

Harris County Texas Comprehensive Turbidity Study Results Report

Prepared in cooperation with the Harris County Flood Control District

Project ID: Z100-00-00-Y053



EIH Technical Report # 12-001

2/28/2012
University of Houston-Clear Lake
Environmental Institute of Houston





Harris County Texas Comprehensive Turbidity Study Results Report



Prepared By Environmental Institute of Houston

University of Houston-Clear Lake
George Guillen, Executive Director
Jenny Oakley, Environmental Scientist
Kristen Vale, Research Associate

Mustafa Mokrech, GIS Analyst
Misty Shepard, Research Associate
Amanda Moss, Research Associate

Principal Investigator

George Guillen
Environmental Institute of Houston
University of Houston Clear Lake
2700 Bay Area Blvd
Houston, Texas 77058

Prepared in cooperation with and for the Harris County Flood Control District

Robert E. Snoza II, Project Manager
Environmental Services Division
9900 Northwest Freeway
Houston, TX 7709

* Photographs of TSS & SS Filters from Harris County waterways, by Jenny Oakley & Misty Shepard.

TABLE OF CONTENTS

EXECUTIVE SUMMARY 8

INTRODUCTION 10

 PROBLEM STATEMENT10

 BACKGROUND11

 STUDY OBJECTIVE13

METHODOLOGY 14

 LITERATURE REVIEW14

 HISTORICAL DATA ANALYSIS.....14

 NEW DATA COLLECTION AND ANALYSIS14

Site Selection Process15

Field Site Surveys.....31

Laboratory Sample Processing and Sample Calculations33

Sub-watershed Delineation34

Rainfall Accumulation and Run-off Modeling35

SOIL TEXTURE 36

Analysis of Survey Field Data36

RESULTS..... 38

 LITERATURE REVIEW38

 HISTORICAL DATA ANALYSIS.....41

 ANALYSIS OF NEW FIELD STUDY DATA44

Sampling Events44

Site Characteristics.....44

Automated Monitoring50

Periodic Monitoring Results60

SYNTHESIS AND CONCLUSION 86

RECOMMENDATIONS 88

LITERATURE CITED 89

APPENDICES..... 91

 APPENDIX 1: SITE CLASSIFICATION CLUSTER ANALYSIS DATA (ELECTRONIC SUPPLEMENT)92

 APPENDIX 2: PHOTOGRAPH RECORD (ELECTRONIC SUPPLEMENT)93

 APPENDIX 3: INTERACTIVE GOOGLE EARTH MAP (ELECTRONIC SUPPLEMENT)98

 APPENDIX 4: FORMS AND DATASHEETS100

 APPENDIX 5: CALIBRATION DATA (ELECTRONIC SUPPLEMENT).....103

 APPENDIX 6: ARCGIS TECHNICAL METHODS.....104

 APPENDIX 7: HYDROLOGICAL SOIL TYPES AND IMPERVIOUSNESS BY SITE SPECIFIC WATERSHEDS.112

 APPENDIX 8: PARENT 2010 HISTORICAL DATA REVIEW DATABASE (ELECTRONIC SUPPLEMENT)133

 APPENDIX 9: HISTORICAL DATABASE (ELECTRONIC SUPPLEMENT)134

9.A: Harris County Historical Data134

9.B: EIH CRP NTU Historical Database134

 APPENDIX 10: DEPLOYED SONDE DATA (ELECTRONIC SUPPLEMENT)135

 APPENDIX 11: FLOW DATA (ELECTRONIC SUPPLEMENT)136

 APPENDIX 12: RAINFALL DATA (ELECTRONIC SUPPLEMENT).....137

 12.A. DAILY RAINFALL DATA137

 12.B. HOURLY RAINFALL DATA137

APPENDIX 13: MASTER DATA (ELECTRONIC SUPPLEMENT)138
13.A. MASTER DATABASE.....138
13.B. LAB BENCH SHEETS138
13.C. FIELD DATASHEETS138
APPENDIX 14: ARCGIS RUNOFF DATA (ELECTRONIC SUPPLEMENT).....139

List of Figures

FIGURE 1. THE STATISTICAL CLUSTERING OF SITES BASED UPON LAND USE AND COVER, AND SOIL TYPE.17

FIGURE 2. MAP OF RECONNAISSANCE SITES, AS LISTED IN TABLE 3.....19

FIGURE 3. MAP SHOWING LOCATION OF SAMPLING SITES ON FINAL LIST, INCLUDING AS AND PM SITES, AS LISTED IN TABLE 4.21

FIGURE 4. PHOTOGRAPHS OF PM SITE 1C, USGS GAGE 8074810, BRAYS BAYOU AT GESSNER DR, HOUSTON, TEXAS.22

FIGURE 5. PHOTOGRAPHS OF PM SITE 1E, USGS GAGE 8073700, BUFFALO BAYOU AT PINEY POINT, TEXAS.22

FIGURE 6. PHOTOGRAPHS OF PM SITE 1F, USGS GAGE 8073600, BUFFALO BAYOU AT W. BELT DR. AT HOUSTON, TEXAS.23

FIGURE 7. PHOTOGRAPHS OF AS SITE 1G, USGS GAGE 8076997, CLEAR CREEK AT MYKAWA ST., NEAR PEARLAND, TEXAS.23

FIGURE 8. PHOTOGRAPHS OF PM SITE 1H, USGS GAGE 8068740, CYPRESS CREEK AT HOUSE-HAHL RD, NEAR CYPRESS, TEXAS.24

FIGURE 9. PHOTOGRAPHS OF PM SITE 1J, USGS GAGE 8075763, HUNTING BAYOU AT HOFFMAN ST., HOUSTON, TEXAS.....24

FIGURE 10. PHOTOGRAPHS OF PM SITE 1K, USGS GAGE 807577630, HUNTING BAYOU AT IH 610, HOUSTON, TEXAS.25

FIGURE 11. PHOTOGRAPHS OF PM SITE 1M, USGS GAGE 8072760, LANGHAM CREEK AT W. LITTLE YORK RD NEAR ADDICKS, TEXAS. 25

FIGURE 12. PHOTOGRAPHS OF PM SITE 1P, USGS GAGE 8075730, VINCE BAYOU AT W. HARRIS AVENUE IN PASADENA, TEXAS.26

FIGURE 13. PHOTOGRAPHS OF PM SITE 2A, USGS GAGE 8068800, CYPRESS CREEK AT GRANT RD., NEAR CYPRESS, TEXAS.26

FIGURE 14. PHOTOGRAPHS OF AS SITE 2B, USGS GAGE 8068900, CYPRESS CREEK AT STUEBNER-AIRLINE RD., NEAR WESTFIELD, TEXAS.27

FIGURE 15. PHOTOGRAPHS OF PM SITE 2D, USGS GAGE 8076000, GREENS BAYOU NEAR HOUSTON, TEXAS.27

FIGURE 16. PHOTOGRAPHS OF PM SITE 2E, USGS GAGE 8075900, GREENS BAYOU NEAR US HWY 75, NEAR HOUSTON, TEXAS.27

FIGURE 17. PHOTOGRAPH OF PM SITE 2G, USGS GAGE 8074020, WHITEOAK BAYOU AT ALABONSON RD. AT HOUSTON, TEXAS.28

FIGURE 18. PHOTOGRAPHS OF AS SITE 3A, USGS GAGE 8068720, CYPRESS CREEK AT KATY-HOCKLEY RD., NEAR HOCKLEY, TEXAS.28

FIGURE 19. PHOTOGRAPHS OF AS SITE 4A, USGS GAGE 8074760, BRAYS BAYOU AT ALIEF, TEXAS.29

FIGURE 20. PHOTOGRAPHS OF PM SITE 4B, USGS GAGE 8073500, BUFFALO BAYOU NEAR ADDICKS, TEXAS.29

FIGURE 21. PHOTOGRAPHS OF PM SITE 5A, USGS GAGE 8075000, BRAYS BAYOU AT HOUSTON, TEXAS.....30

FIGURE 22. PHOTOGRAPHS OF AS SITE 5B, USGS GAGE 8076500, HALLS BAYOU AT HOUSTON, TEXAS.....30

FIGURE 23. PHOTOGRAPHS OF PM SITE 5C, USGS GAGE 8074500, WHITEOAK BAYOU AT HOUSTON, TEXAS.....30

FIGURE 24. PVC AND LOCK BOX DATA SONDE DEPLOYMENT METHODS, SITES 1G (LEFT) AND 3A (RIGHT).31

FIGURE 25. (A) PORTABLE TURBIDITY METER FOR FIELD NTU READINGS; (B) FIELD PERSONNEL TAKING DEPTH AND GRAB SAMPLES; (C) FIELD PERSONNEL TAKING SSC SAMPLES; (D) FIELD PERSONNEL TAKING FLOW MEASUREMENTS AND SONDE READINGS.....32

FIGURE 26. SUSPENDED SEDIMENT SAMPLERS USED THROUGHOUT STUDY33

FIGURE 27. ANALYSIS OF TURBIDITY DATA FOR THE BRAZOS RIVER BASIN UTILIZED IN (PARENT 2009).....40

FIGURE 28. ANALYSIS OF TURBIDITY DATA FOR THE TRINITY RIVER BASIN UTILIZED IN (PARENT 2009).40

FIGURE 29. NTU MEASUREMENTS OBTAINED BY MONITORING AT 69 SITES IN HARRIS, BRAZORIA, AND GALVESTON COUNTIES FROM 12-1-2005 TO 7-18-2011. N = 1,445.41

FIGURE 30. PAIRED NTU VS. SD MEASUREMENTS OBTAINED BY MONITORING AT 69 SITES IN HARRIS, BRAZORIA AND GALVESTON COUNTIES FROM 12-1-2005 TO 7-18-2011. N = 1,44542

FIGURE 31. RESULTS OF REGRESSION ON LOG-TRANSFORMED, PAIRED NTU VS. SD MEASUREMENTS OBTAINED BY MONITORING AT 69 SITES IN HARRIS, BRAZORIA AND GALVESTON COUNTIES FROM 12-1-2005 TO 7-18-2011. N = 1,44542

FIGURE 32. PAIRED NTU VS. TSS MEASUREMENTS OBTAINED BY MONITORING AT 69 SITES IN HARRIS, BRAZORIA AND GALVESTON COUNTIES FROM 12-1-2005 TO 7-18-2011. N = 1,44543

FIGURE 33. RESULTS OF REGRESSION ON LOG-TRANSFORMED, PAIRED NTU VS. TSS MEASUREMENTS OBTAINED BY MONITORING AT 69 SITES IN HARRIS, BRAZORIA AND GALVESTON COUNTIES FROM 12-1-2005 TO 7-18-2011. N = 1,44543

FIGURE 34. WATERSHED AREA LOCATED ABOVE EACH MONITORING SITE, INCLUDING AMOUNTS OF IMPERVIOUS LAND COVER.47

FIGURE 35. MEDIAN STREAM WIDTH DURING STUDY PERIOD AT EACH SURVEY SITE. NOTE: SITE 3A WAS OFTEN INTERMITTENT, SO MEDIAN STREAM WIDTH WAS EQUIVALENT TO MEDIAN POOL WIDTH.47

FIGURE 36. MEDIAN STREAMFLOW OBSERVED DURING THE STUDY PERIOD AT EACH SITE. STREAMFLOW BASED ON VALUES OBSERVED DURING ACTIVE MONITORING.48

FIGURE 37. STATE OF TEXAS DROUGHT INDEX MAP FOR APRIL 19, 2011 DEPICTING CURRENT CONDITIONS IN HARRIS COUNTY. DATA SOURCE: NATIONAL DROUGHT MITIGATION CENTER: ([HTTP://DROUGHT.UNL.EDU/](http://drought.unl.edu/)).48

FIGURE 38. STATE OF TEXAS DROUGHT INDEX MAP ON AUGUST 2, 2011 DEPICTING CURRENT CONDITIONS IN HARRIS COUNTY. DATA SOURCE: NATIONAL DROUGHT MITIGATION CENTER: ([HTTP://DROUGHT.UNL.EDU/](http://drought.unl.edu/)).49

FIGURE 39. STATE OF TEXAS DROUGHT INDEX MAP ON NOVEMBER 22, 2011 DEPICTING CURRENT CONDITIONS IN HARRIS COUNTY. DATA SOURCE: NATIONAL DROUGHT MITIGATION CENTER: ([HTTP://DROUGHT.UNL.EDU/](http://drought.unl.edu/)).49

FIGURE 40. CUMULATIVE DISTRIBUTION OF TURBIDITY NTU OBSERVED DURING THIS STUDY FROM ALL DATASONDES (N = 28,783, OUT OF 31,339 ORIGINAL NTU READINGS, EXCLUDING VALUES < 0). VALUES MARKED BY THE VERTICAL BLUE LINE DENOTE THE 10TH, 25TH, MEDIAN, 75TH AND 90TH PERCENTILE.50

FIGURE 41. BOXPLOT OF TURBIDITY NTU VALUES RECORDED BY AUTOMATED DATASONDE SAMPLERS.....51

FIGURE 42. ESTIMATES OF AVERAGE AND ASSOCIATED 95% CONFIDENCE INTERVALS FOR NTU RECORDED BY AUTOMATED SAMPLERS DURING THE STUDY IN 2011.51

FIGURE 43. TURBIDITY (NTU) AND FLOW (LOG SCALE) OBSERVED AT SITE 1G FROM MAY TO SEPTEMBER 2011. NOTE: THIS ANALYSIS CONTAINS SOME NEGATIVE NTU VALUES THAT WERE NOT TRUNCATED.52

FIGURE 44. TURBIDITY VS. FLOW (LOG SCALE) AT SITE 1G OBSERVED DURING THE STUDY. NOTE: THIS ANALYSIS CONTAINS SOME NEGATIVE NTU VALUES THAT WERE NOT TRUNCATED.....53

FIGURE 45. TURBIDITY (NTU) AND FLOW (LOG SCALE) OBSERVED AT SITE 2B FROM MAY TO SEPTEMBER 2011. NOTE: THIS ANALYSIS CONTAINS SOME NEGATIVE NTU VALUES THAT WERE NOT TRUNCATED.54

FIGURE 46. TURBIDITY VS. FLOW (LOG SCALE) AT SITE 2B OBSERVED DURING THE STUDY. NOTE: THIS ANALYSIS CONTAINS SOME NEGATIVE NTU VALUES THAT WERE NOT TRUNCATED. DURING MOST OF THE PROJECT, LOWER STREAM FLOWS (< 150cfs) BELOW THE RATING CURVE FOR THIS SITE NOT RECORDED BY THE USGS GAGE. CONSEQUENTLY, MATCHING TURBIDITY VALUES ARE NOT DEPICTED FOR THOSE PERIODS.54

FIGURE 47. TRENDS IN TURBIDITY (NTU) MEASURED BY THE YSI DATASONDE AND STREAMFLOW (CFS) AT SITE 3A DURING THE STUDY PERIOD. ALL NTU VALUES WERE UTILIZED FOR THIS DISPLAY, INCLUDING NEGATIVE NUMBERS.55

FIGURE 48. RELATIONSHIP OF TURBIDITY VERSUS STREAMFLOW BASED ON AUTOMATED MONITORING DATA AT SITE 3A. ALL NTU VALUES WERE UTILIZED FOR THIS DISPLAY, INCLUDING NEGATIVE NUMBERS.55

FIGURE 49. TRENDS IN TURBIDITY AND STREAMFLOW BASED ON AUTOMATED MONITORING DATA AT SITE 4A DURING THE STUDY PERIOD. ALL NTU VALUES WERE UTILIZED FOR THIS DISPLAY, INCLUDING NEGATIVE NUMBERS.56

FIGURE 50. RELATIONSHIP BETWEEN TURBIDITY VERSUS STREAMFLOW BASED ON AUTOMATED MONITORING DATA AT SITE 4A. ALL NTU VALUES WERE UTILIZED FOR THIS DISPLAY INCLUDING NEGATIVE NUMBERS. NOTE LOG SCALE OF X-AXIS (FLOW).57

FIGURE 51. TRENDS IN TURBIDITY AND STREAMFLOW BASED ON AUTOMATED MONITORING DATA OBSERVED AT SITE 5B DURING THE STUDY PERIOD. NOTE THAT ALL NTU VALUES WERE UTILIZED FOR THIS DISPLAY, INCLUDING NEGATIVE NUMBER, AND THE LOG SCALE USED FOR STREAMFLOW.57

FIGURE 52. RELATIONSHIP BETWEEN TURBIDITY VERSUS STREAMFLOW AT SITE 5B BASED ON AUTOMATED MONITORING DATA. ALL NTU VALUES WERE UTILIZED FOR THIS DISPLAY, INCLUDING NEGATIVE NUMBERS. NOTE LOG SCALE OF X-AXIS (FLOW).58

FIGURE 53. TYPE-1 HYSTERESIS LOOP OR SUSPENDED-SEDIMENT CONCENTRATIONS FOR TWO STORMFLOW EVENTS SHOWING (1) CONCENTRATIONS HIGHER ON THE RISING LIMB THAN THE FALLING LIMB AND (2) SEDIMENT EXHAUSTION EFFECTS FOR THE SECOND, LARGER FLOOD (FROM HUDSON (2003) REFERENCED IN BRANDES ET AL. (2009)).59

FIGURE 54. EXAMPLE OF SITE 2B (LOCATED IN A LARGE WATERSHED), COMPARING NORMAL “DRY” CONDITIONS (LEFT) AND RAIN INFLUENCED “WET” CONDITIONS (RIGHT). NOTE THE APPEARANCE OF INCREASED SUSPENDED SEDIMENT IN THE FAST FLOWING WATER.59

FIGURE 55. CUMULATIVE DISTRIBUTION OF ADJUSTED STREAMFLOW (CFS + 0.01) ACROSS ALL SITES DURING THIS STUDY. LOGNORMAL CDF = BLUE LINE.....60

FIGURE 56. STREAMFLOW LEVELS OBSERVED DURING COLLECTION OF TSS AND NTU SAMPLES IN 2011.61

FIGURE 57. STREAMFLOW MEASUREMENTS DURING BASE FLOW CONDITIONS AND WET WEATHER SAMPLING FOR TSS AND NTU AT EACH SITE GROUPING.62

FIGURE 58. EMPIRICAL CUMULATIVE DISTRIBUTION FUNCTION (CDF) OF SD (M) ACROSS ALL SITES DURING THIS STUDY. LOGNORMAL CDF = BLUE LINE.....62

FIGURE 59. SECCHI DISK READINGS AT EACH SITE OF THE STUDY. N = 761 GRAB SAMPLES ONLY63

FIGURE 60. SECCHI DISK READINGS FOR EACH SITE GROUP. N = 761.....63

FIGURE 61. EMPIRICAL CUMULATIVE DISTRIBUTION FUNCTION (CDF) OF NTU ACROSS ALL SITES DURING THIS STUDY. LOGNORMAL CDF = BLUE LINE64

FIGURE 62. THE 95% CONFIDENCE INTERVAL OF THE MEAN NTU BY SITE. N = 76265

FIGURE 63. THE 95% CONFIDENCE INTERVAL OF THE MEAN NTU FOR EACH SITE GROUP EVALUATED DURING THE STUDY. N = 76265

FIGURE 64. EMPIRICAL CUMULATIVE DISTRIBUTION FUNCTION (CDF) OF TSS. LOGNORMAL CDF = BLUE LINE.66

FIGURE 65. THE 95% CONFIDENCE INTERVAL OF THE MEAN TSS AT EACH SITE. SITE N = 74966

FIGURE 66. THE 95% CONFIDENCE INTERVAL OF THE MEAN TSS VS. SITE GROUP. N=749.....67

FIGURE 67. THE RELATIONSHIP OF TSS VERSUS STREAMFLOW FOR EACH SITE BASED ON DATA FROM PERIODIC MONITORING (PM) EVENTS.68

FIGURE 68. TRENDS IN TSS (LOG SCALE) VS. PERCENT MAXIMUM STREAMFLOW FOR ALL MONITORED SITES.....68

FIGURE 69. TRENDS IN SD (LOG SCALE) VERSUS STREAMFLOW FOR ALL MONITORED SITES.69

FIGURE 70. TRENDS IN SD (LOG SCALE) VERSUS PERCENT MAXIMUM STREAMFLOW FOR ALL SITES.....69

FIGURE 71. TURBIDITY (NTU) (LOG SCALE) VERSUS STREAMFLOW FOR ALL SITES.....70

FIGURE 72. TURBIDITY (NTU) (LOG SCALE) VERSUS PERCENT MAXIMUM STREAMFLOW FOR ALL SITES. STREAMFLOW DATA WAS OBTAINED FROM MATCHING VALUES.70

FIGURE 73. REGRESSION OF LOG₁₀ TSS VERSUS LOG₁₀ SD BASED ON 727 GRAB SAMPLES. NOTE LOG SCALE.72

FIGURE 74. NON-LINEAR MODEL OF TSS (MG/L) VERSUS SD (M). R = 0.789; R² = 0.623, OUTER RED SHADING = 95% CONFIDENCE INTERVAL FOR MEAN.72

FIGURE 75. REGRESSION OF LOG₁₀ NTU VERSUS LOG₁₀ SD TRANSPARENCY BASED ON 727 GRAB SAMPLES. NOTE LOG SCALE.73

FIGURE 76. NON-LINEAR MODEL OF TURBIDITY (NTU) VERSUS SD (M). R = 0.827; R² = 0.683, OUTER RED SHADING = 95% CONFIDENCE INTERVAL FOR MEAN.73

FIGURE 77. REGRESSION OF LOG₁₀ NTU VERSUS LOG₁₀ TSS USING GRAB SAMPLE RESULTS FROM THIS STUDY. NOTE LOG SCALE AXIS. ...75

FIGURE 78. NON-LINEAR MODEL OF TURBIDITY (NTU) VERSUS TSS (MG/L). R = 0.827; R² = 0.685, OUTER RED SHADING = 95% CONFIDENCE INTERVAL FOR THE MEAN.75

FIGURE 79. LOG₁₀ TSS VERSUS LOG₁₀ NTU REGRESSION MODEL BASED ON 728 GRAB SAMPLES. NOTE LOG AXIS SCALE.76

FIGURE 80. NON-LINEAR MODEL OF TSS (MG/L) VERSUS TURBIDITY (NTU). R = 0.816; R² = 0.666, INNER DARKER RED SHADING = 95% CONFIDENCE INTERVAL FOR MEAN, OUTER LIGHT RED SHADING = 95% PREDICTION INTERVAL FOR INDIVIDUAL VALUES.76

FIGURE 81. ESTIMATED DISTRIBUTION OF DERIVED NTU LEVELS FOR HISTORICAL HARRIS COUNTY SITES (1/01-9/11) USING PREDICTIVE LOG-LOG REGRESSION MODEL FROM CURRENT STUDY FOR TSS AND SD.77

FIGURE 82. COMPARISON OF DERIVED NTU VALUES FOR HARRIS COUNTY SITES USING HISTORICAL TSS VERSUS SD VALUES DURING THE LAST 10 YEARS. 1/01 TO 9/11. (PEARSON CORRELATION COEFFICIENT (R) FOR NTU VALUES DERIVED FROM TSS VS. SD = 0.658, P = 0.000)77

FIGURE 83. DISTRIBUTION OF PREDICTED NTU VERSUS PERCENT IMPERVIOUS LAND IN HARRIS COUNTY MAJOR WATERSHEDS AS DEFINED BY HUC 10 DESIGNATION.....78

FIGURE 84. DISTRIBUTION OF PREDICTED NTU VERSUS HISTORICAL RAINFALL INCIDENCE IN HARRIS COUNTY APPLYING THE REGIONAL REGRESSION MODEL TO PAST SD DATA.78

FIGURE 85. ESTIMATED LOADING IN KG SSC/D DERIVED FROM USGS GAGE READINGS AND SSC MEASUREMENTS AT EACH SITE, VERSUS PERCENT IMPERVIOUS LAND IN THE CONTRIBUTING WATERSHED LOCATED ABOVE SAMPLING SITE DURING THE FIELD STUDY.80

FIGURE 86. ESTIMATED LOADING OF SUSPENDED SOLIDS IN KG SSC/DAY/HECTARE DERIVED FROM USGS GAGE READINGS AND SSC MEASUREMENTS AT EACH SITE VERSUS PERCENT IMPERVIOUS AREA LOCATED ABOVE SITES MONITORED DURING APRIL TO NOVEMBER 2011.80

FIGURE 87. ESTIMATED LOADING IN KG SSC/D EXTRAPOLATED FROM 1) STREAMFLOW DERIVED FROM USGS GAGE READINGS AND SSC MEASUREMENTS AND 2) ESTIMATED QUANTITIES OF TOTAL RUNOFF FROM THE UPSTREAM WATERSHED DERIVED FROM RAINFALL-RUNOFF MODEL PREDICTIONS ADJUSTED FOR LAND USE AND RAINFALL PATTERNS.81

FIGURE 88. ESTIMATED RUNOFF IN SEDIMENTS (SSC) IN KG/D/HECTARE EXTRAPOLATED TO WATERSHED RUNOFF QUANTITIES, BASED ON 1) STREAMFLOW DERIVED FROM USGS GAGE READINGS AND SSC MEASUREMENTS AND 2) ESTIMATED QUANTITIES OF TOTAL RUNOFF FROM THE UPSTREAM WATERSHED DERIVED FROM RAINFALL-RUNOFF MODEL PREDICTIONS ADJUSTED FOR LAND USE AND RAINFALL PATTERNS.81

FIGURE 89. DISTRIBUTION OF SUSPENDED SOLIDS CONCENTRATION (SSC) OBSERVED AT EACH MONITORING SITE DURING 2011.....82

FIGURE 90. DISTRIBUTION OF SSC BY SITE GROUP DURING 2011.82

FIGURE 91. RELATIONSHIP OF MEASURED SSC VERSUS OBSERVED STREAMFLOW ACROSS ALL STUDY SITES.83

FIGURE 92. RELATIONSHIP OF MEASURED SUSPENDED SOLIDS VERSUS OBSERVED STREAMFLOW ACROSS ALL STUDY SITES EXCLUDING SITE 3A. LINES ON GRAPH REPRESENT LINEAR REGRESSION MODEL FITS FOR EACH GROUP AND COMBINED (PURPLE LINE FIT). CORRESPONDING R² VALUES FOR EACH GROUP MODEL ARE OVERALL = 12.5%, 1 = 6.4%; 2 = 29.3%, 4 = 20.9%, AND 5=56.0%.83

FIGURE 93. RELATIONSHIP OF MEASURED TURBIDITY (NTU) VERSUS OBSERVED STREAMFLOW ACROSS ALL STUDY SITES EXCLUDING SITE 3A. LINES ON GRAPH REPRESENT LINEAR REGRESSION MODEL FITS FOR EACH GROUP AND COMBINED (PURPLE LINE FIT). CORRESPONDING R² VALUES FOR EACH GROUP MODEL ARE OVERALL = 4.5%, 1 = 2.5%; 2 = 48.4%, 4 = 6.2%, AND 5=51.0%.....84

FIGURE 94. EXAMPLE OF CONSTRUCTION ACTIVITY OBSERVED DURING THE STUDY PERIOD AT SITE 1K.85

FIGURE 95. COMPARISON OF NTU LEVELS AT SITES WHERE CONSTRUCTION ACTIVITIES WERE OBSERVED DURING VARYING STREAMFLOW
CONDITIONS85

List of Tables

TABLE 1. LIST OF GAGE AND ASSOCIATED WATERSHED TRAITS USED TO CLASSIFY AND GROUP SIMILAR SITES. USGS = UNITED STATES GEOLOGICAL SERVICE. HGAC=HOUSTON-GLAVESTON AREA COUNCIL. NRCS=NATIONAL RESOURCE CONSERVATION SERVICE. 16

TABLE 2. GENERAL DESCRIPTION OF THE CHARACTERS WITHIN EACH WATERSHED TYPE (↓= LOW OR DEPRESSED, ↑ = HIGH OR ELEVATED, ↔ = MODERATE CONDITIONS).17

TABLE 3. LIST OF ALL 29 POTENTIAL STUDY SITES ORGANIZED BY WATERSHED/CLUSTER TYPE. THESE SITES WERE VISITED DURING RECONNAISSANCE SURVEYS TO EVALUATE ACCESS ISSUES PRIOR TO THE STUDY.....18

TABLE 4. FINAL LIST OF SITES MONITORED THROUGHOUT STUDY, DIFFERENTIATED BY SAMPLE TYPE (AUTO-SAMPLING (AS) OR PERIODIC MONITORING (PM)), AND SITE TYPE. HCFWS = HARRIS COUNTY FLOOD WARNING SYSTEM.20

TABLE 5. CANDIDATE NRCS HYDROLOGICAL SOIL GROUPS USED FOR CLASSIFICATION DURING THIS STUDY.....36

TABLE 6. COMPARISON OF PREDICTIVE MODELS FOR TURBIDITY REPORTED BY (PARENT 2009).39

TABLE 7. SAMPLING CONDUCTED DURING THE STUDY PERIOD EXTENDING FROM APRIL TO DECEMBER 2011. *NO DATASONDES LOGGED DATA DURING THIS SAMPLE PERIOD. **NO SAMPLES WERE TAKEN DURING THIS SITE VISIT. AS SITES DATASONDES WERE DEPLOYED DURING SAMPLE 1 AND RETRIEVED DURING SAMPLE 3 FOR EACH SAMPLE PERIOD, UNLESS OTHERWISE STATED.45

TABLE 8. SUMMARY OF SITE CHARACTERISTICS OBSERVED DURING THE STUDY. *FLOW VALUE FROM ENTIRE SONDE DEPLOYMENT SAMPLE PERIOD (CFS). **FLOW VALUES FROM SONDE DEPLOYMENT SAMPLE PERIOD NOT AVAILABLE, USGS GAGE DOES NOT RECORD BASE FLOW CONDITIONS. DSLSR = DAYS SINCE LAST SIGNIFICANT RAINFALL. MIN.= MINIMUM, MED.=MEDIAN, MAX.=MAXIMUM. 46

TABLE 9. RESULTS OF CORRELATION ANALYSIS BETWEEN PAIRED TSS, NTU AND SD MEASUREMENTS AND THEIR LOG₁₀ TRANSFORMATIONS.71

Executive Summary

Harris County and adjacent counties are experiencing increased construction activities associated with new and ongoing residential and industrial development. Stormwater detention ponds and structures have been required in many of these areas to reduce flood risks associated with increased stormwater runoff caused by the increasing amounts of impermeable surfaces associated with urbanization. The immediate construction activities and resulting higher amount of impermeable surfaces associated with new streets and structures, can generate excessive amounts of fine sediments which are transported by stormwater runoff. These discharges can increase the amount of suspended solids in receiving streams. This increase in sediment load can increase turbidity leading to potential negative effects including excessive downstream sedimentation, shading of aquatic plants, and reduced survival of stream fish and benthic organisms. A common method for the reduction of flood risks associated with new development is the construction of stormwater detention ponds. During the construction of these detention ponds, soil is excavated, also increasing the probability of sediment runoff from the construction site. In response, the Environmental Protection Agency (EPA) and states have developed Best Management Practices (BMPs) for construction activities, under their National Pollution Discharge Elimination System (NPDES) National Menu of Stormwater Best Management Practices. Most recently, the EPA issued a numeric limit for effluent turbidity (280 NTU) in their 2009 final effluent guideline rule for the *Construction and Development Point Source Category*. This ruling established national monitoring requirements and enforceable numeric limitations on stormwater discharges from construction sites. The proposed numeric discharge limit was based primarily on best achievable technology and not to reach any specific instream numeric criterion. However, effective January 4, 2011, the EPA withdrew the limit of 280 nephelometric turbidity units (NTU) to correct a calculation error that was identified in petitions filed by industry representatives. The EPA decided to seek additional treatment performance data from construction and development sites before proposing a revised numeric turbidity limit. The EPA published a notice in the Federal Register on January 3, 2012 requesting additional data on performance of technologies in controlling turbidity in stormwater discharges from construction sites. The EPA accepted comments through March 5, 2012. The following report provides additional information on ambient levels of turbidity within southeast Texas streams that can be used to further refine and develop appropriate discharge standards for NTU, based on ambient water quality conditions.

In anticipation of the potential future changes to stormwater effluent limits, the Harris County Flood Control District (HCFCD) partnered with the Environmental Institute of Houston (EIH) of the University of Houston-Clear Lake (UHCL) to: 1) conduct a review of existing scientific literature and local and regional data; 2) conduct new field studies to examine ambient levels of turbidity as measured by various methods; and 3) to develop a comprehensive database of recent data (<10 years) within the region. By reviewing available data, predictive relationships were developed between Secchi depth, TSS, and NTU values. New, additional data was collected in order to evaluate the potential ranges of turbidity as measured by NTU under a varying flow regime. Finally estimates of sediment loading using suspended solids concentration (SSC) measurements were compared to flow regimes and land use to gain a better understanding of how these two factors affect turbidity in urban streams. This new information will be useful to water quality managers and the regulatory community charged with the responsibility of governing sediments, turbidity, and other related issues.

The approach used during this study was to collect paired turbidity (NTU), Secchi disk (SD) transparency (m), TSS (mg/L), and SSC (mg/L) data at 15 sites with watersheds representing a broad spectrum of soil and land-use/land-cover types. These sites were classified as periodic monitoring (PM) sites where only instantaneous grab samples were collected. Streamflow data was collected at all sites from continuously recording United States Geological Survey (USGS) gages. At five additional

automated sampling (AS) sites, YSI multiparameter datasondes equipped with nephelometers were deployed for approximately 1 month during four monitoring periods (Apr-May, Jun-Jul, Aug-Sept and/or Sep-Oct, and Nov-Dec), including wet weather conditions to continuously monitor water temperature, specific conductance, pH, dissolved oxygen, depth, and NTU. Automated monitoring measurements were conducted at half-hour increments. Continuous recording streamflow data was obtained at all sites using USGS gage data, however, due to the lack of low flow gage data at one site (2B), a Sontek Acoustic Doppler Velocimeter (ADV) flow meter was used to take periodic measurements.

Historical data collected by EIH for the Clean Rivers Program (CRP) during 2005 to 2011 document the majority of the NTU measurements ranged between 5 and 75 NTU. The most frequent measurements ranged between 5 and 20 NTU. Values never exceeded 275 NTU. During April to December 2011 automated monitoring datasondes deployed at 5 sites collected a total of 28,783 NTU measurements that were ultimately used in our analysis. The 10th, 25th, median, 75th and 95th percentile NTU values were 7, 13, 26, 60 and 381 respectively, and ranged between 0 and 1,778. During periodic monitoring, an additional 729 paired measurements of NTU and TSS, 728 measurements of SD and 715 streamflow measurements were obtained. The lowest and highest turbidity values were 3.51 and 187 NTU, respectively. Average turbidity values were generally below 40 NTU. Predictive models were developed between turbidity measurements (NTU) and historically collected data using other types of measures of water clarity including TSS and SD. Log transformed SD measurements and turbidity (NTU) were used to develop a predictive linear regression model. This model fit the data well ($r^2 = 0.834$). Log transformed SD measurements explained 83.4% of the variation in log transformed NTU values. This model was used to reconstruct past turbidity values in Harris County by converting historical TSS and SD readings into turbidity (NTU) values. The majority of derived historical Harris County NTU values ranged between 5 and 50 NTU. However, this study was conducted during a severe drought. Therefore the statistical relationships developed between streamflow and turbidity may be biased by the reliance on low flow data sets.

Empirical levels of NTU observed in this study and others show that turbidity levels can be highly variable and elevated immediately after storm flows and/or when bottom sediment is disturbed. Land use and the type of soils influence the various measures of turbidity with high amounts of impervious surface influencing the amount of runoff, streamflow and associated measures of turbidity. This recognized pattern was not consistent in this study. This may be due to the non-linear response associated with sediment transport in streams. In order to evaluate the role of the hydrological sequence of flood pulses on sediment mobilization, we recommend a closer examination of individual hydrographs, and analyzing not only the relationship of absolute streamflow versus turbidity, but also evaluating the rate of change (+ or – delta change in flow) in flow and how it influences sediment transport. Past literature has documented that stormflow hydrographs are frequently characterized by higher suspended sediment concentrations during the rising limb than the falling limb, referred to as a type-1 hysteresis loop.

The development of Geographic Information System (GIS) based land-use data and estimated runoff estimates utilizing empirically derived runoff coefficients for different hydrological soil types and impervious land, coupled with actual measured suspended sediment and streamflow, provides a unique synthesis of these data. This information will serve as an excellent starting point and framework for testing various hypotheses on how BMPs influences suspended sediment loading into the watershed.

Due to the drought conditions encountered during the study, it is recommended that additional studies be conducted during higher flow regimes. There is sufficient evidence to suggest that higher turbidity values are possible during higher streamflow in many of these waterbodies studied. In addition, more detailed automated monitoring focused on evaluating the temporal changes in turbidity associated with the changes in flow including the relative amount and direction of change.

The proposed 280 NTU standard that was withdrawn by EPA, would have been below ambient levels of turbidity in Harris County streams during stormflows and, depending on the watershed, may be close to some ambient base flow conditions. Therefore, in these situations, an effluent limitation close to the 280 NTU value may be difficult to attain given the clay soils present in many of the watersheds found in Harris County and the historically high turbidity levels (>300 NTU) encountered in at least 10% of the monitoring events as documented by this study.

Introduction

Problem Statement

Construction activities associated with new urban development include roads, buildings, stream channelization and stormwater management structures including stormwater detention ponds. During the construction of these structures, soil is excavated increasing the runoff of sediment, nutrients, and other pollutants from the construction site. In an effort to control these sources of pollutants, the Environmental Protection Agency (EPA) and states have developed Best Management Practices (BMPs) for construction activities. These BMPs are presented under the National Pollution Discharge Elimination System (NPDES) National Menu of Stormwater Best Management Practices (http://cfpub.epa.gov/npdes/stormwater/menuofbmps/index.cfm?action=min_measure&min_measure_id=4).

To monitor compliance with these new BMP regulations EPA has selected turbidity as an easily measured indicator of the presence of a number of pollutants. EPA recently issued a numeric limit of 280 Nephelometric Turbidity Units (NTU) in the 2009 final effluent guideline rule for the *Construction and Development Point Source Category*. This ruling established national monitoring requirements and enforceable numeric limitations for stormwater discharges from construction sites (<http://water.epa.gov/scitech/wastetech/guide/construction/index.cfm>) (Environmental Protection Agency 2009b). The proposed numeric discharge limit was based primarily on best achievable technology and not to achieve any specific instream numeric criterion. In summary, the rule stated that beginning no later than August 2, 2010, during any construction activity that disturbs 20 or more acres of land at one time, and no later than February 2, 2014, during construction activity that disturbs ten or more acres of land area at one time, the following requirements apply:

- (a) (1) the average turbidity of any discharge for any day must not exceed a pollutant daily maximum turbidity value of 280 NTU. (a) (2) Conduct monitoring consistent with requirements established by the permitting authority. Each sample must be analyzed for turbidity in accordance with methods specified by the permitting authority.
- (b) If stormwater discharges in any day occur as a result of a storm event in that same day that is larger than the local 2-year, 24-hour storm, the effluent limitation in paragraph (a) (1) of this section does not apply for that day.

The proposed standard was based on an analysis conducted by the EPA, which examined current state water quality standards, available technology, and existing representative data on the industry for the model technology, polymer-aided settling (Environmental Protection Agency 2009a). The limitations for turbidity were provided as the maximum daily discharge limitation. The daily maximum limitation is an estimate of the 99th percentile of the distribution of daily measurements. The percentile for the daily maximum limitation was estimated using the product of the long-term average and the variability factor derived from data that represent the performance of the model technology under all conditions when properly operated and controlled. The EPA estimated the long-term average and variability factor using a statistical model based on a lognormal distribution. The long-term average of 64.13 NTU was the median value of 25 long-term averages collected from 25 treatment systems (Environmental Protection Agency 2009a). Using its standard approach for effluent guidelines, the EPA calculated the value of the daily maximum limitation (280 NTU) using the product of the long-term average (64.13 NTU) and daily variability factor (4.322):

$$\begin{aligned}\text{Daily Maximum Limitation} &= \text{Long-Term Average} \times \text{Variability Factor} \\ &= (64.13 \text{ NTU}) \times (4.322) = 277.17 \text{ NTU}\end{aligned}$$

EPA rounded the value of the limitation to two significant digits (i.e., 280 NTU) (Environmental Protection Agency 2009a). Furthermore, the EPA tested the daily maximum limitation against current data for reasonability and use of proper distributional assumptions.

The EPA withdrew the limit of 280 NTU to correct a calculation error that was identified in petitions filed by industry representatives, effective January 4, 2011 (Environmental Protection Agency 2010). In order to ensure that they adequately characterize the best performance achievable by the technology, the EPA decided to seek additional treatment performance data from construction and development sites before proposing a revised numeric turbidity limit (Environmental Protection Agency 2010). The EPA published a notice in the Federal Register on January 3, 2012 requesting additional data on performance of technologies in controlling turbidity in stormwater discharges from construction sites (Environmental Protection Agency 2012). The notice also requested information on other topics relevant to establishing numeric effluent limitations for stormwater discharges from these sites. The EPA will be accepting comments through March 5, 2012. This report provides additional information that can be used to further refine and develop appropriate discharge standards for NTU, based on ambient levels of turbidity within southeast Texas waterways.

Background

Elevated turbidity in streams can be detrimental to aquatic life and should be regulated to maintain levels as close as possible to natural, region-specific levels that support aquatic life (Berry et al. 2003). In streams and larger rivers, turbidity is influenced by various proximate causes, including sediment load, algal blooms, and dissolved colored substances. Soil conditions, land use (e.g. urbanization, farming, and hard surfaces), discharges, and nutrients can alter turbidity levels in receiving streams (Water 1995). Extensive urbanization can increase stream turbidity due to elevated levels of erosion and runoff from impervious surfaces, including streets and parking lots.

The impact of increased turbidity on streams biota is dependent upon constituents causing turbidity, levels of turbidity and duration of exposure (Newcombe and MacDonald 1991). For example, short exposures of suspended sand and clay may cause minimal impacts on stream organisms, whereas prolonged exposure to fine clays and coating of benthic communities can cause extensive impacts on primary producers including periphyton. (Berry et al. 2003) reviewed much of the literature on the

impacts associated with increased turbidity. However, much of their summary data was focused on coldwater fisheries, including salmonids, and is presented in terms of suspended solids in units of mg/L. These values would need to be converted to NTU units to utilize them in setting any guidelines to protect aquatic systems. The range of concentrations that caused mortality in fish and invertebrates varied considerably and was influenced primarily by life stage. In some cases concentrations as high as 40,000 mg/L did not cause any observable impacts to adult fishes while much lower concentrations (<100 mg/L) could negatively impact larval stages and planktonic organisms. (Newcombe and MacDonald 1991) recognized that high concentrations alone were not sufficient to characterize the impacts of elevated suspended sediments but also the duration of exposure. They developed a stress index that combined the concentration (mg/L) and duration (hours) in one coefficient defined as: $\log_e^* (C \times D)$.

Various states have developed numeric and narrative sediment-related criteria that affect turbidity (Environmental Protection Agency 2009a). These take the form of a variety of magnitudes, duration and frequencies that focus on background levels of 10 to 150 NTU in freshwater streams. A few states also have numeric TSS criteria (e.g. 25 mg/L) for coldwater clear streams. These are usually accompanied by frequency of attainment qualifiers, such as “not to exceed a certain level more than 20% of the time”.

Currently there are many ways to measure the turbidity, or the inverse of this property, clarity of water (Clesceri et al. 1998). It can be measured directly as an optical property of water. Particles in water will scatter a light beam focused on them. This scattered light can be measured with a nephelometer with the detector setup at a 90 degree angle to the light beam. More light reaches the detector if there are many small particles scattering the source beam than if there are few. The units of turbidity obtained from a calibrated nephelometer are referred to as Nephelometric Turbidity Units NTU. To some extent, the amount of light that reflects for a given amount of particulate is dependent upon properties of the particles such as their shape, color, and reflectivity. Turbidity scattering is also affected by particle size; heavier particles settle too quickly and do not contribute to a turbidity reading.

One of the most common methods used to measure turbidity indirectly is Secchi disk (SD) transparency, which is used for routine water quality monitoring. This methodology yields easily understandable data on the depth at which a disk, with alternating black and white shading, disappears from sight when lowered and raised in the water column. The depth is then recorded as a measure of the transparency of the water (inversely related to turbidity). The SD has the advantage of integrating turbidity over depth and is quick, easy, and inexpensive to use. In addition, it can be used to derive a crude estimate of the vertical attenuation coefficient (K_d), a parameter describing the depth of light penetration that supports aquatic plant life (Kirk 1994). Most historical ambient monitoring (e.g. both EPA sponsored and State of Texas Clean Rivers Program – CRP) conducted within Texas and Harris County and adjacent areas have utilized standard SD transparency measurements using Texas Commission on Environmental Quality (TCEQ) methodology to evaluate turbidity trends in various basins (Texas Commission of Environmental Quality 2008).

Another common water quality measurement used to indirectly assess turbidity is total suspended solids (TSS) measured by method 2540 D in Standard Methods (Clesceri et al. 1998). A correlation between turbidity and TSS is somewhat unique for each location or situation. Since NTU is an optical property of water and is affected by the particles’ physical properties, there is no easy, universal conversion to other measurements involving mass. A general rule of thumb, often reported in the literature, is that 1 mg/L TSS \approx 1.0 to 1.5 NTU’s of turbidity {Lake Superior Streams, 2012 #30}. However, this rule of thumb is only an approximation. Although TSS can certainly affect turbidity and cause direct impacts on both

benthic and free swimming organisms, it is not the sole constituent that can affect turbidity, as measured by SD or other methods. Since flow intensity varies with depth, it affects both concentration and size of the sediment particles suspended within an entire water column. TSS is typically obtained from a single, surface grab, and as such, is unsuitable for estimation of sediment transport (Gray et al. 2000).

The United States Geological Survey (USGS) collects considerable amounts of suspended solids concentration (SSC) data for use in sediment transport studies. This data is collected using a time and volume-integrated sampler to ensure that a flow-weighted estimate of the suspended sediment is collected (Edwards and Glysson 1999). This flow weighted method is important due to the rapid settling velocity of sand fractions in a water sample (Edwards and Glysson 1999). Unlike the TSS analysis, which uses an aliquot of the sample, the SSC determination is normally conducted on the entire sample. However, both measurements yield concentrations of sediment in mg/L. The method used for laboratory measurement of SSC is ASTM D3977-97 (American Society for Testing and Materials 2007). Results of the TSS analytical method tend to produce data that are negatively biased from 25 to 34 percent with respect to SSC analyses collected at the same time and can vary widely with different flows at a given site (Gray et al. 2000).

In order to compare historical ambient turbidity levels measured in different units with the new proposed discharge limits in units of NTU, it is necessary to convert historical TSS and SD measurements into NTU values. One approach to accomplish this conversion is to use existing predictive models published in literature to convert values from one unit to the other. These predictive models are often not very accurate because they are influenced by regional conditions, such as the source of turbidity (e.g. color versus suspended solids), soil types, and sediment size distribution. In other words, a model developed in one watershed may not be able to predict the variable in other watersheds with a high degree of accuracy, due to the presence of different sources of turbidity.

A preferred alternative approach is to develop predictive relationships between the more common historical measurement (e.g. SD and TSS) and the new proposed standard unit (e.g. NTU) using data from within the watershed of interest or similar waterbodies. Recently, predictive models were developed between turbidity NTU (independent variable) and SD clarity (dependent variable) in adjacent watersheds in Texas (Parent 2009). This is in contrast to our objective of using SD or TSS as the independent variables to estimate historical and future NTU levels. These models utilized data from various monitoring organizations and watersheds, including the Trinity, Brazos, Sabine, and Colorado Rivers. In total, 6,915 samples were evaluated. Measurements taken both in the field and in a lab were considered. The results of their analysis show a strong, inverse relationship between the water properties of turbidity and Secchi depth. Another, unpublished, local source of data is paired SD and NTU measurements conducted by UHCL during routine CRP monitoring from 2005 to 2011. Preliminary examination of this data suggests a strong relationship between SD clarity and turbidity (NTU).

Study Objective

The objective of this study was to characterize ambient turbidity levels existing in streams, rivers, and bayous within and adjacent to Harris County. Harris and adjacent counties are some of the most urbanized areas in the state of Texas, as well as the nation, and will be experiencing ongoing, rapid population growth within the next few decades. In 2010, the estimated population of Harris County was 4,092,459 (U.S. Census Bureau 2012). The city of Houston is currently ranked as the fourth most populous city in the United States (U.S. Census Bureau 2010). By 2040, the population of Harris County, and adjacent counties, is expected to increase by 4.2 million residents (Office of the State Demographer 2012). This geographic area is unique in having a high annual rainfall, flat topography,

and highly erodible clay soils. Therefore, there will be an ongoing need to build stormwater detention ponds to mitigate increasing flood risks. Future construction activity will be affected by any regulatory changes regarding stormwater effluent limits.

In anticipation of the potential changes to stormwater effluent limits, the Harris County Flood Control District (HCFCD) partnered with the Environmental Institute of Houston (EIH) of the University of Houston-Clear Lake (UHCL) to: 1) conduct a review of existing scientific literature and local and regional data; 2) develop models between Secchi depth, TSS, and NTU to create a comprehensive database of recent data (≤ 10 years) within the region; and 3) conduct new field studies to examine ambient levels of turbidity measured by various methods and how they are influenced by instream and watershed conditions. This new information will be useful to water quality managers and the regulatory community charged with the responsibility of managing sediments, turbidity, and other related issues.

Methodology

Literature Review

A review of recent literature on the relationship of nephelometric turbidity measures and other methods (including SD transparency and total suspended solids) was conducted. This involved a review of recently published articles and agency literature. Particular emphasis was placed on articles that synthesized the findings of scientific studies and research involving similar land use and soils. Literature search engines at the University of Houston-Clear Lake and other online services, including *Google Scholar*, were used to carry out this extensive survey. Key words including *TSS*, *NTU*, *Secchi disk*, *conversion*, and *relationship* were used to locate recently published literature. In addition, the senior author of this study possessed several recent synthesis articles on this topic. Finally, Harris County (past employee - Trent Martin), provided a technical report describing several models developed from ambient water quality data provided by the Lower Colorado, Brazos, Sabine and Trinity River Authorities (Parent 2009).

Historical Data Analysis

Data from 2005 to 2011 collected by EIH for CRP sites located in Harris, Brazoria, and Galveston counties was compiled and used to develop predictive models. EIH collected additional samples that were analyzed with a HF Scientific DRT-15CE Turbidimeter to generate estimates of turbidity in NTU. The results of these measurements were paired with the data obtained from the routine monitoring and analyses of TSS, SD transparency, and streamflow conducted during this same period. These data were subsequently used to relate NTU (dependent variable) to TSS and SD measurements (independent variables). In addition, the relationship of NTU and flow regime was also examined at non-tidal sites. The predictive models based upon historical data, along with new data collected during this study, were then used to estimate past NTU levels using historical SD and/or TSS data measurements collected by other entities through the CRP in Harris County, extending back 10 years. We restricted our application of these models to the most recent 10 years of data, since land use and cover was likely different in prior years and not reflective of current watershed conditions.

New Data Collection and Analysis

During this study, targeted monitoring was conducted at sites in Harris County to gain additional information regarding turbidity and the relationship of this parameter and with other related variables

that have been historically monitored historically to evaluate turbidity. In addition, the role of streamflow regime was evaluated for each site. The potential monitoring locations were chosen at sites where USGS gage stations were operating, to facilitate comparison of water quality data with stream discharge data. Nearly all sites were also co-located with a rain gages operated through the HCFCD's Flood Warning System (HCFWS). The final sampling sites were selected through a statistical screening process (described below in Site Selection Process) taking into account various factors, including: historical data availability, current gage operation, representation of the broad spectrum of land use in Harris County, and comprehensive geographic coverage of major watersheds.

Paired turbidity (NTU), SD (m), TSS (mg/L), and SSC (mg/L) data were collected at sites with contributing watersheds representing a broad spectrum of soil and land-use/land-cover types. These sites were classified as periodic monitoring (PM) sites where and only instantaneous grab samples for the aforementioned parameters were collected. Streamflow data was collected at all sites from continuously recording USGS gages.

Additionally, YSI multiparameter datasondes equipped with nephelometers were deployed at automated sampling (AS) locations throughout Harris county. These data sondes were deployed for approximately 1 month during four monitoring periods (Apr-May, Jun-Jul, Aug-Sept and/or Sep-Oct, and Nov-Dec), and including wet weather conditions to continuously monitored water temperature, specific conductance, pH, dissolved oxygen, depth, and NTU (including those during wet weather conditions, when present). Automated monitoring measurements were conducted at half-hour increments. Continuous recording streamflow data was obtained at all sites using either USGS gage data or, due to the lack of low flow gage data at one site, with a SonTek Acoustic Doppler Velocimeter (ADV) flow meter. At this site, the ADV flow meter was used to measure streamflow during deployment and retrieval of the sonde, as well as any grab sample site visits. At all AS sites, water (TSS and SSC) samples were also collected and SD measurements were made as described for the PM sites.

Site Selection Process

Twenty-nine potential sites were selected based on the availability of USGS gage stations to provide hydrology data, and to ensure broad geographic coverage within the county. Nearly all sites were also co-located with a rain gages operated through the HCFCD's Flood Warning System (HCFWS). Using GIS analysis and information provided by the USGS, an upstream contributing watershed was delineated for each gage site (see Sub-watershed Delineation). Data on the mean, median, maximum and minimum daily flows of record, period of record, and year of maximum and minimum flows was obtained for each gage. Data on the amount of different types of land use and land cover within each contributing watershed was obtained from the Houston-Galveston Area Council (H-GAC) (Meyer 2008). The 2008 land cover data uses a 10-category classification, which follows the hierarchical classification scheme utilized by the National Land Cover Data (NLCD). The types and amounts of major soil groups within each watershed were obtained from the Natural Resource Conservation Service (NRCS) database (<http://soils.usda.gov/>). These selected metrics based on soil classification type, land use/land cover, and hydrological data were used to classify the 29 potential sites based on their similarity. A reduced matrix containing fewer, key characters was used for subsequent statistical analyses and classification of sites based on common traits (Table 1).

Table 1. List of gage and associated watershed traits used to classify and group similar sites. USGS = United States Geological Service. HGAC=Houston-Glaveston Area Council. NRCS=National Resource Conservation Service.

Number	Metric	Units	Data Source
1	Year_Min Year of minimum discharge of record	Year	USGS Gage
2	Year_Max Year of maximum discharge of record	Year	USGS Gage
3	Period_Years Years of operation	Years	USGS Gage
4	MinDischarge_Archived	cfs	USGS Gage
5	MaxDischarge_Archived	cfs	USGS Gage
6	Developed_High_Intensity_LC	m ²	HGAC Land use
7	Developed_Low_Intensity_LC	m ²	HGAC Land use
8	Developed_Open_Space_LC	m ²	HGAC Land use
9	Cultivated_LC	m ²	HGAC Land use
10	Grassland_LC	m ²	HGAC Land use
11	Forest_LC	m ²	HGAC Land use
12	Woody_Wetland_LC	m ²	HGAC Land use
13	Herbaceous_wetland_LC	m ²	HGAC Land use
14	Barren_LC	m ²	HGAC Land use
15	Water_LC	m ²	HGAC Land use
16	LOAMY_FINE_SD	m ²	NRCS Soil Type
17	FINE_SANDY_SD	m ²	NRCS Soil Type
18	COMPLEX_SD	m ²	NRCS Soil Type
19	CLAY_SD	m ²	NRCS Soil Type
20	LOAM_SD	m ²	NRCS Soil Type
22	CLAY_LOAM_SD	m ²	NRCS Soil Type
23	WATER_SD	m ²	NRCS Soil Type
24	SILT_LOAM_SD	m ²	NRCS Soil Type
25	FINE_SAND_SD	m ²	NRCS Soil Type
26	ARENTS_SD	m ²	NRCS Soil Type
27	URBAN_LAND_SD	m ²	NRCS Soil Type

We employed the Clustan[®] statistical software package to conduct a cluster analysis of sites to determine the most reasonable number of groupings of sites based on their similarity (Wishart 2006). The cluster analysis algorithm utilized Wards method, squared Euclidean distance, and un-weighted, standardized variables. The “Best Cut” method was subsequently used to identify a reasonable number of groups based on similarity of groups. Based on the results of this analysis, five unique watersheds, or site types, were differentiated. The analysis was re-run using the Minitab[®] statistical package to generate presentation quality graphics (Figure 1). The algorithm in Minitab[®] also utilized Wards method, squared Euclidean distance, and un-weighted, standardized variables. The major characteristic of each site and watershed area group is listed in Table 2. Data used to conduct the cluster analysis is provided in electronic format in Appendix 1.

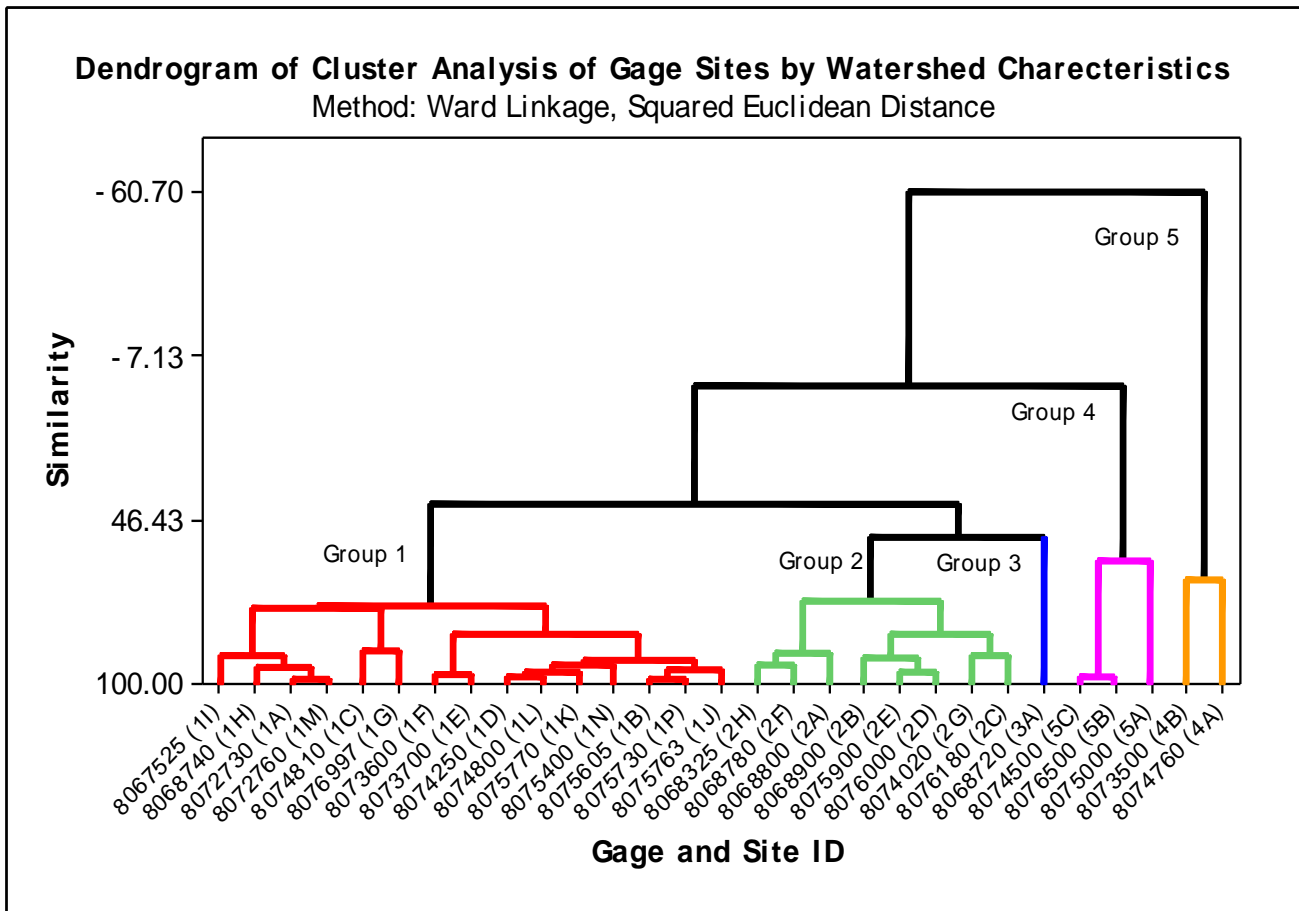


Figure 1. The statistical clustering of sites based upon land use and cover, and soil type.

Table 2. General description of the characters within each watershed type (↓ = low or depressed, ↑ = high or elevated, ↔ = moderate conditions).

Site Type	Hydrology (maximum discharge)	Land Use - Land Cover	Soil Type
1	↓	↓ High Density ↓ Forest	↓ Clay
2	↔	↑ Forest	↔ Sandy
3	↔	↓ High Density	↑ Sandy
4	↑	↑ High Density	↑ Clay
		↑ Forest	↔ Sandy
5	↑	↑ High Density	↓ Clay

The potential sites were surveyed to evaluate accessibility, possible datasonde deployment locations, and overall site quality for sampling. These 29 sites (Table 3) were then reduced down to the final 20 study sites (Table 4 and Figure 3). Reasons for eliminating some of the sites were: inaccessibility, flows too low for sample collection, and close proximity to another site of the same type with better accessibility. Ultimately, five automatic sampling (AS) sites and fifteen periodic monitoring (PM) sites were chosen as representative sites within each unique watershed type. Photographs illustrating the general

characteristics of each sample site are depicted in Figure 4 through Figure 23. Electronic copies of all site photographs are provided in Appendix 2 and the location of each site is provided as an interactive Google Earth map in Appendix 3.

Table 3. List of all 29 potential study sites organized by watershed/cluster type. These sites were visited during reconnaissance surveys to evaluate access issues prior to the study.

Cluster	Latitude	Longitude	Location Description	Watershed Name	USGS No.
1A	29.830783	-95.686891	Bear Ck nr Barker, TX	Addicks Reservoir	8072730
1B	29.656619	-95.229101	Berry Bayou @ Nevada St., South Houston, TX	Sims Bayou	8075605
1C	29.672732	-95.528277	Brays Bayou at Gessner Dr, Houston, TX	Brays Bayou	8074810
1D	29.828004	-95.469385	Brickhouse Gully at Costa Rica St, Houston, TX	White Oak Bayou	8074250
1E	29.746896	-95.523554	Buffalo Bayou at Piney Point, TX	Buffalo Bayou	8073700
1F	29.762173	-95.557721	Buffalo Bayou at W Belt Dr at Houston, TX	Buffalo Bayou	8073600
1G	29.596899	-95.297437	Clear Creek @ Mykawa St., nr Pearland, TX	Clear Creek	8076997
1H	29.959112	-95.717725	Cypress Ck at House-Hahl Rd nr Cypress, TX	Cypress Creek	8068740
1I	29.770782	-94.999650	Goose Ck at Baytown, TX	Spring Gully & Goose Creek	8067525
1J	29.808837	-95.313270	Hunting Bayou @ Hoffman St., Houston, TX	Hunting Bayou	8075763
1K	29.793282	-95.267991	Hunting Bayou at IH 610, Houston, TX	Hunting Bayou	8075770
1L	29.656621	-95.562166	Keegans Bayou at Roark Rd nr Houston, TX	Brays Bayou	8074800
1M	29.867170	-95.646612	Langham Ck at W Little York Rd nr Addicks, TX	Addicks Reservoir	8072760
1N	29.618844	-95.446052	Sims Bayou at Hiram Clarke St, Houston, TX	Sims Bayou	8075400
1P	29.694674	-95.216323	Vince Bayou at Pasadena, TX	Vince Bayou	8075730
2A	29.973556	-95.598555	Cypress Ck at Grant Rd nr Cypress, TX	Cypress Creek	8068800
2B	30.006610	-95.511885	Cypress Ck at Stuebner-Airline Rd nr Westfield, TX	Cypress Creek	8068900
2C	29.933861	-95.233961	Garners Bayou nr Humble, TX	Greens Bayou	8076180
2D	29.918278	-95.306880	Greens Bayou nr Houston, TX	Greens Bayou	8076000
2E	29.956889	-95.417994	Greens Bayou nr US Hwy 75 nr Houston, TX	Greens Bayou	8075900
2F	30.016054	-95.697446	Little Cypress Ck nr Cypress, TX	Little Cypress Creek	8068780
2G	29.870781	-95.480496	Whiteoak Bayou at Alabonson Rd at Houston, TX	White Oak Bayou	8074020
2H	30.105495	-95.546608	Willow Ck nr Tomball, TX	Willow Creek	8068325
3A	29.950224	-95.808284	Cypress Ck at Katy-Hockley Rd nr Hockley, TX	Cypress Creek	8068720
4A	29.709120	-95.583000	Brays Bayou at Alief, TX	Brays Bayou	8074760
4B	29.761896	-95.605778	Buffalo Bayou nr Addicks, TX	Buffalo Bayou	8073500
5A	29.697175	-95.412162	Brays Bayou at Houston, TX	Brays Bayou	8075000
5B	29.861891	-95.334936	Halls Bayou at Houston, TX	Greens Bayou	8076500
5C	29.775228	-95.397161	Whiteoak Bayou at Houston, TX	White Oak Bayou	8074500

Table 4. Final list of sites monitored throughout study, differentiated by sample type (auto-sampling (AS) or periodic monitoring (PM)), and site type. HCFWS = Harris County Flood Warning System.

Sample Type	Site Type	Site Letter	Site Description	Latitude	Longitude	Waterbody Name	HCFCD Unit	USGS ID	HCFWS Gage ID
AS	1	G	Clear Creek @ Mykawa St., nr Pearland, TX	29.59651	-95.29732	Clear Creek	A100-00-00	8076997	180
	2	B	Cypress Ck at Stuebner-Airline Rd nr Westfield, TX	30.00666	-95.51192	Cypress Creek	K100-00-00	8068900	1140
	3	A	Cypress Ck at Katy-Hockley Rd nr Hockley, TX	29.95013	-95.80827	Cypress Creek	K100-00-00	8068720	1180
	4	A	Brays Bayou at Alief, TX	29.70912	-95.58300	Brays Bayou	D100-00-00	8074760	470
	5	B	Halls Bayou at Houston, TX	29.86191	-95.33480	Greens Bayou	P118-00-00	8076500	1680
PM	1	C	Brays Bayou at Gessner Dr, Houston, TX	29.67256	-95.52803	Brays Bayou	D100-00-00	8074810	460
		E	Buffalo Bayou at Piney Point, TX	29.74690	-95.52355	Buffalo Bayou	W100-00-00	8073700	2260
		F	Buffalo Bayou at W Belt Dr at Houston, TX	29.76238	-95.55758	Buffalo Bayou	W100-00-00	8073600	2270
		H	Cypress Ck at House-Hahl Rd nr Cypress, TX	29.95928	-95.71778	Cypress Creek	K100-00-00	8068740	1175
		J	Hunting Bayou @ Hoffman St., Houston, TX	29.80869	-95.31293	Hunting Bayou	H100-00-00	8075763	840
		K	Hunting Bayou at IH 610, Houston, TX	29.79345	-95.26791	Hunting Bayou	H100-00-00	8075770	830
		M	Langham Ck at W Little York Rd nr Addicks, TX	29.86776	-95.64773	Addicks Reservoir	U100-00-00	8072760	2120
	P	Vince Bayou at W Harris Ave in Pasadena, TX	29.69801	-95.21680	Vince Bayou	I100-00-00	8075730	920	
	2	A	Cypress Ck at Grant Rd nr Cypress, TX	29.97368	-95.59876	Cypress Creek	K100-00-00	8068800	1160
		D	Greens Bayou nr Houston, TX	29.91843	-95.30618	Greens Bayou	P100-00-00	8076000	1640
		E	Greens Bayou nr US Hwy 75 nr Houston, TX	29.95614	-95.41573	Greens Bayou	P100-00-00	8075900	1660
		G	Whiteoak Bayou at Alabonson Rd at Houston, TX	29.87066	-95.48052	White Oak Bayou	E100-00-00	8074020	545
	4	B	Buffalo Bayou nr Addicks, TX	29.76185	-95.60610	Buffalo Bayou	W100-00-00	8073500	2290
	5	A	Brays Bayou at Houston, TX	29.69734	-95.41194	Brays Bayou	D100-00-00	8075000	420
		C	Whiteoak Bayou at Houston, TX	29.77520	-95.39717	White Oak Bayou	E100-00-00	8074500	520

Field Survey Sites

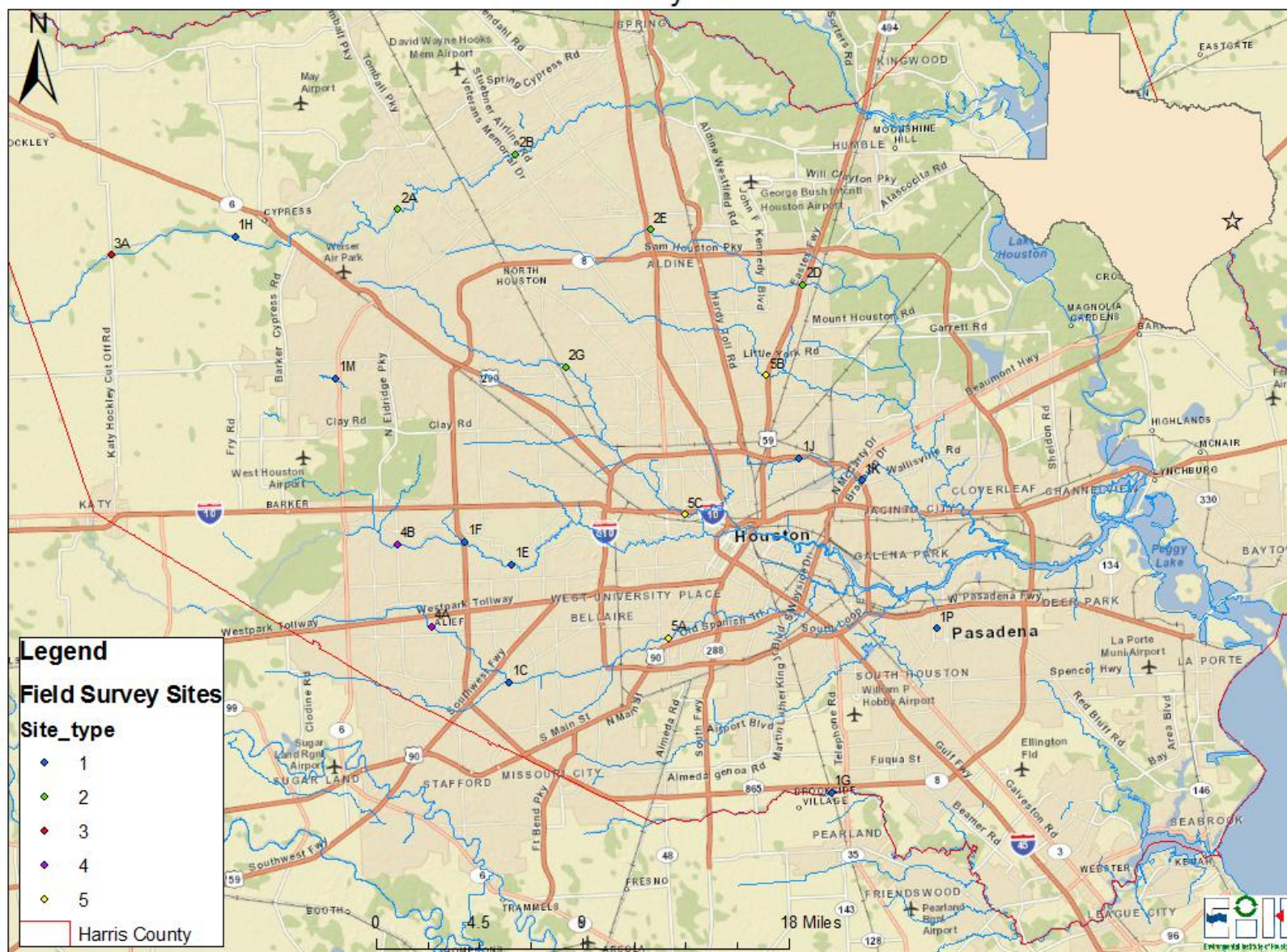


Figure 3. Map showing location of sampling sites on final list, including AS and PM sites, as listed in Table 4.

The final set of monitoring sites exhibited a wide range of channel forms, bottom substrate, and riparian vegetation types (Figure 3 and Table 4). Individual site descriptions and pictures are listed below. Since these photographs were taken at particular sample locations, they did not necessarily depict the overall watershed characteristics. Also, channel substrate was not included in the cluster analysis and tended to vary within each site type.

Site 1C, Brays Bayou at Gessner, was a concrete-lined, trapezoidal channel located next to USGS gage 8074810 and HCFWS rain gage 180 (Figure 4). Accumulated sediment particles were found along various portions of the streambank. Maximum water depth was less than 3 ft. deep. The stream was approximately 25 ft. wide. The surrounding area was suburban residential, with two golf courses located nearby and along the banks.



Figure 4. Photographs of PM site 1C, USGS gage 8074810, Brays Bayou at Gessner Dr, Houston, Texas.

In contrast, Site 1E, Buffalo Bayou at Piney Point (USGS gage 8073700; HCFWS gage 2260) exhibited a more natural channel form with soft bottom sediments including fine sands. It had an approximate maximum depth of 3.6ft and minimum width of 28ft (Figure 5). Although the riparian zone was forested, there was still a high concentration of adjacent residential land.



Figure 5. Photographs of PM site 1E, USGS gage 8073700, Buffalo Bayou at Piney Point, Texas.

The area surrounding site 1F, Buffalo Bayou at West Belt Drive (USGS gage 8073600 and HCFWS gage 2270), was very similar to that at 1E. However, the immediate area possessed a combination of concrete-lined banks and new, large cobble/rip-rap (Figure 6). The width and depth of this site was 40ft. and 3.9ft. respectively.



Figure 6. Photographs of PM site 1F, USGS gage 8073600, Buffalo Bayou at W. Belt Dr. at Houston, Texas.

Site 1G was an AS site located on Clear Creek next to USGS gage 8076997. Located very near to the South Sam Houston Tollway, it had a cleared and mowed riparian zone with light industrial and undeveloped, though maintained, lands surrounding. Moderately sloped banks line this relatively narrow and shallow channelized creek, with approximate maximum depth and minimum width of 3.7ft and 7.5ft (Figure 7). The substrate was sandy clay and quite firm throughout most of the site with some softer, boggy spots, especially around bends where the water slowed or eddied.



Figure 7. Photographs of AS site 1G, USGS gage 8076997, Clear Creek at Mykawa St., near Pearland, Texas.

Exhibiting similar widths and depths as 1G, site 1H was located in a much more rural section of Harris County on Cypress Creek (Figure 8). It had tree-lined, moderately steep banks, with a powerline corridor crossing upstream and a large golf course adjacent downstream. Although it is so rural and relatively near to the headwaters, this site showed definite evidence of channelization.



Figure 8. Photographs of PM site 1H, USGS gage 8068740, Cypress Creek at House-Hahl Rd, near Cypress, Texas.

Sites 1J and 1K (Figure 9 and Figure 10) were both located on Hunting Bayou, approximately 4 river miles apart and adjacent to Loop 610. They were co-located with USGS gages 8068470 and 8075763 and HCFWS gages 840 and 830, respectively. Both sites were channelized and highly urbanized outside of the immediate vicinity. The maximum stream width at these sites was relatively small (< 25ft), and the maximum water depths were less than 2 feet. These sampling locations and the rest of the Type 1 sites all had grassy, mowed/maintained riparian zones.



Figure 9. Photographs of PM site 1J, USGS gage 8075763, Hunting Bayou at Hoffman St., Houston, Texas.



Figure 10. Photographs of PM site 1K, USGS gage 807577630, Hunting Bayou at IH 610, Houston, Texas.

Site 1M was located on Langham Creek in a suburban residential area, next to USGS gage 8072760 and HCFWS gage 2120. Again, the stream was quite narrow and shallow. This site had markedly clearer water than every other site and a sandy bottom (Figure 11).



Figure 11. Photographs of PM site 1M, USGS gage 8072760, Langham Creek at W. Little York Rd near Addicks, Texas.

Site 1P was unique, in that it was the only one that was tidally influenced. As expected, the water levels varied considerably, from less than 3ft to nearly 5ft deep and widths between 40 and 50ft. The USGS gage station (8075730) is located upstream of the site and is nontidal. The clay substrate was littered with riprap at the bridge. Beyond the treeline visible in Figure 12, the land was mostly residential with an adjacent commercial center.

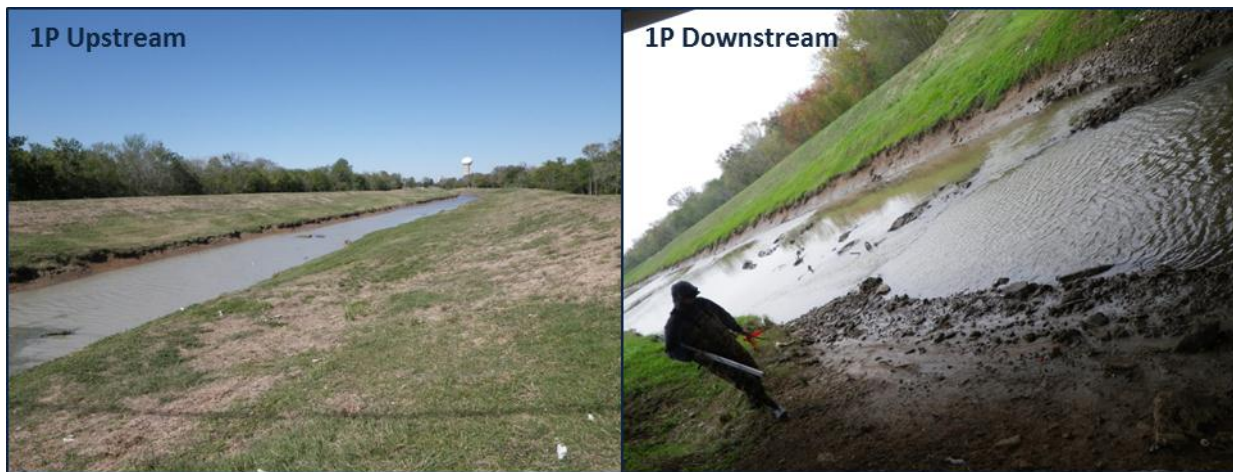


Figure 12. Photographs of PM site 1P, USGS gage 8075730, Vince Bayou at W. Harris Avenue in Pasadena, Texas.

Sites 2A, 2B, and 2D were located at Cypress Creek at Grant Rd., near Cypress, Cypress Creek at Stuebner-Airline near Westfield, and Greens Bayou in Houston, respectively. Site 2B was an AS site. All of these waterbodies were moderately-sized streams ranging from 15 to 30 ft wide (Figure 13 to Figure 15). Bottom sediments were clay and silt. The stream banks are vegetated with grass, appeared mowed with and the adjacent land being covered with small shrubs and trees. Land use was largely rural to suburban.



Figure 13. Photographs of PM site 2A, USGS gage 8068800, Cypress Creek at Grant Rd., near Cypress, Texas.



Figure 14. Photographs of AS site 2B, USGS gage 8068900, Cypress Creek at Stuebner-Airline Rd., near Westfield, Texas.



Figure 15. Photographs of PM site 2D, USGS gage 8076000, Greens Bayou near Houston, Texas.

Sites 2E and 2G were approximately 2 ft. deep and ranged in size between 9 to 35 ft wide respectively (Figure 16 and Figure 17). Both were located in suburban areas. The stream banks were covered with mowed grass. Both streams lacked natural meanders and appeared to be channelized for flood water conveyance.



Figure 16. Photographs of PM site 2E, USGS gage 8075900, Greens Bayou near US Hwy 75, near Houston, Texas.



Figure 17. Photograph of PM site 2G, USGS gage 8074020, Whiteoak Bayou at Alabonson Rd. at Houston, Texas.

Site 3A, was an AS site which was colocated next to the USGS gage 8068720 at Cypress Creek at Katy-Hockley Rd., near Hockley, Texas (Figure 18). This site had heavily vegetated banks and the immediate surrounding land use could be characterized as rural with forested land composed of thick underbrush and trees. This small stream had a maximum depth of 0.5 to 1 ft. and width of 6-7 ft.

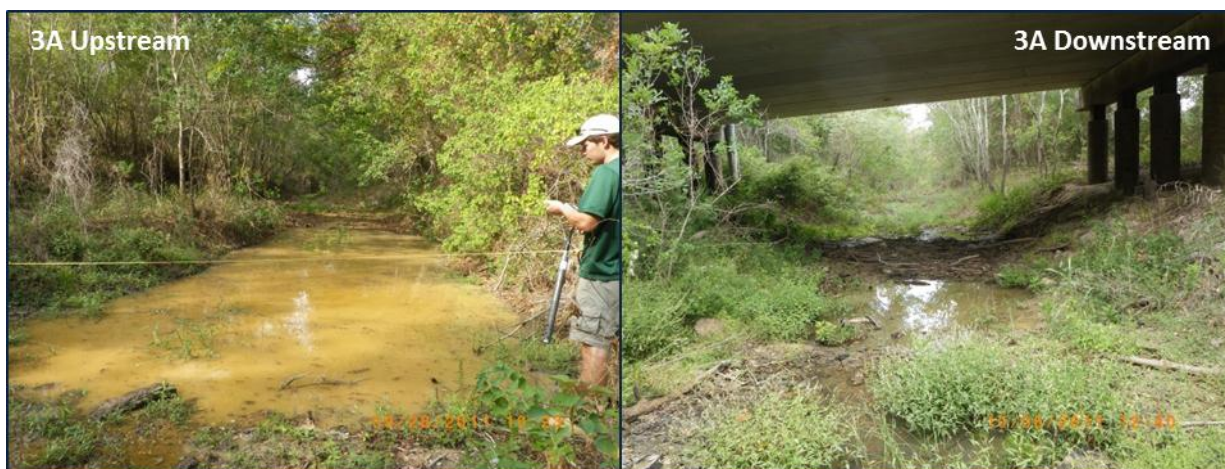


Figure 18. Photographs of AS site 3A, USGS gage 8068720, Cypress Creek at Katy-Hockley Rd., near Hockley, Texas.

Sites 4A and 4B were located at Brays Bayou near Beltway 8 at USGS gage 8074760, and Buffalo near Addicks at USGS gage 8073500 respectively (Figure 19 and Figure 20). Site 4A was designated as an AS site. Both sites were located near residential areas. The stream channel lacked significant meanders. Site 4A had mowed grassy banks with adjacent housing. Site 4B was located near Addicks Reservoir and had heavily vegetated banks with woody debris. The stream width and depth was 1 ft. and 22 ft. respectively at site 4A, and 2 ft. and 45 ft. respectively at site 4B.



Figure 19. Photographs of AS site 4A, USGS gage 8074760, Brays Bayou at Alief, Texas.



Figure 20. Photographs of PM site 4B, USGS gage 8073500, Buffalo Bayou near Addicks, Texas.

The last group of sites consisted of several urban bayous including sites 5A, 5B and 5C (Figure 21 and Figure 23). Site 5A was located at USGS gage 8075000 on Brays Bayou near the intersection of South Main and S. Braeswood. This portion of Brays Bayou was a trapezoidal concrete lined bayou surrounded by extensive urban and suburban development. The channel dimensions during the initial site visit was 2.5 ft. deep by 38 ft. wide. Site 5B was an AS site located adjacent to USGS gage 8076500 at Halls Bayou. The substrate type was concrete lined under the bridge, but earthen up and down stream. There was a public park located on the left bank upstream of the bridge. Site 5C was located at USGS gage 8074500 at Whiteoak Bayou surrounded by residential and urban development. This site was concrete lined and had relatively high velocities at base-flow conditions.



Figure 21. Photographs of PM site 5A, USGS gage 8075000, Brays Bayou at Houston, Texas.



Figure 22. Photographs of AS site 5B, USGS gage 8076500, Halls Bayou at Houston, Texas.



Figure 23. Photographs of PM site 5C, USGS gage 8074500, Whiteoak Bayou at Houston, Texas.

Field Site Surveys

Sampling occurred periodically during several 30-day periods, with a minimum of 2 wet weather, or “rain-influenced”, events for each site. This ensured coverage over a variety of conditions and seasons, including spring (April and May), summer (June to August), fall (September and October) and winter (November and December) 2011. At AS sites, a YSI 6920V2 automated datasonde, equipped with a model number 6136 nephelometer probe, was used to monitor water quality and turbidity during the deployment period. Two attachment methods were used for sonde placement: a horizontal lock box anchored into the substrate at the middle of the stream or a PVC tube strapped to the downstream side of a bridge piling (Figure 24). The method used was dependent upon the site conditions; sites 1G and 2B used PVC, while sites 3A, 4A, and 5B used lock boxes. Sondes and lock boxes were provided by the HCFCD.



Figure 24. PVC and lock box data sonde deployment methods, sites 1G (left) and 3A (right).

At AS sites, a minimum of three grab samples were collected per monitoring period. Grab samples and instantaneous measurements of water quality were taken at the beginning, midpoint, and end of the period, during which the continuous logging datasonde was deployed. At the midpoint sampling events, the automated datasondes were also checked for proper operation and to clear debris or sediment from the area surrounding the sonde and deployment container.

At PM sites, instantaneous measurements and grab samples were collected at the beginning and end of the deployment period defined for AS sites. At both AS and PM sites, immediately following a rain event, a field team was deployed to take additional grab samples and field parameters at sites that were most influenced by the rainfall and subsequent increased streamflow. The sampling protocol was the same used as during dry weather periods.

Various water quality parameters and observations were collected at every site to evaluate the turbidity and suspended sediment content (Figure 25). Parameters collected at every site were NTU, SD, TSS, and SSC. To determine sampling locations, stream width was divided into 3 equal increments (left, middle, right), and samples were collected at the midpoint of each section. SD, NTU, and TSS were collected as near-surface grab samples (top 0.3m of water, excluding any surface film). Depth and flow-integrated SSC samples were collected using a sampler specific to sampling conditions (described below). Samples for TSS and SSC were preserved in a cooler on wet ice throughout the day and

processed within 7 days of collection. NTU readings were performed in the field within 15min of collection with a LaMotte 2020we portable turbidity meter (Figure 25). Secchi disk transparency was also read in the field with a standard, alternating black and white disk at the bottom of a 1m tube. Field splits were taken once daily for each TSS, SSC, and NTU sample for quality control. Field split data was reviewed for reasonability and then averaged with the corresponding original sample before use in data analysis.



Figure 25. (a) Portable turbidity meter for field NTU readings; (b) field personnel taking depth and grab samples; (c) field personnel taking SSC samples; (d) field personnel taking flow measurements and sonde readings

Additional water quality variables were measured at the midpoint of the stream with a YSI 600XLM multi-parameter sonde. These parameters include temperature, pH, dissolved oxygen, and specific conductance. Days since last significant rainfall, present weather, discharge, gage height, water color, water odor, and thalweg depth were supplemental measurements and observations recorded at each site during sampling. Present weather was coded as follows: 1 = clear, 2 = partly cloudy, 3 = cloudy, 4 = rain. Any activities or conditions that may have affected turbidity, such as construction or recent mowing along banks, was also noted and, often, photographed (Appendix 2).

SSC samples were collected using samplers that integrate the depth and flow. USGS standard equipment and techniques were used (Edwards and Glysson 1999). Suspended solid concentration was taken first at the deepest sampling point (left, middle, or right) first. The sampler was moved through the entire

water column at a constant rate, with the nozzle facing upstream, into the current. The goal was to make one pass, i.e. down and back up, to obtain a full, one-liter bottle at the deepest section. Deployment time was used as a rough assurance metric based upon the depth and deployment time of the initial sample. For example, if the depth is approximately one-third of the initial, then the time should also be about one-third. Each section's SSC was composited in either the lab or the field resulting in one SSC sample per site. In some instances, the water depth was too shallow or flow was absent (i.e. only isolated pools at site) to allow for proper use of sampler. Grab samples were taken at these sites and are noted in the report. A model DH-81 with a 1/4" nozzle was the most frequently used (Figure 26). However, high flow conditions required a bridge-deployable model, DH-76 using 1/4" and 3/16" nozzles. In the instances when two field crews were in the field at the same time, another model, DH-48 with a 1/4" nozzle, was used. All of the sampler models are pictured in Figure 26.

All methods used during water quality sampling and sonde deployment followed protocol outlined in the TCEQ Surface Water Quality Monitoring manual (Texas Commission of Environmental Quality 2008). All instruments were calibrated prior to deployment and checked for instrument drift after use each day or upon retrieval. All forms and data sheets used to compile data are provided in Appendix 4. Calibration data in electronic format is provided in Appendix 5.

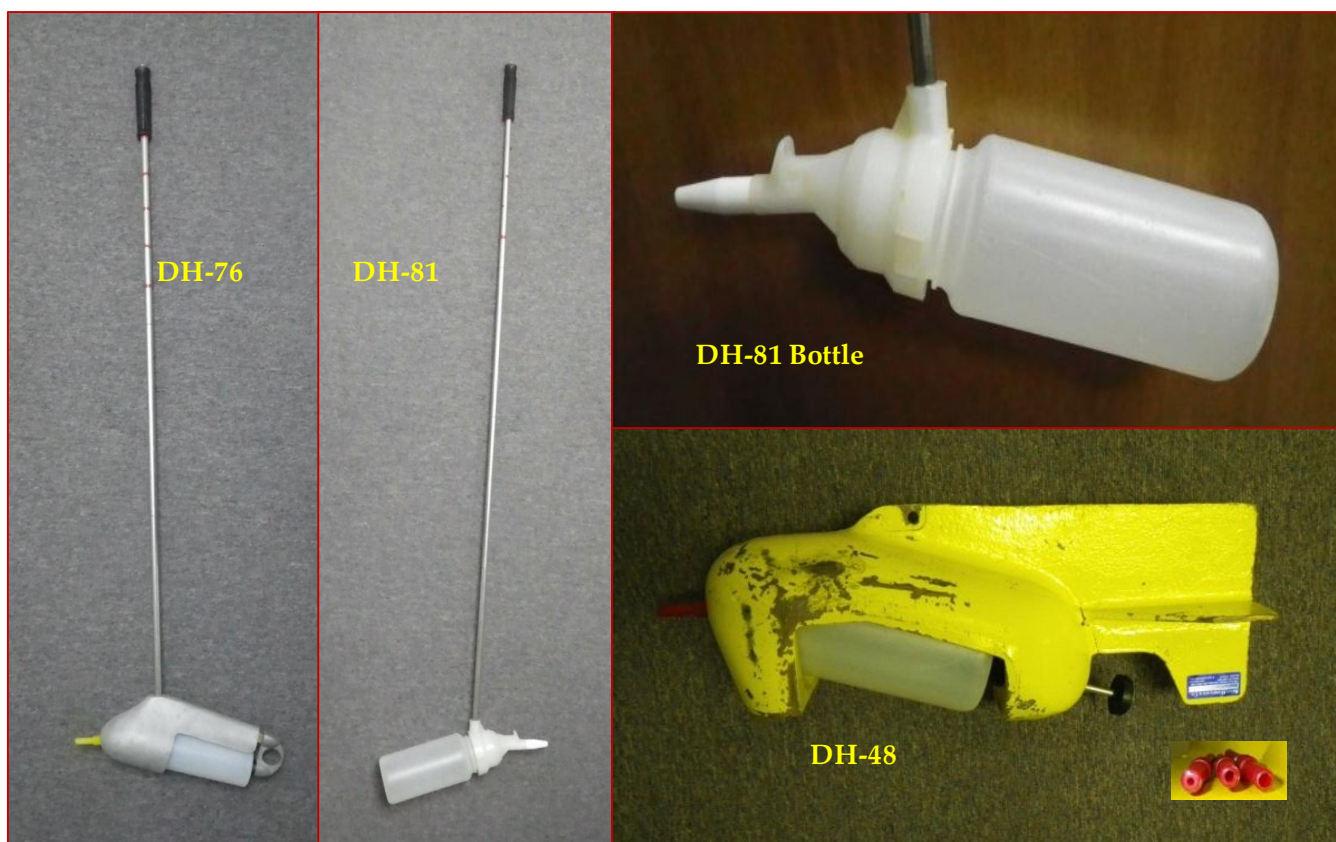


Figure 26. Suspended sediment samplers used throughout study

Laboratory Sample Processing and Sample Calculations

Samples for TSS and SSC were processed at the UHCL laboratory following APHA and ASTM filtration methods with the following modification (American Society for Testing and Materials 2007; Clesceri et al. 1998). For SSC estimation we did not use a Gooch crucible. Instead we followed the exact

same APHA procedures for TSS filtration delineated in the Clesceri et al. (1998), with the exception of measuring and recording total sample volume in addition to filtered volume. Standard Methods compliant Hach pre-weighed, glass-fiber filters were used for a majority of the samples. If pre-weighed filters were not available, filters were prepared in-house according to APHA and ASTM methods. All samples were filtered within the 7 day holding time and refrigerated when storage was required. A varying volume of the homogenized TSS and SSC samples was filtered for each site and recorded. Filters were then dried to a constant weight. The initial weight (W_i) was subtracted from the final weight (W_f) to get the total weight of the sediment (W_s) on the filter using the following equation:

$$W_f - W_i = W_s$$

Sediment weight (W_s) was multiplied by 1000mL and then divided by the volume filtered (V_f) to obtain the value for TSS or SSC in mg/L. Composite values for both TSS and SSC were calculated by taking the sum of the site's sediment weights and dividing by the sum of the volumes filtered. Equations are described below.

$$\text{Equation for individual sample calculation: } \text{TSS}_i \text{ or } \text{SSC}_i \text{ mg/L} = \frac{(1000\text{mL})(W_f - W_i) \text{ mg}}{(V_f) \text{ mL}}$$

$$\text{Equation for composite calculation: } \text{TSS}_c \text{ or } \text{SSC}_c \text{ mg/L} = \frac{(1000\text{mL}) \sum (W_s) \text{ mg}}{\sum (V_f) \text{ mL}}$$

Sub-watershed Delineation

The analysis of surface water hydrology was conducted using the Spatial Analyst facilities in ArcGIS 10 to define the upstream flow and to delineate the watersheds for a number of predefined locations (technically called pour points). These points represent the locations of the active USGS stations in this study. The analysis was based on the principle that a uniform rainfall pattern throughout the investigated region will cause water to flow from one location to another using the nearest steepest path. This flow combines with other paths and accumulates to form the total of upstream flows. Where flows in adjacent cells move away from each other, it suggests that a local watershed exists. Streams combine into larger regions described as stream basins, with boundaries known as watersheds (de Smith et al. 2009). This analysis was based on many assumptions including: (i) uniform precipitation; (ii) flows take place entirely across surfaces; (iii) flows grow as a linear function with distance and are not altered by the slope values, just by the direction; and (iv) there are no barriers to flow (de Smith et al. 2009). The main inputs into this analysis are a Digital Elevation Model (DEM) that is a grid file (i.e. 30 m spatial grid) of surface elevations and the pour points (i.e. the locations of the active USGS stations); while the output is a grid file defining the watersheds associated with the pour points. The main analysis steps include:

- Removing artificial depressions (also known as sinks) from the initial 30m DEM to ensure that flows are continuous across the surface; the “Fill” tool was used.
- Creating the flow direction image using the “Flow Direction” tool
- Creating the accumulated flow image using the “Flow Accumulation” tool
- The USGS stations were relocated appropriately on the defined accumulated flow image to be used as pour points.
- The watersheds of the USGS stations were delineated using the “Watershed” tool.
- The delineated watersheds were validated against the National Watershed Boundary Dataset.

More details on the technical methodology used to construct the watershed model can be found in Appendix 6.

Rainfall Accumulation and Run-off Modeling

Runoff was calculated with the consideration of the upstream area that may influence each monitoring station. This was achieved by identifying the rain gages that are surrounding and within the sub-watersheds. A total number of 99 rain gages were selected after excluding a number of gages that were associated with suspicious readings (e.g., reported daily rainfall amount of over 25in, when all adjacent gages reported zero precipitation, etc.). Afterwards, the area of influence from each rain gage was estimated and constructed in ArcGIS using the Thiessen polygon algorithm, which can proportionally divide and distribute the gage coverage into gage regions. These regions are generally known as Thiessen or Voronoi polygons. The rain gage regions were intersected with the watershed layer to exclude the parts located outside the watersheds. In this manner, the weight for each rain gage station was calculated as a percentage of the total of all individual gage region areas located within the upstream watershed area for each monitoring and associated streamflow station.

The direct runoff from each rainfall event was calculated using the NRCS Runoff Curve Number method. The method was developed by the U.S. Department of Agriculture and Natural Resources Conservation Service (NRCS), which is formally known as the Soil Conservation Service (SCS). The primary inputs include the runoff curve number, rainfall, and the drainage area size. The method is based on the notion that for a single storm, the ratio of actual soil retention after runoff begins to the potential retention, is equal to the ratio of direct runoff to the storm rainfall (USDA-SCS 1985). This principle, after algebraic manipulation and application of simplifying assumptions, results in equation (1) that is found in the National Engineering Handbook (USDA-SCS 1985) where Q is runoff (inch) and P is rainfall (inch):

$$(1) \quad Q = \frac{(P-0.2S)^2}{P+0.8S}$$

S is the potential maximum soil moisture retention after runoff begins (inch). This parameter was calculated from equation (2) using the runoff Curve Number (CN):

$$(2) \quad S = \frac{1000}{CN} - 10$$

Initial abstraction, I_a , is water retained before runoff, due to processes, such as infiltration or interception by vegetation, and is directly related to S as in the equation (3).

$$(3) \quad I_a = 0.2S$$

The CN values usually range from 30 to 100 with lower numbers indicating lower runoff while larger numbers are related to increasing runoff potential. The CN is an empirical parameter that is primarily related to soil characteristics and land use (surface cover). In general, the infiltration rate of the soil surface is affected by surface conditions and soil profiles. As soil profiles may be considerably altered due to urbanization, the hydrological soil groups (HSG) are established according to the texture of the surface soil as described below (Table 5). In general, the “Group A” soils are associated with the lowest runoff potential and high infiltration rates even when thoroughly wetted, while the “Group D” soils are associated with the highest runoff potential, as it has very low infiltration rates when thoroughly wetted. In this analysis, the hydrological soil groups are extracted from the NRCS soil data. We found that only two soil groups (C and D) were located within the investigated watersheds (Appendix 7, Figures A7.1-A7.20).

Table 5. Candidate NRCS hydrological soil groups used for classification during this study.

HSG	Soil Texture
A	Sand, loamy sand, or sandy loam
B	Silt loam or loam
C	Sandy clay loam
D	Clay loam, silty clay loam, sandy clay, silty clay, or clay

We also recognized that the range of land use/cover for determining the CN values could be narrowed down to two main categories: impervious surfaces and pervious surfaces. For this purpose, the national impervious data set was used to calculate the percentage of imperviousness for each subwatershed (2006 national land cover database, http://www.mrlc.gov/nlcd06_data.php). The CN for the impervious category were given a value of 98, regardless of the underlying HSG. The pervious category for C and D hydrological groups were given average-weighted numbers based on the land use/cover types and their percentage classes within the subwatersheds. As a result, three groups of CN values were created: 1) CN value (98) for impervious surfaces; 2) CN values for pervious surfaces with hydrological soil group C (they range between 73 and 83); and 3) CN values for pervious surfaces with hydrological soil condition D (they range between 79 and 86). The three groups of CN values were then combined based on the percentages of impervious and pervious surfaces of each upstream area.

The runoff at each monitoring station was calculated for all hourly and daily rainfalls using equations 1 and 2 above once the rainfall exceeded the initial abstraction, as expressed in equation 3 above. The area of each subwatershed and the weights of each rain gage were used to calculate the total estimated runoff in cubic feet at each monitoring station. We evaluated the effect of the estimated runoff on observed NTU and SD levels, and TSS concentrations and loading, by comparing the 1-day (estimated runoff from the day of sampling) and 3-day cumulative volumes of estimated runoff to the observed stream flow, NTU, SSC, SD and TSS values.

Analysis of Survey Field Data

All data collected during the study were statistically analyzed using the Minitab statistical software package. Non-linear models were fitted using CurveExpert[®] Professional v1.5.0 (<http://www.curveexpert.net/>). The analyses consisted of multiple components including:

- 1) Evaluating statistical moments (means, percentiles) of NTU measurements historically collected.
- 2) Evaluating the relationship of historical NTU measurements to other measures of turbidity, including TSS and SD through the use of linear regression analysis.
- 3) Evaluating statistical moments (means, percentiles) of NTU measurements collected during this study, including measures obtained through automated samplers and grab samples.
- 4) Evaluating relationship of NTU measurements to other measures of turbidity made during this study, including TSS and SD through the use of linear and non-linear regression analysis.
- 5) Evaluating the relationships of turbidity measurements and land use/cover through visual evaluation of boxplots and mean confidence intervals.
- 6) Estimation and comparison of stream sediment loads derived from SSC measurements at respective study sites and site groupings to evaluate the relationship of land use and flow on sediment load.
- 7) Applying predictive regression models developed by this study to historical data sets in Harris County to generate statistical moments (means, percentiles) of predicted NTU measurements.

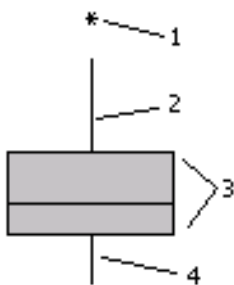
During the analysis of data generated during our field study, several data quality issues arose that needed to be addressed. During examination of the data, we attempted to correct, if possible, and exclude, if necessary, any values that were erroneously recorded. This included laboratory results that were either impossible or highly unlikely. For example, values of TSS that were negative due to errors in initial weighing of filters were excluded from further analysis. In some cases, obvious errors associated with misplacement of a decimal point were corrected by comparing to the other replicate samples' results.

The field deployed automated sampler datasondes recorded some potential erroneous values that were difficult to “correct” due to the lack of any obvious source of error. Records of zero or negative NTU values generated by the field datasondes were observed, but infrequently. For the purpose of describing the data distribution, these values were included, since they usually represented less than 5% of the total record for a parameter at that station in most cases. One major source of this error can be attributed to fouling or inclusion of air in the measuring chamber. The manufacturer, YSI, stated that:

“it is important to remember that field optical measurements are particularly susceptible to fouling, not only from long term build up of biological and chemical debris, but also to shorter term formation of bubbles from outgassing of the environmental water”(YSI 2012).

They further state that these bubbles can generally be removed in short-term sampling applications by simply agitating the sonde manually. However, for studies longer than a few hours where the user is not present at the site, the quality of the turbidity data obtained with a turbidity sensor that has no capability of mechanical cleaning is likely to be poor. Our instrument probes were equipped with a mechanical wiper that reduces the likelihood of this source of error. Since our instruments were successfully calibrated and passed post deployment validation tests, it is likely that possible turbulence in the flowing river may have exposed the probe to excessive bubbles, causing some of the negative readings. Also, excessive build-up of sediment on units deployed within boxes on the substrate was seen infrequently but may have been responsible for some of the high turbidity readings observed in the datasonde. Since it is impossible to rule out whether an extremely high reading was a true error in the measurement due to fouling or just excessive turbidity, we chose to retain the data for the purposes of descriptive statistical characterization. However, for regression analyses, we censored our dataset by removing zeros and negative values since the data was log-transformed prior to analysis and this method is incompatible with these values. Similarly, for grab samples and/or instantaneous water quality readings, we infrequently censored (removed) some of the very high values if they were at least an order of magnitude higher when compared to replicate measurements or there were apparent transcription errors.

As previously stated, to facilitate comparison of sites and sample periods, we used boxplots to display the distribution of data at each class grouping. Boxplots are useful for comparing the central tendency and distribution of data. The default boxplot display produced by Minitab[®] software and used in this report consisted of the following components:



- 1 **Outlier (*)** – Observation that is beyond the upper or lower whisker
- 2 **Upper whisker** – Extends to the maximum data point within 1.5 box heights from the top of the box
- 3 **Interquartile range box** – Middle 50% of the data
 - Top line – Q3 (third quartile). 75% of the data are less than or equal to this value.
 - Middle line – Q2 (median). 50% of the data are less than or equal to this value.
 - Bottom line – Q1 (first quartile). 25% of the data are less than or equal to this value.
- 4 **Lower whisker** – Extends to the minimum data point within 1.5 box heights from the bottom of the box

Results

Literature Review

Past studies on the prediction of turbidity measured by nephelometric methods have been performed both regionally and at other locations (Anderson and Davic 2004; Dahlgren et al. 2004). Dahlgren et al. (2004) found strong, statistically significant relationships between TSS, SD and NTU while studying various stream systems in California. The following predictive models were produced for several river systems: [*Assume $\text{Log}(\text{NTU}) = a + b(\text{Log SD cm})$*]

Bay-Delta waterways

$$Y = -0.95x + 2.53 \quad R^2 = 0.71, P < 0.001$$

Stockton Ship Channel

$$Y = -1.1x + 3.03 \quad R^2 = 0.85, p < 0.001$$

Central Valley Rivers

$$Y = 1.16x + 2.91 \quad R^2 = 0.79; p < 0.001$$

Similarly, they found statistically significant though less strong relationships between log-transformed TSS (mg/L), the dependent variable, and log-transformed SD (cm), the independent variable. They are listed below: [*Assume $\text{Log}(\text{TSS}) = a + b(\text{Log SD cm})$*]

Stockton Ship Channel

$$Y = -1.17x + 3.13 \quad R^2 = 0.51; p < 0.001$$

Central Valley Rivers

$$Y = -0.93x + 2.89 \quad R^2 = 0.60; p < 0.001$$

Anderson and Davic (2004) conducted similar studies on 12 streams in northeast Ohio. They simultaneously collected and compared various measures of turbidity, including NTU, TSS, and various transparency tubes readings. Statistically significant relationships developed from their data include:

Given: $\text{Log}(\text{TSS}) = a + b(\text{Log}(\text{Tube reading (cm)}^{-2}))$

$$Y = 3.58 + 0.704x \quad r^2 = 0.844$$

$$Y = 3.85 + 0.807x \quad r^2 = 0.858$$

$$Y = 3.88 + 0.794x \quad r^2 = 0.846$$

Given: $\text{Log}(\text{NTU}) = a + b(\text{Log}(\text{Tube reading (cm)}^{-2}))$

$$Y = 3.45 + 0.668x \quad r^2 = 0.934$$

$$Y = 3.66 + 0.748x \quad r^2 = 0.936$$

$$Y = 3.76 + 0.769x \quad r^2 = 0.928$$

Where $\{\text{Tube reading (cm)}^{-2}\}$ is the inverse square transformation X^{-2} .

The X^{-2} transformation is unfamiliar to the author and is not often used in water quality studies. Based on the more common inverse transformation, X^{-1} , we assume the square of the number is taken and then the inverse. In the case of this study, (Anderson and Davic 2004), they further manipulated the data by log transforming this number. The statistical properties are difficult to determine given the dual transformation process.

More recently, Parent (2009) examined multiple data sets in Texas from several river basins, including Brazos, Lavaca-Navidad, Nueces, Sabine and Trinity Rivers. These data were provided to Parent (2009) by the respective river authorities. Parent (2009) examined a total of 6,915 samples. This consisted of matching SD (meters) and NTU measurements. They conducted their analyses two ways on the combined data set; 1) taking the indefinite (less than/greater than) values and assigning the value of the detection limit for values below this threshold and 2) discarding the indefinite values discarding values below the detection limit. They also conducted their analyses on the individual river basin data sets using only the definite values. They found significant relationships between SD and NTU in each analysis. These two measures of turbidity were highly correlated. However, their analysis relied on a general functional form where SD is the dependent (Y) variable and NTU is the independent variable (X). In other words, they were trying to predict SD from NTU levels. This is the inverse of what we were attempting to accomplish, which is predicting NTU from historical SD readings. The results of their analyses are reported in Table 6.

Table 6. Comparison of predictive models for turbidity reported by (Parent 2009).

Data Source: River Authorities	Power Equation R^2 $Y = a X^b$	Spearman's Non-parametric Statistic r_s	Number of Observations	Data manipulation
All	0.6688 $Y = 1.7786x^{-0.541}$	-0.6688	6915	Indefinite values converted to detection limit
All	0.691 $Y = 1.970x^{-0.589}$	-0.691	6793	Indefinite values excluded
Brazos	0.6394 $Y = 1.5505x^{-0.599}$	-0.78	2008	Indefinite values excluded
Lavaca-Navidad	0.5018 $Y = 1.5184x^{-0.495}$	-0.63	283	Indefinite values excluded
Nueces	0.565 $Y = 1.6106x^{-0.531}$	-0.71	171	Indefinite values excluded
Sabine	0.7955 $Y = 2.1658x^{-0.527}$	-0.89	1898	Indefinite values excluded
Trinity	0.7287 $Y = 2.1515x^{-0.607}$	-0.84	2433	Indefinite values excluded

We utilized the data provided by (Parent 2009) and conducted a regression analysis of the \log_{10} transformed data using the censored data set for the Brazos and Trinity Rivers. These are the closest basins to the Harris County study area. The results of our regression analysis of the Brazos and Trinity River data are depicted in Figure 27 and Figure 28. The original data used to conduct these analyses are provided in electronic format in Appendix 8. The log-transformed NTU and SD readings were highly correlated ($r = .80$ and 0.82 for the Brazos and Trinity Rivers, respectively). Both models provided fairly good fits with SD explaining 64% and 67.8% of the variability in turbidity measurements.

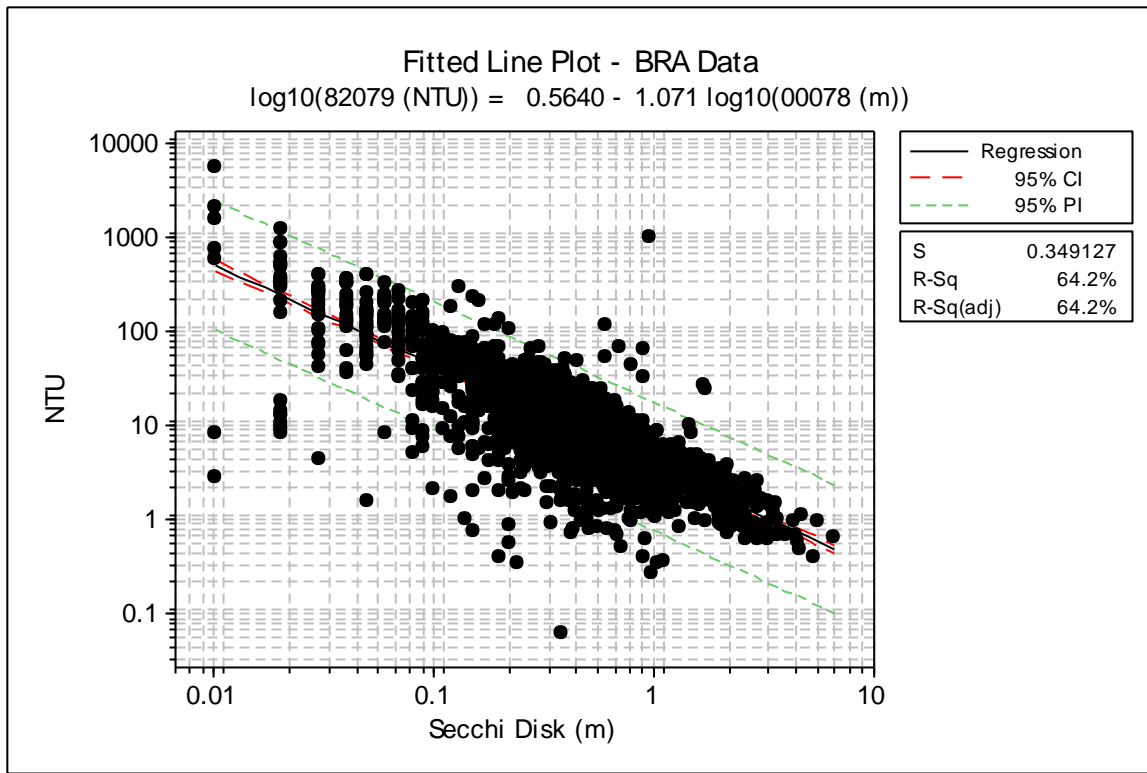


Figure 27. Analysis of turbidity data for the Brazos River Basin utilized in (Parent 2009).

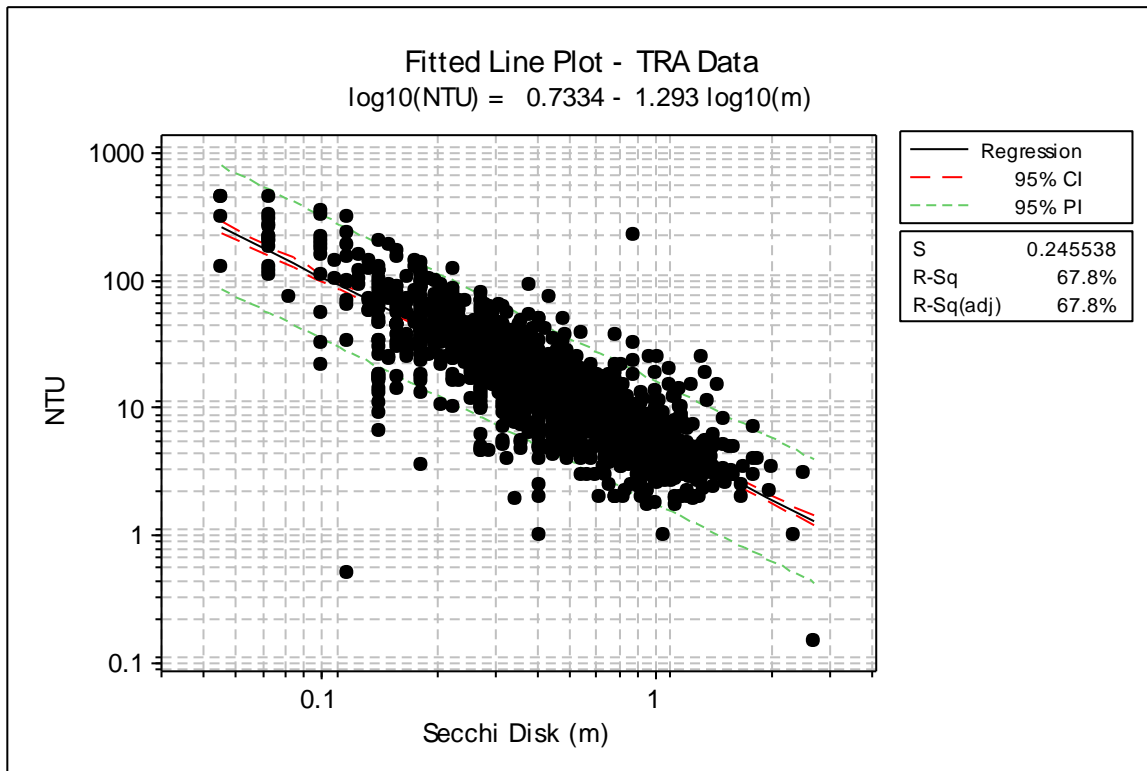


Figure 28. Analysis of turbidity data for the Trinity River Basin utilized in (Parent 2009).

Historical Data Analysis

Historical data collected by EIH from 2005 to 2011 document that the majority of the NTU measurements collected in Brazoria, Galveston, and Harris Counties ranged between 5 and 75 NTU (Figure 29). The data appears to have a log-normal distribution based on the skewed distribution. The most frequent measurements ranged between 5 and 20 NTU. Values never exceeded 275 NTU. We evaluated the relationship of these variables by using a log-log transformation of the variables and subjecting these to linear regression. Statistically significant, moderately strong relationships existed between the \log_{10} transformed NTU and SD readings (Figure 30 and Figure 31). However, only a relatively weak relationship was observed between historical NTU and TSS values (Figure 32 and Figure 33). Historical data used in this analysis are provided in electronic format in Appendix 9.

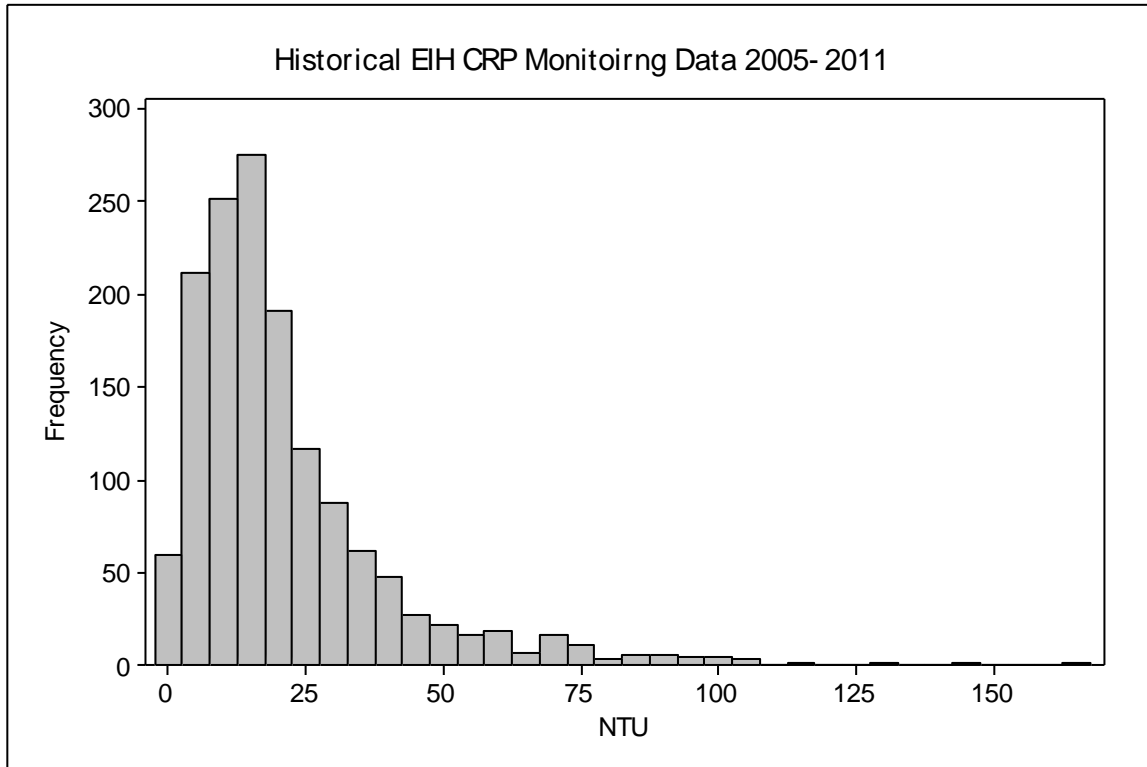


Figure 29. NTU measurements obtained by monitoring at 69 sites in Harris, Brazoria, and Galveston counties from 12-1-2005 to 7-18-2011. N = 1,445.

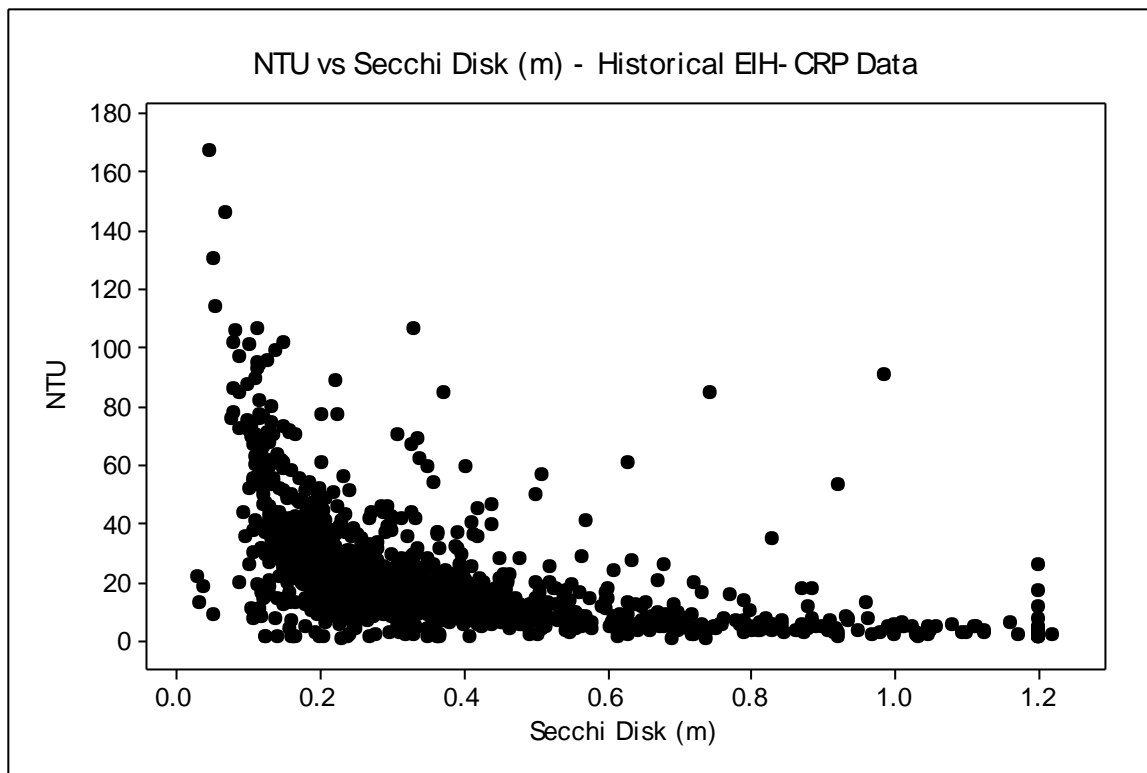


Figure 30. Paired NTU vs. SD measurements obtained by monitoring at 69 sites in Harris, Brazoria and Galveston counties from 12-1-2005 to 7-18-2011. N = 1,445

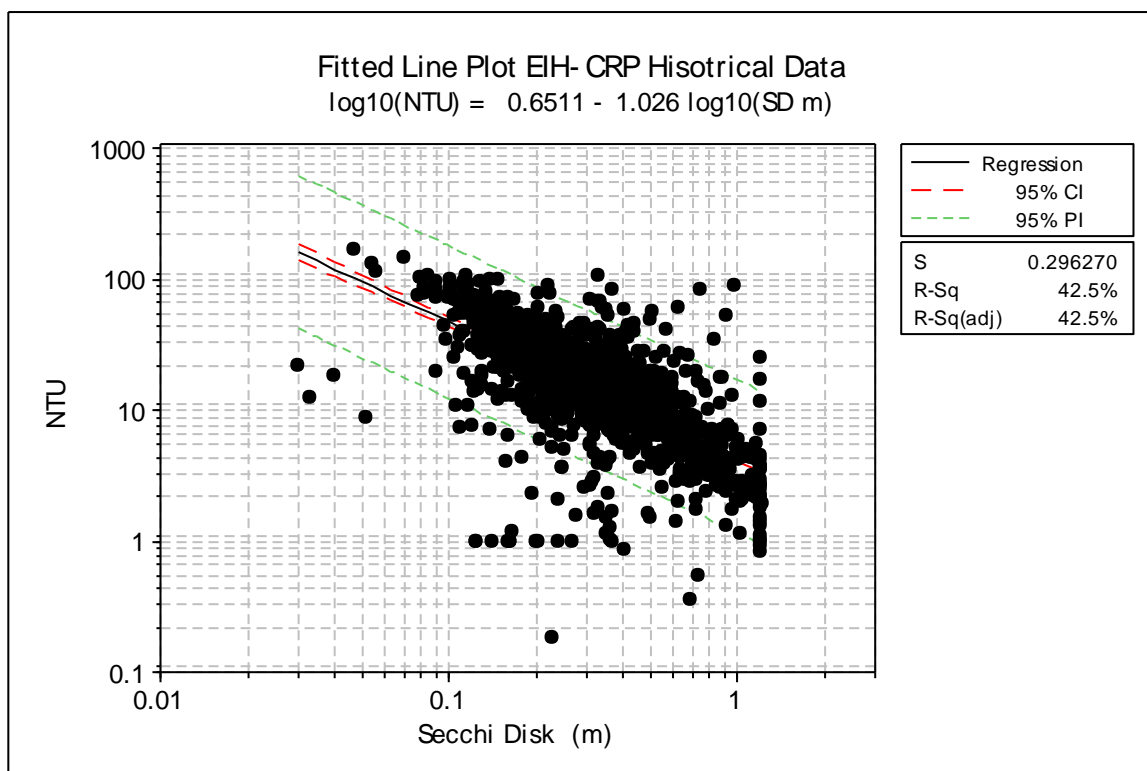


Figure 31. Results of regression on log-transformed, paired NTU vs. SD measurements obtained by monitoring at 69 sites in Harris, Brazoria and Galveston counties from 12-1-2005 to 7-18-2011. N = 1,445

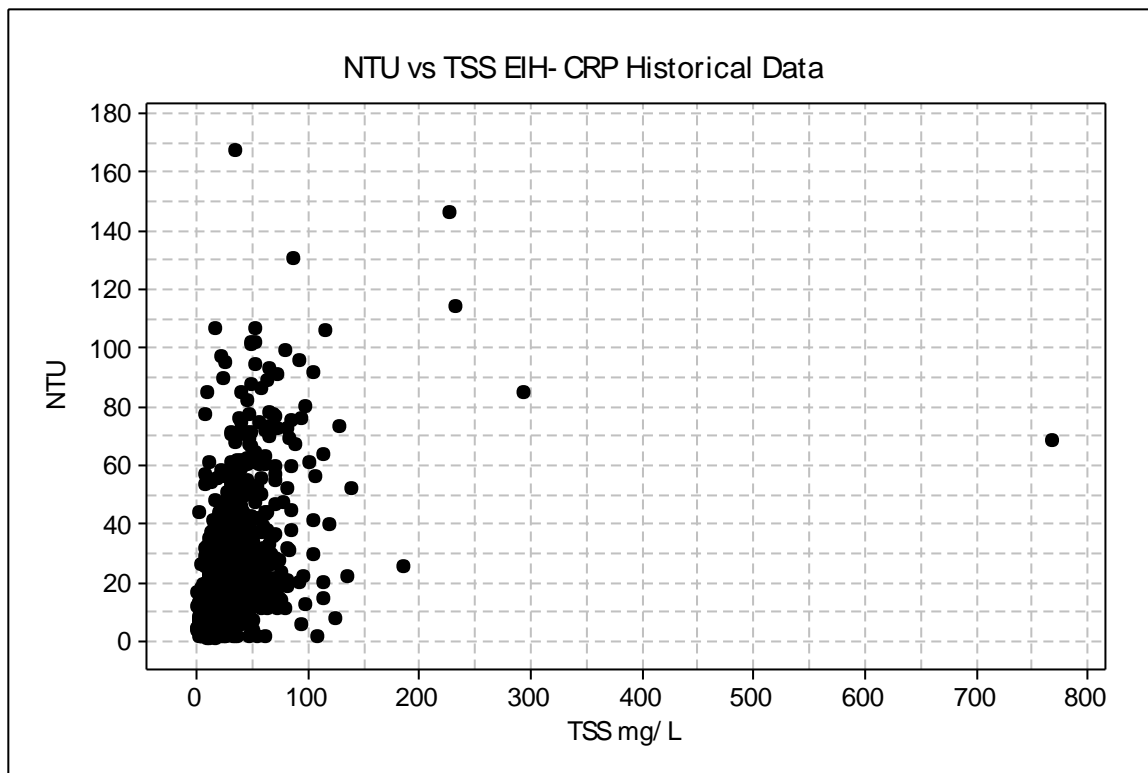


Figure 32. Paired NTU vs. TSS measurements obtained by monitoring at 69 sites in Harris, Brazoria and Galveston counties from 12-1-2005 to 7-18-2011. N = 1,445

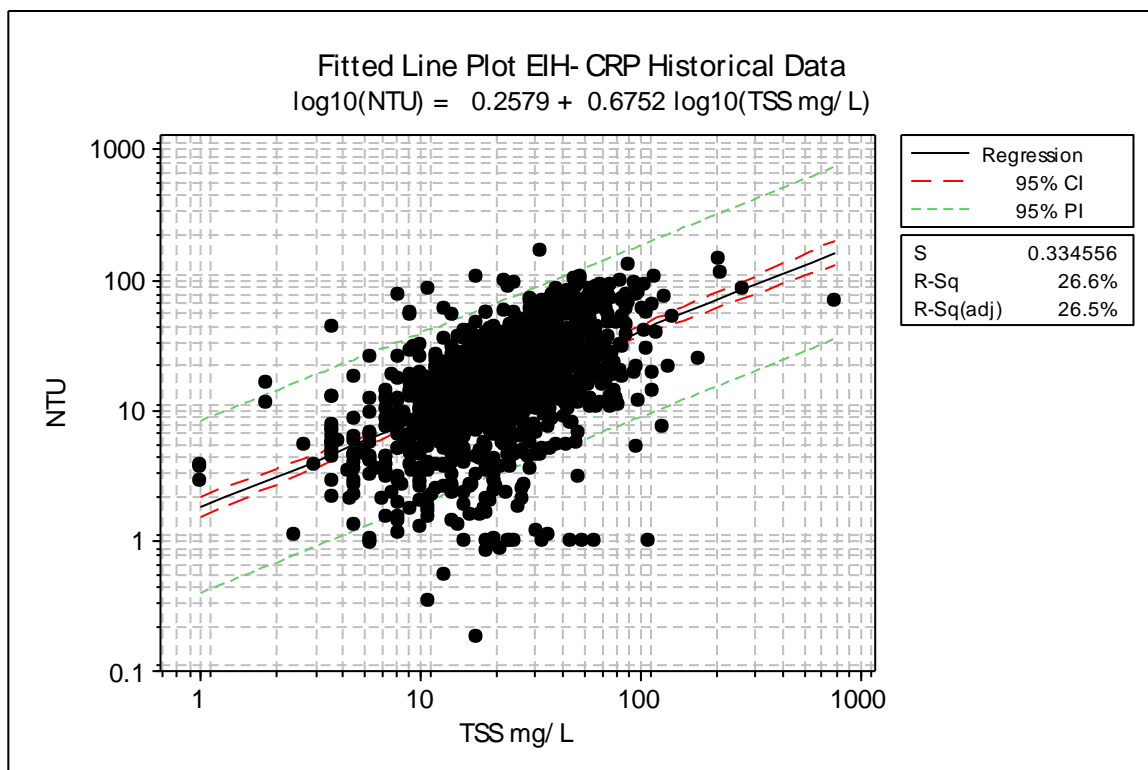


Figure 33. Results of regression on log transformed, paired NTU vs. TSS measurements obtained by monitoring at 69 sites in Harris, Brazoria and Galveston counties from 12-1-2005 to 7-18-2011. N = 1,445

Analysis of New Field Study Data

Sampling Events

Environmental sampling was conducted over a period extending from April to December 2011 covering 5 distinct monitoring periods (Table 7). During monitoring period 3a, late summer-fall (August-September), automated monitoring was not conducted. Therefore, automated monitoring was conducted during the early fall period (September-October, 3b). Periodic monitoring grab samples were, however, obtained during each monitoring period.

Site Characteristics

Physical data obtained onsite and from the watershed analysis are summarized in Table 7. Electronic versions of data derived from datasonde measurements, USGS-provided and measured streamflow, rainfall, water quality, and rainfall-runoff analyses are provided in Appendices 10-14. The streams varied considerably in terms of size, amount of impervious area, and flow regime. The largest watersheds were associated with sites 1E, 1F and 4B, which all exceeded 70,000 hectares (173,000 acres, 270 miles²) (Figure 34). It should be noted that, when compared to official published USGS gage estimates of contributing watersheds, our watershed estimates from 1.3 to 33% with a average deviation of 9.8%. However, the relative order of watershed sizes by site was not affected. Watersheds having the greatest percent of impervious surface (i.e. urbanized) were located in the small to medium-sized watersheds (sites 1C, 1J, 1K, 1P, 4A, 5A, and 5C) (Figure 34).

Stream morphology and flow regime did not strongly correlate with watershed size or percentage of impervious area (Figure 35 and Figure 36). Overall, median streamflow did exhibit moderate but significant positive correlations with watershed size and the amount of impervious surface ($r = 0.570$, $p = 0.009$; $r = 0.622$, $p = 0.003$ respectively). In addition, the percentage of impervious area was significantly negatively-correlated with the size of the watershed ($r = -0.611$, $p = 0.004$). Highest observed median streamflow occurred at site 5A which possessed a moderate size watershed, a high percentage of impervious surfaces, and the widest stream width (Figure 34 to Figure 36). It should be noted that at Site 3A, the only site which represented group 3 as defined by the initial cluster analysis, lacked streamflow during most periods when the datasonde was deployed. Observable streamflow was only present during one monitoring period. For the rest of the study the area immediately upstream of site 3A was composed of isolated pools or was completely dry (Figure 36 and Table 7).

The lack of strong correlations between median streamflow and overall watershed size or the amount of impervious land may be due to the drought conditions and the resulting low streamflows that existed and persisted throughout the study. Harris County, like the rest of the state of Texas, was experiencing an extended, severe drought (Figure 37 to

Figure 39). Consequently, rainfall and streamflow were generally below normal, and most flows likely consisted primarily of return wastewater within many urban streams in Harris County. For example, examination of official archived historical data at site 5C (USGS gage site 08074500) for the months of April through September showed that flows were lower than the historical lower quartile and median streamflows during April, May, June, August, and September. Streamflow during July was approximately equal to the historical median monthly flow for this month. However, these values are not adjusted for the increase in base flows that have occurred over the last 30 years due to urbanization.

Table 7. Sampling conducted during the study period extending from April to December 2011. *No Datasondes logged data during this sample period. **No samples were taken during this site visit. AS Sites datasondes were deployed during Sample 1 and retrieved during Sample 3 for each sample period, unless otherwise stated.

Sample Type	Site	Sample Period 1				Sample Period 2				Sample Period 3a*				Sample Period 3b				Sample Period 4					
		Sample 1	Sample 2	Rain Sample	Sample 3	Sample 1	Sample 2	Rain Sample	Sample 3	Sample 1	Sample 2	Rain Sample	Sample 3	Sample 1	Sample 2	Rain Sample	Sample 3	Sample 1	Sample 2	Rain Sample	Sample 3	Sonde retrieve **	
AS	1G	4/18	5/3	-	5/12	6/28	7/11	7/19	7/28	8/24	9/13	-	9/29	10/5	10/20	-	-	11/2	11/9	11/22	11/9	12/7	12/14
	2B	4/18	5/3	5/13	5/10	6/29	7/11	-	7/29	8/25	9/13	-	9/28	10/6	10/20	-	-	11/3	11/8	11/22	11/22	12/8	12/14
	3A	4/18	5/3	5/13	5/11	6/27	7/11	-	7/27	8/25	9/13	-	9/28	10/6	10/20	10/10	-	11/3	11/8	11/22	-	12/8	12/14
	4A	4/18	5/3	5/13	5/12	6/28	7/11	-	7/28	8/24	9/13	-	9/29	10/5	10/20	-	-	11/2	11/9	11/22	-	12/5	12/14
	5B	4/18	5/3	-	5/16	6/29	7/11	7/19	7/29	8/23	9/13	-	9/30	10/5	10/20	10/28	-	11/1	11/10	11/22	11/22	12/6	12/14
PM	1C	4/20	-	-	5/12	6/28	-	-	7/28	8/24	-	9/19	9/29	10/5	-	-	-	11/2	11/9	-	11/9	12/7	-
	1E	4/20	-	-	5/12	6/28	-	-	7/28	8/24	-	9/19	9/29	10/5	-	-	-	11/2	11/9	-	11/9	12/7	-
	1F	4/20	-	-	5/12	6/28	-	-	7/28	8/24	-	9/19	9/29	10/5	-	-	-	11/2	11/9	-	11/9	12/7	-
	1H	4/19	-	5/13	5/11	6/27	-	-	7/27	8/25	-	8/25	9/28	10/6	-	10/10	-	11/3	11/8	-	-	12/8	-
	1J	4/20	-	-	5/16	6/29	-	7/19	7/29	8/23	-	-	9/30	10/5	-	10/10	-	11/1	11/10	-	-	12/6	-
	1K	4/20	-	-	5/16	6/29	-	7/19	7/29	8/23	-	-	9/30	10/5	-	10/10; 10/28	-	11/1	11/10	-	-	12/6	-
	1M	4/19	-	5/13	5/11	6/27	-	-	7/27	8/25	-	-	9/28	10/6	-	10/10	-	11/3	11/8	-	-	12/8	-
	1P	4/26	5/3	-	5/16	6/29	-	7/19	7/29	8/23	-	-	9/30	10/5	-	10/10	-	11/1	11/10	-	-	12/6	-
	2A	4/19	-	5/13	5/11	6/27	-	-	7/27	8/25	-	8/25	9/28	10/6	-	-	-	11/3	11/8	-	-	12/8	-
	2D	4/19	-	-	5/16	6/29	-	7/19	7/29	8/23	-	-	9/30	10/5	-	-	-	11/1	11/10	-	-	12/5	-
	2E	4/19	-	-	5/11	6/27	-	7/19	7/27	8/25	-	-	9/28	10/6	-	-	-	11/3	11/8	-	-	12/6	-
	2G	4/19	-	-	5/11	6/27	-	-	7/27	8/23	-	-	9/30	10/5	-	10/10; 10/28	-	11/1	11/10	-	-	12/5	-
	4B	4/20	-	5/13	5/12	6/28	-	-	7/28	8/24	-	-	9/29	10/5	-	10/28	-	11/2	11/9	-	-	12/7	-
	5A	4/20	-	-	5/12	6/28	-	-	7/28	8/24	-	9/19	9/29	10/5	-	-	-	11/2	11/9	-	-	12/5	-
	5C	4/20	-	-	5/16	6/27	-	-	7/27	8/23	-	9/19	9/30	10/5	-	-	-	11/1	11/10	-	-	12/5	-

Table 8. Summary of site characteristics observed during the study. *Flow value from entire sonde deployment sample period (cfs). **Flow values from sonde deployment sample period not available, USGS gage does not record base flow conditions. DSLSR = Days Since Last Significant Rainfall. Min.= Minimum, Med.=Median, Max.=Maximum.

Sample Type	Site	USGS ID	Sub-Watershed Area (ha)	% Impervious Area	Min. Flow (cfs)	Med. Flow (cfs)	Max. Flow (cfs)	Med. #DSLRS (days)	Min. Thalweg (m)	Med. Thalweg (m)	Max. Thalweg (m)	Min. Width (m)	Med. Width (m)	Max. Width (m)
AS	1G	8076997	8360	15.6	4.1 (2.3*)	6.5 (13.0*)	81.0 (381.0*)	12.0	0.25	0.54	1.14	2.8	7.0	9.5
	2B	8068900	49246	8.7	6.4 (**)	21.8 (**)	139.4 (**)	9.5	0.55	0.83	1.48	10.1	11.1	16.8
	3A	8068720	27847	0.8	0.0 (0.0*)	0.0 (0.0*)	0.4 (0.4*)	10.0	0.14	0.22	0.42	2.3	5.1	7.0
	4A	8074760	4325	47.2	21.0 (8.5*)	26.0 (26.0*)	103.0 (963.0*)	6.0	0.38	0.51	0.84	6.8	7.7	9.0
	5B	8076500	8490	38.3	3.2 (2.6*)	7.5 (5.7*)	36.0 (830.0*)	5.0	0.14	0.67	0.76	4.4	9.9	10.7
PM	1C	8074810	13158	50.9	40.0	59.0	261.0	12.0	0.69	0.78	0.85	8.4	15.4	18.0
	1E	8073700	79439	19.6	72.0	84.0	444.0	6.0	0.65	0.90	1.50	8.4	9.9	16.0
	1F	8073600	77918	19.0	77.0	86.0	380.0	10.0	0.50	0.90	1.40	11.0	13.1	17.8
	1H	8068740	35526	1.6	0.6	2.2	60.0	7.0	0.36	0.65	0.92	2.4	4.2	6.7
	1J	8075763	1337	56.2	0.3	1.7	180.0	4.5	0.28	0.46	1.62	2.9	6.5	17.0
	1K	8075770	3988	50.9	2.2	6.4	48.0	4.0	0.15	0.35	1.57	3.1	6.1	9.0
	1M	8072760	6914	19.4	5.3	6.3	70.0	6.0	0.24	0.49	1.11	3.0	5.0	30.2
	1P	8075730	1810	50.3	0.2	3.3	31.0	6.0	0.36	1.13	1.46	6.4	15.0	16.8
	2A	8068800	41267	4.7	4.4	7.3	271.0	5.0	0.21	0.29	1.11	5.2	6.5	13.0
	2D	8076000	16036	36.6	27.0	31.0	916.0	5.0	0.60	0.64	2.56	7.7	12.3	16.8
	2E	8075900	9050	37.1	14.0	21.0	546.0	7.0	0.64	0.72	1.83	3.6	4.5	10.7
	2G	8074020	8512	40.7	11.0	19.0	220.0	4.5	0.60	0.81	1.07	11.5	13.1	14.1
	4B	8073500	74586	17.5	58.0	76.5	169.0	4.5	0.70	0.86	1.08	12.5	13.0	16.8
	5A	8075000	24201	52.9	80.0	104.0	1370.0	6.0	0.83	0.89	1.71	15.0	18.1	23.8
5C	8074500	21221	45.8	19.0	36.0	811.0	4.0	0.42	0.49	1.71	3.2	3.5	12.9	

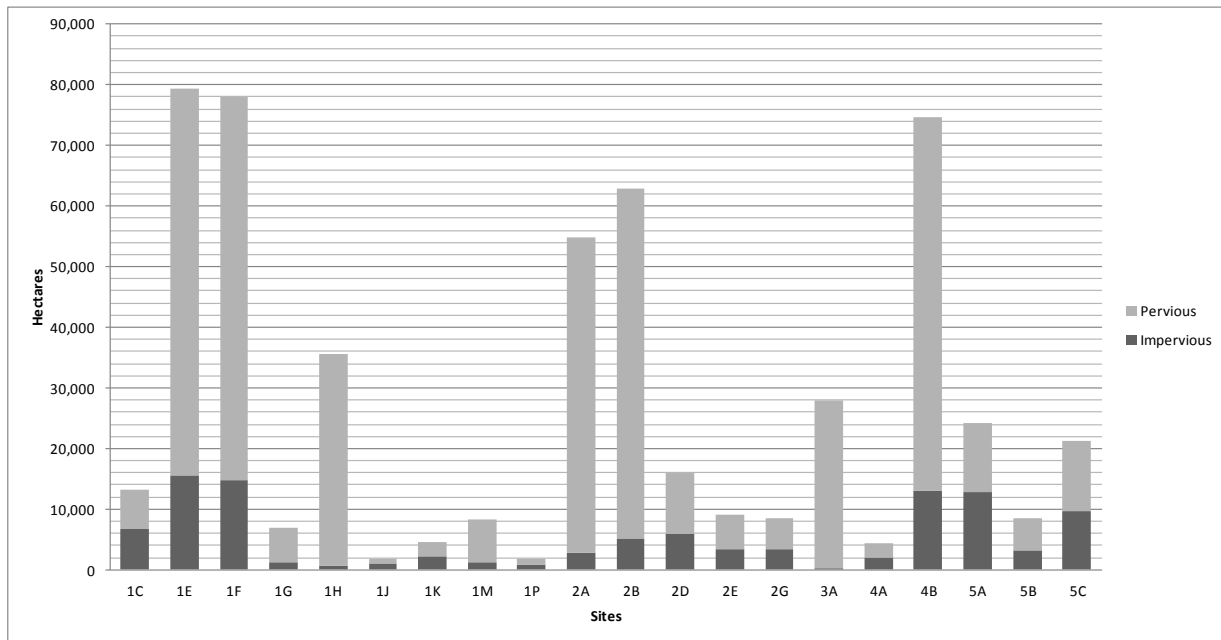


Figure 34. Watershed area located above each monitoring site, including amounts of impervious land cover.

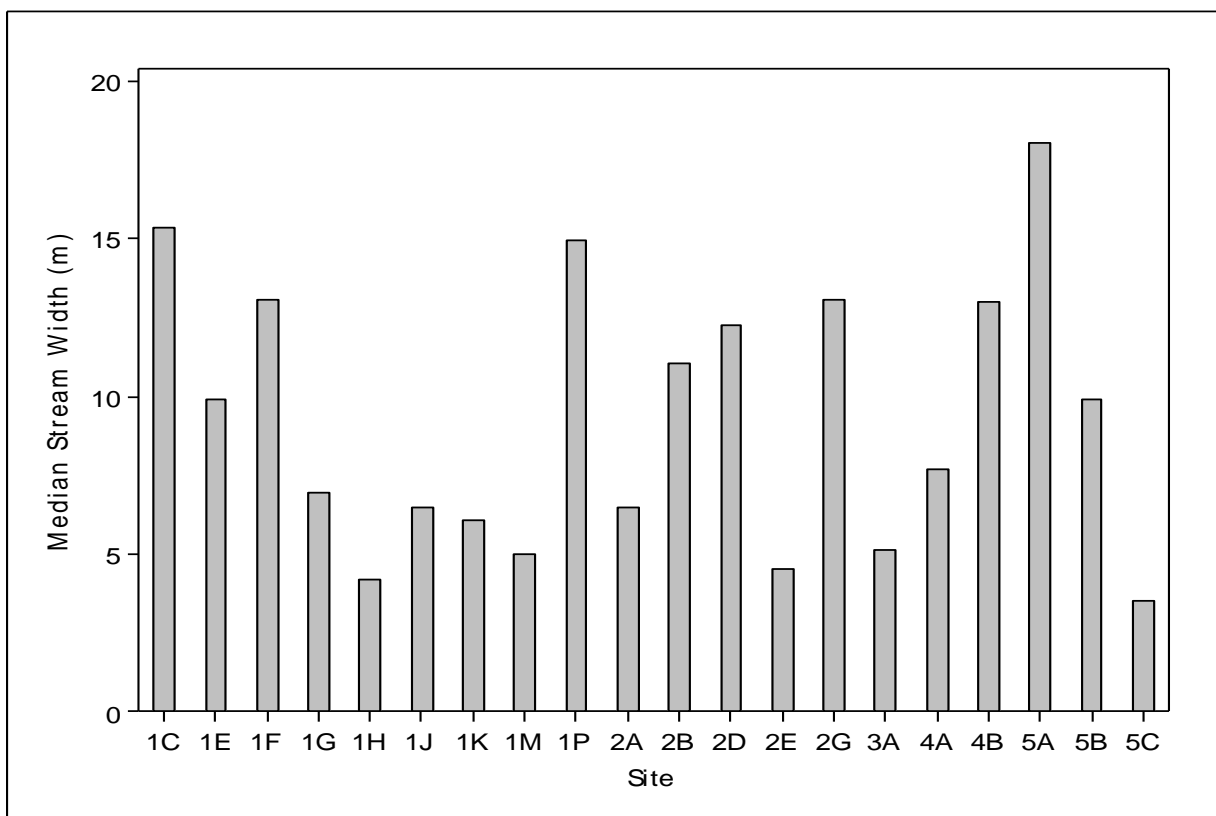


Figure 35. Median stream width during study period at each survey site. Note: Site 3A was often intermittent, so median stream width was equivalent to median pool width.

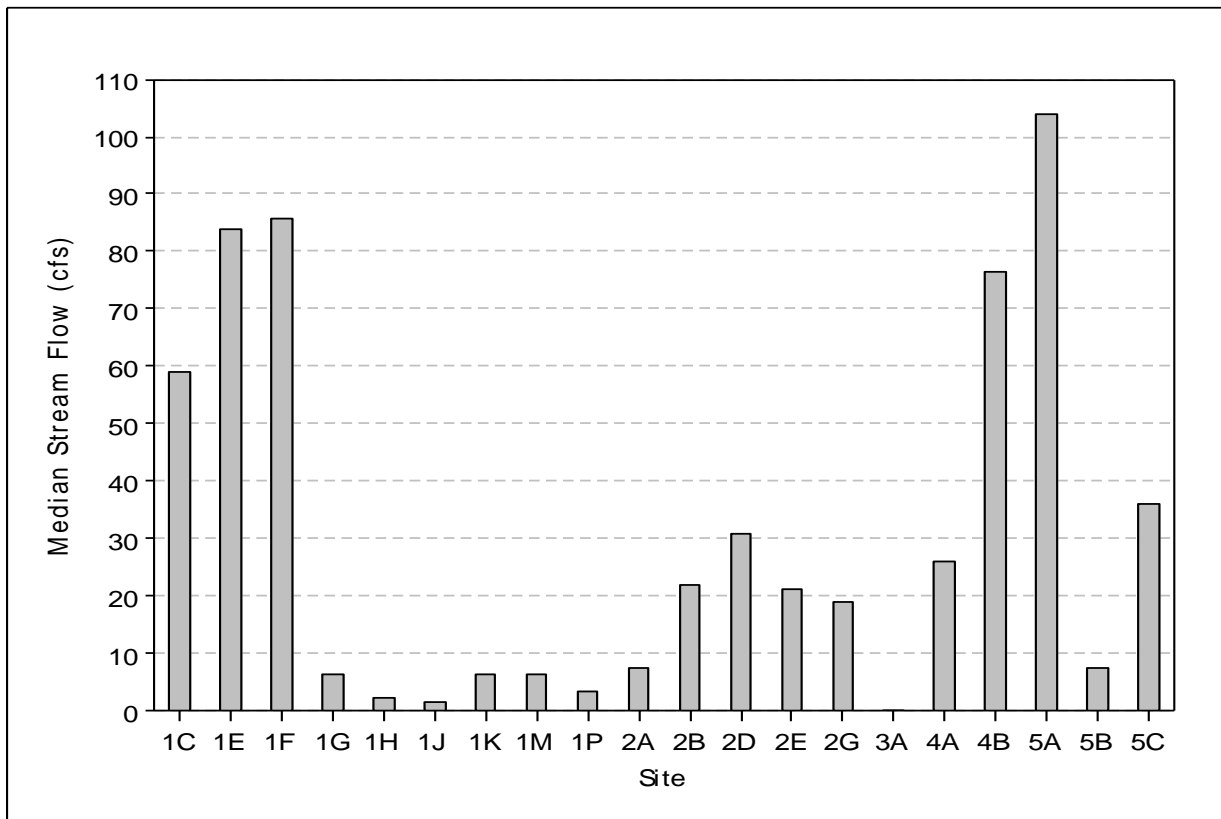


Figure 36. Median streamflow observed during the study period at each site. Streamflow based on values observed during active monitoring.

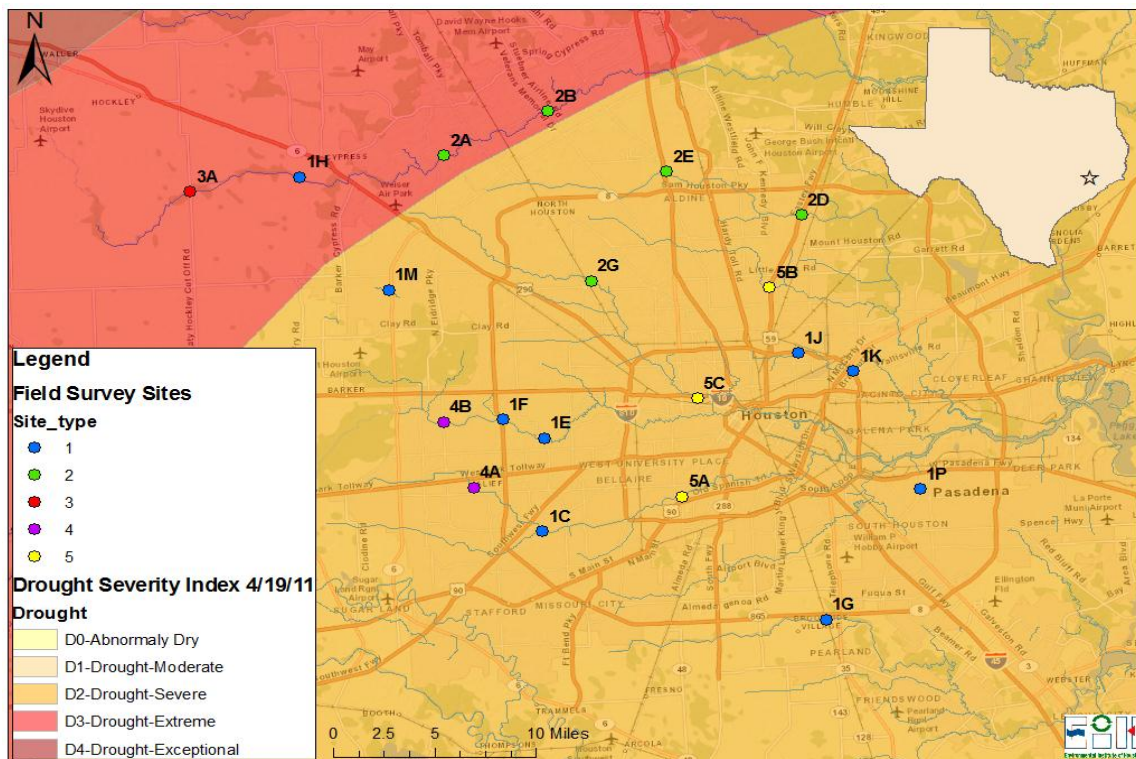


Figure 37. State of Texas drought index map for April 19, 2011 depicting current conditions in Harris County. Data Source: National Drought Mitigation Center: (<http://drought.unl.edu/>).

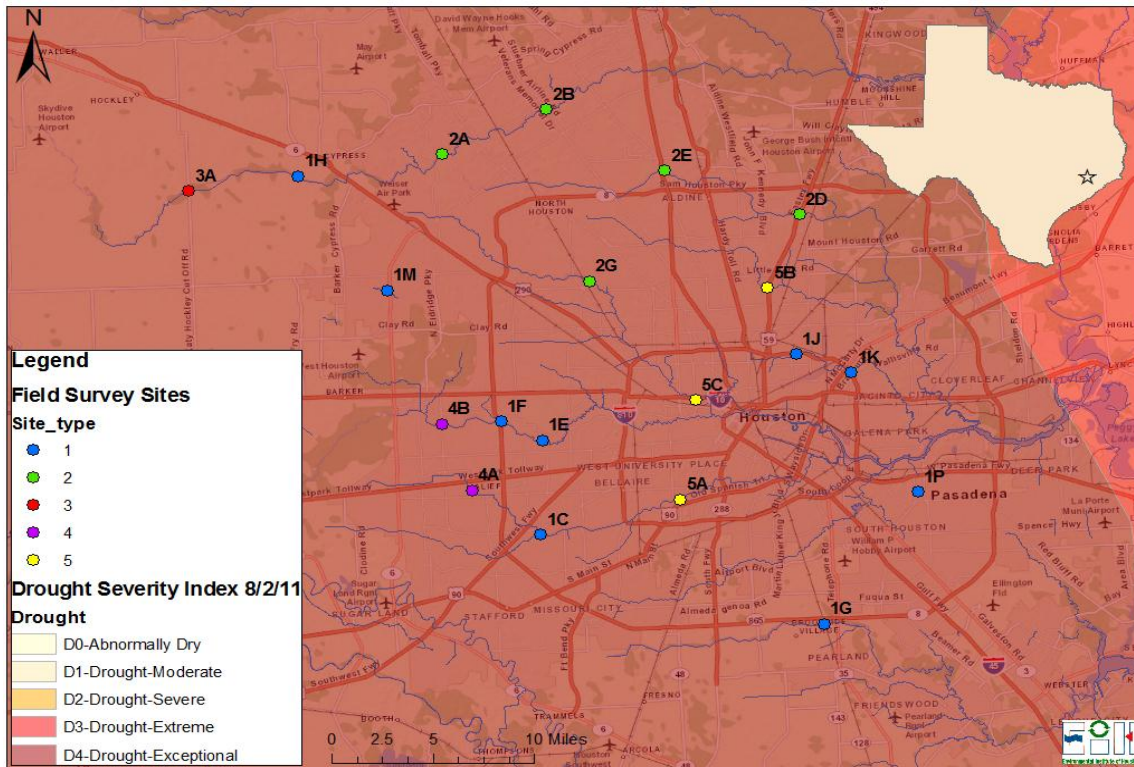


Figure 38. State of Texas drought index map on August 2, 2011 depicting current conditions in Harris County. Data Source: National Drought Mitigation Center: (<http://drought.unl.edu/>).

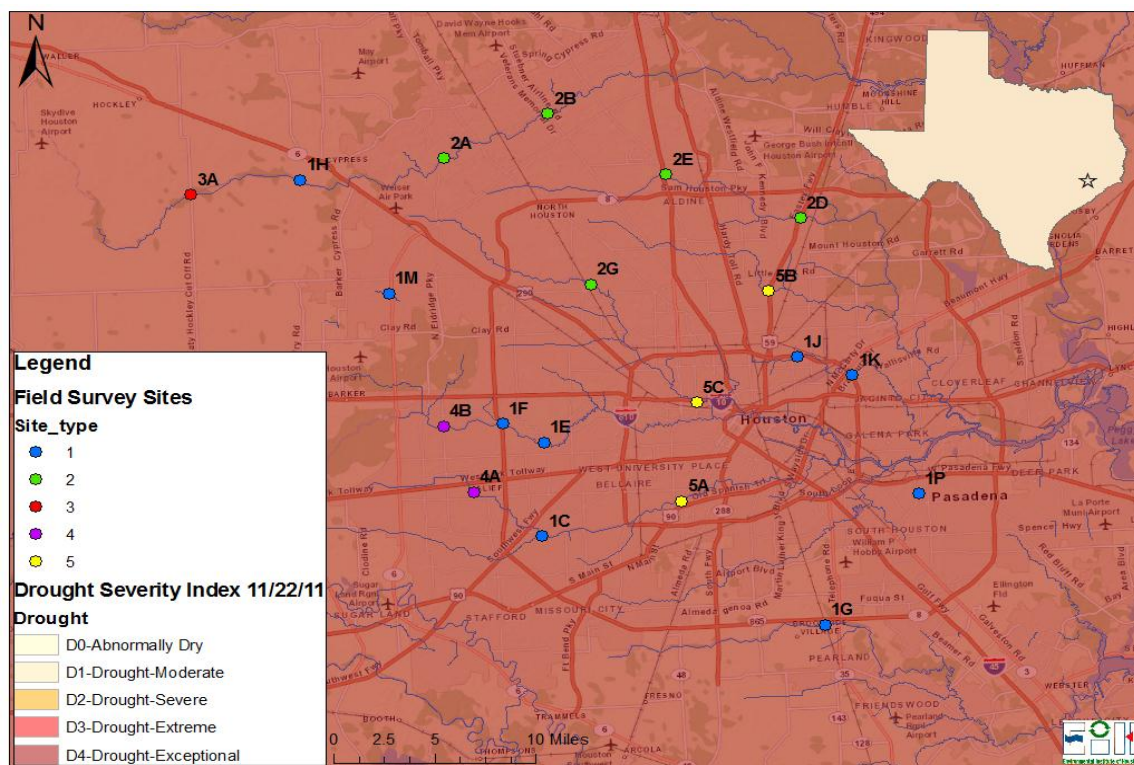


Figure 39. State of Texas drought index map on November 22, 2011 depicting current conditions in Harris County. Data Source: National Drought Mitigation Center: (<http://drought.unl.edu/>).

Automated Monitoring

Automated monitoring datasondes deployed at 5 sites collected a total of 31,339 NTU measurements. However, 2,556 NTU values were negative; suggesting that the turbidity probe may have been exposed to air due to turbulent flows or low water levels. Therefore, only 28,783 measurements (91.8%) were used in our analysis (Figure 40). The 10th, 25th, median, 75th and 95th percentile NTU values were 7, 13, 26, 60 and 381 respectively, and ranged between 0 and 1,778. Median NTU values were higher at site 3A. This site often experienced extremely low or zero flows. During these periods water was only found in stagnant pools. The presence of stagnant water and easily disturbed, silty sediment during low flow may have caused unrepresentative or skewed turbidity readings due to disturbance and/or suspended algae. Highly discolored water caused by dissolved organic material was also frequently observed at site 3A. Each AS site, however, had some extremely high values denoted as outliers on the boxplot (Figure 41). Due to the narrow distribution of values, (9.8, 12.6, 16.0 NTU corresponding to the 25th, median, and 75th percentiles respectively), the majority of remaining values associated with site 5B appeared to be outlier values. Sites 2B and 5B had the highest and lowest overall average NTU values (Figure 42). The site 5B datasonde was deployed on the bottom of the stream bed. We did observe periods where the instrument had been surrounded by a highly concentrated suspension of fine silt. At site 5B, streamflow was also often very low.

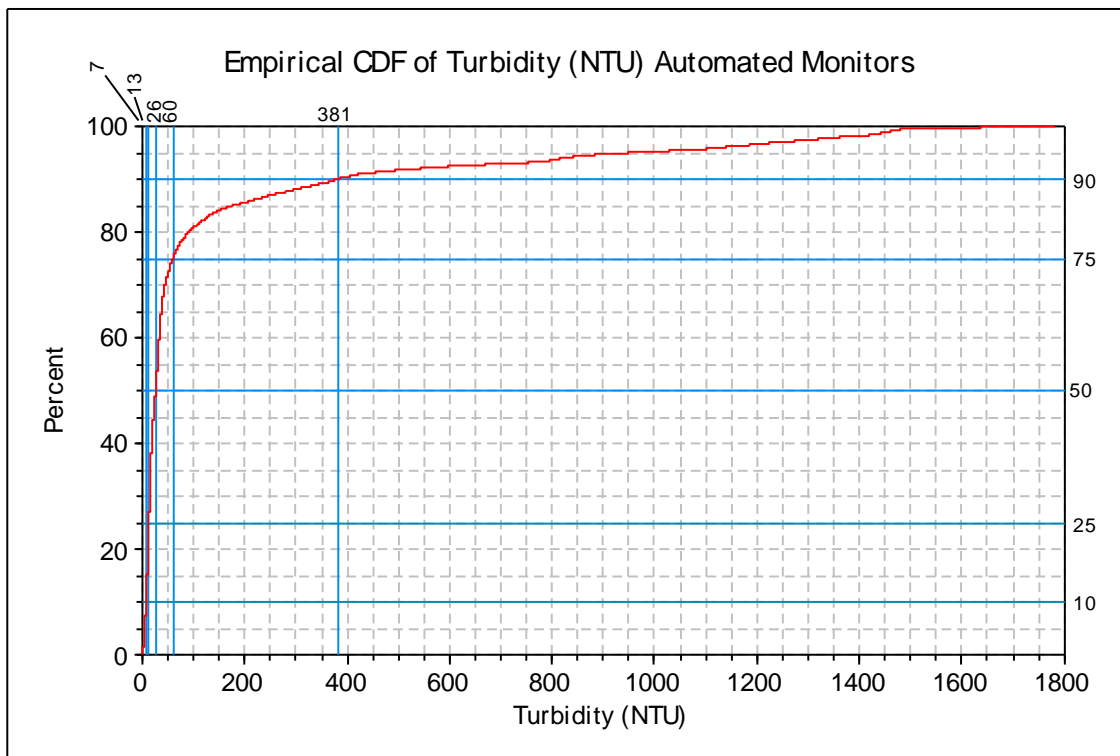


Figure 40. Cumulative distribution of turbidity NTU observed during this study from all datasondes (N = 28,783, out of 31,339 original NTU readings, excluding values < 0). Values marked by the vertical blue line denote the 10th, 25th, median, 75th and 90th percentile.

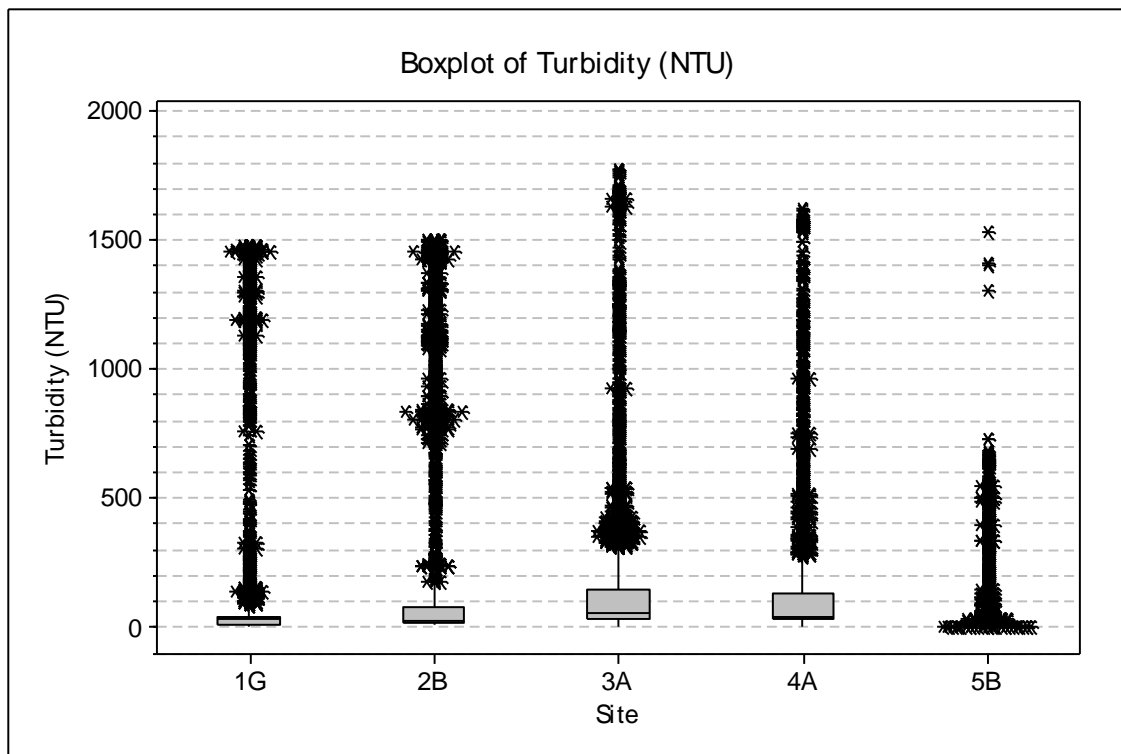


Figure 41. Boxplot of turbidity NTU values recorded by automated datasonde samplers.

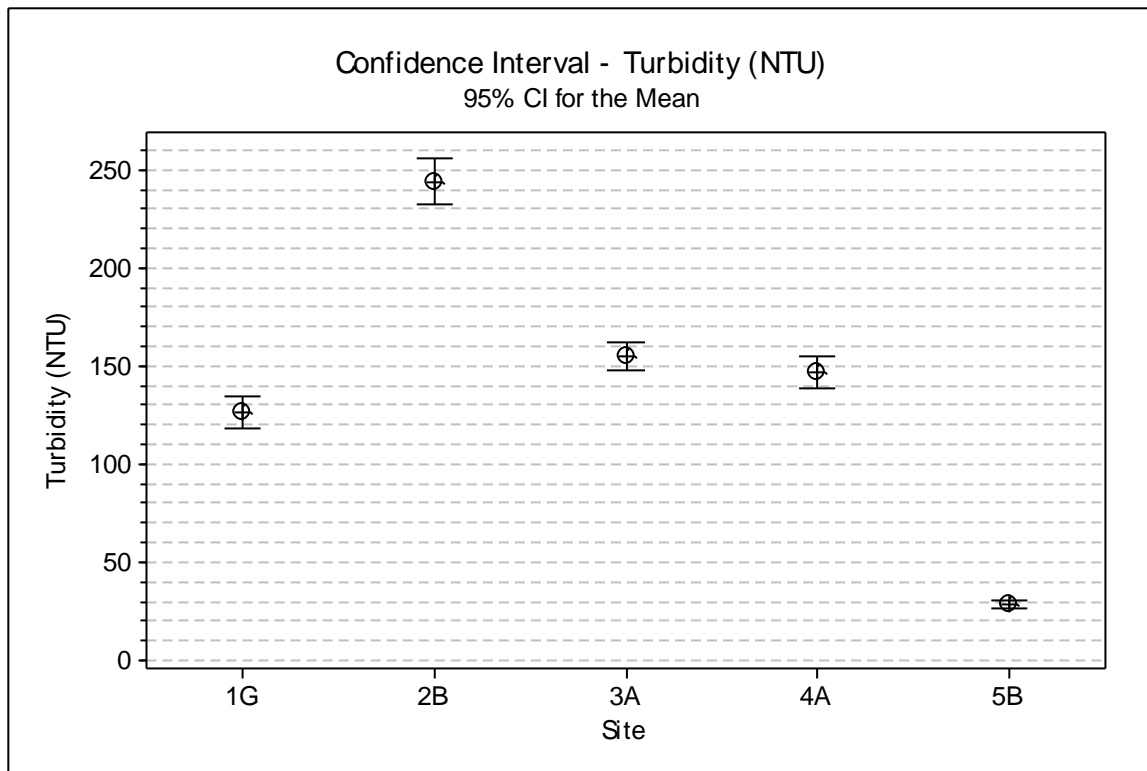


Figure 42. Estimates of average and associated 95% confidence intervals for NTU recorded by automated samplers during the study in 2011.

Coupled temporal trends between turbidity and streamflow were difficult to detect based on automated sampler (YSI datasonde) results (Figure 43 to Figure 52). This may be due to multiple factors, including lack of sufficient reliable streamflow data, which occurred at site 2B and 3A. In addition, individual hydrographs were not evaluated for more subtle patterns in sediment transport and turbidity associated with “first flush” hydrodynamics. Strong positive correlations between suspended sediment and streamflow during the rising limb of the hydrograph may have been masked by evaluating this large data set using simple linear regression analysis between turbidity measures and streamflow. In addition, no regard was given for whether streamflow was increasing after prolonged low flows, or if it was receding after a large pulse of water, associated with heavy rains, had flushed the system. This non-linear response would confound simple statistical approaches dependent on normally distributed data and linear responses to external stressors.

During the study period, the datasonde deployed at site 1G recorded extremely high turbidities (>1000 NTU) during October. At this site, it does appear streamflow did, in many cases, increase prior to parallel increases in NTU levels. This suggests that increased flows resuspended or introduced suspended particles and increased turbidity (Figure 43). Furthermore, the highest NTU levels generally occurred at intermediate levels of streamflow, suggesting that the increased energy, from rising water levels and associated runoff, contributes new sediment from the watershed and resuspends bottom sediment, quickly increasing turbidity (Figure 44).

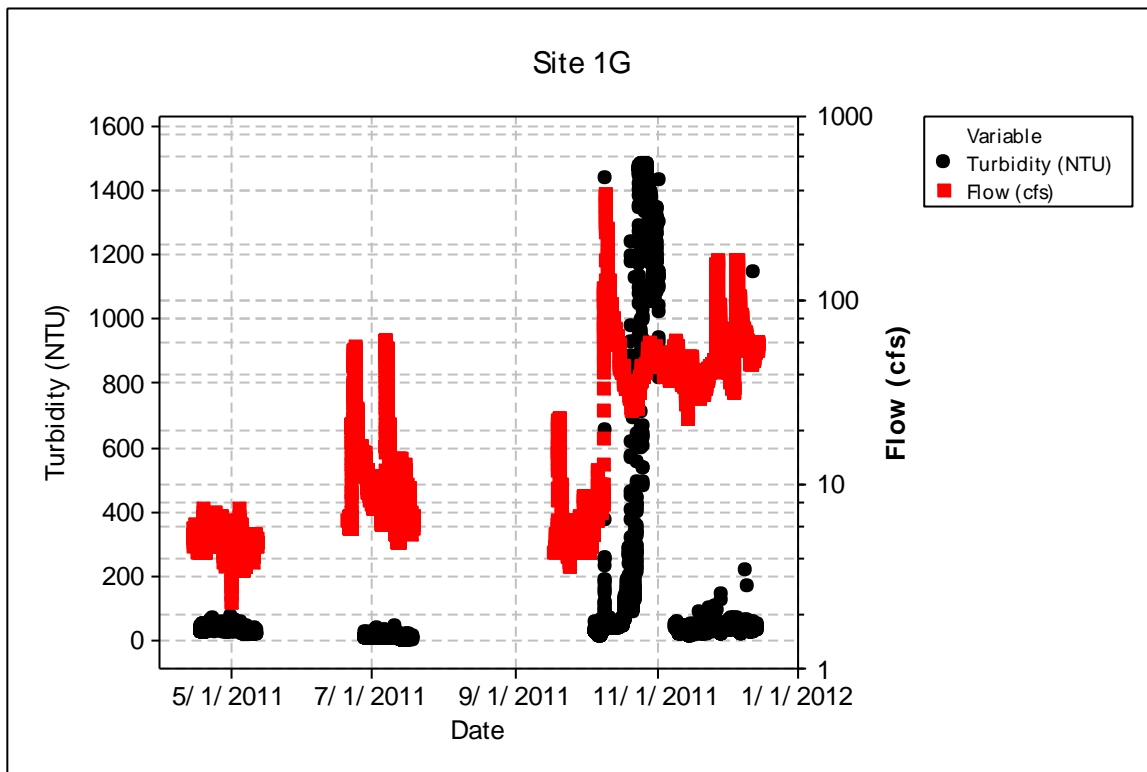


Figure 43. Turbidity (NTU) and flow (log scale) observed at site 1G from May to September 2011. Note: this analysis contains some negative NTU values that were not truncated.

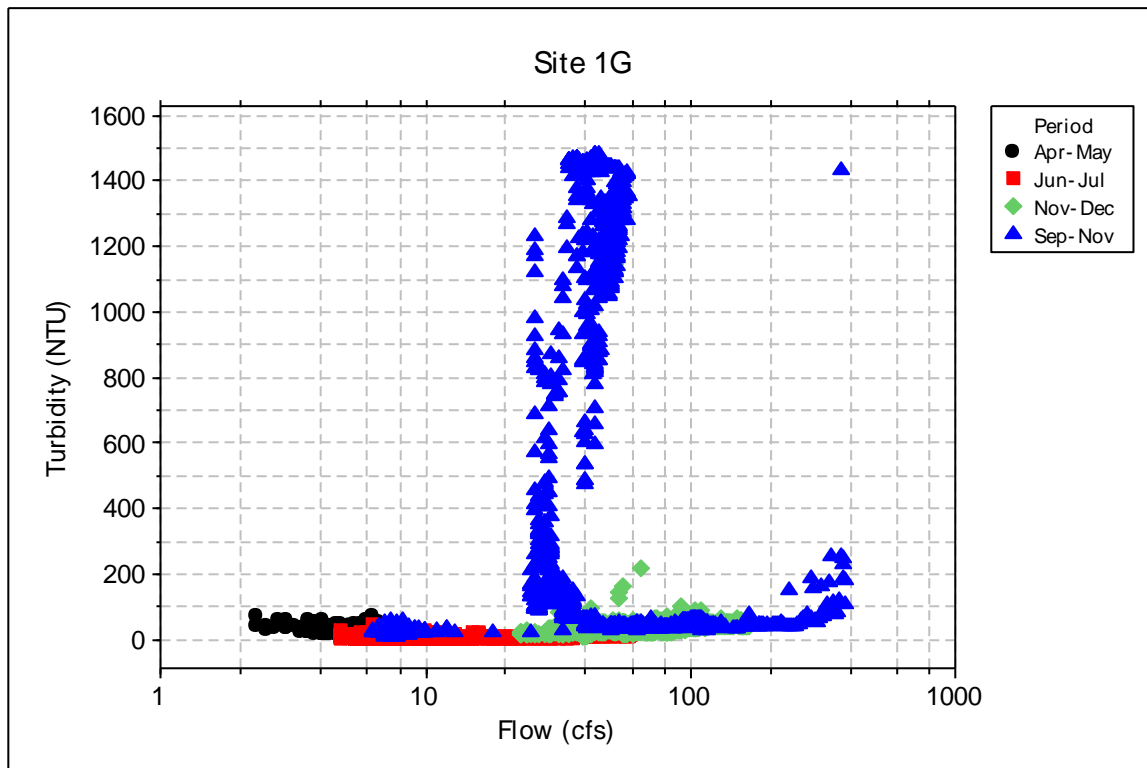


Figure 44. Turbidity vs. flow (log scale) at site 1G observed during the study. Note: this analysis contains some negative NTU values that were not truncated.

As previously mentioned, the low flows or limited datasonde data at sites 2B and 3A, limited our ability to derive strong inferences regarding the role of streamflow on turbidity (Figure 46 - Figure 48). Very high turbidity (>1000 NTU) was recorded during spring and fall months at both sites. These elevated turbidity readings did not appear to be associated with high streamflow conditions. At site 2B, water levels were frequently too low to obtain a reliable gage reading and converted flow estimate. We spoke to USGS and obtained a rating curve for this site. But we have been unable to obtain matching streamflow and lower gage readings to extend the rating curve to estimate flows in that range. One possible method to extend the streamflow record at lower flows is to use the nearest upstream and downstream gage to develop a predictive relationship for the missing data period. This method should be explored in future analyses.

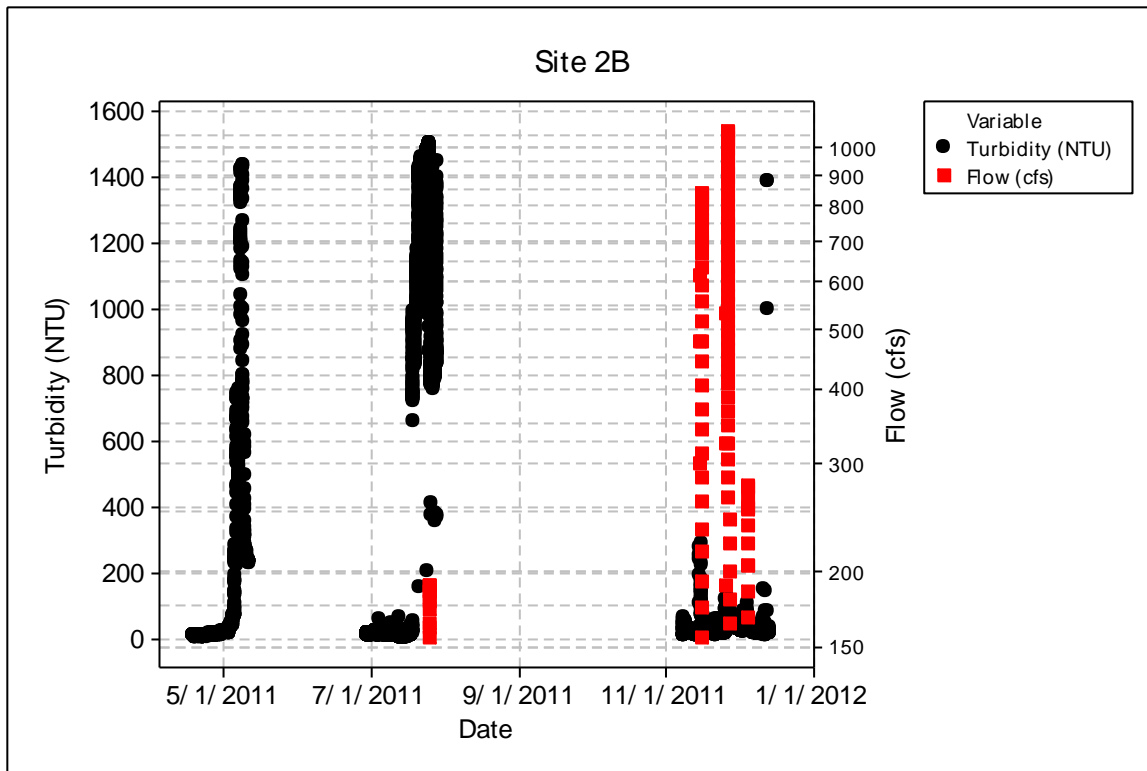


Figure 45. Turbidity (NTU) and flow (log scale) observed at site 2B from May to September 2011. Note: this analysis contains some negative NTU values that were not truncated.

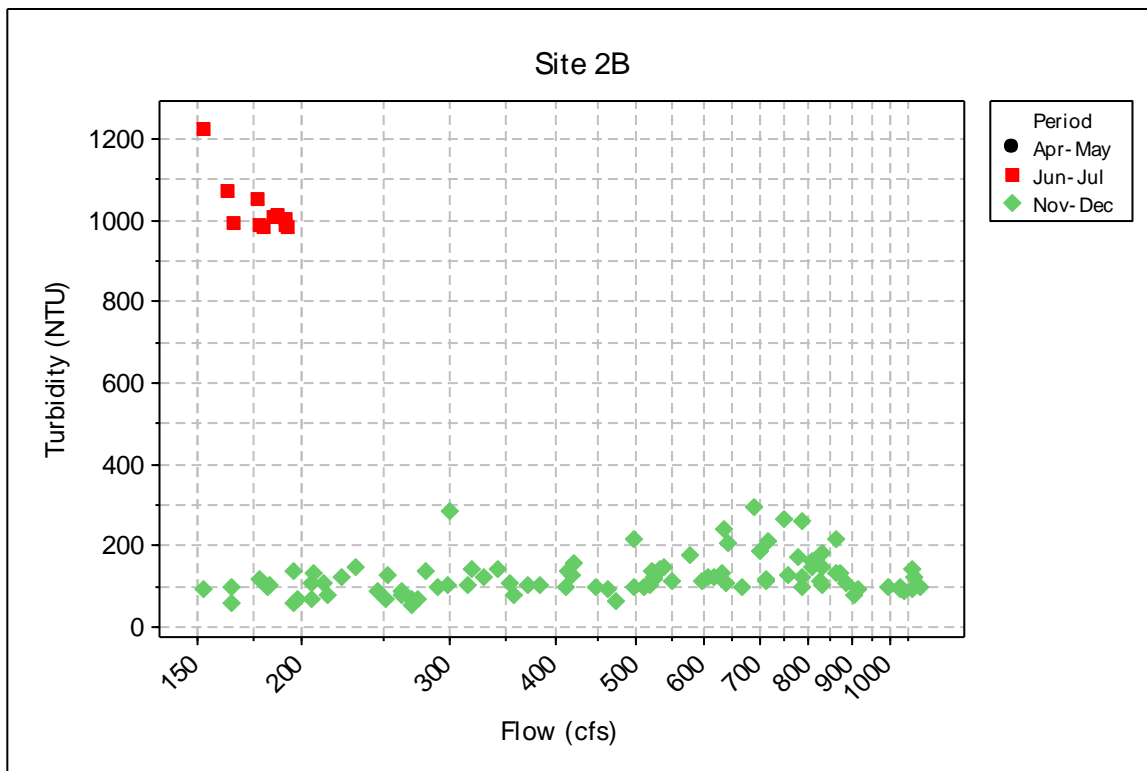


Figure 46. Turbidity vs. flow (log scale) at site 2B observed during the study. Note: this analysis contains some negative NTU values that were not truncated. During most of the project, lower stream flows (< 150cfs) below the rating curve for this site not recorded by the USGS gage. Consequently, matching turbidity values are not depicted for those periods.

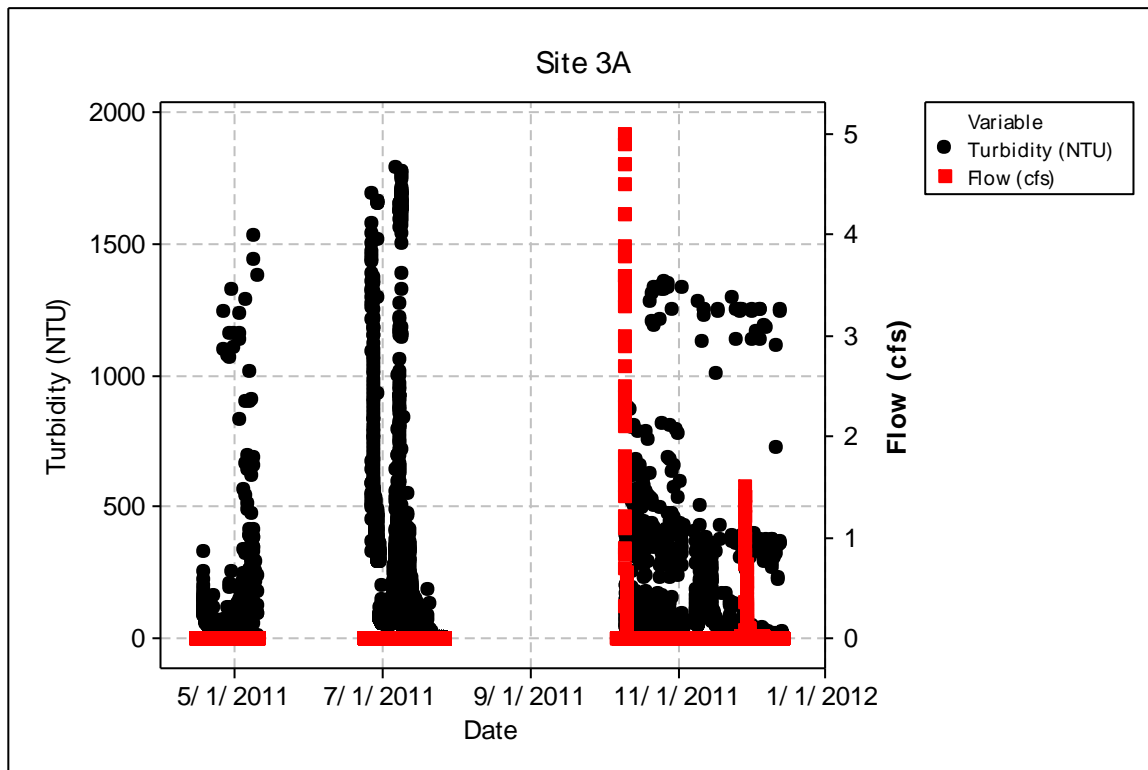


Figure 47. Trends in turbidity (NTU) measured by the YSI datasonde and streamflow (cfs) at site 3A during the study period. All NTU values were utilized for this display, including negative numbers.

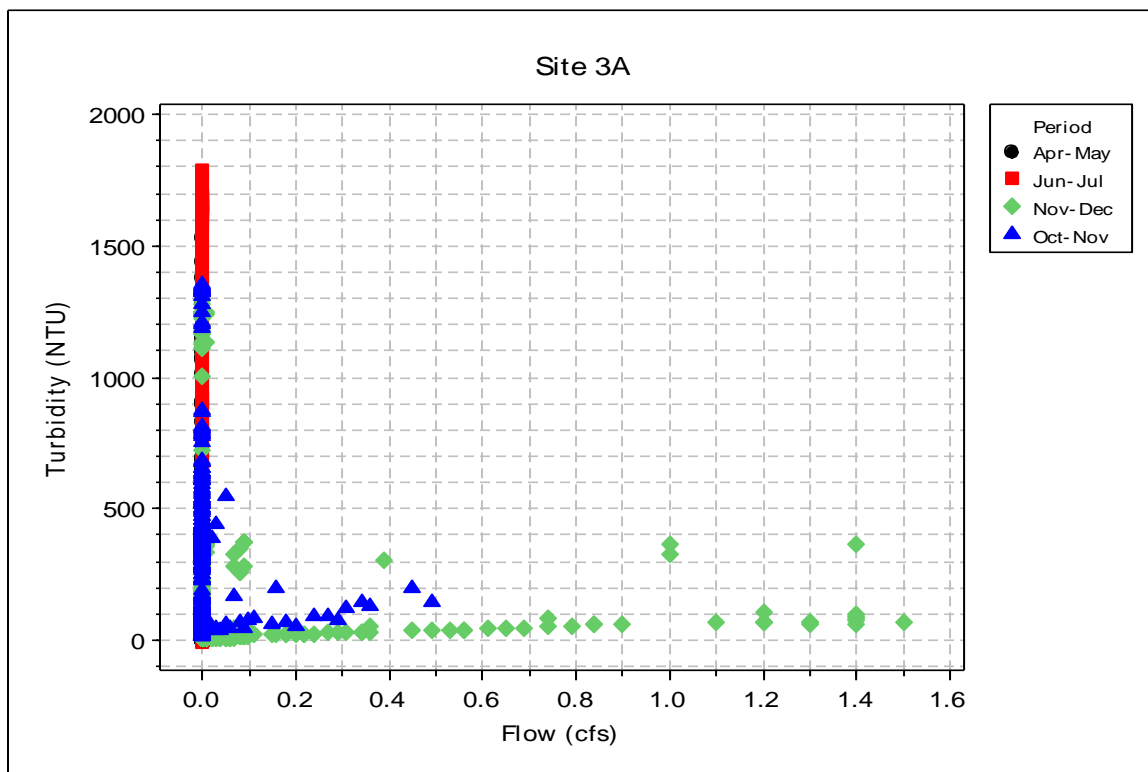


Figure 48. Relationship of turbidity versus streamflow based on automated monitoring data at site 3A. All NTU values were utilized for this display, including negative numbers.

Similar to site 1G, site 4A generally exhibited increasing levels of turbidity shortly after increased streamflow and had the highest readings (1400 to 1600 NTU) at intermediate flows (20 - 40cfs) versus extremely high flows (Figure 49 and Figure 50). Site 5B, however, did not appear to exhibit a consistent relationship between flow and observed turbidity (Figure 51 and Figure 52). Elevated turbidity above 400 NTU was observed frequently in the fall of 2011, and infrequently observed as high as 1500 NTU during summer months.

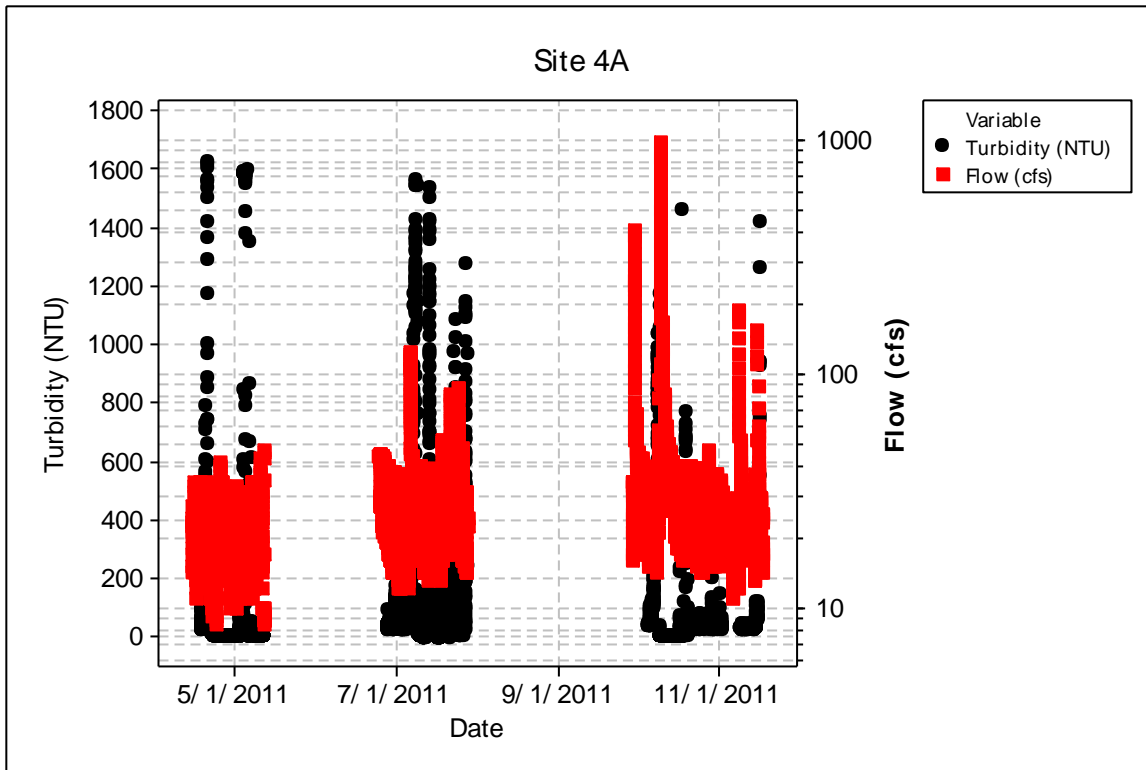


Figure 49. Trends in turbidity and streamflow based on automated monitoring data at site 4A during the study period. All NTU values were utilized for this display, including negative numbers.

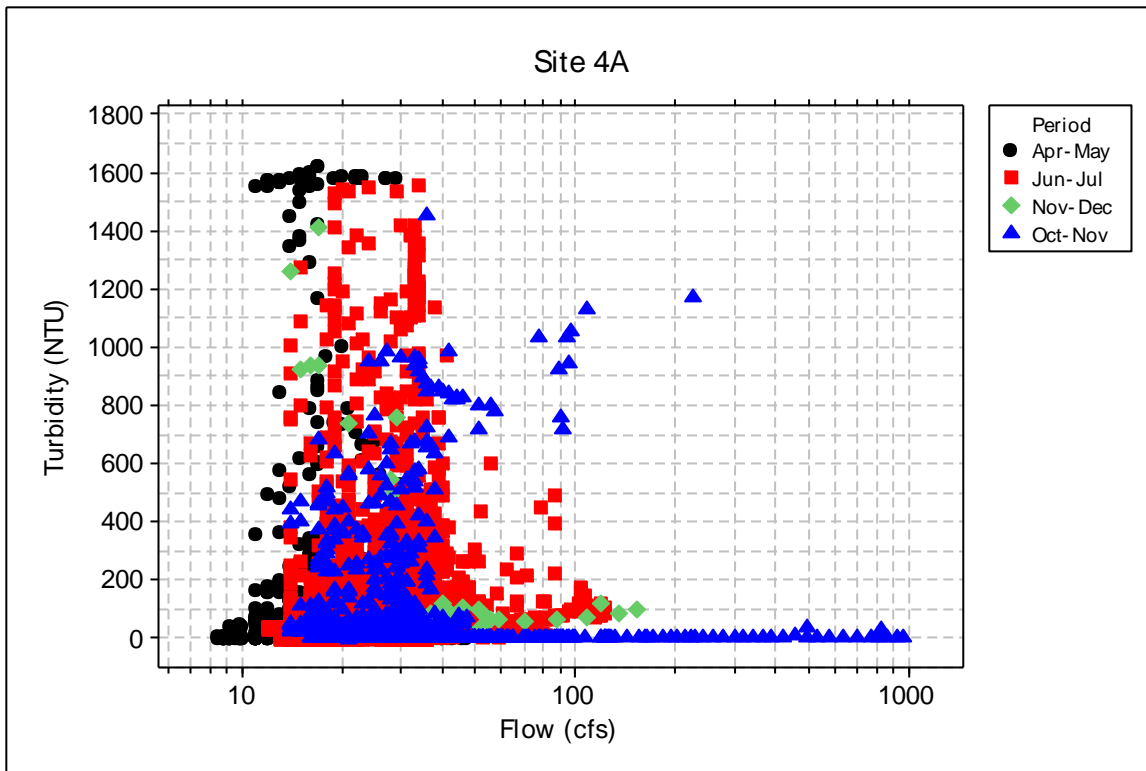


Figure 50. Relationship between turbidity versus streamflow based on automated monitoring data at site 4A. All NTU values were utilized for this display including negative numbers. Note log scale of x-axis (flow).

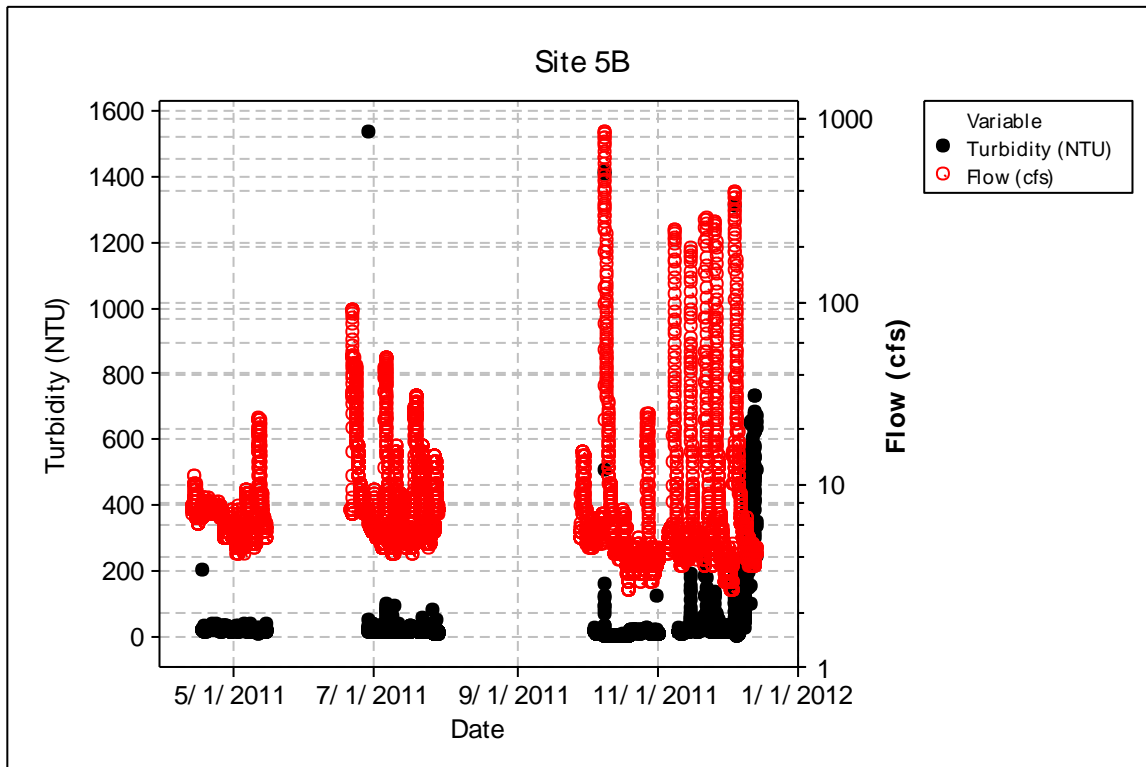


Figure 51. Trends in turbidity and streamflow based on automated monitoring data observed at site 5B during the study period. Note that all NTU values were utilized for this display, including negative number, and the log scale used for streamflow.

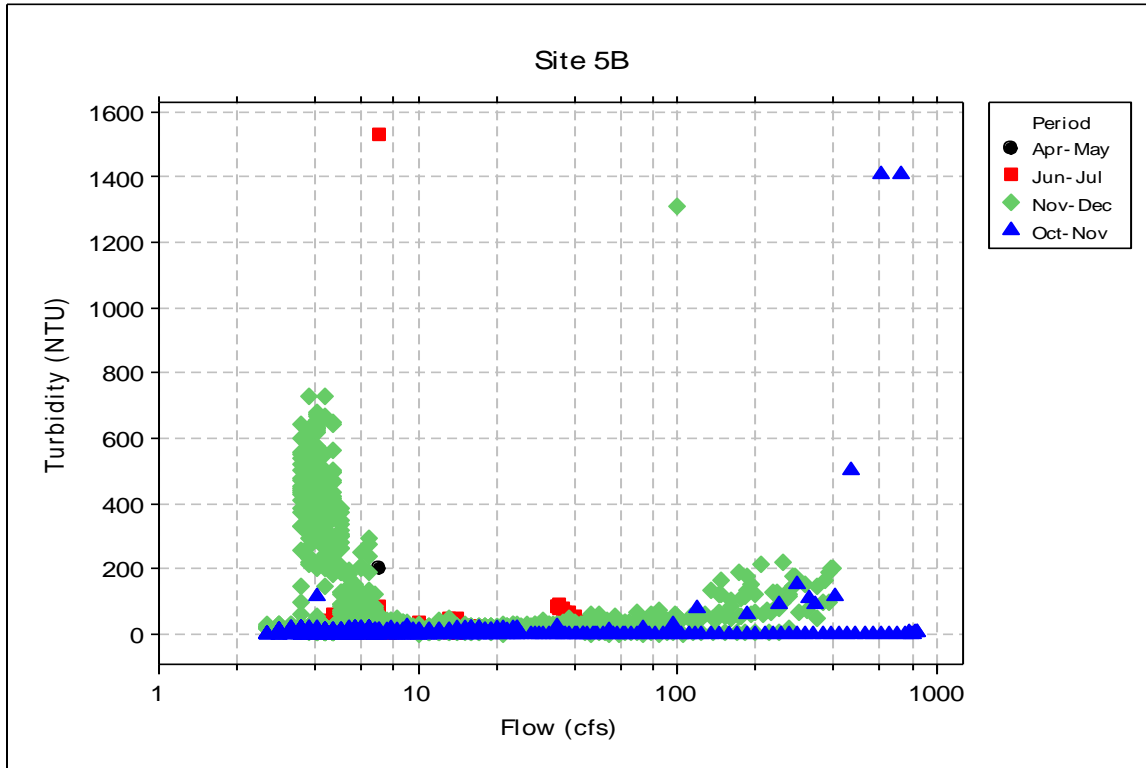


Figure 52. Relationship between turbidity versus streamflow at site 5B based on automated monitoring data. All NTU values were utilized for this display, including negative numbers. Note log scale of x-axis (flow).

Stormflow hydrographs are frequently characterized by higher suspended sediment concentrations during the rising limb than the falling limb, referred to as a type-1 hysteresis loop (Figure 53) (Brandes et al. 2009). In addition, the timing between storm events also influences the availability of fine-grained sediment from the watershed, such that an initial stormflow following relatively dry conditions usually has a greater SSC than subsequent flows of similar magnitude (Figure 54). We will need to further evaluate these data against non-linear modeling approaches to determine if this occurred during our study, i.e. modal response to increases flows which exhibits a different response in the dependent variable (turbidity) during the increasing arm of the hydrograph versus on the receding end when flows again equal the same magnitude.

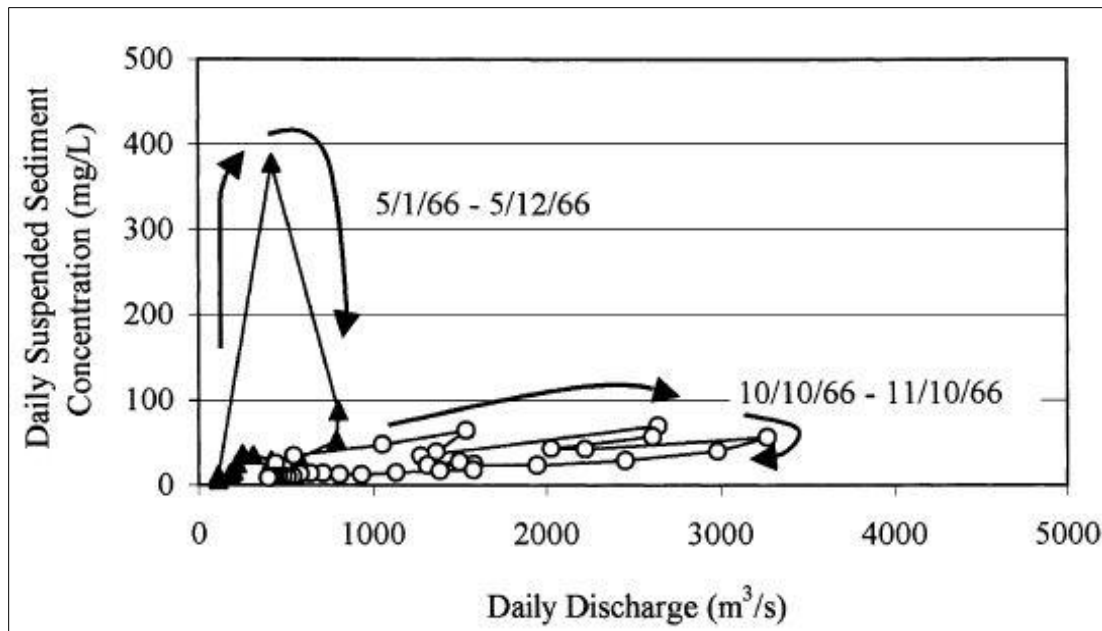


Figure 53. Type-1 hysteresis loop or suspended-sediment concentrations for two stormflow events showing (1) concentrations higher on the rising limb than the falling limb and (2) sediment exhaustion effects for the second, larger flood (from Hudson (2003) referenced in Brandes et al. (2009)).

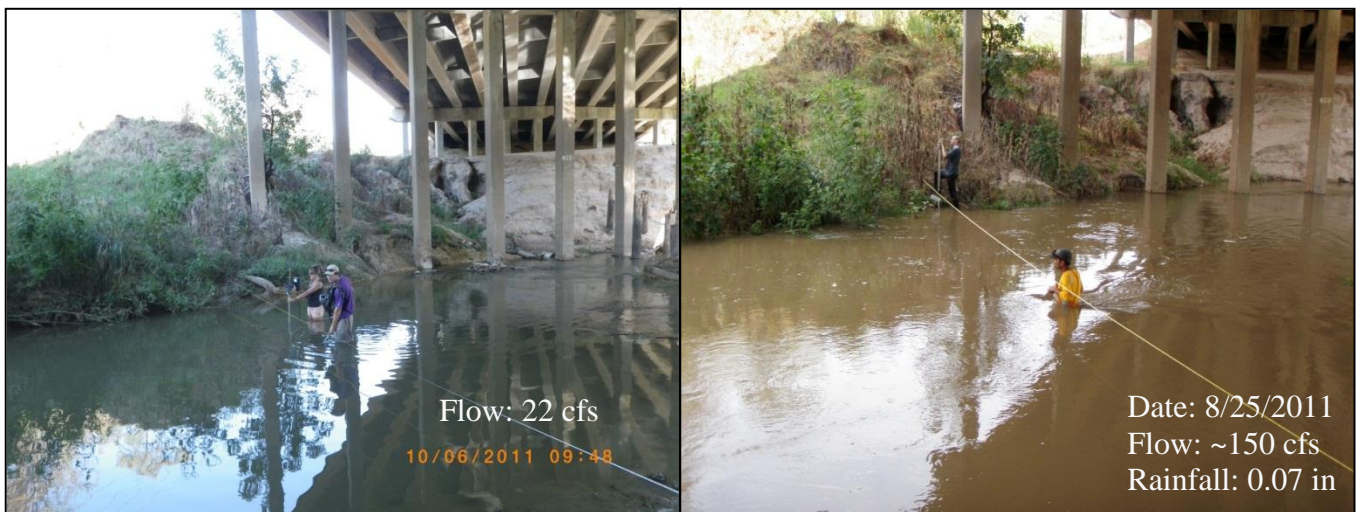


Figure 54. Example of site 2B (located in a large watershed), comparing normal “dry” conditions (left) and rain influenced “wet” conditions (right). Note the appearance of increased suspended sediment in the fast flowing water.

Periodic Monitoring Results

During the study, periodic monitoring yielded hundreds of paired measurements of NTU; including 729 with TSS, 728 with SD and 715 with streamflow. The untransformed streamflow data did not appear to fit the normal distribution. Therefore we attempted to fit the lognormal distribution. In order to do this we had to add 0.01 to each measurement to allow log transformation of zero flow values. This distribution of adjusted streamflow appeared to follow the lognormal distribution (Figure 55). Using this approach and converting back to the original data units suggests that the mean streamflow during PM events was 14 cfs overall for all sites. The estimated 10th and 90th percentile values were 1 and 273 cfs, respectively. The lowest and highest recorded untransformed streamflow were 0 and 1,370 cfs at the 3A and 5A sites, respectively.

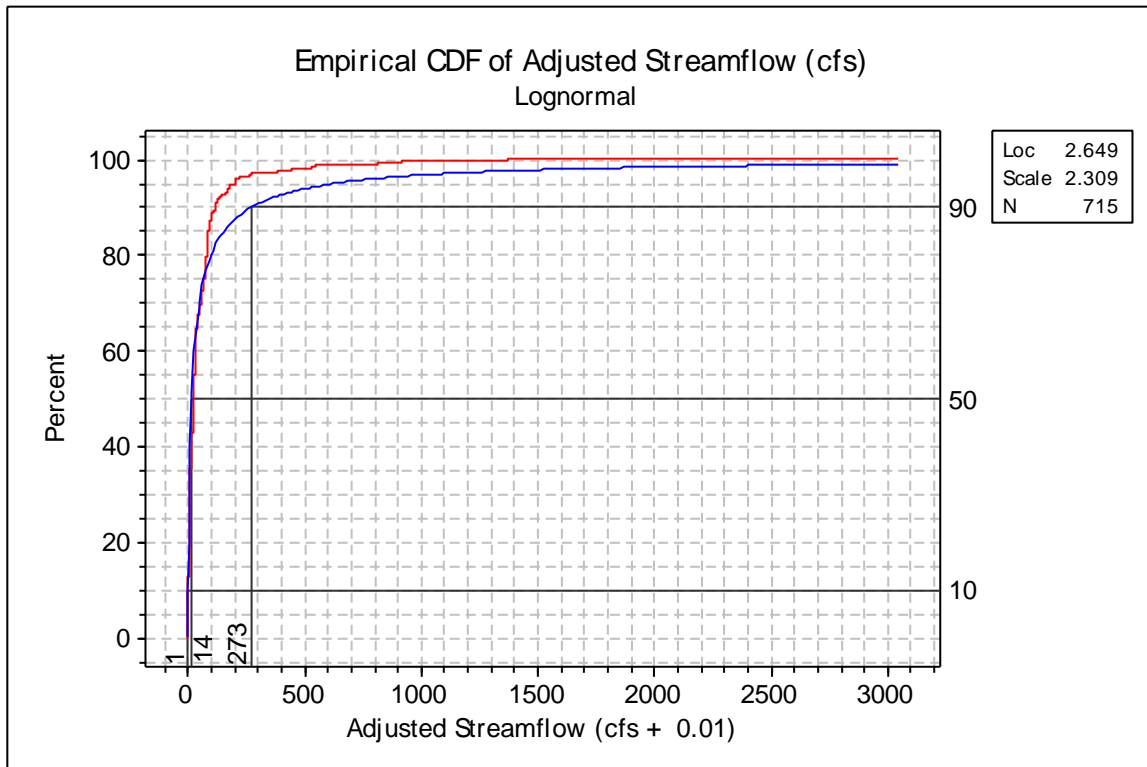


Figure 55. Cumulative distribution of adjusted streamflow (cfs + 0.01) across all sites during this study. Lognormal CDF = blue line.

During 2011, the highest average streamflow observed during TSS and NTU PM grab sampling events was recorded at site 5A (mean 250 cfs) (Figure 56). The lowest (<40 cfs) average streamflow occurred at sites 1G-1P and 5B. Site 3A had the lowest overall mean streamflow (0 cfs), and was only flowing during one site visit, otherwise the water consisted of intermittent pools. Streamflow measured during wet weather sampling was significantly higher in comparison to dry weather periods (Figure 57). The only exception appeared to be site 3A where streamflow was low during the entire study period. Secchi disk transparency best fit the log-normal distribution (Figure 58). The lowest and highest SD values were 0.020 and 1.208 meters at sites 3A and 1H respectively. Average SD values varied considerably but the highest mean values were generally recorded at the 1H, 1M and 5B sites (Figure 59). Site groups 3 and 4 had the overall lowest average SD values (Figure 59).

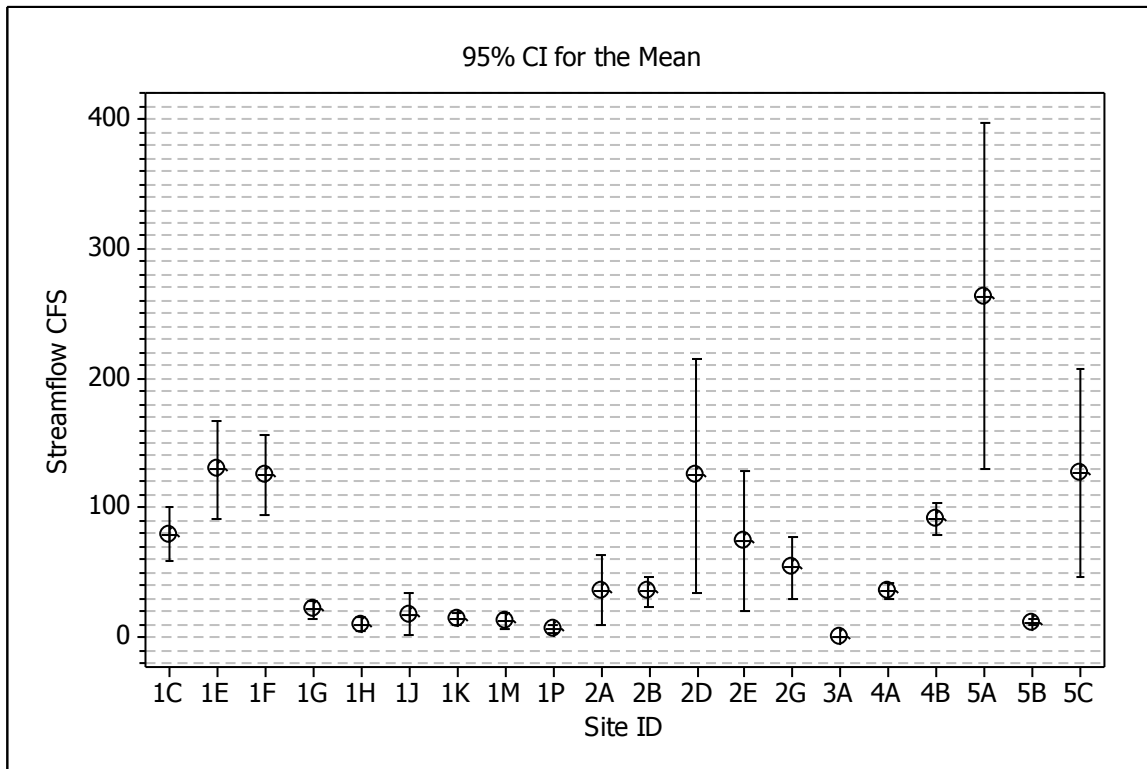


Figure 56. Streamflow levels observed during collection of TSS and NTU samples in 2011.

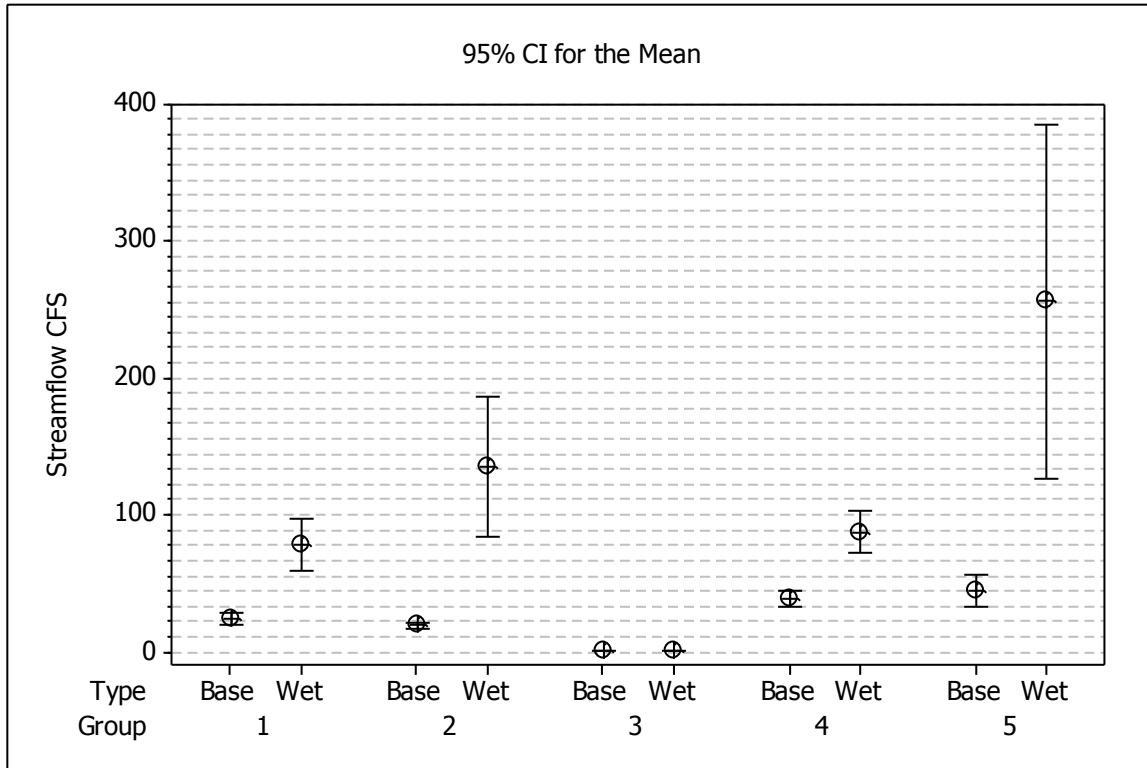


Figure 57. Streamflow measurements during base flow conditions and wet weather sampling for TSS and NTU at each site grouping.

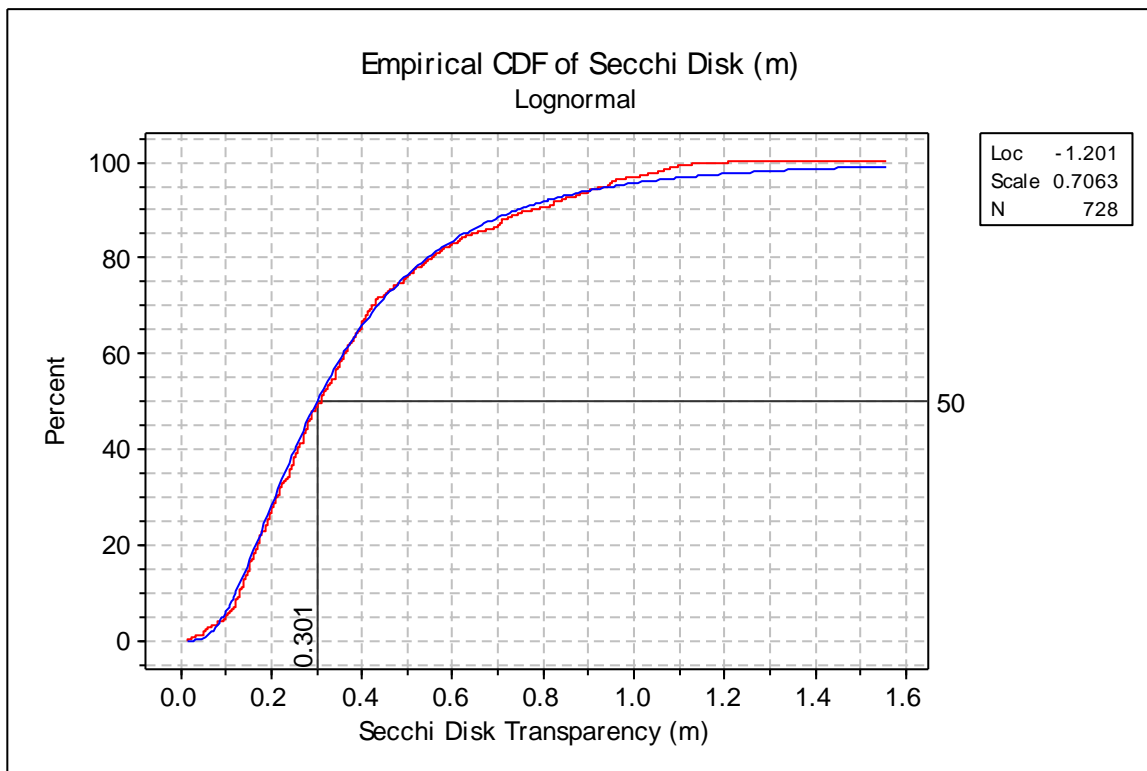


Figure 58. Empirical cumulative distribution function (CDF) of SD (m) across all sites during this study. Lognormal CDF = blue line

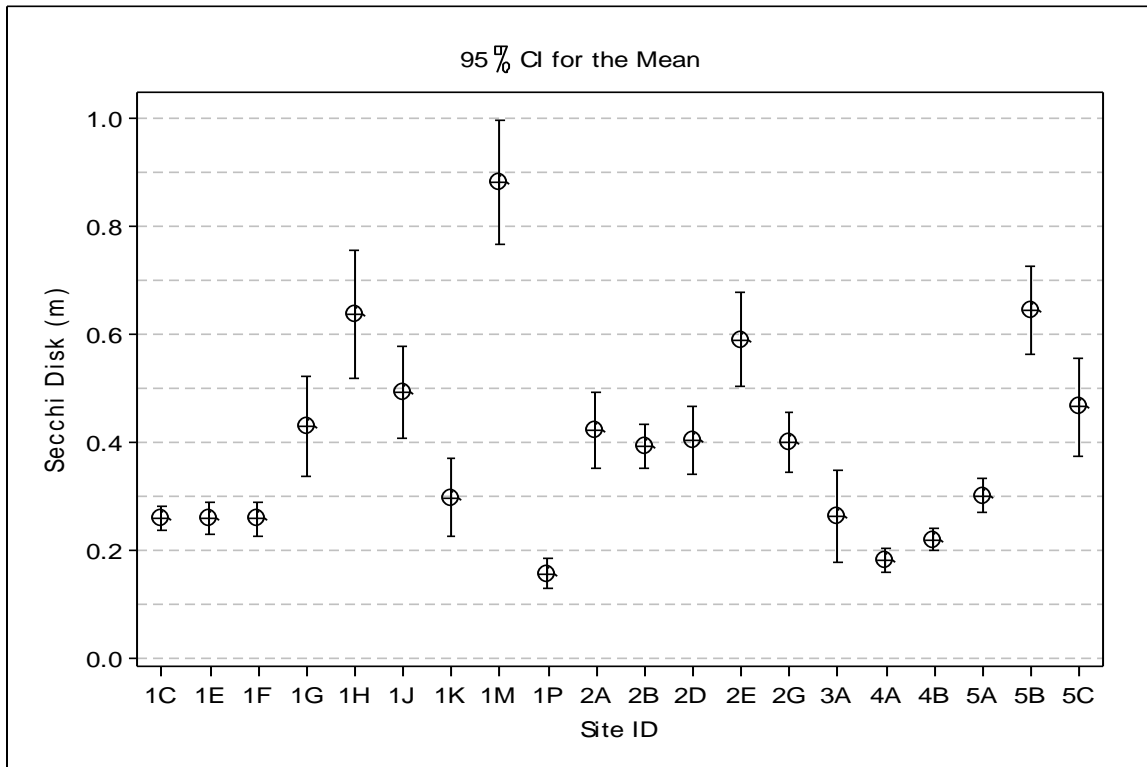


Figure 59. Secchi disk readings at each site of the study. N = 761 Grab samples only

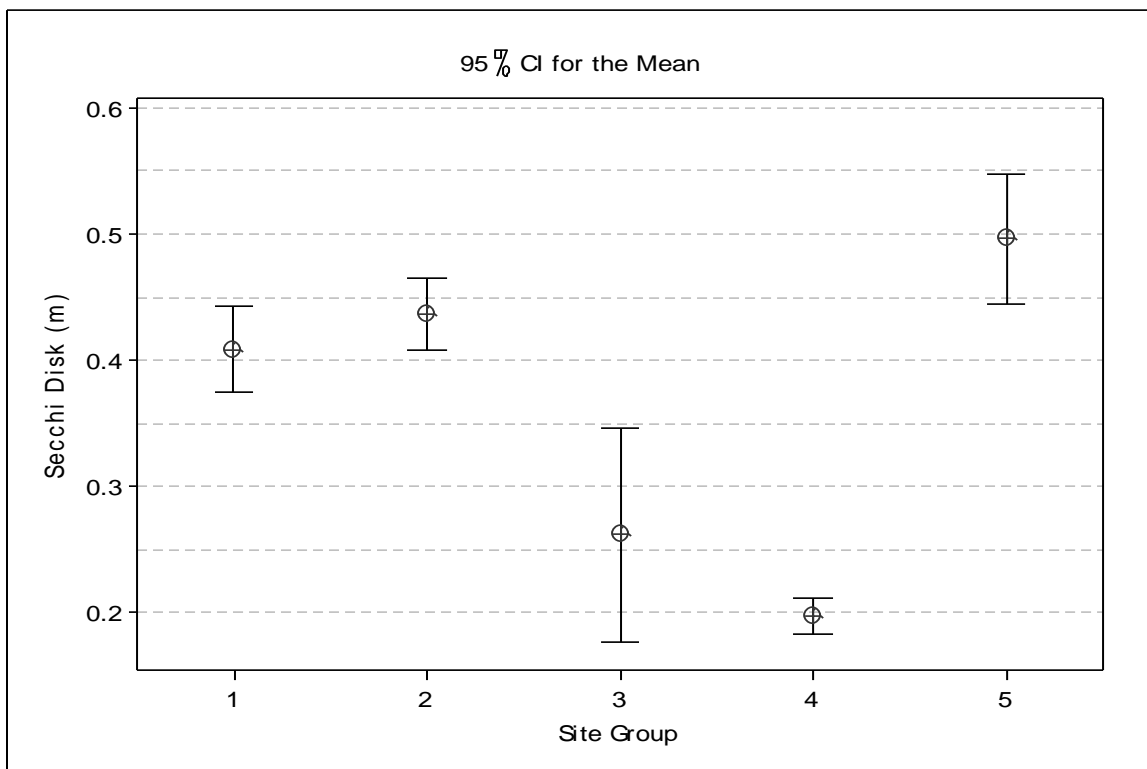


Figure 60. Secchi disk readings for each site group. N = 761

Turbidity data best fit the log-normal distribution (Figure 61). The lowest and highest turbidity values were 3.51 and 187 NTU at sites 1M and 1P, respectively. Average turbidity values were generally below 40 NTU, but the highest mean values were recorded at the 1P and 4A sites (Figure 62). Site group 3 (site 3A) had the overall highest average NTU values (Figure 63).

Total suspended solids data best fit the log-normal distribution (Figure 64). The lowest and highest TSS values were 0.49 and 841.4 mg/L at sites 1H and 3A, respectively. Average TSS values were generally below 100 mg/L. The highest mean value was recorded at site 3A (Figure 65). Site group 3 (site 3A) had the overall highest average TSS values (Figure 66).

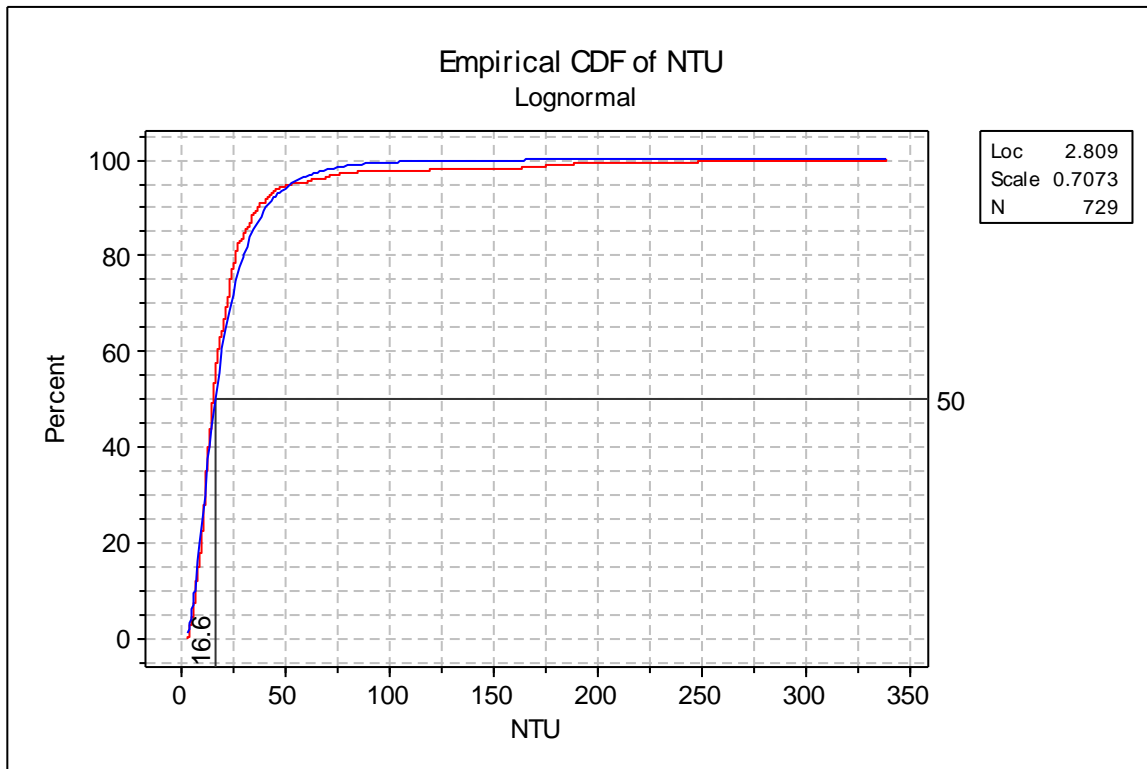


Figure 61. Empirical cumulative distribution function (CDF) of NTU across all sites during this study. Lognormal CDF = blue line

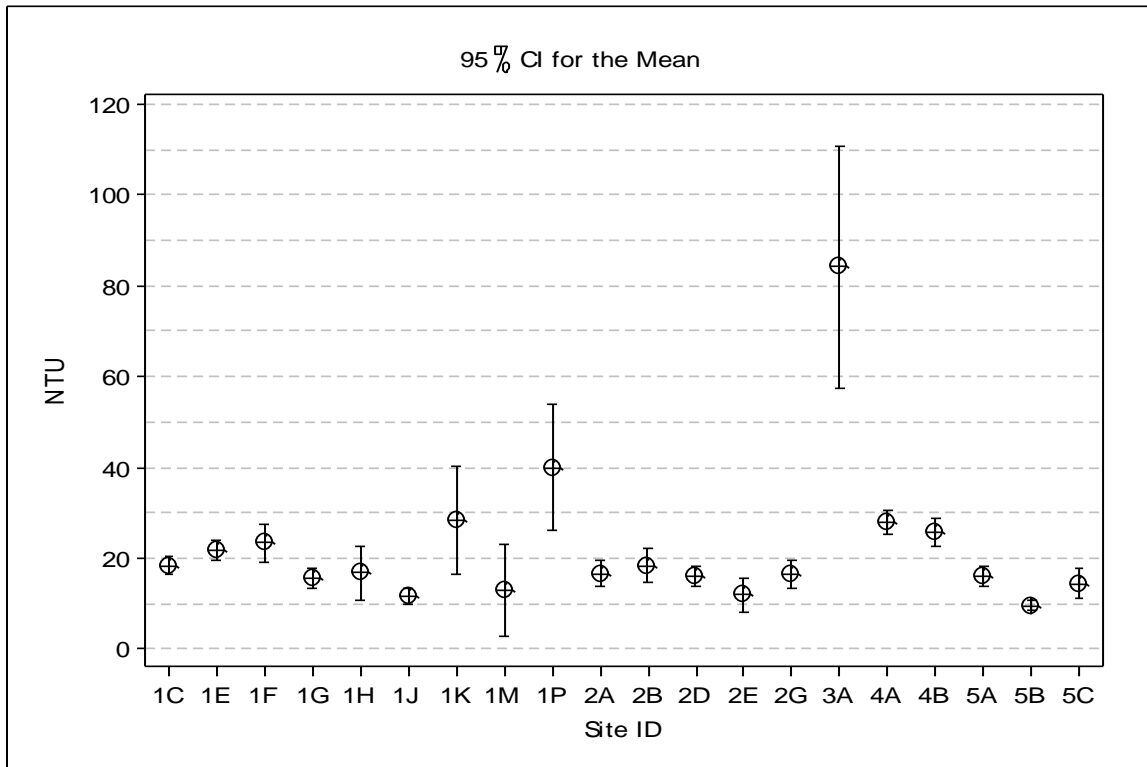


Figure 62. The 95% confidence interval of the mean NTU by site. N = 762

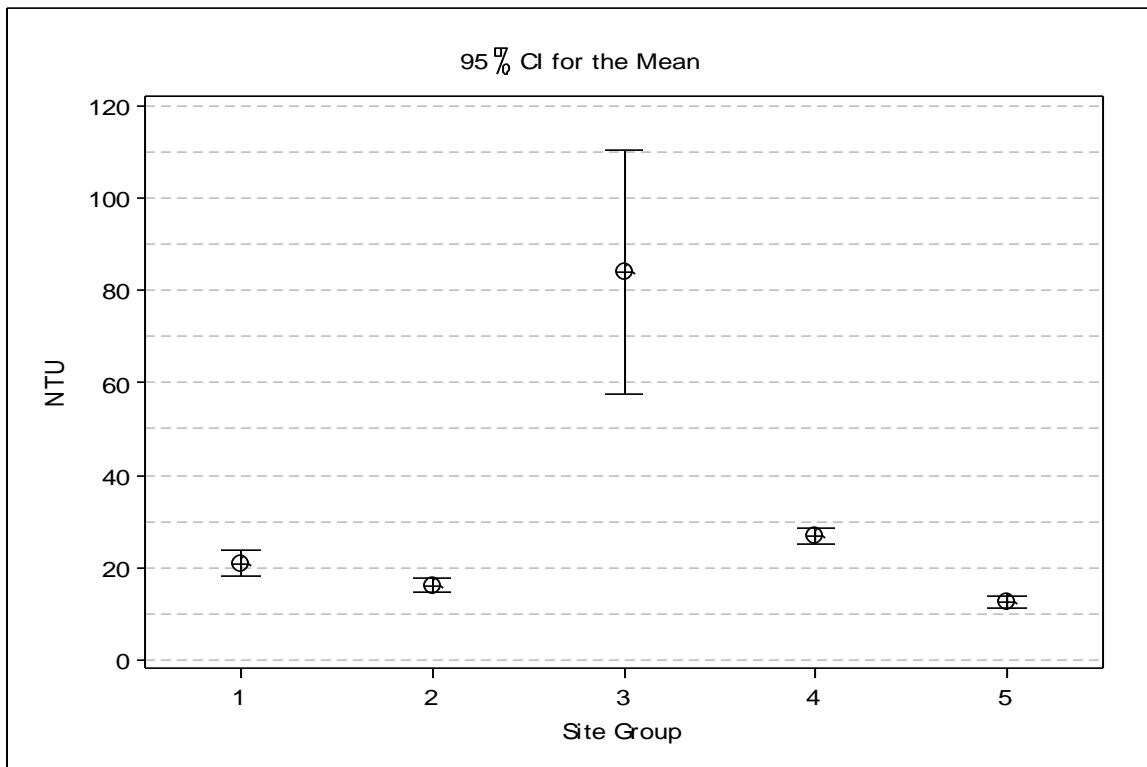


Figure 63. The 95% confidence interval of the mean NTU for each site group evaluated during the study. N = 762

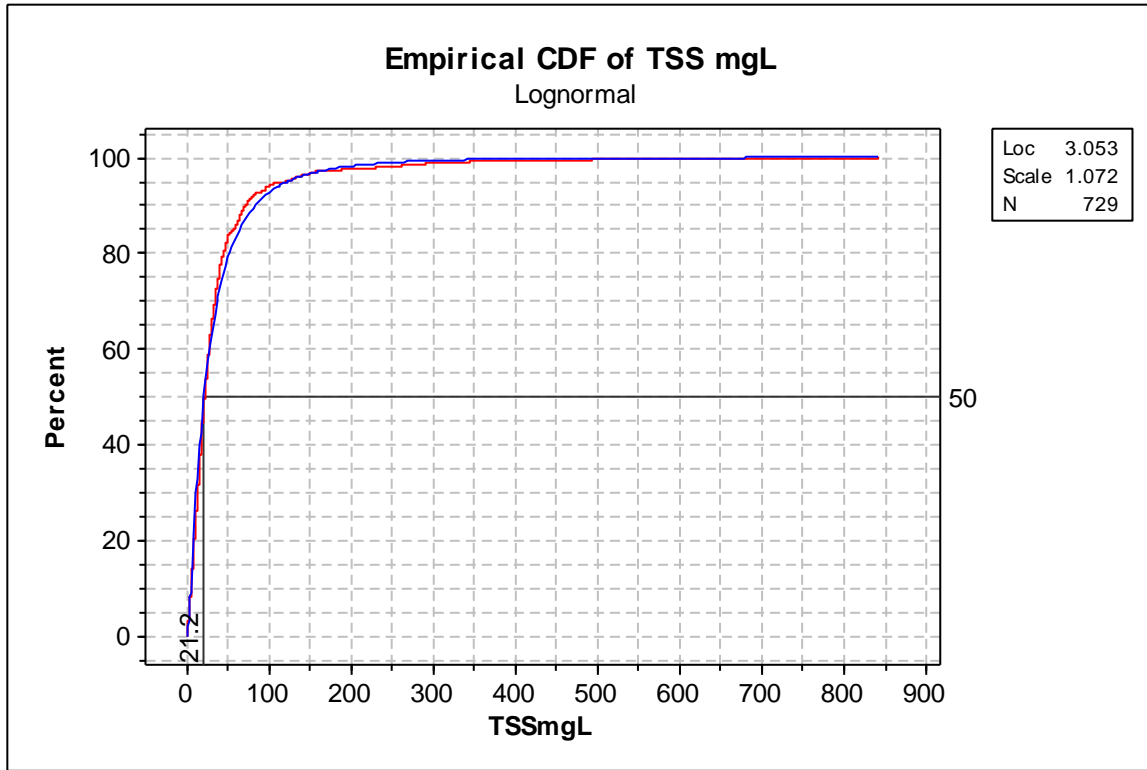


Figure 64. Empirical cumulative distribution function (CDF) of TSS. Lognormal CDF = blue line.

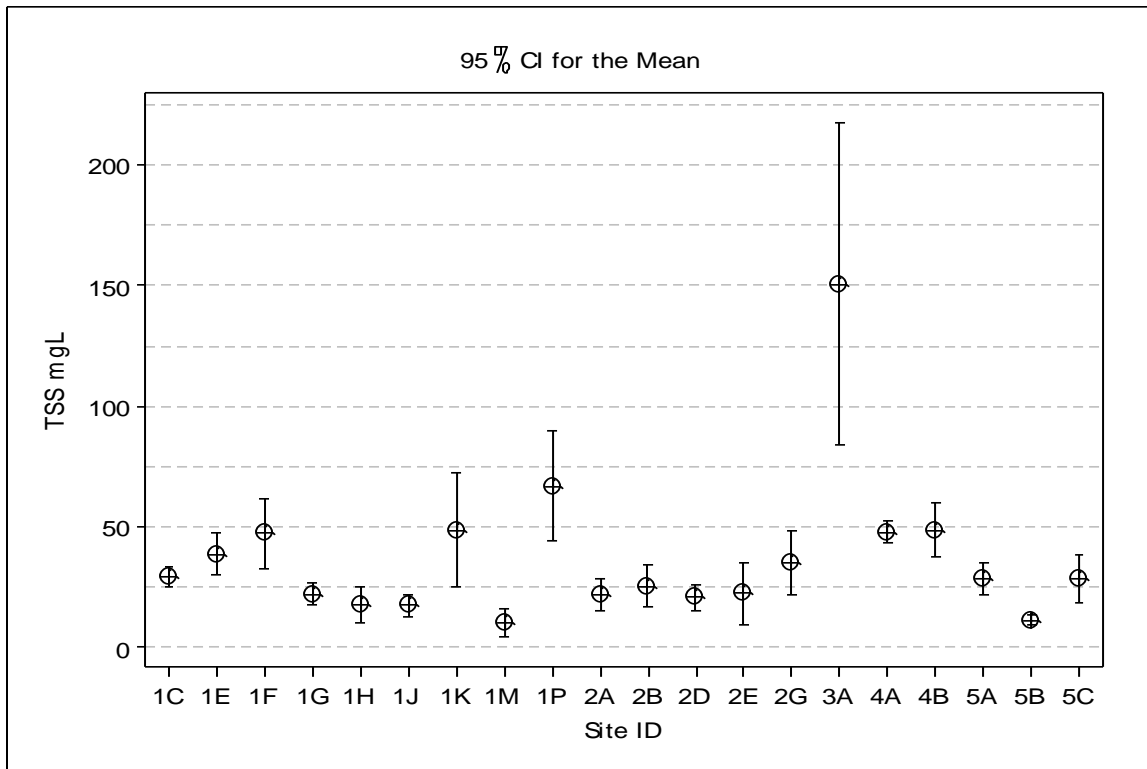


Figure 65. The 95% confidence interval of the mean TSS at each site. Site N = 749

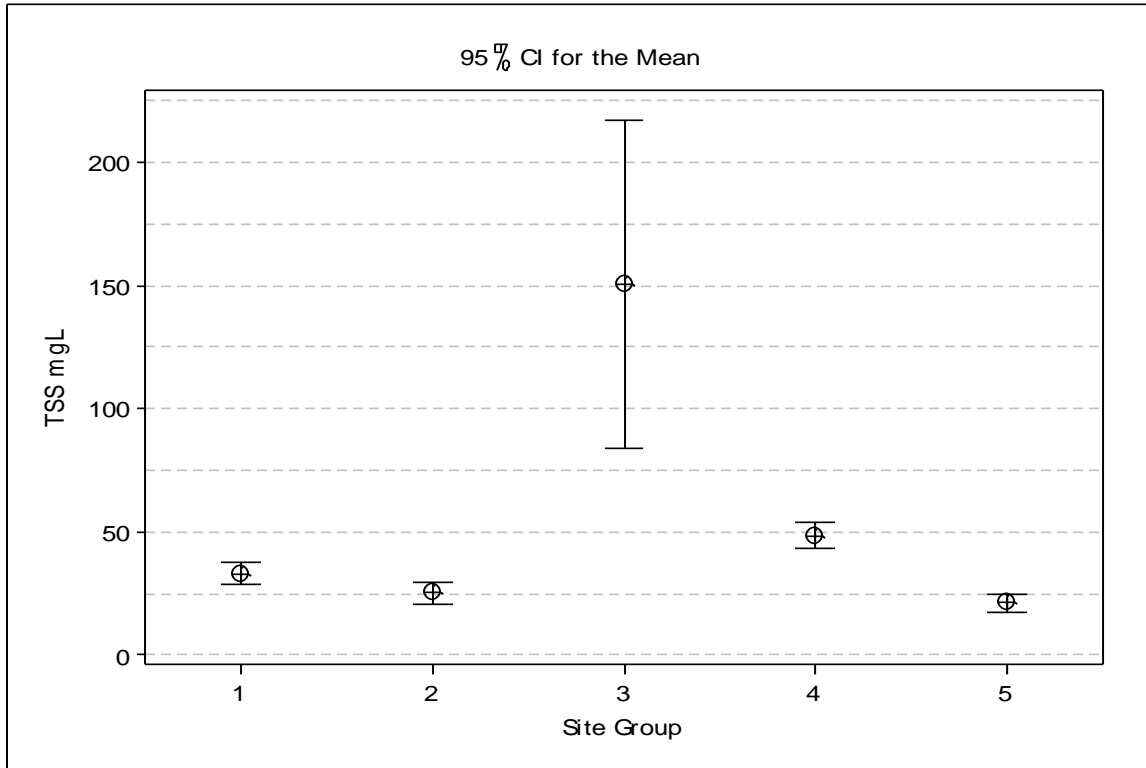


Figure 66. The 95% confidence interval of the mean TSS vs. site group. N=749

A total of 255 paired computed average values for TSS, SD, NTU and streamflow values were derived from the PM events to evaluate the relationship of streamflow and the variables listed. Average TSS values were highly variable at lower streamflow but generally increased to 200 mg/L at 400 cfs (Figure 67). The highest variability in average TSS values occurred at low flows at site 3A. Since streamflow is a function of watershed and stream size, we also analyzed the relationship of TSS concentration and the calculated percent of maximum streamflow recorded at each site during the study (%Maxflow), corresponding to the observed matching streamflow (Figure 68). Except for site 3A, the trend appeared to be more distinct with higher average TSS occurring as streamflow approached maximum observed flow for each waterbody (Figure 68).

Similar trends in average SD were observed with site 3A having a wide range of values over low streamflows (Figure 69 and Figure 70). The trend was most evident when evaluating the response of SD versus %Maxflow. For all sites except 3A, the minimum SD values occurred as %Maxflow exceeded 50%. Similarly, the response of average NTU values followed the pattern of TSS and SD with the maximum NTU values occurring as %Maxflow exceeded 90% (Figure 71 and Figure 72). As with the other metrics, NTU values varied extensively over very low flows, and in particular at site 3A.

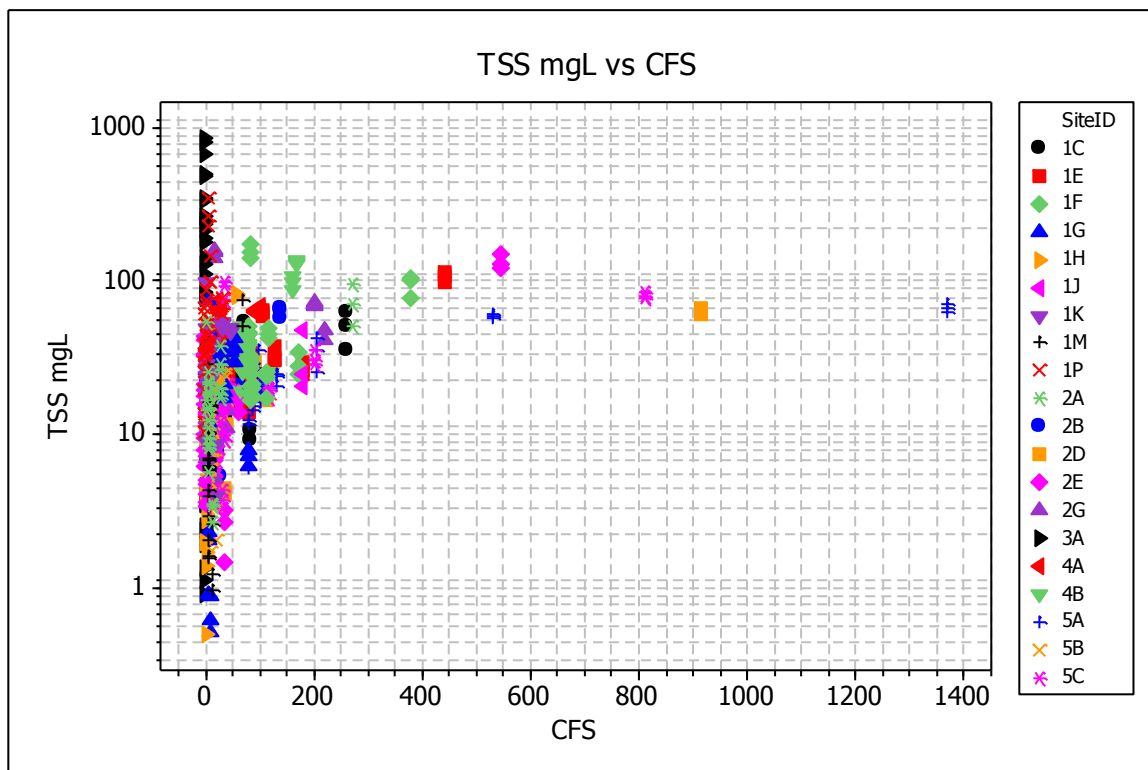


Figure 67. The relationship of TSS versus streamflow for each site based on data from periodic monitoring (PM) events.

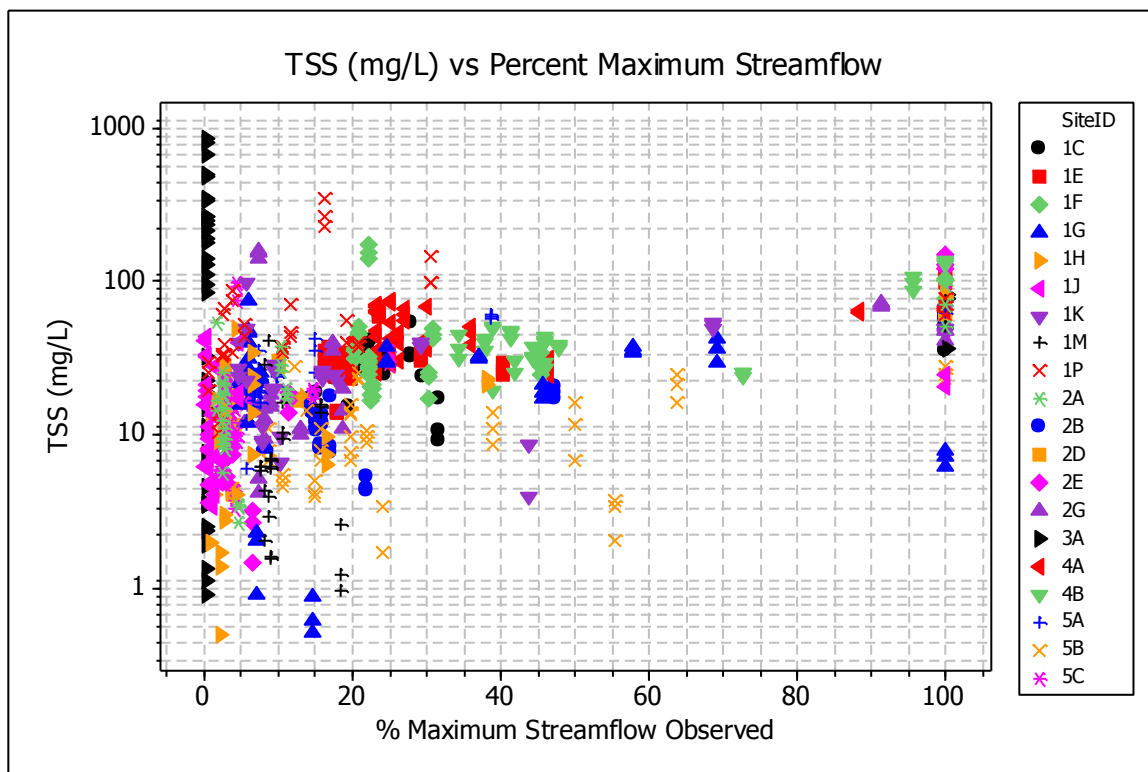


Figure 68. Trends in TSS (log scale) vs. percent maximum streamflow for all monitored sites.

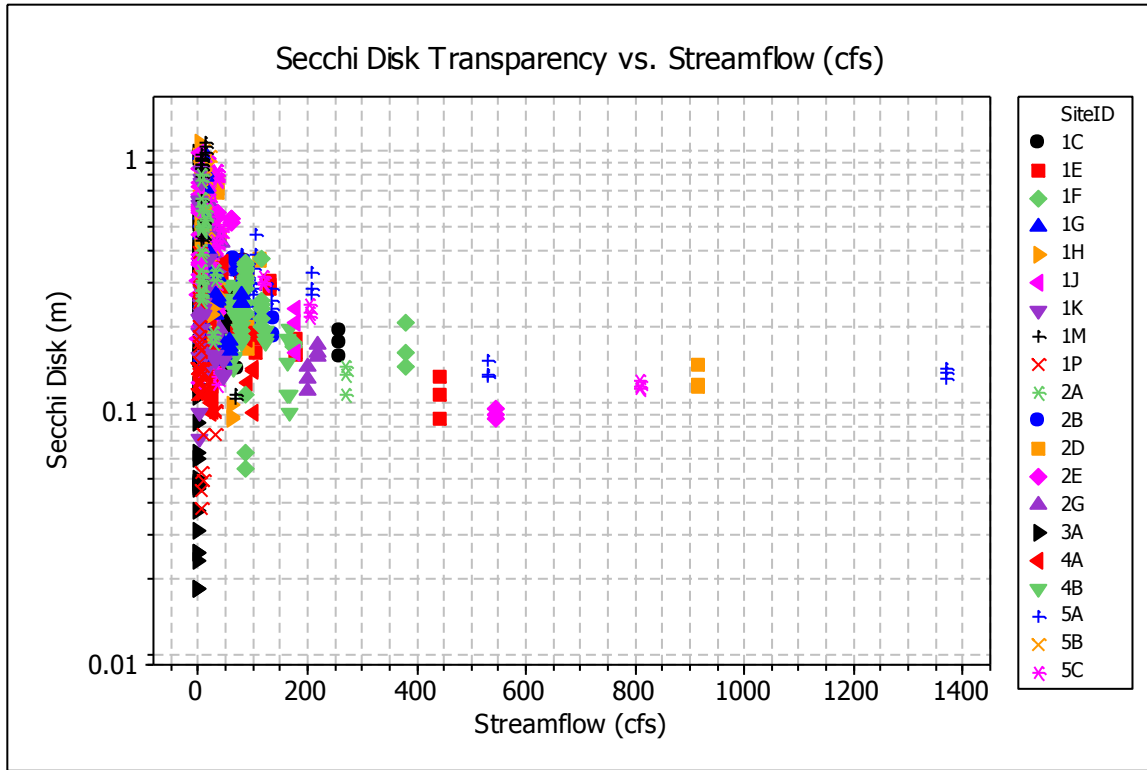


Figure 69. Trends in SD (log scale) versus streamflow for all monitored sites.

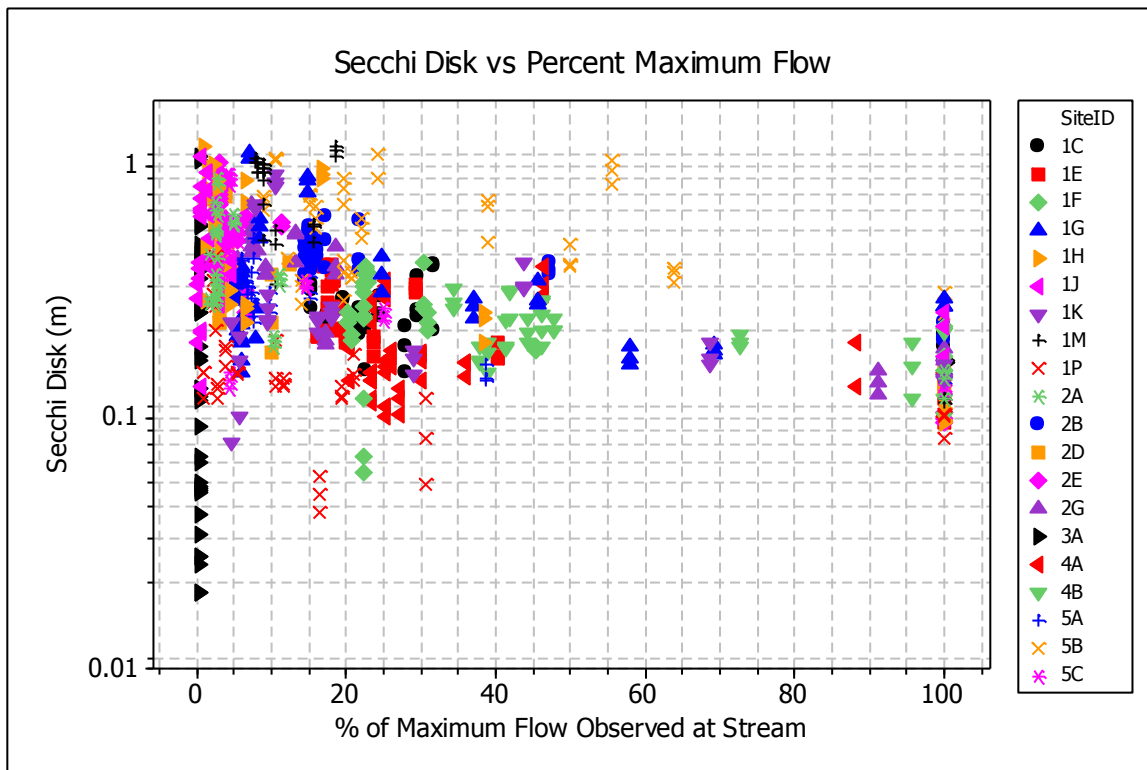


Figure 70. Trends in SD (log scale) versus percent maximum streamflow for all sites.

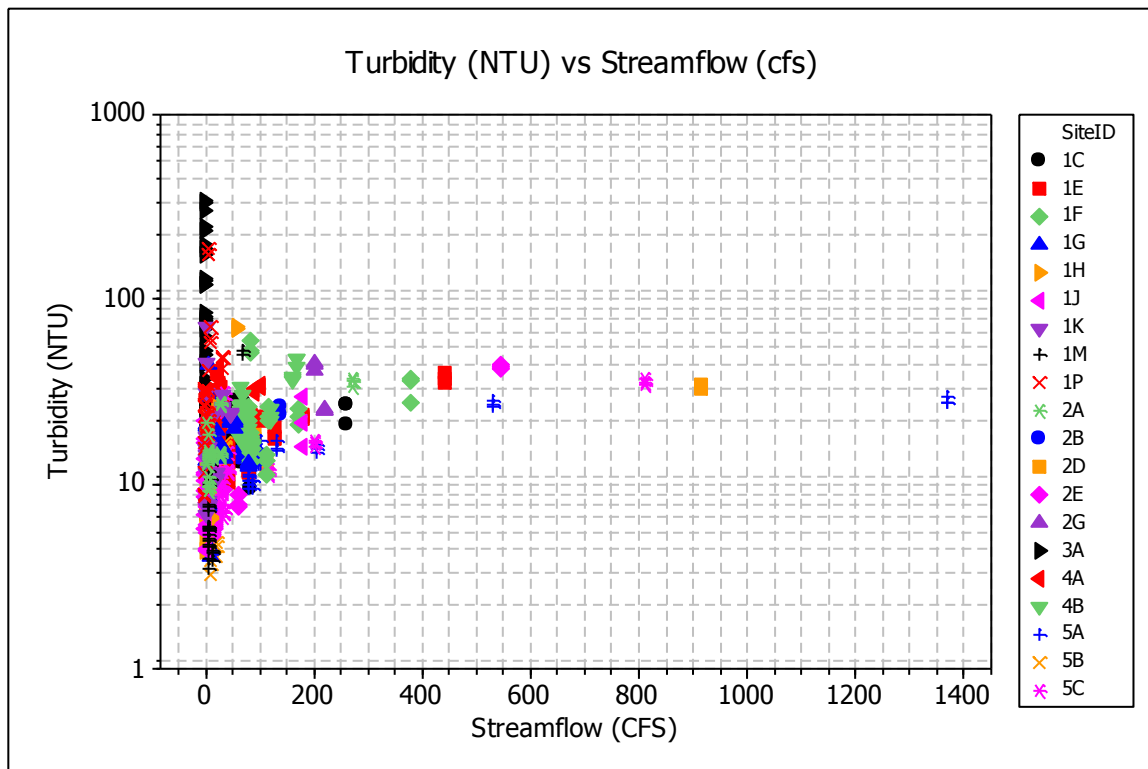


Figure 71. Turbidity (NTU) (log scale) versus streamflow for all sites.

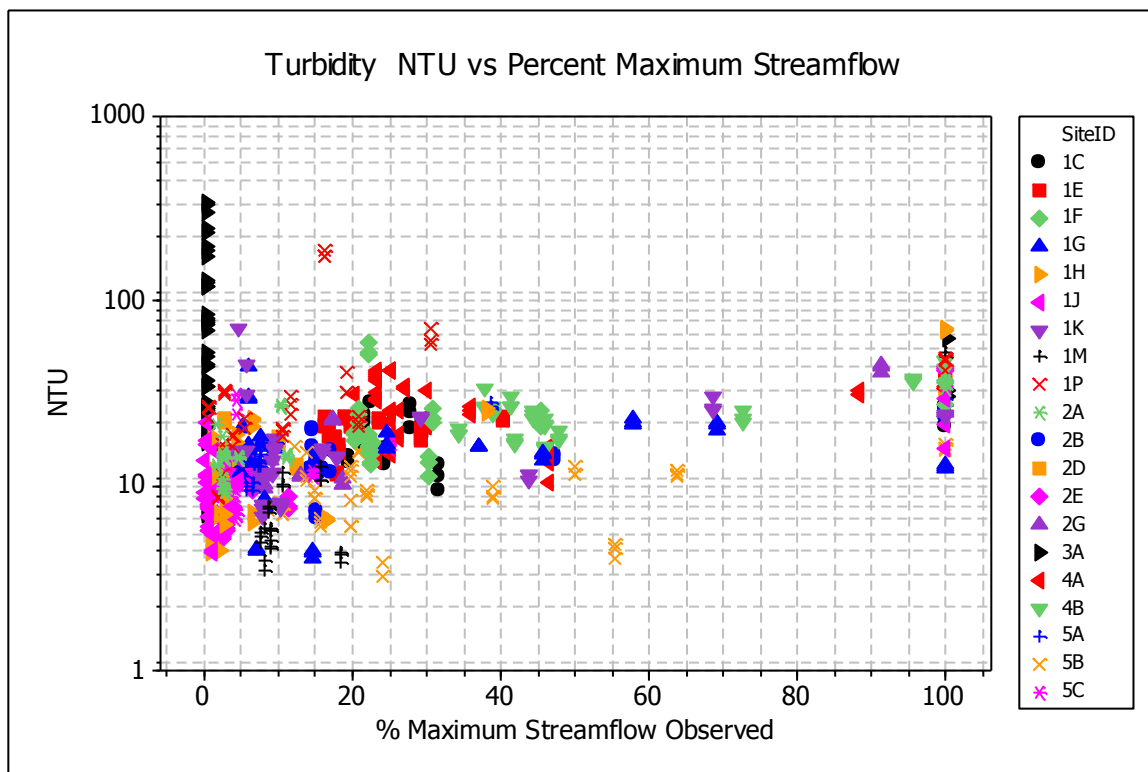


Figure 72. Turbidity (NTU) (log scale) versus percent maximum streamflow for all sites. Streamflow data was obtained from matching values.

During PM, sampling yielded paired measurements of 729 NTU and TSS, and 728 SD measurements. The relationship between these variables was evaluated using linear regression analysis. In order to maximize the use of the data set, we constructed statistical models using NTU, both as an independent variable to predict TSS, and as a dependent variable that can be predicted from TSS or SD readings. The distribution of each of these variables fit the log-normal distribution. Linear models have the desirable trait of having a closed analytical solution. We therefore decided to use a log-log transformation of both variables, otherwise called a power model. However, when possible, we also utilized an untransformed non-linear power model to provide an alternative option for future analysis. Prior to constructing the regression analysis we conducted a simple correlation analysis between paired TSS, NTU and SD measurements and their \log_{10} transformations. The following Pearson correlation coefficients and associated p-values were observed (Table 9).

Table 9. Results of correlation analysis between paired TSS, NTU and SD measurements and their \log_{10} transformations.

Pair	r	p
NTU – SD	-0.436	0.000
TSS – SD	-0.401	0.000
TSS – NTU	0.817	0.000
\log_{10} NTU – \log_{10} SD	-0.913	0.000
\log_{10} TSS – \log_{10} SD	-0.847	0.000
\log_{10} TSS – \log_{10} TSS	0.812	0.000

The higher correlation coefficients and significant p-values suggest that the use of log transformed variables, are an appropriate transformation to remove non-linearity. However, the untransformed TSS and NTU values were highly correlated even without being log transformed.

Linear regression models of the log transformed SD and TSS values yield a fairly predictive model of TSS (Figure 73). The model suggested that as SD readings increase (i.e. turbidity declines, clarity increases) the TSS content will decline as well. The log transformed SD measurements explained 71.7% of the variation in log transformed TSS values. The non-linear power function model also provided an alternative predictive model. Based on this model, the SD measurements explained 62.3% of the variation in TSS (Figure 74).

The log transformed SD measurements and NTU linear regression model fit the data well ($r^2 = 0.834$) (Figure 75). Log transformed SD measurements explained 83.4% of the variation in log transformed NTU values. The non-linear power model using untransformed variables also produced a moderately predictive model (Figure 76). The untransformed SD measurements explained 62.3% of the variation in NTU values.

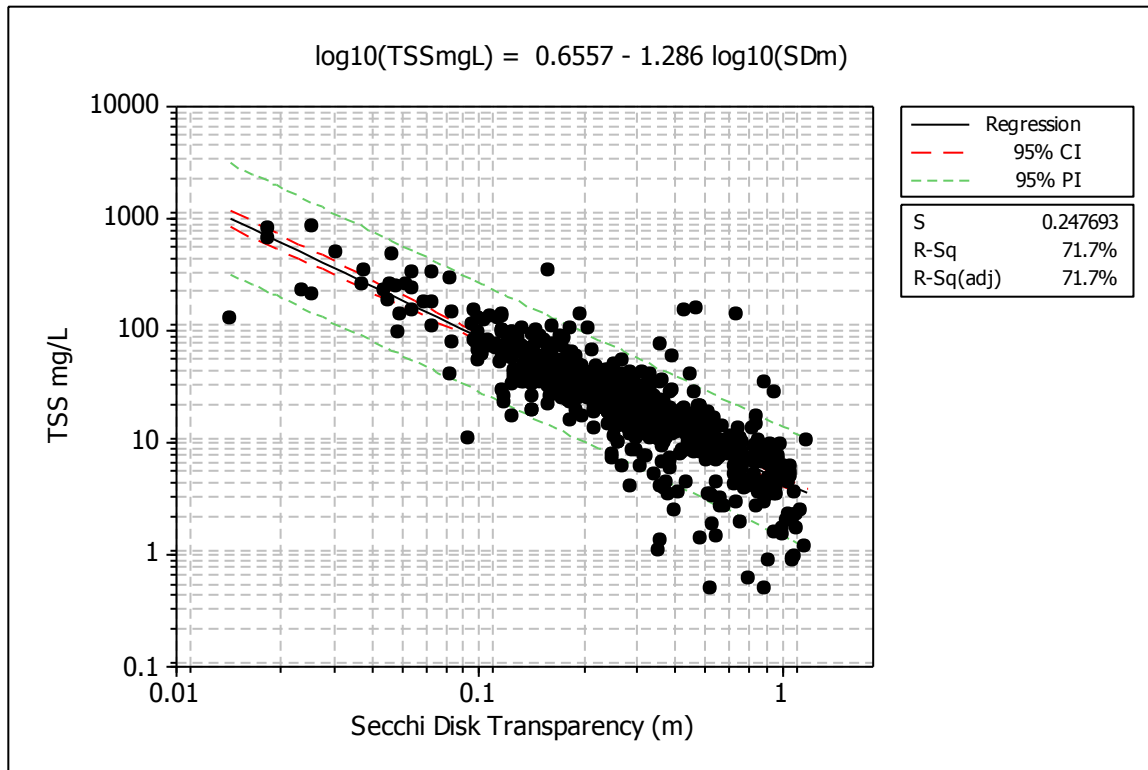


Figure 73. Regression of \log_{10} TSS versus \log_{10} SD based on 727 grab samples. Note log scale.

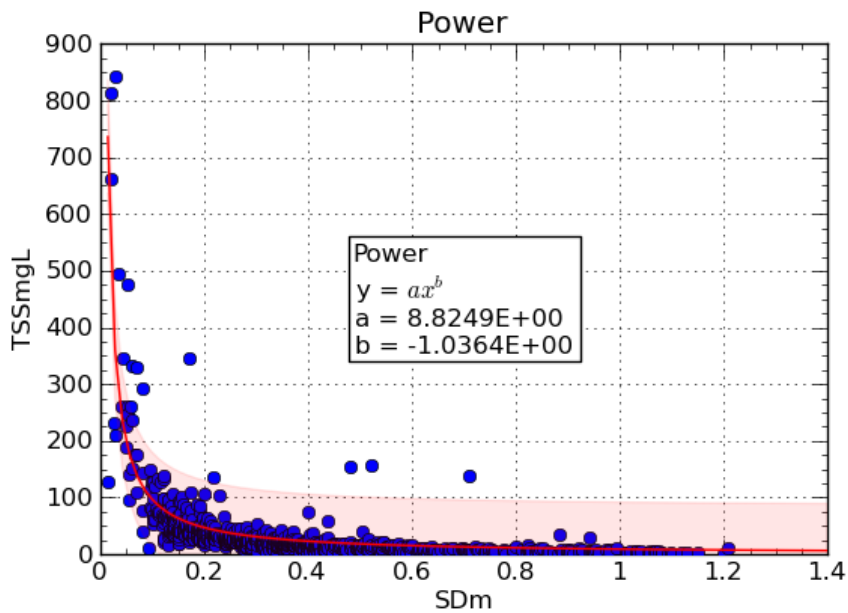


Figure 74. Non-linear model of TSS (mg/L) versus SD (m). $R = 0.789$; $R^2 = 0.623$, outer red shading = 95% confidence interval for mean.

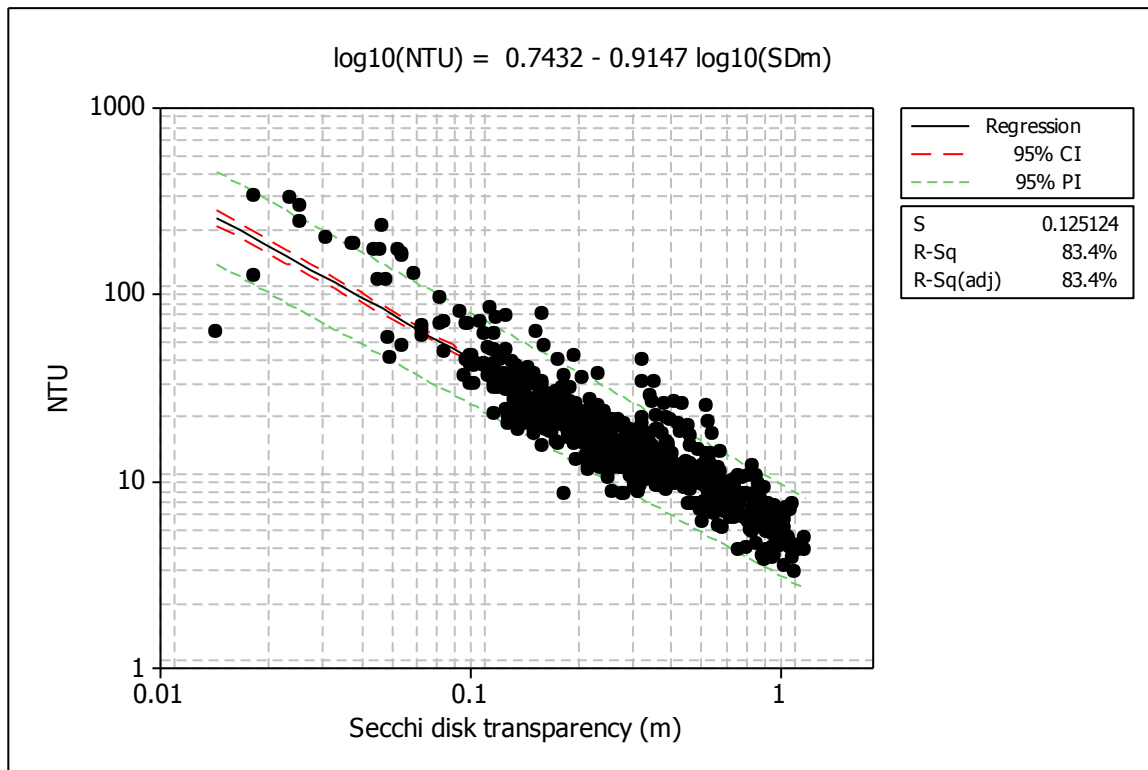


Figure 75. Regression of Log_{10} NTU versus Log_{10} SD transparency based on 727 grab samples. Note log scale.

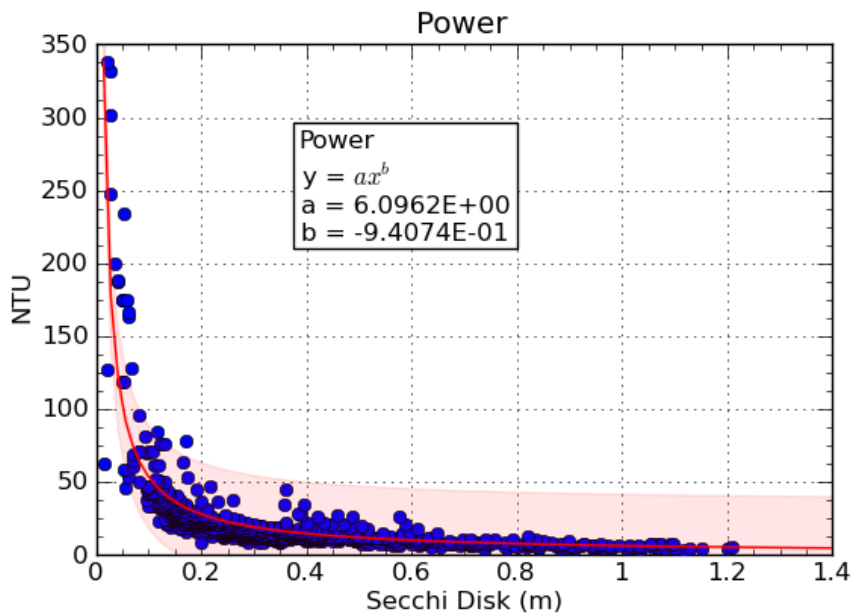


Figure 76. Non-linear model of turbidity (NTU) versus SD (m). $R = 0.827$; $R^2 = 0.683$, outer red shading = 95% confidence interval for mean.

The linear regression model of log transformed TSS values and NTU concentrations yielded a moderately well fit model (Figure 77). The log transformed TSS values explained 65.9% of the variation in the log transformed NTU values. The non-linear regression model fit the data slightly better and yielded a more predictive model. Using the non-linear model, TSS values explained 68.5% of the variation in NTU values (Figure 78).

The last log transformed linear regression model was constructed to predict log TSS from log NTU values (Figure 79). This model fit the data moderately well, with log NTU explaining 65.9% of the variation in log TSS values. The non-linear model was only slightly better with NTU explaining 66.6% of the variation in TSS values.

After completing the construction of the various regression models, we used the two log-transformed regression models that predict NTU using SD and TSS values to estimate and hind cast NTU values for monitoring events archived in the CRP database for Harris County (Figure 81). Although both methods yielded overlapping NTU values, the SD derived distribution contained more values due to the higher number of historical SD values. Where paired TSS and SD data existed, we estimated NTU using both methods. These paired values were analyzed using linear correlation analysis. Although significant, the positive relationship between the different derived NTU values was only moderately strong, $r = 0.658$ (Figure 82). Therefore, users should use caution when using NTU values derived from different predictive models. In general, values generated from the regression model based on log transformed SD and NTU values should be used when possible, since that model was the best fitting and most predictive equation (Figure 75). The majority of derived Harris County NTU values ranged between 5 and 50 NTU.

After estimating the distribution of historical NTU values in Harris County, we compared the distribution of those values with percent impervious land use in the associated HUC 10 units where the original SD and TSS data was collected. The distribution of estimated NTU values varied considerably over the entire range of amounts of impervious land. However at higher percentages of impervious land the upper range of NTU values generally increased (Figure 83). There did not appear to be a discernible relationship between rainfall patterns and predicted historical NTU values (Figure 84).

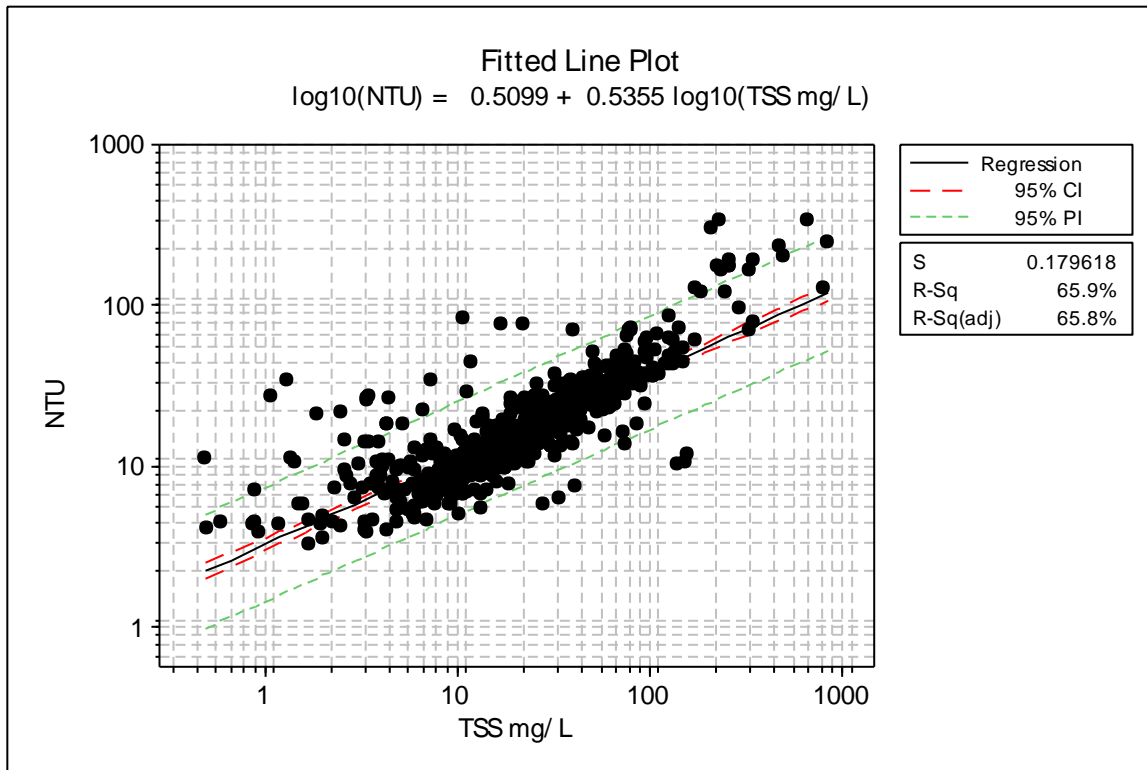


Figure 77. Regression of \log_{10} NTU versus \log_{10} TSS using grab sample results from this study. Note log scale axis.

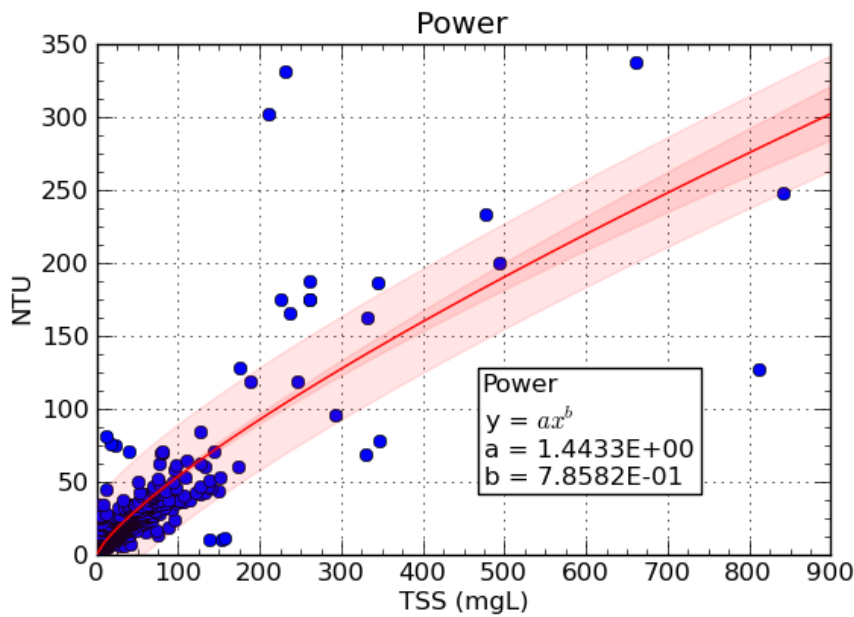


Figure 78. Non-linear model of turbidity (NTU) versus TSS (mg/L). $R = 0.827$; $R^2 = 0.685$, outer red shading = 95% confidence interval for the mean.

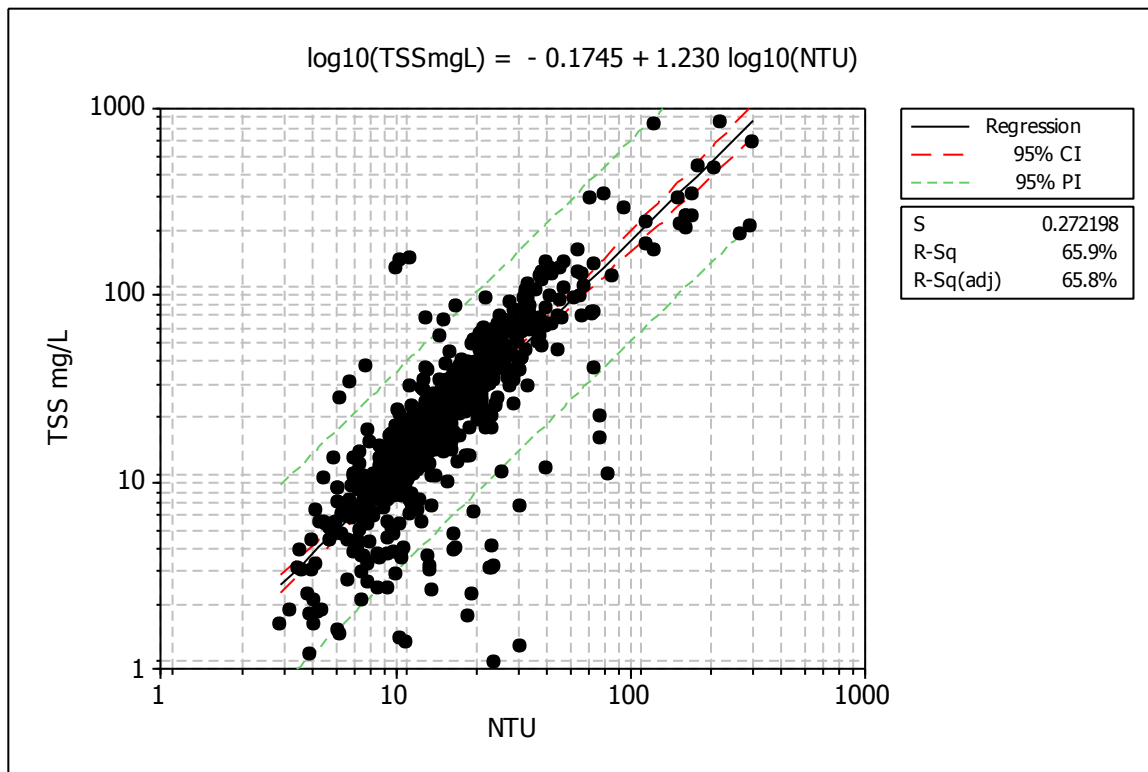


Figure 79. \log_{10} TSS versus \log_{10} NTU regression model based on 728 grab samples. Note log axis scale.

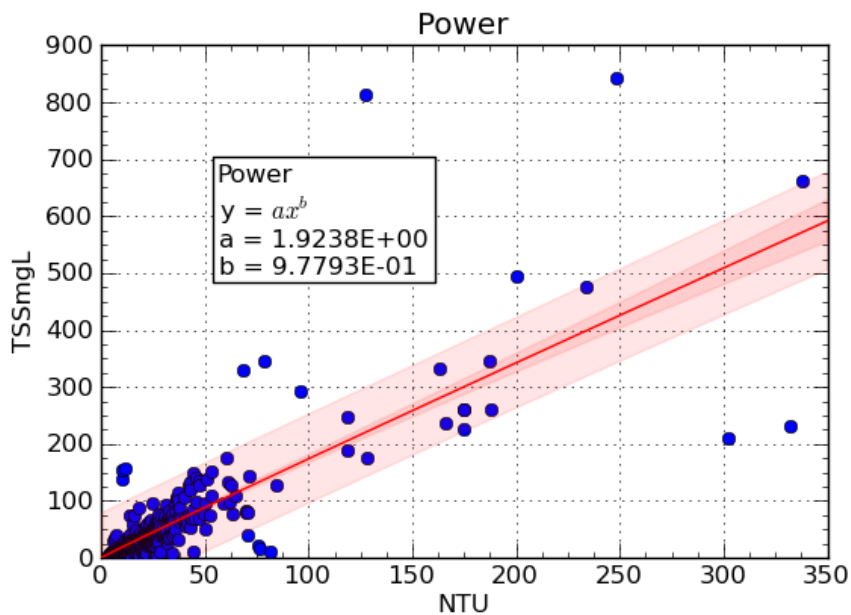


Figure 80. Non-linear model of TSS (mg/L) versus turbidity (NTU). $R = 0.816$; $R^2 = 0.666$, inner darker red shading = 95% confidence interval for mean, outer light red shading = 95% prediction interval for individual values.

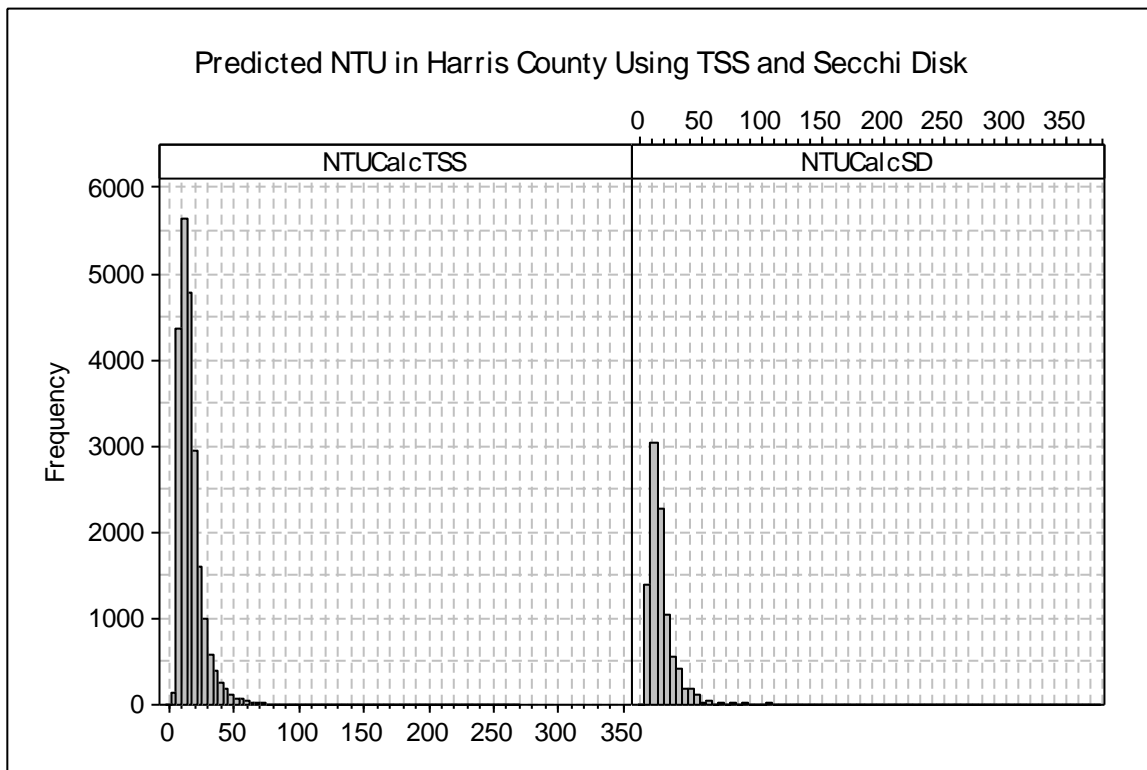


Figure 81. Estimated distribution of derived NTU levels for historical Harris County sites (1/01-9/11) using predictive log-log regression model from current study for TSS and SD.

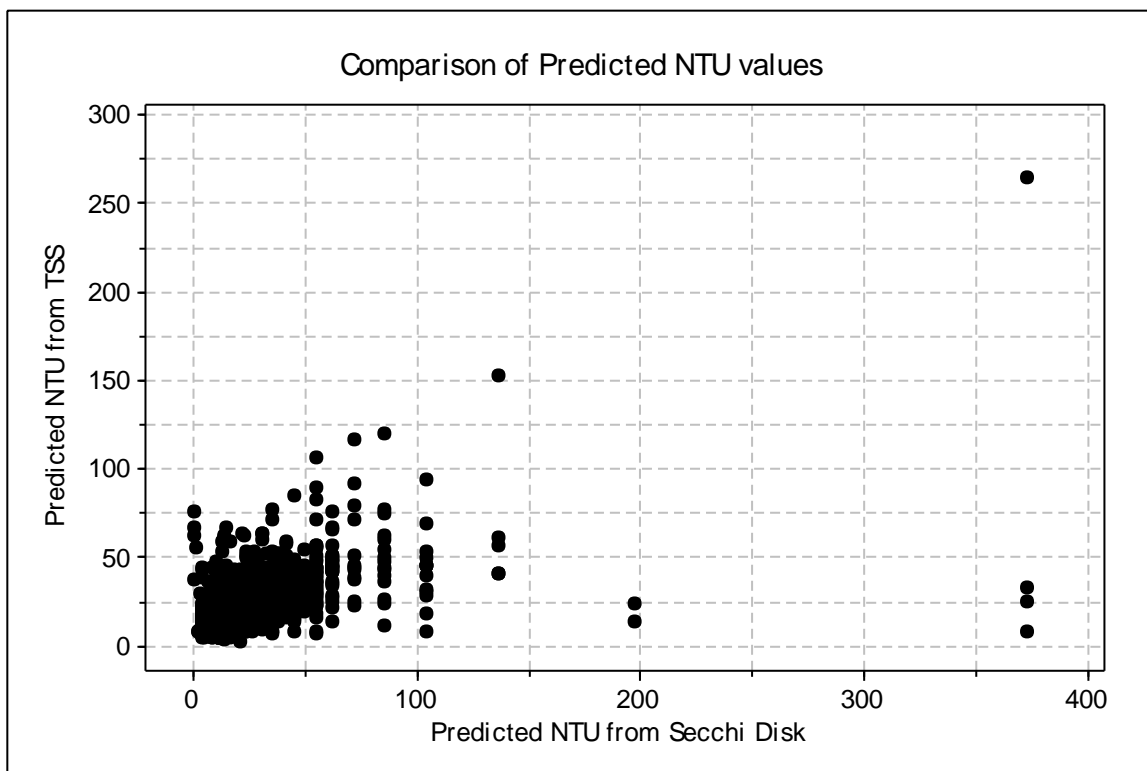


Figure 82. Comparison of derived NTU values for Harris County sites using historical TSS versus SD values during the last 10 years. 1/01 to 9/11. (Pearson correlation coefficient (r) for NTU values derived from TSS vs. SD = 0.658, $p = 0.000$)

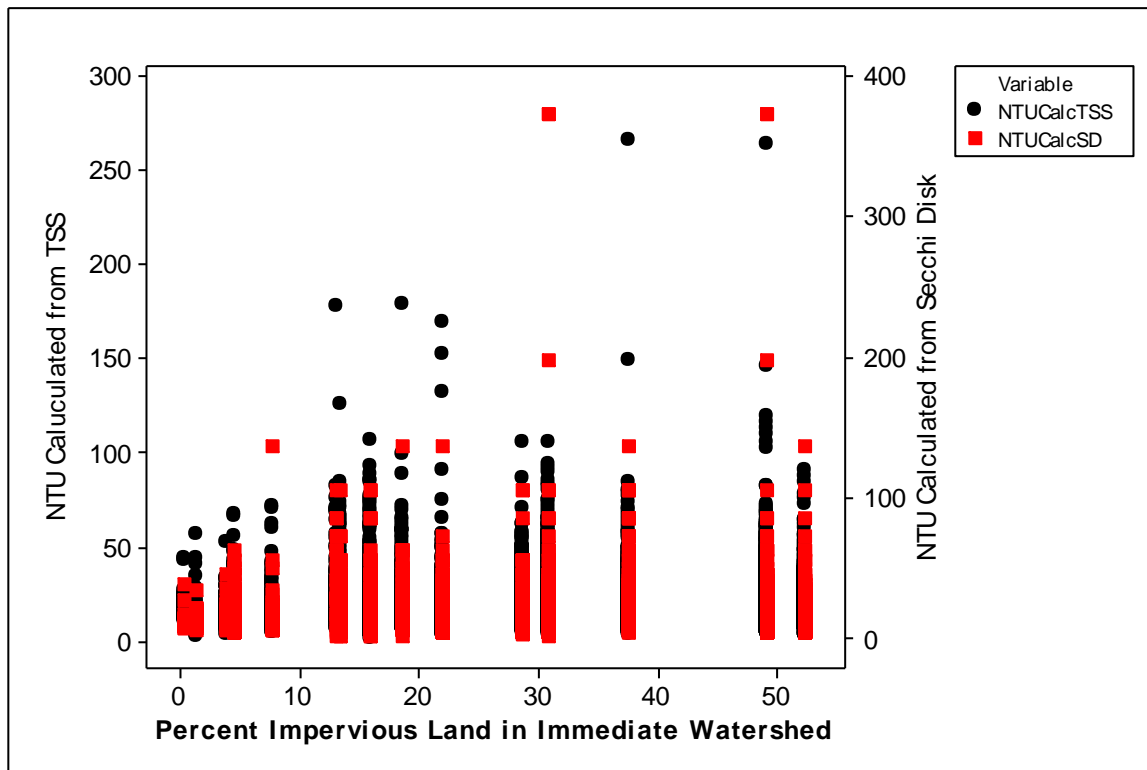


Figure 83. Distribution of predicted NTU versus percent impervious land in Harris County major watersheds as defined by HUC 10 designation.

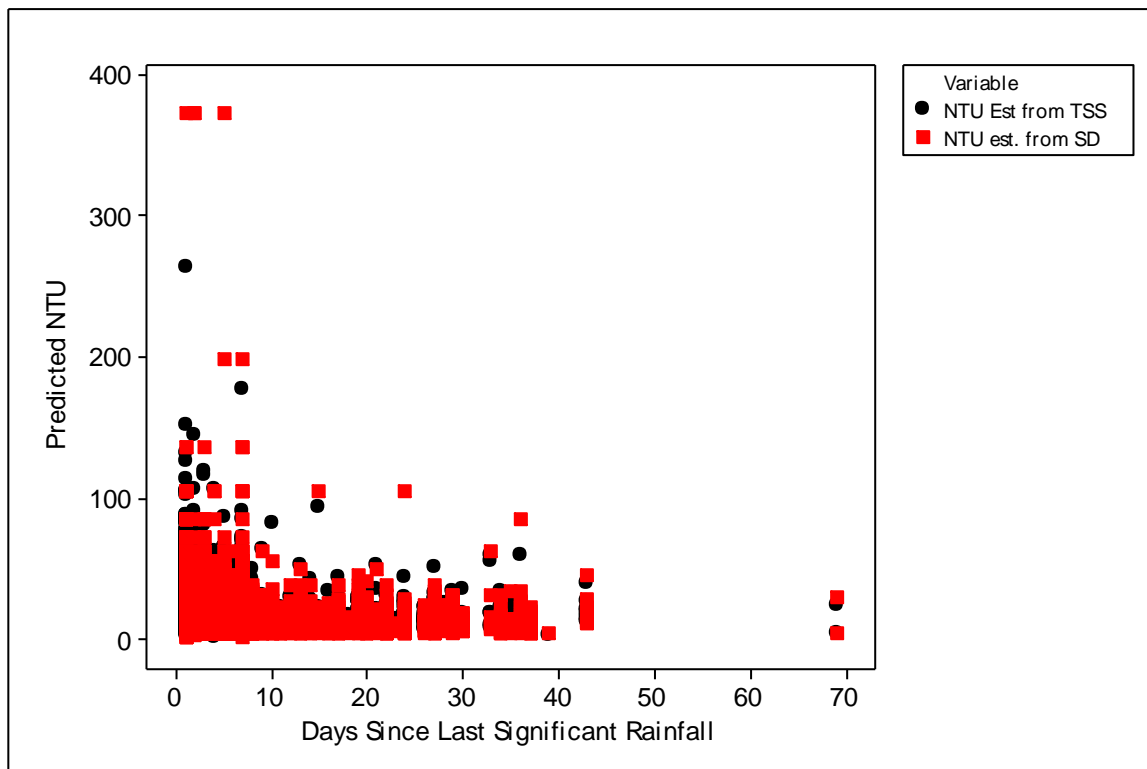


Figure 84. Distribution of predicted NTU versus historical rainfall incidence in Harris County applying the regional regression model to past SD data.

The final analysis conducted was to evaluate the potential yield of SSC versus percent impervious area based on the runoff projections. The runoff projections were produced by our rainfall-runoff analysis using various hydrological soil groups and impervious land cover estimates for several weighted rainfall scenarios observed during the field study in 2011. These estimates were produced based on streamflow estimated from USGS gage readings and measured SSC values for that date. This data was used to derive raw loading estimates (kg SSC/d) and adjusted for the amount of land per watershed in kg SSC/d/hectare. Under both analyses there was a definite trend of increasing sediment loads with percent impervious surface (Figure 85 and Figure 86). The amount of SSC derived from USGS gage readings, SSC measurements and the amount of predicted runoff however showed a non-linear trend where higher levels of loading occurred at intermediate flows (Figure 87 and Figure 88).

Although highly variable, SSC levels were generally highest at 3A (group 3), with the higher median values at both 1P and 3A (Figure 89 and Figure 90). However, there did not appear to be a strong correlation or pattern associated with increased streamflow (Figure 91). Site 3A frequently had low flows and did not have a high amount of impervious land within the upstream watershed. It is therefore difficult to postulate what is the cause of the elevated NTU, TSS and SSC observed at this site. It may be that human or animal traffic have disturbed bottom sediments in this shallow stream, or algal blooms contributed during non-flowing stagnant periods. We concluded that if the data from site 3A was removed a stronger relationship between flow and SSC would likely emerge. Therefore we reanalyzed this relationship with the data from site 3A removed (Figure 92). The relationship between streamflow and observed SSC levels appeared to be stronger and highly influenced by which groups are included in the analysis. The following significant ($p < 0.01$) regression relationships were observed overall and within individual site groupings.

1) All groups excluding 3A

1a) $SS \text{ mg/L} = 26.3 + 0.0753 \text{ flow (cfs)}$; $R^2 = 12.5\%$

1b) $\log_{10}(SS \text{ mg/L}) = 1.009 + 0.2348 \log_{10}(\text{cfs})$; $R^2 = 11.8\%$

Upon further examination we also found that two outliers (very low SS values) and flows were observed at the 1M site, located on Langham Ck at West Little York Rd near Addicks. We removed this site from further examination and found, however, that the overall regression model fit did not improve.

2) All groups excluding 3A and 1M

2a) $SS \text{ mg/L} = 27.5 + 0.0722 \text{ streamflow (cfs)}$; $R^2 = 11.8\%$

2b) $\log_{10}(SS \text{ mg/L}) = 1.111 + 0.1877 \log_{10}(\text{streamflow cfs})$; $R^2 = 11.8\%$

Finally we examined the predictive relationship between streamflow and SS by site group. Groups 1 and 3 showed no major improvement in the predictive linear model (low R^2) when we subset the data by groups. We did observe a better fit (higher r^2), between the two variables for groups 2, 4 and 5 (Figure 92).

3) Group 2

3a) $SS \text{ mg/L} = 17.0 + 0.108 \text{ streamflow (cfs)}$; $R^2 = 29.3.1\%$

3b) $\log_{10}(SS \text{ mg/L}) = 0.5825 + 0.4377 \log_{10}(\text{streamflow cfs})$; $R^2 = 30.5\%$

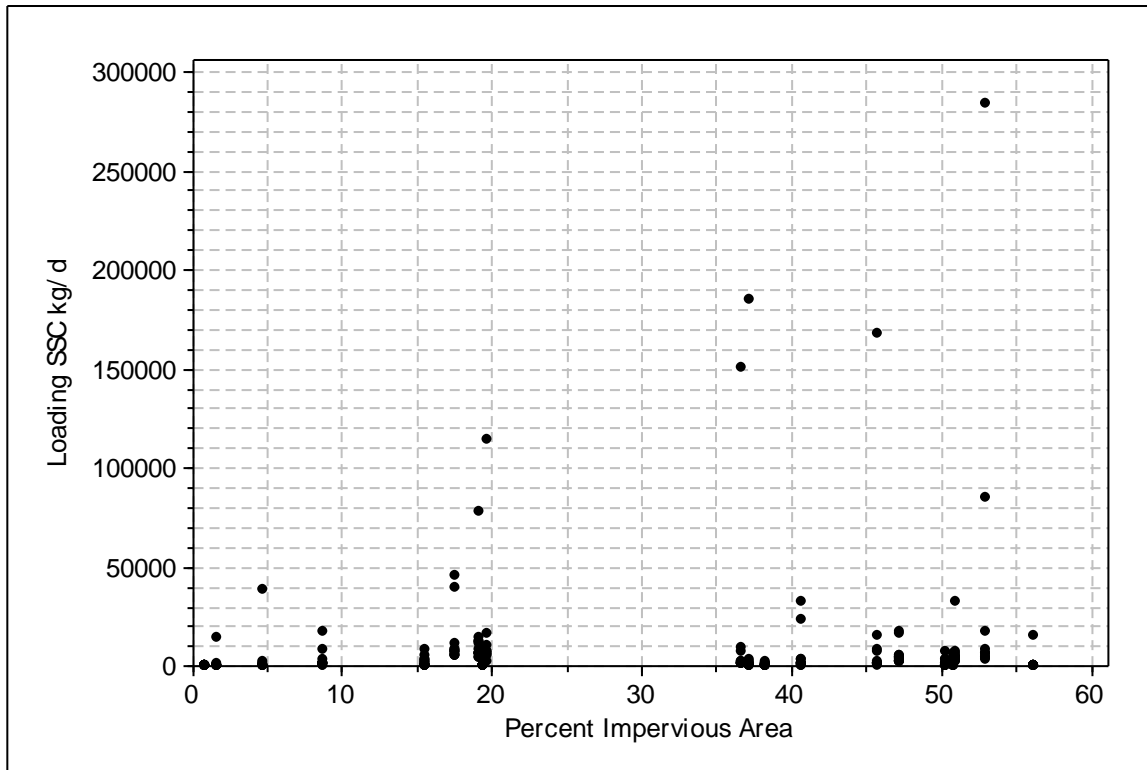


Figure 85. Estimated loading in kg SSC/d derived from USGS gage readings and SSC measurements at each site, versus percent impervious land in the contributing watershed located above sampling site during the field study.

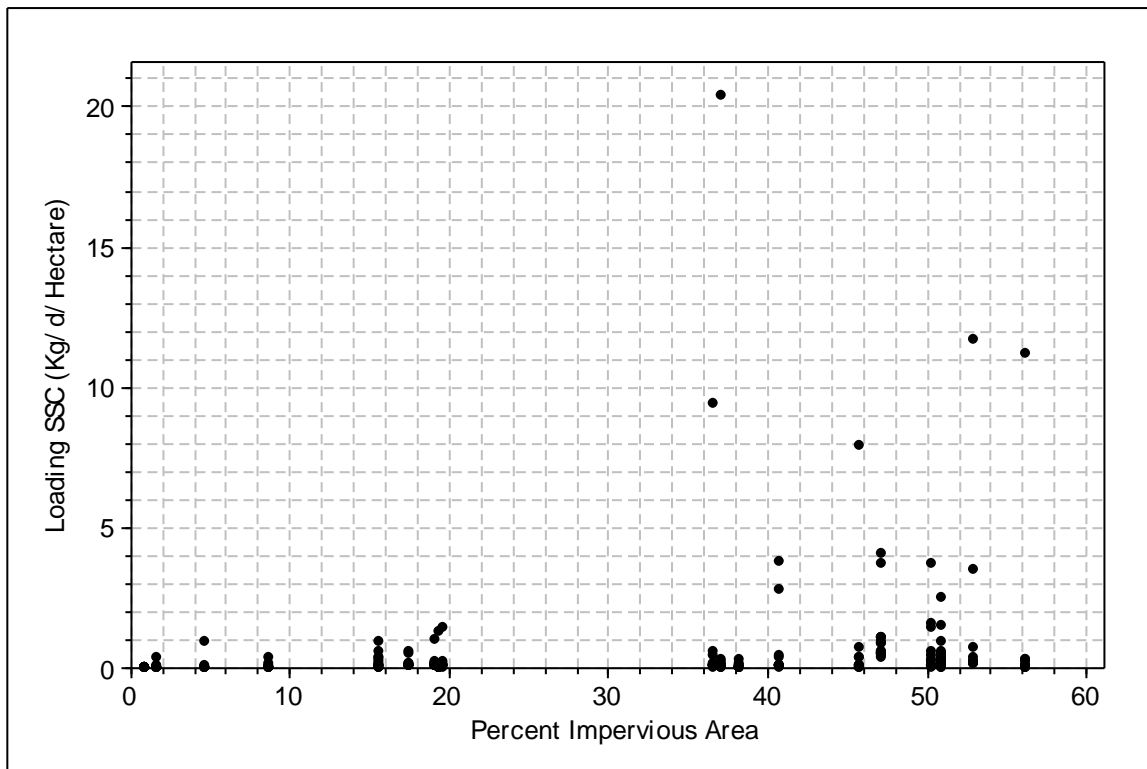


Figure 86. Estimated loading of suspended solids in kg SSC/day/hectare derived from USGS gage readings and SSC measurements at each site versus percent impervious area located above sites monitored during April to November 2011.

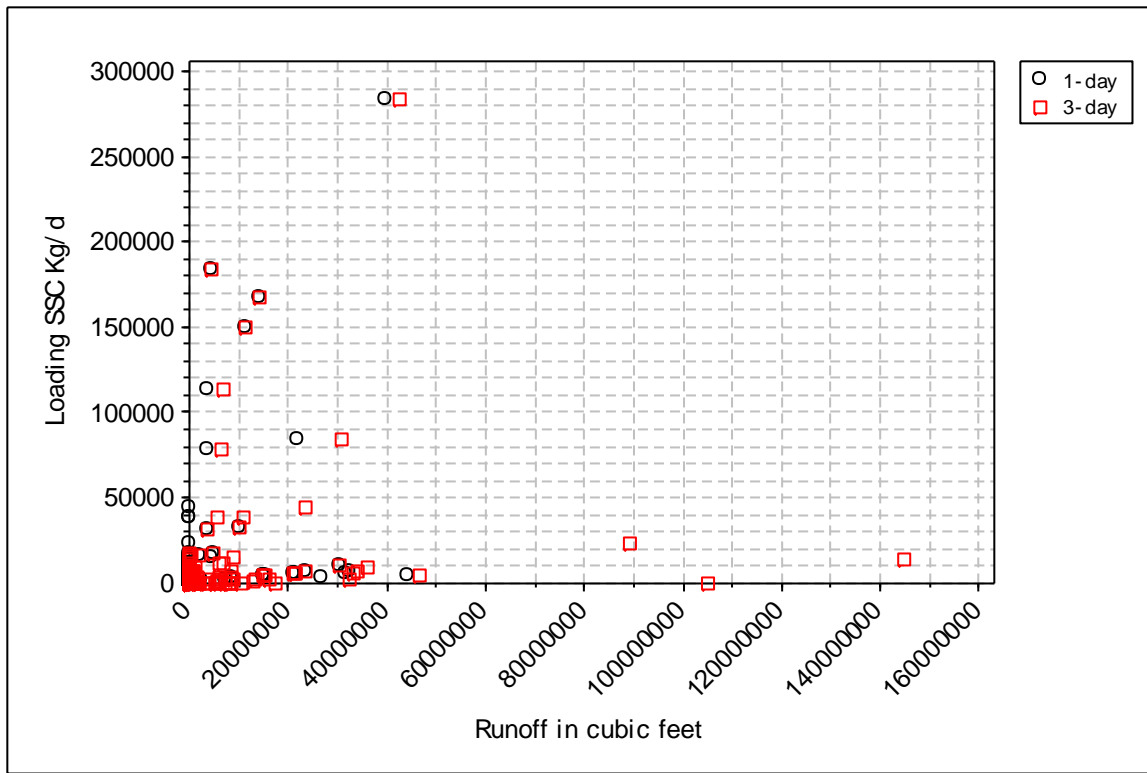


Figure 87. Estimated loading in kg SSC/d extrapolated from 1) streamflow derived from USGS gage readings and SSC measurements and 2) estimated quantities of total runoff from the upstream watershed derived from rainfall-runoff model predictions adjusted for land use and rainfall patterns.

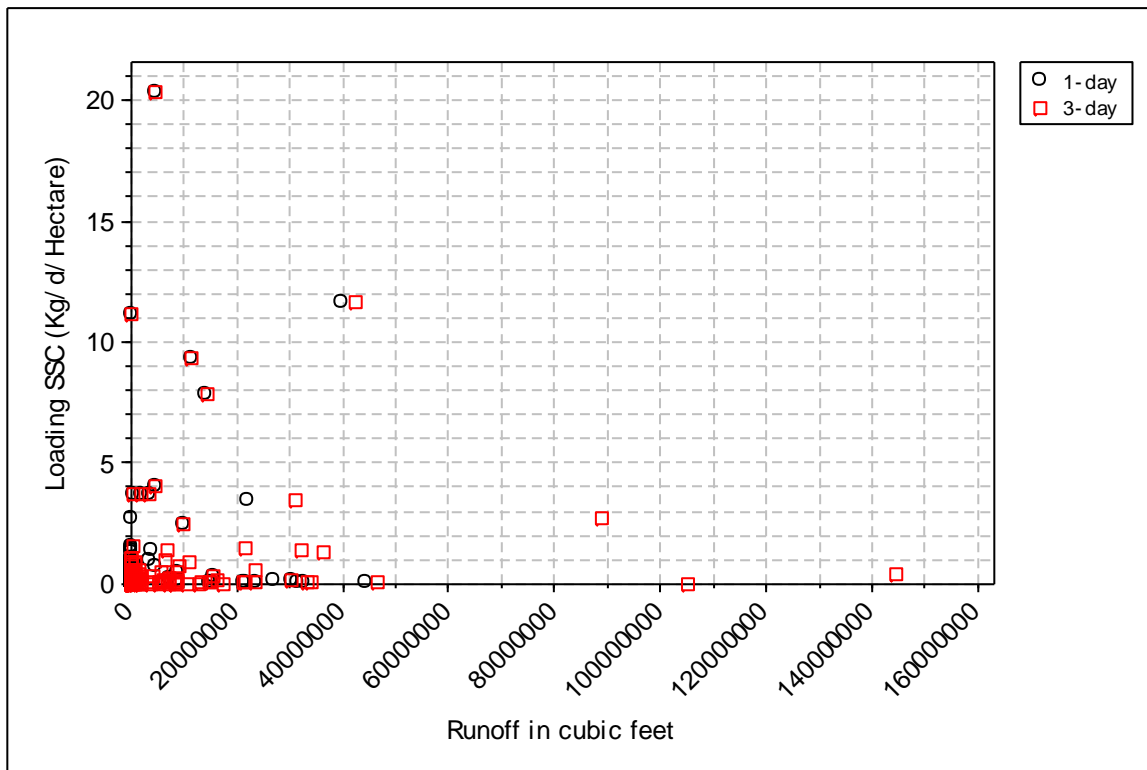


Figure 88. Estimated runoff in sediments (SSC) in kg/d/hectare extrapolated to watershed runoff quantities, based on 1) streamflow derived from USGS gage readings and SSC measurements and 2) estimated quantities of total runoff from the upstream watershed derived from rainfall-runoff model predictions adjusted for land use and rainfall patterns.

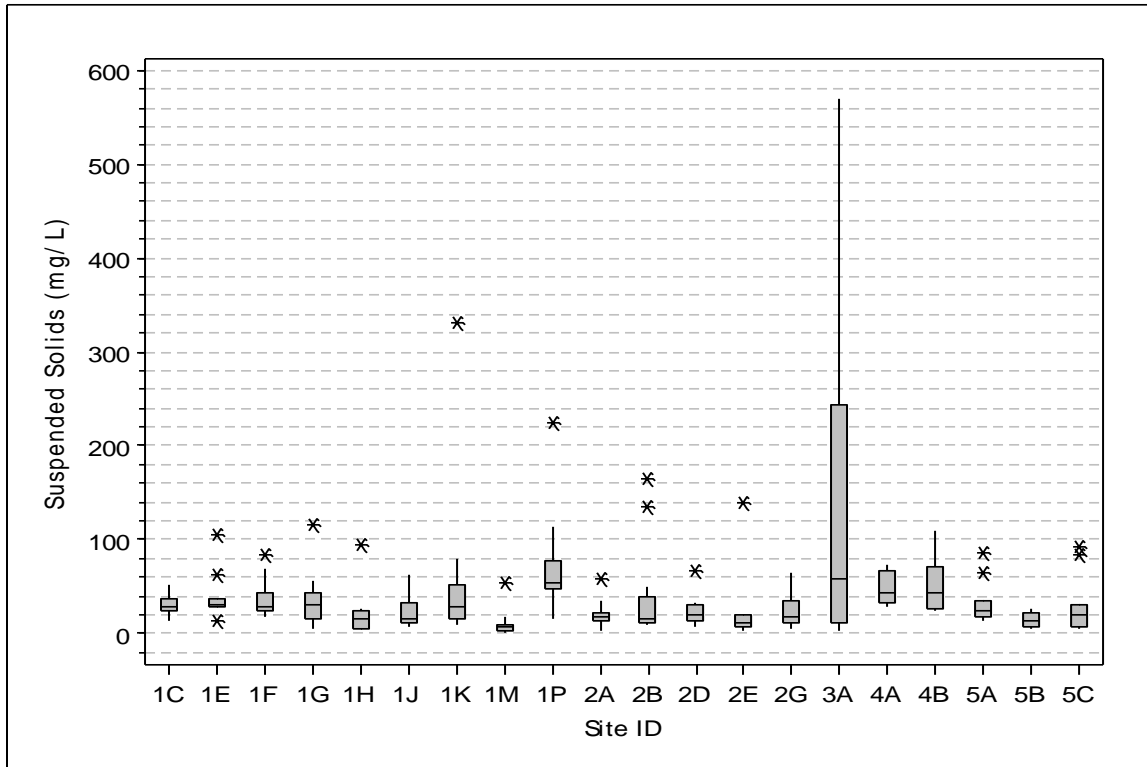


Figure 89. Distribution of suspended solids concentration (SSC) observed at each monitoring site during 2011.

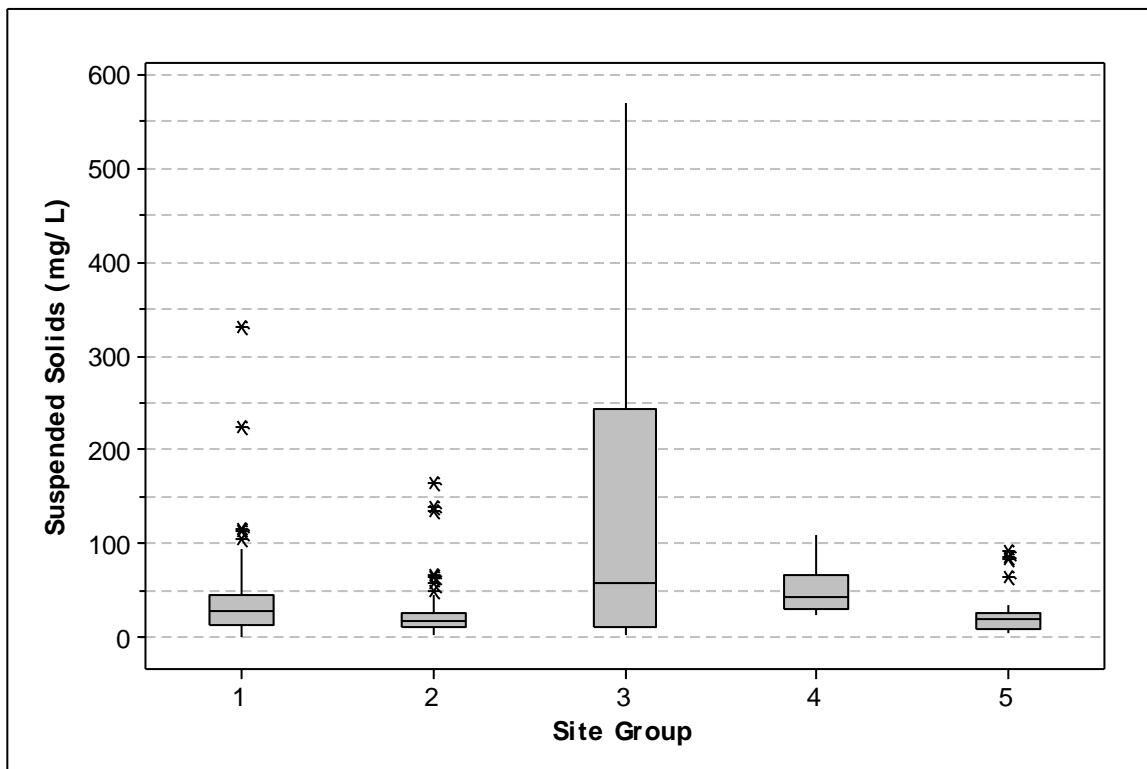


Figure 90. Distribution of SSC by site group during 2011.

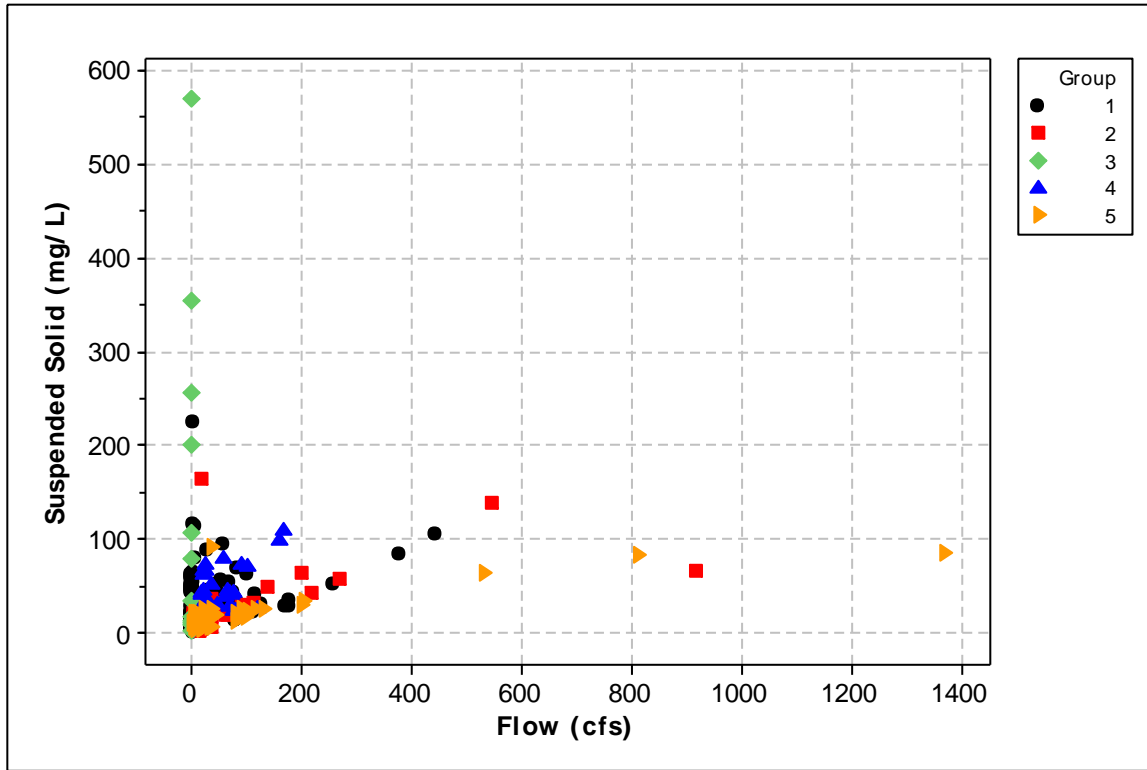


Figure 91. Relationship of measured SSC versus observed streamflow across all study sites.

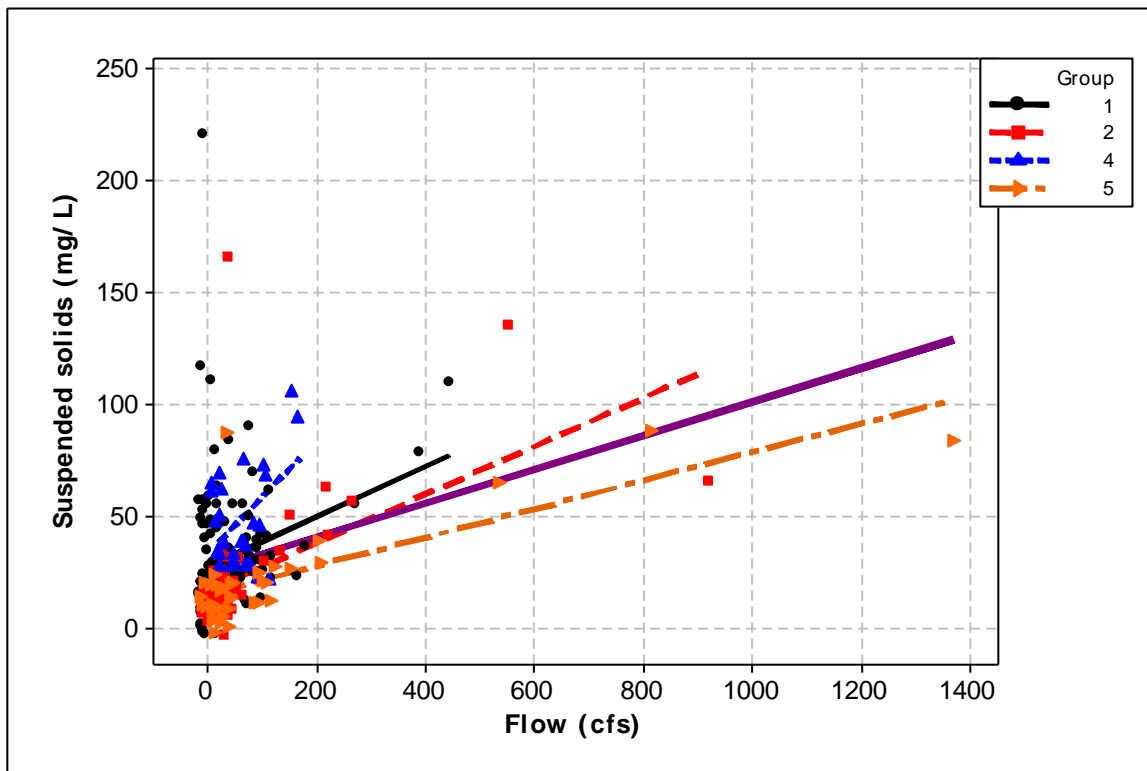


Figure 92. Relationship of measured suspended solids versus observed streamflow across all study sites excluding site 3A. Lines on graph represent linear regression model fits for each group and combined (purple line fit). Corresponding r^2 values for each group model are overall = 12.5%, 1 = 6.4%; 2 = 29.3%, 4 = 20.9%, and 5=56.0%.

4) Group 4

4a) $SS\text{ mg/L} = 34.0 + 0.250 \text{ streamflow (cfs)}$; $R^2 = 20.9\%$

4b) $\log_{10}(SS\text{ mg/L}) = 1.424 + 0.1337 \log_{10}(\text{streamflow cfs})$; $R^2 = 0.4\%$

5) Group 5

5a) $SS\text{ mg/L} = 15.7 + 0.0633 \text{ streamflow (cfs)}$; $R^2 = 56.0\%$

5b) $\log_{10}(SS\text{ mg/L}) = 0.6874 + 0.3503 \log_{10}(\text{streamflow cfs})$; $R^2(\text{adj}) = 41.7\%$

Similar relationships were observed between turbidity (NTU) and streamflow and are depicted below in Figure 93.

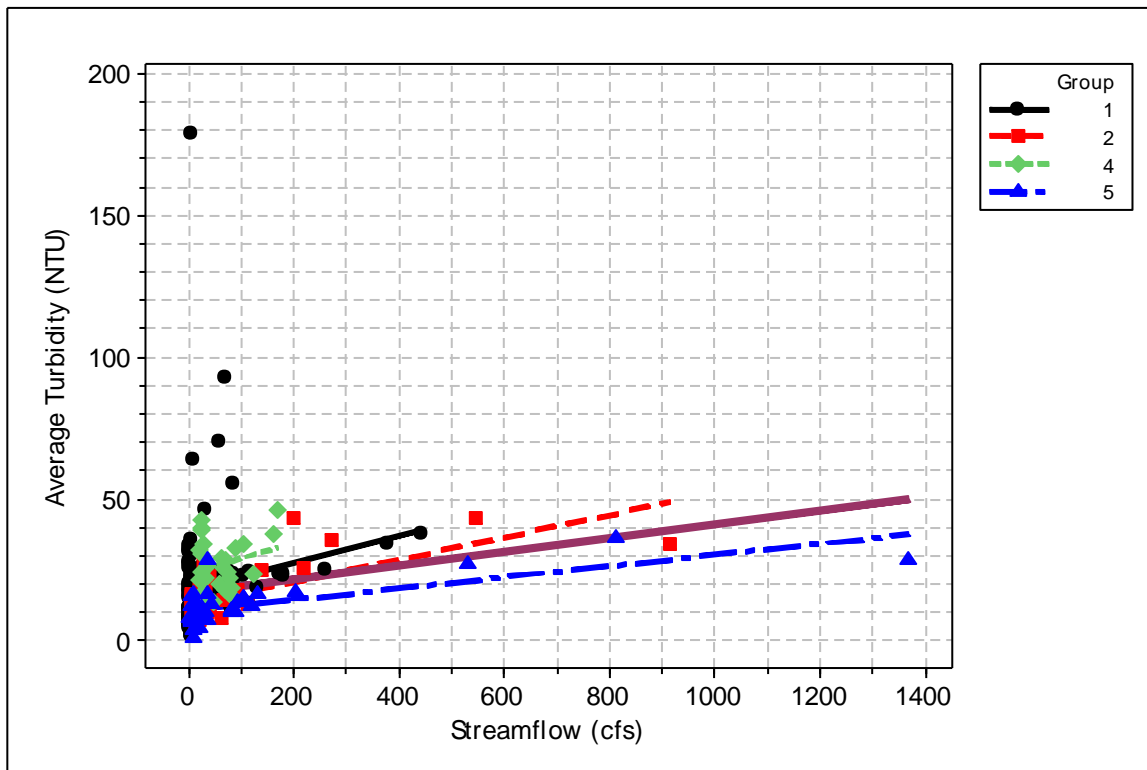


Figure 93. Relationship of measured turbidity (NTU) versus observed streamflow across all study sites excluding site 3A. Lines on graph represent linear regression model fits for each group and combined (purple line fit). Corresponding r^2 values for each group model are overall = 4.5%, 1 = 2.5%; 2 = 48.4%, 4 = 6.2%, and 5=51.0%.

Turbidity at site groupings 2 and 5 appeared to have the strongest response to streamflow (Figure 52 and Figure 93). Therefore it appears that the ability to predict suspended sediment concentrations and associated turbidity is heavily influenced by watershed characteristics, and are difficult to relate directly to streamflow alone, except in the context of comparing trends within a watershed or between watersheds with similar physical characteristics. This relationship is particularly confounded during low flow conditions in streams with high silt content, which are easily disturbed. We did observe intermittent activity at several monitoring sites including 1F, 1K and 5B (Figure 94 and Figure 95). We examined patterns of SSC on dates when construction activity was observed at these sites and those when they were not. Data collected during the study produced inconclusive results (Figure 95). Higher NTU values were observed during construction days at 1F, while the inverse was observed at 1K. At site 5B, there did not appear to be a strong pattern either way.



Figure 94. Example of construction activity observed during the study period at site 1K.

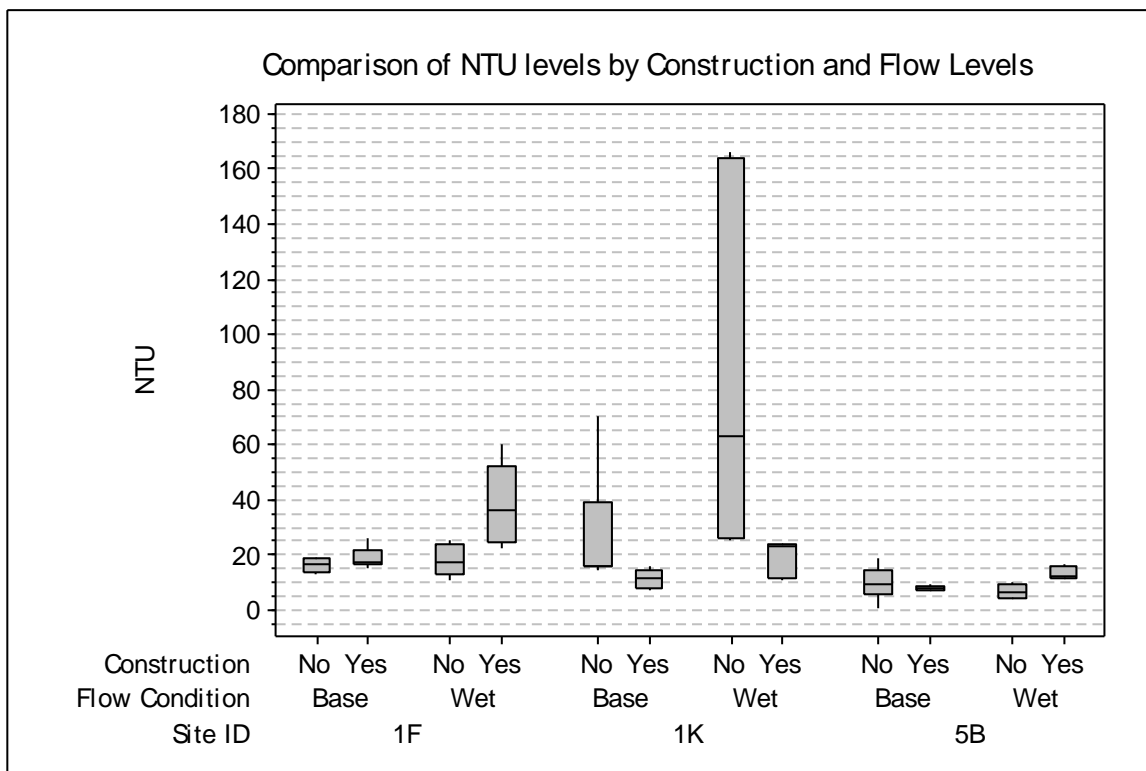


Figure 95. Comparison of NTU levels at sites where construction activities were observed during varying streamflow conditions.

Synthesis and Conclusion

The results of this study provide critical information on the levels and distribution of various measures of turbidity and sediment loading including NTU, SD, TSS and SSC. These newly collected data provide much needed information on the influence of land-use and flow regime on stream turbidity levels. The following major observations and conclusions can be made based on our analysis of historical and recently collected data.

1. Empirical levels of NTU observed in this study and others show that turbidity can be highly variable and elevated immediately after storm flows and when bottom sediments are disturbed. The general trend of increasing turbidity, TSS and SSC and decreasing SD levels was confounded by the highly variable data measured at site 3A. This site had extremely high turbidity, TSS, SSC and low SD levels. Therefore this one site would often strongly influence the relationship of flow regime, land-use and any turbidity/clarity measure evaluated. We therefore re-analyzed the data without this site. The re-analysis documented that the relationship between streamflow and suspended solids and turbidity is highly influenced by watershed conditions.

2. Land use and the type of land and soils influence the various measures of turbidity. High amounts of impervious surface influence the amount of runoff, streamflow and associated measures of turbidity. However, this pattern was not consistent. This may be due to the non-linear response associated with sediment transport in streams. As previously discussed, the phenomenon described as the “Type-1 hysteresis loop” describes the differential behavior of SSC and predicts that higher concentrations of SSC will occur during the rising limb of the hydrograph rather than the falling limb and that mobilization of these sediments initially may result in sediment exhaustion effects during subsequent stormflows. In order to evaluate the role of the hydrological sequence of flood pulses on sediment mobilization, we recommend a closer examination of individual hydrographs, and analyzing not only the relationship of absolute streamflow versus turbidity, but also evaluating the rate of change (+ or – delta change in flow) in flow and how it influences sediment transport.

3. Our data show ambient levels of turbidity as measured by NTU, SD and TSS are highly variable but, apparently within the range of concentrations that support warmwater aquatic life in sluggish coastal bayous. These waterbodies have naturally high turbidity levels that have not been sufficiently characterized. This turbidity is due in part to the easily suspended clay substrate that it is very common within the coastal zone of Texas. The distribution of NTU values based on periodic and automated monitoring ranged from near zero to near 1,800 NTU. Maximum values exceeding 1600 NTU were observed at several sites. These high values occurred regardless of land-use type. The median value derived from periodic monitoring and automated monitoring was approximately 16.6 and 26 NTU, respectively. The 90th percentile value based on automated monitoring was 381 NTU. These recent data agree with historical values collected by EIH for the CRP program in Brazoria and Galveston counties, which documented that the majority of historical turbidity measurements ranged between 5 and 25 NTU.

4. Predictive models relating TSS to NTU and vice versa do not have very good fit ($r^2 < 0.70$). However, these models can be used to provide rough estimates of TSS or NTU if one of these parameters is available and the other is missing.

5. The NTU versus SD regression models provided a much better statistical fit and are suitable for local watersheds in Harris County for deriving NTU values from historical SD values. The model with the highest r^2 was the log-log NTU and SD model which had an r^2 of 83.4%. We recommend the use of this

model for deriving NTU values from SD readings. This model and the associated coefficients are similar to other linear log transformed models reported in the literature by other investigators, which also report good statistical fits. These studies are documented in this report.

6. Several issues may have affected and compromised our efforts to characterize ambient levels of turbidity and associated variables. For example, at site 3A, the only site in its type group, a datasonde was deployed but, due to the drought, streamflow was low or absent with the exception of one major event. During the rest of the study the stream consisted of either disconnected pools only or was completely dry. During these periods, the probe may have been exposed temporarily. Silting-in of sonde boxes deployed along the stream bottom was also a problem, especially at site 5B. We cleaned out the boxes during midpoint sampling events, but this schedule may not have been sufficient, especially after rainstorms, to completely remove accumulated silt. Also, other debris/biofouling may have been an issue. These factors can lead to abnormally low and high turbidity levels due to physical coating and covering of the probe, or the introduction of air bubbles respectively.

7. At Site 2B, we were not able to use many of the turbidity readings to develop flow-turbidity relationships due to incomplete USGS gage flow records at low flow periods. We attempted to try to fill in the long gap periods by extending the existing rating curves, with supplemental flow measurements and use of available upstream/downstream flow data from existing USGS gage data. However, we were not able to accomplish this at this time and will need additional resources to develop this relationship.

8. Site 1P was actually a tidal site, so, although flow was measured at an upstream gage near this site, the flow regime is affected by tidal fluctuations. This may have affected the measurement of true streamflow and therefore biased readings from this site used in the development of streamflow turbidity relationships.

9. This study was conducted during a severe drought. Therefore the statistical relationships developed between streamflow and turbidity may be biased by the reliance on low flow data sets.

10. The discoloration of water due to dissolved organic tannins may cause a lower turbidity (NTU) reading unrelated to TSS concentrations. During the study, several sites had “tea-colored” water some or all of the time (e.g. 3A and 1H). This turbidity is not related to TSS, and affects the statistical relationship of NTU and other variables including streamflow, and TSS. In addition, as previously noted, turbidity levels at site 3A were highly variable and elevated.

11. The development of GIS based land-use data and runoff estimates utilizing empirical runoff coefficients for different hydrological soil types and impervious land coupled with actual measured suspended sediment and streamflow is a unique synthesis of data. These data provide an excellent starting point and framework for testing various hypothesis on how best management practices influences suspended sediment loading into the watershed.

Recommendations

Due to the drought conditions encountered during the study, it is recommended that additional studies be conducted during higher/normal flow regimes. There is sufficient evidence to suggest that higher turbidity values are possible during higher streamflow in many of the waterbodies studied. In addition, more detailed automated monitoring focused on evaluating the temporal changes in turbidity associated with the changes in flow including the relative amount and direction of change is recommended.

Close quantitative examination of other properties that may affect turbidity (including color and the presence of suspended and floating algae) is needed during future studies to evaluate the role of these variables and influence on apparent turbidity measurements. This can be done using standard color scales such as the Platinum Cobalt and/or Forel-Ule scales and concurrent measurement of chlorophyll-*a* pigments and TDS. By incorporating these variables into future monitoring efforts the major contributing factors influencing turbidity can be quantified.

The proposed 280 NTU standard that was withdrawn by EPA, would have been below ambient levels of turbidity in Harris County streams during stormflows and, depending on the watershed, may be close to some ambient base flow conditions. Therefore in these situations an effluent limitation close to the 280 NTU value may actually be difficult to attain given the clay soils present in many of the watersheds found in Harris County and the historically high turbidity levels (>300 NTU) encountered in at least 10% of the monitoring events as documented by this study.

Literature Cited

- American Society for Testing and Materials. 2007. Standard test methods for determining sediment concentration in water samples. ASTM, West Conshohocken, PA.
- Anderson, P., and R. D. Davic. 2004. Use of transparency tubes for rapid assessment of total suspended solids and turbidity in streams. *Lake and Reservoir Management* 20(2):110-120.
- Berry, W., N. Rubinstein, B. Melzian, and B. Hill. 2003. Internal Report - The biological effects of suspended and bedded sediment (SAB) in aquatic systems: a review. Environmental Protection Agency, Narragansett, RI.
- Brandes, B., and coauthors. 2009. Fluvial sediment transport as an overlay to instream flow recommendations for the environmental flows allocation process. Senate Bill 3 Science Advisory Committee, Austin, Texas.
- Clesceri, L. S., A. E. Greenberg, and A. D. Eaton, editors. 1998. Standard Methods for the Examination of Water and Wastewater, 20th edition. American Public Health Association, American Water Works Association and Water Environment Federation, Washington, D.C.
- Dahlgren, R., E. Van Nieuwenhuyse, and G. Litton. 2004. Transparency tube provides reliable water-quality measurements. *California Agriculture* (July-September):249.
- De Smith, M. J., M. F. Goodchild, and P. A. Longley. 2009. *Geospatial Analysis: A comprehensive Guide To Principles, Techniques and Software Tools.*, 3rd edition.
- Edwards, T. K., and G. D. Glysson. 1999. Field Measurements for Methods for Fluvial Sediment. Book 3. Chapter C2. Techniques of the Water-Resources Investigations of the U.S. Geological Survey, Reston, Virginia.
- Environmental Protection Agency. 2009a. Development document for final effluent guidelines and standards for the construction and development category. Environmental Protection Agency, Washington, D.C.
- Environmental Protection Agency. 2009b. Direct Final Rule Staying Numeric Limitation for the Construction and Development Point Source Category 40 CFR Part 450. 62996-63058. Federal Register/ Volume 74, No. 229/ December 1, 2009/ Rules and Regulations. , Washington, D.C. <http://water.epa.gov/scitech/wastetech/guide/construction/index.cfm>
- Environmental Protection Agency. 2010. Direct Final Rule Staying Numeric Limitation for the Construction and Development Point Source Category 40 CFR Part 450. 682215-68218. Federal Register/ Volume 75, No. 214/ November 5, 2010/ Rules and Regulations., Washington, D.C.
- Environmental Protection Agency, D. W., D.C. 2012. Effluent limitations guidelines and standards for the construction and development point source category Federal Register/ Volume 77, No. 1/ January 3, 2012/ Notices Environmental Protection Agency, Washington, D.C.
- Gray, J. R., G. D. Glysson, L. M. Turcios, and G. E. Schwarz. 2000. Comparability of suspended-sediment concentration and total suspended solids data. United States Geological Survey, Reston, VA.
- Hudson, P. F. 2003. Event sequence and sediment exhaustion in the lower Panuco Basin, Mexico. *Catena* 52:57-76.
- Meyer, R. 2008. Houston-Galveston Area Council 2008 Land Cover Image Processing Protocol. Duluth, MN. http://www.h-gac.com/community/socioeconomic/land_use/default.aspx
- Newcombe, C. P., and D. D. MacDonald. 1991. Effects of suspended sediments on aquatic ecosystems. *North American Journal of Fisheries Management* 11:72-82.
- Office of the State Demographer. 2012. Texas and Region 4 Demographic Characteristics and Trends: Presented Region 4 Education Service Center January 3, 2012, Houston, TX, Austin, TX. .
- Parent, E. 2009. Statistical analysis of turbidity (NTU) and secchi disk clarity: Memorandum and Report to the Harris County Storm Water Quality Section. Dannebaum Engineering Corporation.

- Texas Commission of Environmental Quality. 2008. Surface water quality monitoring procedures, volume 1. Physical and chemical monitoring methods for water, sediment, and tissue. . Texas Commission on Environmental Quality, Austin, Texas.
- U.S. Census Bureau. 2010. United States Census 2010: Interactive Population Map. U.S. Census Bureau. <http://2010.census.gov/2010census/popmap/>
- U.S. Census Bureau. 2012. State and County Quickfacts: Harris County. U.S. Census Bureau, Washington, D.C. <http://quickfacts.census.gov/qfd/states/48/48201.html>
- USDA-SCS. 1985. National Engineering Handbook, Section 4 – Hydrology. USDA-NRCS (Previously SCS). Washington, D.C.
- Water, T. F., editor. 1995. Sediment in streams: sources, biological effects and control. American Fisheries Society, Bethesda, MD.
- Wishart, D. 2006. ClustanGraphics Primer. Clustan Limited, Edinburgh, England.
- YSI. 2012. 6-series multiparameter water quality sondes user manual. YSI Incorporated, Yellow Springs, OH.

Appendices

- Appendix 1: Site Classification Cluster Analysis Data (Electronic Supplement)
- Appendix 2: Photograph Record (Electronic Supplement)
- Appendix 3: Interactive Google Earth Map (Electronic Supplement)
- Appendix 4: Forms and Datasheets
- Appendix 5: Calibration Data (Electronic Supplement)
- Appendix 6: ArcGIS Technical Methods
- Appendix 7: Hydrological Soil Types
- Appendix 8: Parent 2010 Historical Data Review (Electronic Supplement)
- Appendix 9 Historical Database (Electronic Supplement)
 - 3.A: Harris County Historical Data
 - 3.B: NTU Historical Model CRP Database
- Appendix 10: Deployed Sonde Data (Electronic Supplement)
- Appendix 11: Flow Data (Electronic Supplement)
- Appendix 12: Rainfall Data (Electronic Supplement)
 - 12.A: Daily Rainfall Data
 - 12.B: Hourly Rainfall Data
- Appendix 13: Master Project Data Compilation (Electronic Supplement)
 - 13.A: Master Database
 - 13.B: Lab Bench Sheets
 - 13.C: Field Datasheets
- Appendix 14: ArcGIS Technical Methods and Loading Database (Electronic Supplement)

Appendix 1: Site Classification Cluster Analysis Data (Electronic Supplement)

*See Compact Disk at Rear of Report for Electronic Supplements

Appendix 2: Photograph Record (Electronic Supplement)

*See Compact Disk (Appendix 2) for Electronic Supplement

Photograph Number	Site	Sample Period	Site Description	Date	Photograph Description
Turbidity1C-01	1C	Recon	Brays Bayou at Gessner Dr, Houston, TX	3/21/2011	View of right bank, upstream of bridge
Turbidity1C-02	1C	Recon	Brays Bayou at Gessner Dr, Houston, TX	3/21/2011	View downstream from bridge
Turbidity1C-03	1C	Recon	Brays Bayou at Gessner Dr, Houston, TX	3/21/2011	Vertical view of channel showing a depth difference between the sides and middle
Turbidity1C-04	1C	Recon	Brays Bayou at Gessner Dr, Houston, TX	3/21/2011	View of left bank from left bank, upstream of bridge
Turbidity1C-05	1C	Recon	Brays Bayou at Gessner Dr, Houston, TX	3/21/2011	View upstream from bridge
Turbidity1C-06	1C	1	Brays Bayou at Gessner Dr, Houston, TX	4/20/2011	View facing upstream
Turbidity1C-07	1C	1	Brays Bayou at Gessner Dr, Houston, TX	4/20/2011	View facing left bank
Turbidity1C-08	1C	1	Brays Bayou at Gessner Dr, Houston, TX	4/20/2011	View facing downstream
Turbidity1C-09	1C	1	Brays Bayou at Gessner Dr, Houston, TX	4/20/2011	View facing right bank
Turbidity1E-01	1E	Recon	Buffalo Bayou at Piney Point, TX	3/21/2011	View downstream from bridge
Turbidity1E-02	1E	Recon	Buffalo Bayou at Piney Point, TX	3/21/2011	View upstream from bridge
Turbidity1E-03	1E	Recon	Buffalo Bayou at Piney Point, TX	3/21/2011	View of left bank from upstream side of bridge
Turbidity1E-04	1E	Recon	Buffalo Bayou at Piney Point, TX	3/21/2011	View of right bank from upstream side of bridge
Turbidity1E-05	1E	Recon	Buffalo Bayou at Piney Point, TX	3/21/2011	View of left bank from left bank under bridge
Turbidity1E-06	1E	Recon	Buffalo Bayou at Piney Point, TX	3/21/2011	View of right bank from left bank under bridge
Turbidity1E-07	1E	1	Buffalo Bayou at Piney Point, TX	4/20/2011	View facing upstream
Turbidity1E-08	1E	1	Buffalo Bayou at Piney Point, TX	4/20/2011	View facing left bank
Turbidity1E-09	1E	1	Buffalo Bayou at Piney Point, TX	4/20/2011	View facing downstream
Turbidity1E-10	1E	1	Buffalo Bayou at Piney Point, TX	4/20/2011	View facing right bank
Turbidity1F-01	1F	Recon	Buffalo Bayou at W Belt Dr at Houston, TX	3/21/2011	View downstream from bridge
Turbidity1F-02	1F	Recon	Buffalo Bayou at W Belt Dr at Houston, TX	3/21/2011	View of right bank from downstream side of bridge
Turbidity1F-03	1F	Recon	Buffalo Bayou at W Belt Dr at Houston, TX	3/21/2011	View of left bank from downstream side of bridge
Turbidity1F-04	1F	Recon	Buffalo Bayou at W Belt Dr at Houston, TX	3/21/2011	View of box attached to middle of bridge, downstream side, with possible water level sounding cone from bottom
Turbidity1F-05	1F	1	Buffalo Bayou at W Belt Dr at Houston, TX	4/20/2011	View facing upstream from midstream with active construction on left bank
Turbidity1F-06	1F	1	Buffalo Bayou at W Belt Dr at Houston, TX	4/20/2011	View facing left bank from midstream
Turbidity1F-07	1F	1	Buffalo Bayou at W Belt Dr at Houston, TX	4/20/2011	View facing downstream from midstream
Turbidity1F-08	1F	1	Buffalo Bayou at W Belt Dr at Houston, TX	4/20/2011	View facing right bank from midstream
Turbidity1F-09	1F	3a	Buffalo Bayou at W Belt Dr at Houston, TX	8/24/2011	View facing down left bank at culverts from middle of left bank
Turbidity1F-10	1F	3a	Buffalo Bayou at W Belt Dr at Houston, TX	8/24/2011	View of new wire-covered rock and rip rap on left bank from middle of left bank
Turbidity1F-11	1F	3a	Buffalo Bayou at W Belt Dr at Houston, TX	8/24/2011	View of EIH personnel crossing stream and new rip rap on right bank from left bank
Turbidity1F-12	1F	3a	Buffalo Bayou at W Belt Dr at Houston, TX	8/24/2011	View upstream of new and in-progress construction from left bank
Turbidity1F-13	1F	3a	Buffalo Bayou at W Belt Dr at Houston, TX	8/24/2011	View downstream from left bank, some newer construction visible
Turbidity1G-01	1G	Recon	Clear Creek @ Mykawa St, nr Pearland, TX	3/21/2011	View of left bank from left bank, downstream of Mykawa St bridge
Turbidity1G-02	1G	Recon	Clear Creek @ Mykawa St, nr Pearland, TX	3/21/2011	View downstream from railroad bridge
Turbidity1G-03	1G	Recon	Clear Creek @ Mykawa St, nr Pearland, TX	3/21/2011	View of right bank from right bank downstream of Mykawa St bridge
Turbidity1G-04	1G	Recon	Clear Creek @ Mykawa St, nr Pearland, TX	3/21/2011	View of channel and wooden pilings of railroad bridge from right bank
Turbidity1G-05	1G	Recon	Clear Creek @ Mykawa St, nr Pearland, TX	3/21/2011	View upstream from upstream side of Mykawa St bridge
Turbidity1G-06	1G	1	Clear Creek @ Mykawa St, nr Pearland, TX	4/18/2011	Photograph of in situ sonde deployed using PVC housing, attached to railroad bridge pylon near left bank facing downstream
Turbidity1G-07	1G	1	Clear Creek @ Mykawa St, nr Pearland, TX	4/18/2011	Photograph of EIH personnel collecting SS samples under bridge along left bank
Turbidity1G-08	1G	1	Clear Creek @ Mykawa St, nr Pearland, TX	4/18/2011	View facing upstream
Turbidity1G-09	1G	1	Clear Creek @ Mykawa St, nr Pearland, TX	4/18/2011	View facing left bank
Turbidity1G-10	1G	1	Clear Creek @ Mykawa St, nr Pearland, TX	4/18/2011	View facing downstream
Turbidity1G-11	1G	1	Clear Creek @ Mykawa St, nr Pearland, TX	4/18/2011	View facing right bank
Turbidity1G-12	1G	3b	Clear Creek @ Mykawa St, nr Pearland, TX	10/20/2011	View of debris on upstream side of railroad bridge pilings from left bank
Turbidity1G-13	1G	3b	Clear Creek @ Mykawa St, nr Pearland, TX	10/20/2011	View of debris on upstream side of railroad bridge pilings from left bank
Turbidity1G-14	1G	3b	Clear Creek @ Mykawa St, nr Pearland, TX	10/20/2011	View of sonde and debris stuck on RR bridge pilings from midstream
Turbidity1G-15	1G	3b	Clear Creek @ Mykawa St, nr Pearland, TX	10/20/2011	View of sonde and debris stuck on RR bridge pilings from left bank
Turbidity1G-16	1G	3b	Clear Creek @ Mykawa St, nr Pearland, TX	10/20/2011	View of sonde and debris stuck on RR bridge pilings from left bank
Turbidity1G-17	1G	3b	Clear Creek @ Mykawa St, nr Pearland, TX	11/2/2011	View of sonde and debris stuck on RR bridge pilings from left bank
Turbidity1G-18	1G	3b	Clear Creek @ Mykawa St, nr Pearland, TX	11/2/2011	View upstream from left bank, upstream side of RR bridge
Turbidity1G-19	1G	3b	Clear Creek @ Mykawa St, nr Pearland, TX	11/2/2011	View of sonde and debris stuck on RR bridge pilings from left bank
Turbidity1G-20	1G	3b	Clear Creek @ Mykawa St, nr Pearland, TX	11/2/2011	Close-up view of sonde on bridge piling surrounded by debris
Turbidity1G-21	1G	3b	Clear Creek @ Mykawa St, nr Pearland, TX	11/2/2011	View of sonde, debris, and EIH at RR bridge piling
Turbidity1G-22	1G	3b	Clear Creek @ Mykawa St, nr Pearland, TX	11/2/2011	View of sonde probes with sediment settled on them at retrieval
Turbidity1G-23	1G	3b	Clear Creek @ Mykawa St, nr Pearland, TX	11/2/2011	View of sonde probes with mud inside sampling cap at retrieval
Turbidity1G-24	1G	3b	Clear Creek @ Mykawa St, nr Pearland, TX	11/2/2011	View of sonde probes with mud inside sampling cap at retrieval
Turbidity1G-25	1G	3b	Clear Creek @ Mykawa St, nr Pearland, TX	11/2/2011	View of mud/sediment inside PVC tube at sonde retrieval
Turbidity1G-26	1G	4	Clear Creek @ Mykawa St, nr Pearland, TX	12/14/2011	View of debris on upstream side of railroad bridge pilings from left bank
Turbidity1G-27	1G	4	Clear Creek @ Mykawa St, nr Pearland, TX	12/14/2011	View of debris on upstream side of railroad bridge pilings from left bank
Turbidity1G-28	1G	4	Clear Creek @ Mykawa St, nr Pearland, TX	12/14/2011	View of sonde and debris stuck on RR bridge pilings from left bank, cap missing from PVC tube
Turbidity1H-01	1H	Recon	Cypress Ck at House-Hahl Rd nr Cypress, TX	3/11/2011	View upstream from left bank
Turbidity1H-02	1H	Recon	Cypress Ck at House-Hahl Rd nr Cypress, TX	3/11/2011	View of left bank under bridge
Turbidity1H-03	1H	Recon	Cypress Ck at House-Hahl Rd nr Cypress, TX	3/11/2011	View downstream from left bank
Turbidity1H-04	1H	Recon	Cypress Ck at House-Hahl Rd nr Cypress, TX	3/11/2011	View of right bank from left bank
Turbidity1H-05	1H	1	Cypress Ck at House-Hahl Rd nr Cypress, TX	4/19/2011	View facing upstream
Turbidity1H-06	1H	1	Cypress Ck at House-Hahl Rd nr Cypress, TX	4/19/2011	View facing left bank
Turbidity1H-07	1H	1	Cypress Ck at House-Hahl Rd nr Cypress, TX	4/19/2011	View facing downstream
Turbidity1H-08	1H	1	Cypress Ck at House-Hahl Rd nr Cypress, TX	4/19/2011	View facing right bank
Turbidity1H-09	1H	1	Cypress Ck at House-Hahl Rd nr Cypress, TX	5/11/2011	Photograph of mixing between turbid blue water and turbid brownish-green water coming from pipe on left bank
Turbidity1H-10	1H	2	Cypress Ck at House-Hahl Rd nr Cypress, TX	6/27/2011	Photograph of sediment cloud coming from pipe on left bank downstream of bridge
Turbidity1H-11	1H	2	Cypress Ck at House-Hahl Rd nr Cypress, TX	6/27/2011	View facing upstream
Turbidity1H-12	1H	2	Cypress Ck at House-Hahl Rd nr Cypress, TX	6/27/2011	Photograph of mixing in water column of sediment output from pipe on left bank and water from upstream
Turbidity1H-13	1H	3a	Cypress Ck at House-Hahl Rd nr Cypress, TX	8/25/2011	View of vegetation pushed over on banks, evidence of recent higher flows, from left bank facing slightly upstream
Turbidity1H-14	1H	3a	Cypress Ck at House-Hahl Rd nr Cypress, TX	8/25/2011	View of vegetation pushed over on banks, evidence of recent higher flows, from left bank facing downstream
Turbidity1H-15	1H	3b	Cypress Ck at House-Hahl Rd nr Cypress, TX	10/10/2011	View towards downstream of higher water level, post-rain
Turbidity1J-01	1J	Recon	Hunting Bayou @ Hoffman St., Houston, TX	3/11/2011	View upstream from foot bridge
Turbidity1J-02	1J	Recon	Hunting Bayou @ Hoffman St., Houston, TX	3/11/2011	View of left bank with culvert from bridge
Turbidity1J-03	1J	Recon	Hunting Bayou @ Hoffman St., Houston, TX	3/11/2011	View downstream from bridge
Turbidity1J-04	1J	Recon	Hunting Bayou @ Hoffman St., Houston, TX	3/11/2011	View of right bank from bridge
Turbidity1J-05	1J	Recon	Hunting Bayou @ Hoffman St., Houston, TX	3/11/2011	View of lock box with piping from left bank
Turbidity1J-06	1J	1	Hunting Bayou @ Hoffman St., Houston, TX	4/20/2011	View facing right bank
Turbidity1J-07	1J	1	Hunting Bayou @ Hoffman St., Houston, TX	4/20/2011	View facing downstream
Turbidity1J-08	1J	1	Hunting Bayou @ Hoffman St., Houston, TX	4/20/2011	View facing upstream
Turbidity1J-09	1J	1	Hunting Bayou @ Hoffman St., Houston, TX	4/20/2011	View facing left bank

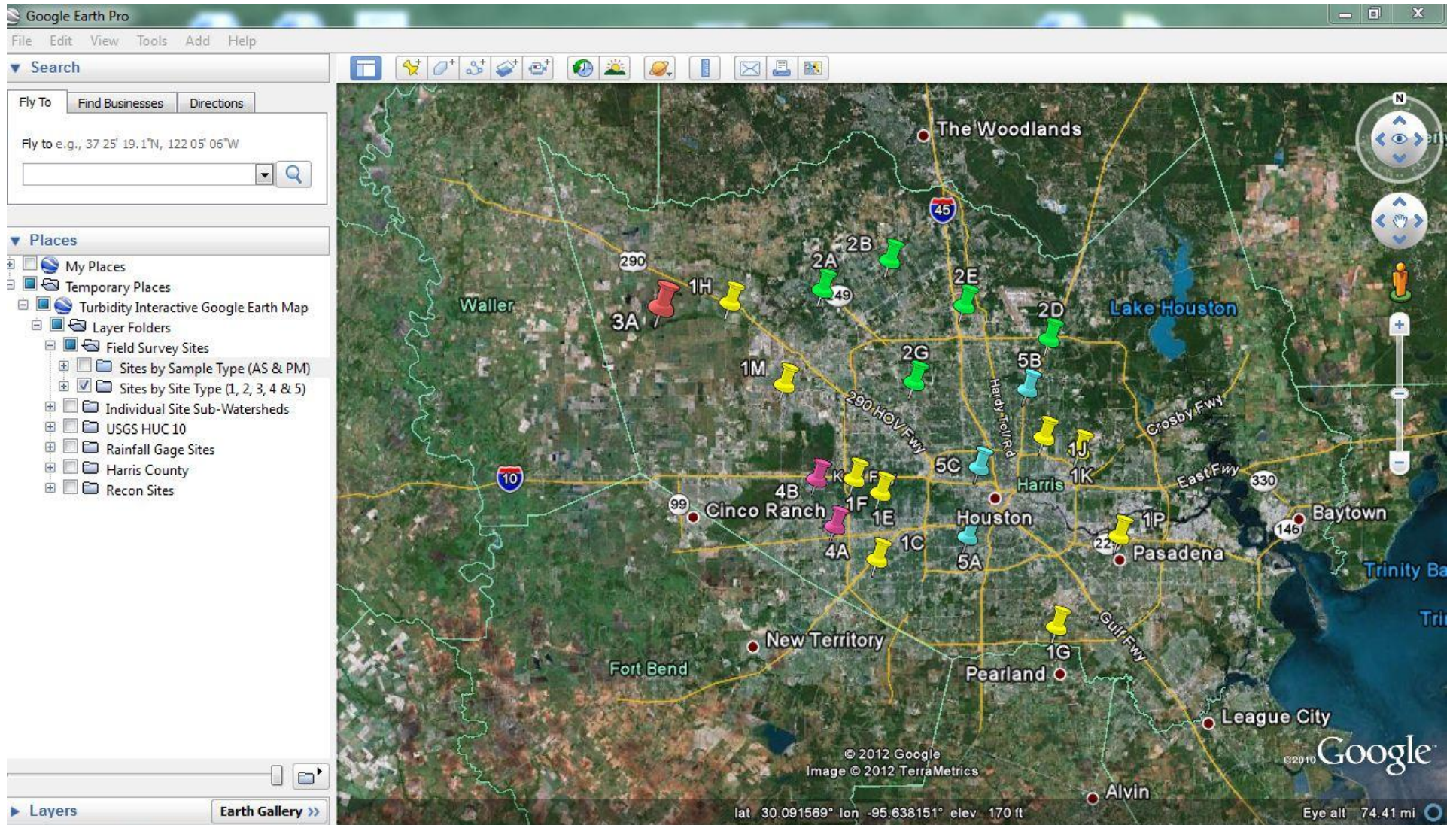
Photograph Number	Site	Sample Period	Site Description	Date	Photograph Description
Turbidity1K-01	1K	Recon	Hunting Bayou at IH 610, Houston, TX	3/11/2011	View upstream from left bank
Turbidity1K-02	1K	Recon	Hunting Bayou at IH 610, Houston, TX	3/11/2011	View of left bank from left bank
Turbidity1K-03	1K	Recon	Hunting Bayou at IH 610, Houston, TX	3/11/2011	View downstream from left bank
Turbidity1K-04	1K	Recon	Hunting Bayou at IH 610, Houston, TX	3/11/2011	View of right bank from left bank
Turbidity1K-05	1K	Recon	Hunting Bayou at IH 610, Houston, TX	3/11/2011	View under bridge, left bank
Turbidity1K-06	1K	Recon	Hunting Bayou at IH 610, Houston, TX	3/11/2011	View of gage station on left bank
Turbidity1K-07	1K	1	Hunting Bayou at IH 610, Houston, TX	4/20/2011	View downstream from midstream
Turbidity1K-08	1K	1	Hunting Bayou at IH 610, Houston, TX	4/20/2011	View of right bank from midstream
Turbidity1K-09	1K	1	Hunting Bayou at IH 610, Houston, TX	4/20/2011	View of left bank from midstream
Turbidity1K-10	1K	1	Hunting Bayou at IH 610, Houston, TX	4/20/2011	View upstream from midstream
Turbidity1K-11	1K	2	Hunting Bayou at IH 610, Houston, TX	7/29/2011	View of high water level due to rainfall taken from top of right bank
Turbidity1K-12	1K	3a	Hunting Bayou at IH 610, Houston, TX	8/23/2011	View upstream of new construction from top of right bank
Turbidity1K-13	1K	3a	Hunting Bayou at IH 610, Houston, TX	8/23/2011	View upstream of new construction from top of right bank
Turbidity1K-14	1K	3a	Hunting Bayou at IH 610, Houston, TX	8/23/2011	View of temporary crossing and grated banks from top of right bank
Turbidity1K-15	1K	3a	Hunting Bayou at IH 610, Houston, TX	8/23/2011	View downstream from right bank under bridge
Turbidity1K-16	1K	4	Hunting Bayou at IH 610, Houston, TX	12/6/2011	View of nearly completed construction on right bank from right bank
Turbidity1K-17	1K	4	Hunting Bayou at IH 610, Houston, TX	12/6/2011	View of nearly completed construction on right bank from right bank
Turbidity1M-01	1M	Recon	Langham Ck at W Little York Rd nr Addicks, TX	3/21/2011	View of left bank from left bank under upstream side of bridge
Turbidity1M-02	1M	Recon	Langham Ck at W Little York Rd nr Addicks, TX	3/21/2011	Wide view of upstream from left bank side of bridge
Turbidity1M-03	1M	Recon	Langham Ck at W Little York Rd nr Addicks, TX	3/21/2011	View upstream from middle of bridge
Turbidity1M-04	1M	Recon	Langham Ck at W Little York Rd nr Addicks, TX	3/21/2011	View of right bank from right bank under upstream side of bridge
Turbidity1M-05	1M	Recon	Langham Ck at W Little York Rd nr Addicks, TX	3/21/2011	View downstream from bridge
Turbidity1M-06	1M	Recon	Langham Ck at W Little York Rd nr Addicks, TX	3/21/2011	View of locked box attached to downstream side of bridge
Turbidity1M-07	1M	1	Langham Ck at W Little York Rd nr Addicks, TX	4/19/2011	View facing upstream
Turbidity1M-08	1M	1	Langham Ck at W Little York Rd nr Addicks, TX	4/19/2011	View facing left bank, EIH personnel collecting SS sample
Turbidity1M-09	1M	1	Langham Ck at W Little York Rd nr Addicks, TX	4/19/2011	View facing downstream
Turbidity1M-10	1M	1	Langham Ck at W Little York Rd nr Addicks, TX	4/19/2011	View facing right bank
Turbidity1M-11	1M	1	Langham Ck at W Little York Rd nr Addicks, TX	5/13/2011	View facing upstream; appears to have recent herbicide use
Turbidity1M-12	1M	1	Langham Ck at W Little York Rd nr Addicks, TX	5/13/2011	View facing left bank; appears to have recent herbicide use
Turbidity1M-13	1M	2	Langham Ck at W Little York Rd nr Addicks, TX	6/27/2011	View facing upstream
Turbidity1M-14	1M	2	Langham Ck at W Little York Rd nr Addicks, TX	6/27/2011	View facing left bank
Turbidity1M-15	1M	2	Langham Ck at W Little York Rd nr Addicks, TX	6/27/2011	View downstream from midchannel
Turbidity1M-16	1M	2	Langham Ck at W Little York Rd nr Addicks, TX	6/27/2011	View of right bank from midchannel
Turbidity1M-17	1M	3b	Langham Ck at W Little York Rd nr Addicks, TX	10/10/2011	View of flooded channel from left bank upstream side of bridge
Turbidity1M-18	1M	3b	Langham Ck at W Little York Rd nr Addicks, TX	10/10/2011	View upstream of flooded channel from left bank
Turbidity1P-01	1P	Recon	Vince Bayou at Pasadena, TX	3/21/2011	View towards channel of fence from dead end road
Turbidity1P-02	1P	Recon	Vince Bayou at Pasadena, TX	3/21/2011	View upstream from left bank
Turbidity1P-03	1P	Recon	Vince Bayou at Pasadena, TX	3/21/2011	View downstream from left bank
Turbidity1P-04	1P	1	Vince Bayou at Pasadena, TX	4/26/2011	View of creek sign on upstream side of bridge
Turbidity1P-05	1P	1	Vince Bayou at Pasadena, TX	4/26/2011	View of right bank taken from left bank under bridge
Turbidity1P-06	1P	1	Vince Bayou at Pasadena, TX	4/26/2011	View of EIH personnel running NTU samples in field
Turbidity1P-07	1P	4	Vince Bayou at Pasadena, TX	11/10/2011	View upstream of low water level due to tide, large debris visible, from top of left bank
Turbidity1P-08	1P	4	Vince Bayou at Pasadena, TX	11/10/2011	View upstream from top of left bank of low water level due to tide, large debris visible
Turbidity1P-09	1P	4	Vince Bayou at Pasadena, TX	11/10/2011	View upstream from left bank of low water level due to tide, large and small debris visible
Turbidity1P-10	1P	4	Vince Bayou at Pasadena, TX	11/10/2011	View upstream from left bank of low water level due to tide, large and small debris visible
Turbidity1P-11	1P	4	Vince Bayou at Pasadena, TX	11/10/2011	View upstream from left bank of low water level due to tide, large and small debris visible
Turbidity1P-12	1P	4	Vince Bayou at Pasadena, TX	12/6/2011	View downstream from left bank of low water level due to tide, EIH personnel visible
Turbidity1P-13	1P	4	Vince Bayou at Pasadena, TX	12/6/2011	View upstream from left bank of low water level due to tide
Turbidity1P-14	1P	4	Vince Bayou at Pasadena, TX	12/6/2011	View directly under bridge from left bank, showing low water level
Turbidity2A-01	2A	Recon	Cypress Ck at Grant Rd nr Cypress, TX	3/11/2011	View upstream from bridge
Turbidity2A-02	2A	Recon	Cypress Ck at Grant Rd nr Cypress, TX	3/11/2011	View of left bank from bridge
Turbidity2A-03	2A	Recon	Cypress Ck at Grant Rd nr Cypress, TX	3/11/2011	View downstream from bridge
Turbidity2A-04	2A	Recon	Cypress Ck at Grant Rd nr Cypress, TX	3/11/2011	View of right bank from bridge
Turbidity2A-05	2A	Recon	Cypress Ck at Grant Rd nr Cypress, TX	3/11/2011	View of gage box and creek sign on right bank
Turbidity2A-06	2A	Recon	Cypress Ck at Grant Rd nr Cypress, TX	3/11/2011	View downstream from left bank under bridge
Turbidity2A-07	2A	1	Cypress Ck at Grant Rd nr Cypress, TX	4/19/2011	View upstream from midchannel
Turbidity2A-08	2A	1	Cypress Ck at Grant Rd nr Cypress, TX	4/19/2011	View of left bank from midchannel; EIH personnel collecting SS sample
Turbidity2A-09	2A	1	Cypress Ck at Grant Rd nr Cypress, TX	4/19/2011	View facing downstream from midchannel
Turbidity2A-10	2A	1	Cypress Ck at Grant Rd nr Cypress, TX	4/19/2011	View facing right bank from midchannel
Turbidity2A-11	2A	1	Cypress Ck at Grant Rd nr Cypress, TX	5/13/2011	View of left bank from left bank showing water line from rain event the day before
Turbidity2A-12	2A	2	Cypress Ck at Grant Rd nr Cypress, TX	6/27/2011	View of EIH personnel rinsing bottles before sampling
Turbidity2A-13	2A	2	Cypress Ck at Grant Rd nr Cypress, TX	6/27/2011	View of EIH personnel collecting SS sample on left bank
Turbidity2B-01	2B	Recon	Cypress Ck at Stuebner-Airline Rd nr Westfield, TX	3/11/2011	View of gage box and creek sign on right bank
Turbidity2B-02	2B	Recon	Cypress Ck at Stuebner-Airline Rd nr Westfield, TX	3/11/2011	View of left bank from bridge
Turbidity2B-03	2B	Recon	Cypress Ck at Stuebner-Airline Rd nr Westfield, TX	3/11/2011	View downstream from bridge
Turbidity2B-04	2B	Recon	Cypress Ck at Stuebner-Airline Rd nr Westfield, TX	3/11/2011	View of right bank from bridge
Turbidity2B-05	2B	Recon	Cypress Ck at Stuebner-Airline Rd nr Westfield, TX	3/11/2011	Vertical view of gage piping on right bank
Turbidity2B-06	2B	Recon	Cypress Ck at Stuebner-Airline Rd nr Westfield, TX	3/11/2011	View under bridge from left bank, towards downstream
Turbidity2B-07	2B	1	Cypress Ck at Stuebner-Airline Rd nr Westfield, TX	4/18/2011	View of EIH personnel deploying datasonde with PVC housing
Turbidity2B-08	2B	1	Cypress Ck at Stuebner-Airline Rd nr Westfield, TX	4/18/2011	View facing upstream from channel
Turbidity2B-09	2B	1	Cypress Ck at Stuebner-Airline Rd nr Westfield, TX	4/18/2011	View facing downstream from channel
Turbidity2B-10	2B	1	Cypress Ck at Stuebner-Airline Rd nr Westfield, TX	4/18/2011	View of right bank from channel
Turbidity2B-11	2B	1	Cypress Ck at Stuebner-Airline Rd nr Westfield, TX	4/18/2011	View of deployed datasonde with PVC housing at deployment
Turbidity2B-12	2B	1	Cypress Ck at Stuebner-Airline Rd nr Westfield, TX	5/11/2011	View of deployed datasonde with PVC housing at retrieval
Turbidity2B-13	2B	3a	Cypress Ck at Stuebner-Airline Rd nr Westfield, TX	8/25/2011	View from right bank of water level and EIH personnel taking samples and flow
Turbidity2B-14	2B	3a	Cypress Ck at Stuebner-Airline Rd nr Westfield, TX	8/25/2011	View of submerged gage piping on right bank
Turbidity2B-15	2B	3a	Cypress Ck at Stuebner-Airline Rd nr Westfield, TX	9/13/2011	View from right bank of low water level, also EIH personnel collecting samples
Turbidity2B-16	2B	3a	Cypress Ck at Stuebner-Airline Rd nr Westfield, TX	9/13/2011	View towards downstream of debris in channel from right bank
Turbidity2B-17	2B	3a	Cypress Ck at Stuebner-Airline Rd nr Westfield, TX	9/13/2011	View of datasonde completely out of water due to low water level
Turbidity2B-18	2B	4	Cypress Ck at Stuebner-Airline Rd nr Westfield, TX	11/22/2011	View from right bank of deployed datasonde at midpoint sampling
Turbidity2B-19	2B	4	Cypress Ck at Stuebner-Airline Rd nr Westfield, TX	11/22/2011	View of right bank from right bank showing debris and erosion evidence of recent water level rise due to rainfall
Turbidity2B-20	2B	4	Cypress Ck at Stuebner-Airline Rd nr Westfield, TX	12/14/2011	View of left bank from right bank under bridge
Turbidity2B-21	2B	4	Cypress Ck at Stuebner-Airline Rd nr Westfield, TX	12/14/2011	View downstream from right bank under bridge
Turbidity2B-22	2B	4	Cypress Ck at Stuebner-Airline Rd nr Westfield, TX	12/14/2011	View of right bank from right bank under bridge
Turbidity2B-23	2B	4	Cypress Ck at Stuebner-Airline Rd nr Westfield, TX	12/14/2011	View upstream from right bank under bridge, EIH personnel in channel taking flow
Turbidity2B-24	2B	4	Cypress Ck at Stuebner-Airline Rd nr Westfield, TX	12/14/2011	View of right bank showing evidence of recent water-level rise due to rainfall
Turbidity2B-25	2B	4	Cypress Ck at Stuebner-Airline Rd nr Westfield, TX	12/14/2011	View of erosion on left bank from right bank under bridge
Turbidity2B-26	2B	4	Cypress Ck at Stuebner-Airline Rd nr Westfield, TX	12/14/2011	View of datasonde probes with some dirt and debris at retrieval
Turbidity2B-27	2B	4	Cypress Ck at Stuebner-Airline Rd nr Westfield, TX	12/14/2011	View of datasonde probes with some dirt and debris at retrieval

Photograph Number	Site	Sample Period	Site Description	Date	Photograph Description
Turbidity2D-01	2D	Recon	Greens Bayou nr Houston, TX	3/11/2011	View upstream from right bank, downstream of bridge
Turbidity2D-02	2D	Recon	Greens Bayou nr Houston, TX	3/11/2011	View of left bank from right bank
Turbidity2D-03	2D	Recon	Greens Bayou nr Houston, TX	3/11/2011	View downstream from bridge
Turbidity2D-04	2D	Recon	Greens Bayou nr Houston, TX	3/11/2011	View of left bank with culvert from bridge, EIH vehicle visible
Turbidity2D-05	2D	Recon	Greens Bayou nr Houston, TX	3/11/2011	Vertical view of left bank from bridge
Turbidity2D-06	2D	1	Greens Bayou nr Houston, TX	4/19/2011	View facing upstream from channel
Turbidity2D-07	2D	1	Greens Bayou nr Houston, TX	4/19/2011	View facing left bank from channel
Turbidity2D-08	2D	1	Greens Bayou nr Houston, TX	4/19/2011	View facing downstream from channel
Turbidity2D-09	2D	1	Greens Bayou nr Houston, TX	4/19/2011	View facing right bank from channel, EIH personnel rinsing bottles
Turbidity2E-01	2E	Recon	Greens Bayou nr US Hwy 75 nr Houston, TX	3/11/2011	View upstream from bridge
Turbidity2E-02	2E	Recon	Greens Bayou nr US Hwy 75 nr Houston, TX	3/11/2011	View of left bank from bridge
Turbidity2E-03	2E	Recon	Greens Bayou nr US Hwy 75 nr Houston, TX	3/11/2011	View downstream from bridge
Turbidity2E-04	2E	Recon	Greens Bayou nr US Hwy 75 nr Houston, TX	3/11/2011	View of right bank from bridge
Turbidity2E-05	2E	Recon	Greens Bayou nr US Hwy 75 nr Houston, TX	3/11/2011	View of bridge from right bank
Turbidity2E-06	2E	1	Greens Bayou nr US Hwy 75 nr Houston, TX	4/19/2011	View facing right bank
Turbidity2E-07	2E	1	Greens Bayou nr US Hwy 75 nr Houston, TX	4/19/2011	View facing downstream
Turbidity2E-08	2E	1	Greens Bayou nr US Hwy 75 nr Houston, TX	4/19/2011	View facing upstream
Turbidity2E-09	2E	1	Greens Bayou nr US Hwy 75 nr Houston, TX	4/19/2011	View facing left bank
Turbidity2E-10	2E	2	Greens Bayou nr US Hwy 75 nr Houston, TX	6/27/2011	View of left bank from right bank, EIH personnel collecting SS samples
Turbidity2E-11	2E	2	Greens Bayou nr US Hwy 75 nr Houston, TX	6/27/2011	View facing upstream taken from right bank
Turbidity2E-12	2E	2	Greens Bayou nr US Hwy 75 nr Houston, TX	6/27/2011	View facing downstream taken from right bank
Turbidity2E-13	2E	4	Greens Bayou nr US Hwy 75 nr Houston, TX	11/8/2011	View of high water level and flow from right bank, downstream
Turbidity2E-14	2E	4	Greens Bayou nr US Hwy 75 nr Houston, TX	11/8/2011	View of high water level and flow at bridge from right bank, downstream
Turbidity2E-15	2E	4	Greens Bayou nr US Hwy 75 nr Houston, TX	11/8/2011	View of high water level and flow from right bank, downstream
Turbidity2E-16	2E	4	Greens Bayou nr US Hwy 75 nr Houston, TX	11/8/2011	View of high water level and flow from right bank, upstream
Turbidity2E-17	2E	4	Greens Bayou nr US Hwy 75 nr Houston, TX	11/8/2011	Vertical view of rushing water from upstream side of bridge
Turbidity2E-18	2E	4	Greens Bayou nr US Hwy 75 nr Houston, TX	11/8/2011	View upstream of high flow from bridge
Turbidity2E-19	2E	4	Greens Bayou nr US Hwy 75 nr Houston, TX	11/8/2011	View of debris caught on sonde (with SS sampler used as a weight) from bridge
Turbidity2G-01	2G	Recon	Whiteoak Bayou at Alabonson Rd at Houston, TX	3/11/2011	View upstream from bridge
Turbidity2G-02	2G	Recon	Whiteoak Bayou at Alabonson Rd at Houston, TX	3/11/2011	View of left bank from bridge
Turbidity2G-03	2G	Recon	Whiteoak Bayou at Alabonson Rd at Houston, TX	3/11/2011	View downstream from bridge
Turbidity2G-04	2G	Recon	Whiteoak Bayou at Alabonson Rd at Houston, TX	3/11/2011	View of right bank from bridge
Turbidity2G-05	2G	1	Whiteoak Bayou at Alabonson Rd at Houston, TX	4/19/2011	View facing left bank
Turbidity2G-06	2G	1	Whiteoak Bayou at Alabonson Rd at Houston, TX	4/19/2011	View facing upstream
Turbidity2G-07	2G	1	Whiteoak Bayou at Alabonson Rd at Houston, TX	4/19/2011	View facing right bank
Turbidity2G-08	2G	1	Whiteoak Bayou at Alabonson Rd at Houston, TX	4/19/2011	View facing downstream
Turbidity2G-09	2G	4	Whiteoak Bayou at Alabonson Rd at Houston, TX	6/27/2011	View of right bank from left bank, EIH personnel collecting SS samples
Turbidity3A-01	3A	Recon	Cypress Ck at Katy-Hockley Rd nr Hockley, TX	3/11/2011	View of creek sign
Turbidity3A-02	3A	Recon	Cypress Ck at Katy-Hockley Rd nr Hockley, TX	3/11/2011	View upstream from bridge
Turbidity3A-03	3A	Recon	Cypress Ck at Katy-Hockley Rd nr Hockley, TX	3/11/2011	View of left bank from bridge, upstream side
Turbidity3A-04	3A	Recon	Cypress Ck at Katy-Hockley Rd nr Hockley, TX	3/11/2011	View downstream from bridge
Turbidity3A-05	3A	Recon	Cypress Ck at Katy-Hockley Rd nr Hockley, TX	3/11/2011	View of right bank from downstream side of bridge
Turbidity3A-06	3A	Recon	Cypress Ck at Katy-Hockley Rd nr Hockley, TX	3/11/2011	View downstream from under bridge, right bank
Turbidity3A-07	3A	1	Cypress Ck at Katy-Hockley Rd nr Hockley, TX	4/18/2011	View facing upstream, EIH personnel collecting SS sample
Turbidity3A-08	3A	1	Cypress Ck at Katy-Hockley Rd nr Hockley, TX	4/18/2011	View facing downstream
Turbidity3A-09	3A	1	Cypress Ck at Katy-Hockley Rd nr Hockley, TX	4/18/2011	View facing left bank
Turbidity3A-10	3A	1	Cypress Ck at Katy-Hockley Rd nr Hockley, TX	4/18/2011	View facing right bank
Turbidity3A-11	3A	1	Cypress Ck at Katy-Hockley Rd nr Hockley, TX	4/18/2011	View of EIH personnel deploying datasonde in lockbox
Turbidity3A-12	3A	1	Cypress Ck at Katy-Hockley Rd nr Hockley, TX	5/3/2011	View of sonde box barely submerged due to water level drop
Turbidity3A-13	3A	1	Cypress Ck at Katy-Hockley Rd nr Hockley, TX	5/11/2011	View of completely exposed sonde box due to water level drop
Turbidity3A-14	3A	1	Cypress Ck at Katy-Hockley Rd nr Hockley, TX	5/11/2011	View of large pool found approximately 100m upstream of bridge where sonde was redeployed
Turbidity3A-15	3A	1	Cypress Ck at Katy-Hockley Rd nr Hockley, TX	5/13/2011	View of small, shallow pools from recent rainfall after bed was dry
Turbidity3A-16	3A	1	Cypress Ck at Katy-Hockley Rd nr Hockley, TX	5/13/2011	View approx 100m upstream of bridge of small, shallow pools from recent rainfall
Turbidity3A-17	3A	2	Cypress Ck at Katy-Hockley Rd nr Hockley, TX	6/27/2011	View of EIH personnel deploying datasonde
Turbidity3A-18	3A	2	Cypress Ck at Katy-Hockley Rd nr Hockley, TX	6/27/2011	View of EIH personnel deploying datasonde, sediment cloud kicked up
Turbidity3A-19	3A	3a	Cypress Ck at Katy-Hockley Rd nr Hockley, TX	8/25/2011	Vertical view of ribbon snake swimming in sampling pool
Turbidity3A-20	3A	3a	Cypress Ck at Katy-Hockley Rd nr Hockley, TX	8/25/2011	View of pool sampled from downstream side
Turbidity3A-21	3A	3a	Cypress Ck at Katy-Hockley Rd nr Hockley, TX	8/25/2011	View of rat snake in sampling pool
Turbidity3A-22	3A	3a	Cypress Ck at Katy-Hockley Rd nr Hockley, TX	8/25/2011	View of rat snake in sampling pool
Turbidity3A-23	3A	3a	Cypress Ck at Katy-Hockley Rd nr Hockley, TX	8/25/2011	View of depth reading in sampling pool
Turbidity3A-24	3A	3a	Cypress Ck at Katy-Hockley Rd nr Hockley, TX	8/25/2011	View of pool approx. 100m upstream of bridge
Turbidity3A-25	3A	3a	Cypress Ck at Katy-Hockley Rd nr Hockley, TX	8/25/2011	View of pool just upstream of bridge
Turbidity3A-26	3A	3a	Cypress Ck at Katy-Hockley Rd nr Hockley, TX	8/25/2011	View downstream from midchannel
Turbidity3A-27	3A	3a	Cypress Ck at Katy-Hockley Rd nr Hockley, TX	8/25/2011	View of leaves and debris under bridge
Turbidity3A-28	3A	3a	Cypress Ck at Katy-Hockley Rd nr Hockley, TX	9/13/2011	Photograph of creek bed during sample period, site completely dry, no samples collected
Turbidity3A-29	3A	3a	Cypress Ck at Katy-Hockley Rd nr Hockley, TX	9/28/2011	View upstream from midchannel
Turbidity3A-30	3A	3a	Cypress Ck at Katy-Hockley Rd nr Hockley, TX	9/28/2011	View downstream from midchannel
Turbidity3A-31	3A	3b	Cypress Ck at Katy-Hockley Rd nr Hockley, TX	10/6/2011	View downstream from midchannel
Turbidity3A-32	3A	3b	Cypress Ck at Katy-Hockley Rd nr Hockley, TX	10/6/2011	View upstream from right bank
Turbidity3A-33	3A	3b	Cypress Ck at Katy-Hockley Rd nr Hockley, TX	10/6/2011	View downstream from bridge
Turbidity3A-34	3A	3b	Cypress Ck at Katy-Hockley Rd nr Hockley, TX	10/10/2011	View upstream from channel after large rainfall event
Turbidity3A-35	3A	3b	Cypress Ck at Katy-Hockley Rd nr Hockley, TX	10/10/2011	View downstream from channel after large rainfall event
Turbidity3A-36	3A	3b	Cypress Ck at Katy-Hockley Rd nr Hockley, TX	10/10/2011	View of EIH personnel in channel at sondebox showing water level
Turbidity3A-37	3A	3b	Cypress Ck at Katy-Hockley Rd nr Hockley, TX	10/20/2011	View upstream from channel near right bank
Turbidity3A-38	3A	4	Cypress Ck at Katy-Hockley Rd nr Hockley, TX	11/22/2011	Vertical view of channel from left bank
Turbidity3A-39	3A	4	Cypress Ck at Katy-Hockley Rd nr Hockley, TX	11/22/2011	View upstream from left bank
Turbidity3A-40	3A	4	Cypress Ck at Katy-Hockley Rd nr Hockley, TX	11/22/2011	View downstream from left bank
Turbidity3A-41	3A	4	Cypress Ck at Katy-Hockley Rd nr Hockley, TX	12/8/2011	View upstream from channel approx. 50m upstream of bridge
Turbidity3A-42	3A	4	Cypress Ck at Katy-Hockley Rd nr Hockley, TX	12/8/2011	View downstream from channel approx. 50m upstream of bridge
Turbidity3A-43	3A	4	Cypress Ck at Katy-Hockley Rd nr Hockley, TX	12/8/2011	View of left bank from right bank, EIH personnel sampling SS
Turbidity4A-01	4A	Recon	Brays Bayou at Alief, TX	3/21/2011	View upstream from bridge
Turbidity4A-02	4A	Recon	Brays Bayou at Alief, TX	3/21/2011	View of top of lock box with pipe on downstream side of bridge
Turbidity4A-03	4A	Recon	Brays Bayou at Alief, TX	3/21/2011	Vertical view of lock box piping going down towards the water
Turbidity4A-04	4A	Recon	Brays Bayou at Alief, TX	3/21/2011	View downstream from bridge, view obstructed by foot bridge
Turbidity4A-05	4A	Recon	Brays Bayou at Alief, TX	3/21/2011	View of right bank from right bank upstream of bridge
Turbidity4A-06	4A	Recon	Brays Bayou at Alief, TX	3/21/2011	View of right bank from left bank under bridge
Turbidity4A-07	4A	Recon	Brays Bayou at Alief, TX	3/21/2011	View of left bank from left bank under bridge, gage piping visible
Turbidity4A-08	4A	1	Brays Bayou at Alief, TX	4/18/2011	View of EIH personnel deploying sonde with lockbox
Turbidity4A-09	4A	1	Brays Bayou at Alief, TX	4/18/2011	View of EIH personnel deploying sonde with lockbox
Turbidity4A-10	4A	2	Brays Bayou at Alief, TX	5/13/2011	View upstream from midchannel, showing slightly elevated water levels

Photograph Number	Site	Sample Period	Site Description	Date	Photograph Description
Turbidity4A-11	4A	3b	Brays Bayou at Alief, TX	10/20/2011	View of sonde probes with settled sediment at retrieval
Turbidity4A-12	4A	3b	Brays Bayou at Alief, TX	10/20/2011	View of sonde probes with settled sediment at retrieval
Turbidity4A-13	4A	4	Brays Bayou at Alief, TX	11/22/2011	View towards upstream showing higher water level from left bank
Turbidity4A-14	4A	4	Brays Bayou at Alief, TX	11/22/2011	View towards bridge showing higher water level from left bank
Turbidity4A-15	4A	4	Brays Bayou at Alief, TX	11/22/2011	View of debris deposited on left bank from high flows
Turbidity4A-16	4A	4	Brays Bayou at Alief, TX	12/5/2011	View of channel from top of left bank showing high water level
Turbidity4A-17	4A	4	Brays Bayou at Alief, TX	12/5/2011	View upstream from left bank showing high water level
Turbidity4A-18	4A	4	Brays Bayou at Alief, TX	12/14/2011	View of sonde probes with settled sediment at retrieval
Turbidity4A-19	4A	4	Brays Bayou at Alief, TX	12/14/2011	View of sonde probes with settled sediment at retrieval
Turbidity4B-01	4B	Recon	Buffalo Bayou nr Addicks, TX	3/21/2011	View upstream and of right bank from right bank under downstream bridge
Turbidity4B-02	4B	Recon	Buffalo Bayou nr Addicks, TX	3/21/2011	View of left bank from right bank under downstream bridge
Turbidity4B-03	4B	Recon	Buffalo Bayou nr Addicks, TX	3/21/2011	View upstream and of left bank from right bank under upstream bridge
Turbidity4B-04	4B	Recon	Buffalo Bayou nr Addicks, TX	3/21/2011	View upstream from upstream bridge
Turbidity4B-05	4B	Recon	Buffalo Bayou nr Addicks, TX	3/21/2011	View of right bank towards downstream from left bank under upstream bridge
Turbidity4B-06	4B	Recon	Buffalo Bayou nr Addicks, TX	3/21/2011	View of EIH personnel on right bank from left bank, good view of bank slope/incline
Turbidity4B-07	4B	Recon	Buffalo Bayou nr Addicks, TX	3/21/2011	Close-up view of culvert on right bank from downstream bridge
Turbidity4B-08	4B	Recon	Buffalo Bayou nr Addicks, TX	3/21/2011	Vertical view of channel downstream from downstream bridge
Turbidity4B-09	4B	Recon	Buffalo Bayou nr Addicks, TX	3/21/2011	View downstream from downstream bridge, view obstructed by piping
Turbidity4B-10	4B	1	Buffalo Bayou nr Addicks, TX	4/20/2011	View facing upstream from midchannel
Turbidity4B-11	4B	1	Buffalo Bayou nr Addicks, TX	4/20/2011	View facing left bank from midchannel
Turbidity4B-12	4B	1	Buffalo Bayou nr Addicks, TX	4/20/2011	View facing downstream from midchannel
Turbidity4B-13	4B	1	Buffalo Bayou nr Addicks, TX	4/20/2011	View facing right bank from midchannel
Turbidity4B-14	4B	1	Buffalo Bayou nr Addicks, TX	5/13/2011	View across channel from left bank during elevated flow, EIH personnel traversing
Turbidity4B-15	4B	1	Buffalo Bayou nr Addicks, TX	5/13/2011	View across channel from left bank during elevated flow, EIH personnel traversing
Turbidity5A-01	5A	Recon	Brays Bayou at Houston, TX	3/11/2011	View upstream from left bank
Turbidity5A-02	5A	Recon	Brays Bayou at Houston, TX	3/11/2011	View of left bank from left bank
Turbidity5A-03	5A	Recon	Brays Bayou at Houston, TX	3/11/2011	View downstream from left bank
Turbidity5A-04	5A	Recon	Brays Bayou at Houston, TX	3/11/2011	View of right bank from left bank
Turbidity5A-05	5A	Recon	Brays Bayou at Houston, TX	3/11/2011	Vertical view of channel contrasting depth difference
Turbidity5A-06	5A	1	Brays Bayou at Houston, TX	4/20/2011	View facing upstream from
Turbidity5A-07	5A	1	Brays Bayou at Houston, TX	4/20/2011	View facing left bank
Turbidity5A-08	5A	1	Brays Bayou at Houston, TX	4/20/2011	View facing downstream
Turbidity5A-09	5A	1	Brays Bayou at Houston, TX	4/20/2011	View facing right bank
Turbidity5A-10	5A	4	Brays Bayou at Houston, TX	12/5/2011	View upstream from bridge of high flow
Turbidity5B-01	5B	Recon	Halls Bayou at Houston, TX	3/11/2011	View upstream from bridge
Turbidity5B-02	5B	Recon	Halls Bayou at Houston, TX	3/11/2011	View of left bank from bridge
Turbidity5B-03	5B	Recon	Halls Bayou at Houston, TX	3/11/2011	View downstream from bridge
Turbidity5B-04	5B	Recon	Halls Bayou at Houston, TX	3/11/2011	View of right bank from bridge
Turbidity5B-05	5B	1	Halls Bayou at Houston, TX	4/18/2011	View facing upstream, also visible: UHCL-EIH personnel placing lockbox housing for in situ sonde
Turbidity5B-06	5B	1	Halls Bayou at Houston, TX	4/18/2011	View facing left bank
Turbidity5B-07	5B	1	Halls Bayou at Houston, TX	4/18/2011	View facing downstream
Turbidity5B-08	5B	1	Halls Bayou at Houston, TX	4/18/2011	View facing right bank
Turbidity5B-09	5B	3a	Halls Bayou at Houston, TX	9/13/2011	Photograph of surface almost completely choked with water lettuce and showing water level drop
Turbidity5B-10	5B	3a	Halls Bayou at Houston, TX	9/13/2011	Photograph of deployed in situ sonde lockbox visible on creek bottom
Turbidity5B-11	5B	3b	Halls Bayou at Houston, TX	10/20/2011	View upstream of construction from top of left bank, EIH personnel in channel
Turbidity5B-12	5B	3b	Halls Bayou at Houston, TX	10/20/2011	View of construction on right bank from top of left bank, EIH personnel in channel
Turbidity5B-13	5B	3b	Halls Bayou at Houston, TX	10/20/2011	View of construction on left bank from top of left bank, EIH personnel in channel
Turbidity5B-14	5B	3b	Halls Bayou at Houston, TX	10/20/2011	View of construction machinery and temp. buildings on left bank
Turbidity5B-15	5B	3b	Halls Bayou at Houston, TX	10/20/2011	View of sediment settled on datasonde probes at retrieval
Turbidity5B-16	5B	3b	Halls Bayou at Houston, TX	10/20/2011	View of sediment settled on datasonde probes at retrieval
Turbidity5B-17	5B	3b	Halls Bayou at Houston, TX	10/20/2011	View of EIH personnel in channel retrieving sonde box
Turbidity5B-18	5B	3b	Halls Bayou at Houston, TX	11/1/2011	View of construction vehicles on left bank
Turbidity5B-19	5B	3b	Halls Bayou at Houston, TX	11/1/2011	View of graded bank and piled up dirt and debris - left bank
Turbidity5B-20	5B	3b	Halls Bayou at Houston, TX	11/1/2011	View of dirt piles left and right banks
Turbidity5B-21	5B	3b	Halls Bayou at Houston, TX	11/1/2011	View of mowing tractor on right bank
Turbidity5B-22	5B	3b	Halls Bayou at Houston, TX	11/1/2011	View of freshly mowed right bank
Turbidity5B-23	5B	3b	Halls Bayou at Houston, TX	11/1/2011	Closer view of dirt piles and machinery on right bank
Turbidity5B-24	5B	3b	Halls Bayou at Houston, TX	11/1/2011	Overview of whole area being worked on
Turbidity5B-25	5B	4	Halls Bayou at Houston, TX	11/10/2011	View of construction machinery and temp. buildings on left bank
Turbidity5B-26	5B	4	Halls Bayou at Houston, TX	11/10/2011	View of dump trucks on newly graded area on left bank
Turbidity5B-27	5B	4	Halls Bayou at Houston, TX	11/10/2011	View of dump trucks on newly graded area on left bank, EIH personnel in channel
Turbidity5B-28	5B	4	Halls Bayou at Houston, TX	11/10/2011	View of fresh tire marks on right bank from left bank, EIH personnel in channel
Turbidity5B-29	5B	4	Halls Bayou at Houston, TX	11/10/2011	View of dump trucks coming into construction area from street, left bank
Turbidity5B-30	5B	4	Halls Bayou at Houston, TX	11/10/2011	View of fresh tire marks on right bank from left bank
Turbidity5B-31	5B	4	Halls Bayou at Houston, TX	11/10/2011	View of EIH personnel in channel
Turbidity5B-32	5B	4	Halls Bayou at Houston, TX	11/22/2011	View of EIH personnel in channel
Turbidity5B-33	5B	4	Halls Bayou at Houston, TX	11/22/2011	View of progressed construction on left bank from left bank
Turbidity5B-34	5B	4	Halls Bayou at Houston, TX	11/22/2011	View upstream from left bank of elevated water level, EIH personnel at bank
Turbidity5B-35	5B	4	Halls Bayou at Houston, TX	11/22/2011	View of EIH personnel sampling in rain
Turbidity5B-36	5B	4	Halls Bayou at Houston, TX	11/22/2011	View of EIH personnel sampling in rain
Turbidity5B-37	5B	4	Halls Bayou at Houston, TX	11/22/2011	View of EIH personnel sampling in rain
Turbidity5B-38	5B	4	Halls Bayou at Houston, TX	11/22/2011	View of EIH personnel in channel checking sonde at midpoint sampling
Turbidity5B-39	5B	4	Halls Bayou at Houston, TX	11/22/2011	View of EIH personnel in channel checking sonde at midpoint sampling
Turbidity5B-40	5B	4	Halls Bayou at Houston, TX	11/22/2011	View towards upstream showing elevated water level from left bank
Turbidity5B-41	5B	4	Halls Bayou at Houston, TX	11/22/2011	View towards bridge showing elevated water level from left bank
Turbidity5B-42	5B	4	Halls Bayou at Houston, TX	12/6/2011	View of progressed construction on left bank from left bank
Turbidity5B-43	5B	4	Halls Bayou at Houston, TX	12/6/2011	View of channel and EIH personnel, tire marks still pronounced on right bank
Turbidity5B-44	5B	4	Halls Bayou at Houston, TX	12/6/2011	Close-up view of eroded pocket on right bank from midchannel
Turbidity5B-45	5B	4	Halls Bayou at Houston, TX	12/14/2011	View of sediment settled on datasonde probes at retrieval
Turbidity5B-46	5B	4	Halls Bayou at Houston, TX	12/14/2011	View of sediment settled on datasonde probes at retrieval
Turbidity5B-47	5B	4	Halls Bayou at Houston, TX	12/14/2011	View of trucks moving around on cleared bank from left bank
Turbidity5C-01	5C	Recon	Whiteoak Bayou at Houston, TX	3/11/2011	View upstream from right bank
Turbidity5C-02	5C	Recon	Whiteoak Bayou at Houston, TX	3/11/2011	View of left bank from right bank
Turbidity5C-03	5C	Recon	Whiteoak Bayou at Houston, TX	3/11/2011	View downstream from bridge
Turbidity5C-04	5C	Recon	Whiteoak Bayou at Houston, TX	3/11/2011	View of right bank from right bank
Turbidity5C-05	5C	Recon	Whiteoak Bayou at Houston, TX	3/11/2011	View downstream from bridge
Turbidity5C-06	5C	1	Whiteoak Bayou at Houston, TX	4/20/2011	View facing left bank
Turbidity5C-07	5C	1	Whiteoak Bayou at Houston, TX	4/20/2011	View facing downstream
Turbidity5C-08	5C	1	Whiteoak Bayou at Houston, TX	4/20/2011	View facing right bank
Turbidity5C-09	5C	1	Whiteoak Bayou at Houston, TX	4/20/2011	View facing upstream
Turbidity5C-10	5C	3a	Whiteoak Bayou at Houston, TX	9/30/2011	View facing downstream from bridge. Flow was high at time of sampling, samples taken from bridge
Turbidity5C-11	5C	3a	Whiteoak Bayou at Houston, TX	9/30/2011	Vertical view of water under downstream side of bridge showing high flow at time of sampling

Appendix 3: Interactive Google Earth Map (Electronic Supplement)

*See Compact Disk at Rear of Report for Electronic Supplements



Example Screen Shot of the Google Earth Interactive Map.

Appendix 4: Forms and Datasheets

Datasheet used for reconnaissance of initial 29 sites

Environmental Institute of Houston - University of Houston Clear Lake HCFCF Turbidity Study Recon.		
Date: _____		Collected By: _____
Site: _____	Lat: _____	Long: _____
Time: arrive _____ depart _____	Photos U__L__D__R__	
Access Notes: _____		<i>(Verify gage)</i>
Sonde Secure Point: _____		
Flow Comments: _____		Wadeable Y N
Sediment Type: _____		Riparian Zone L _____ R _____
Site: _____	Lat: _____	Long: _____
Time: arrive _____ depart _____	Photos U__L__D__R__	
Access Notes: _____		<i>(Verify gage)</i>
Sonde Secure Point: _____		
Flow Comments: _____		Wadeable Y N
Sediment Type: _____		Riparian Zone L _____ R _____
Site: _____	Lat: _____	Long: _____
Time: arrive _____ depart _____	Photos U__L__D__R__	
Access Notes: _____		<i>(Verify gage)</i>
Sonde Secure Point: _____		
Flow Comments: _____		Wadeable Y N
Sediment Type: _____		Riparian Zone L _____ R _____
Site: _____	Lat: _____	Long: _____
Time: arrive _____ depart _____	Photos U__L__D__R__	
Access Notes: _____		<i>(Verify gage)</i>
Sonde Secure Point: _____		
Flow Comments: _____		Wadeable Y N
Sediment Type: _____		Riparian Zone L _____ R _____
Site: _____	Lat: _____	Long: _____
Time: arrive _____ depart _____	Photos U__L__D__R__	
Access Notes: _____		<i>(Verify gage)</i>
Sonde Secure Point: _____		
Flow Comments: _____		Wadeable Y N
Sediment Type: _____		Riparian Zone L _____ R _____
ADDITIONAL INFORMATION & REMARKS ON BACK		

Field datasheet used throughout study at all sampling sites

Environmental Institute of Houston - University of Houston Clear Lake (HCFCD) Turbidity Study Field Data/Sampling Sheet			
Station ID: _____		Date: _____	
Time: arrive _____		sample _____	
depart _____			
Location: _____			
Collected By: _____		Lat: _____	
		Long: _____	
THALWEG FIELD MEASUREMENTS			
	Surface	Middle	Bottom
Temp (C)			
Conductivity (uS)			
Salinity (psu)			
DO (%sat)			
DO mg/L			
pH			
Depth (m)			
Turbidity (probe) (NTU)			
FIELD MEASUREMENTS CONT.			
	Left (facing downstream)	Middle	Right (facing downstream)
Sample Location (m)			
Turbidity (probe) (NTU)			
Turbidity (LaMotte) (NTU)			
TSS			
SS			
SS deployment time			
Total Depth (m)			
Secchi (m)			
FIELD OBSERVATIONS			
<input type="text"/>	Days since last sig. rainfall (From HCOEM gage)	<input type="text"/>	Total Depth at Thalweg (m)
<input type="text"/>	Water Color 1-brownish 2-reddish 3-greenish 4-blackish 5-clear 6-other	<input type="text"/>	UGSG Gage Number
<input type="text"/>	Water Odor 1-sewage 2-chemical 3-rotten egg 4-musky 5-fishy 6-none 7-other	<input type="text"/>	Flow (cfs) (from USGS Gage)
<input type="text"/>	Present Weather 1-clear 2-partly cloudy 3-cloudy 4-rain	<input type="text"/>	Gage height (ft) (from USGS Gage)
<input type="text"/>	Time Sonde Deployed / Retrieved	<input type="text"/>	Water Field Split Collected? (Yes/No)
		<input type="text"/>	Total Stream Width (m)
		<input type="text"/>	Cell Width (m)
SAMPLES			
Container	Preservative	Analysis Requested	Comments
3 x 1L - Plastic	Ice	TSS	water grab from surface layer
4 x 3L or 4L cubetainer - Plastic	Ice	SS	
ADDITIONAL INFORMATION & REMARKS			

Appendix 5: Calibration Data (Electronic Supplement)

*See Compact Disk at Rear of Report for Electronic Supplements

Appendix 6: ArcGIS Technical Methods

Turbidity Study in the Harris County Watersheds

1. Technical Objectives and Steps

1. Delineating the watersheds that are associated with the active USGS stations, where measurements of surface water discharge are available.
2. Extracting the current measurements of surface-water discharge and the archived statistics at the active USGS stations.
3. Linking the active USGS stations to the soil types within watersheds
4. Linking the active USGS stations to the land-use data within watersheds
5. Linking watersheds and streams.
6. Runoff calculation for hourly and daily rainfall datasets

2. Data

- Water-surface discharge at the active USGS stations acquired from the web interface of the National water information system.
- Digital Elevation Model (DEM) acquired from the National Elevation Data at 30 m spatial resolution.
- Multi-resolution land cover 2001 (National dataset)
- Harris County land cover 2008
- Harris County soil map acquired in October 2000 (<http://www.eng.hctx.net/GIS/gis.htm#HCFCD>)
- National soil dataset
- 2008 TCEQ Stream segments
- HCFCD Channels acquired in April 2004 (<http://www.eng.hctx.net/GIS/gis.htm#HCFCD>)
- Watershed Boundary Dataset – National dataset available from the National Resources Conservation Service (NRCS) website
- Sub-watershed delineation of the Tropical Storm Alison Recovery Project (TSARP)
- Hourly rainfall records for 99 rain gages that correspond to the sampling dates and times
- Daily rainfall records for 99 rain gages that correspond to the sampling dates

3. Method

3.1. USGS stations

- 37 active USGS stations in the Harris County were identified with 31 stations having archived statistics for daily surface-water discharge over an operational period ranging between 2 and 74 years. Each station is identified by its number.

- The current statistics of surface-water discharge include water discharge, long-term daily mean and long-term daily median.
- The archived statistics of daily surface-water discharge over the operational periods of the stations include: recent discharge, minimum, 25th percentile, median, mean, 75th percentile, and maximum. Note that there were a few gaps in these statistics.
- Hyperlinks to the above statistics were established in a shapefile to allow an easy access to the latest archived statistics of water-surface discharge at the USGS stations.

3.2. Watershed Analysis

The following steps/processes were implemented using the ArcGIS platform:

- Artificial sinks were removed from the topographical dataset (i.e. DEM at 30 m spatial resolution).
- The flow direction and accumulated flow maps have been created.
- The USGS stations have been located appropriately on the accumulated flow map.
- The watersheds of the USGS stations have been produced.
- The created watersheds have been checked against the National Watershed Boundary Dataset.
- A spatial link has been established between the gage stations and associated watersheds using the station numbers.
- The soil types within watersheds were summarized (using the area in square meter per soil type) and an attribute table was produced. The soil types have been aggregated regardless of the slope. The consideration of the slope can be achieved at much higher scale or at the original soil map scale.
- The land use classes within watershed were summarized for further use in water and hydrology analysis.

3.2.1 Results

Hydrological and rainfall data were spatially aggregated into multiple ArcGIS attribute tables to facilitate spatial analysis. Examples of each of these are illustrated below.

- The attribute table of the daily surface-water discharge and statistics is shown below:

FID	Shape*	StationID	Address	Lat	Long	LTMean	LTMedian	Discharge	Date	Min	Recent	th25	Median	th75	Mean	Max	YearMin	YearMax	Period	Link		
1	Point	8067525	Goose Ck at Baytown, TX	29.770782	-94.99965	10.0	6.30	1.1	02/02	0.31	1.6	1.3	6.3	23	10	28	2009	2007	4	http://waterdata.usgs.gov/bun		
1	Point	8068325	Willow Ck nr Tomball, TX	30.105495	-95.546688	43.0	43.0	3.2	02/02	5.2	2.9	-9999	43	-9999	43	80	2008	2007	2	http://waterdata.usgs.gov/bun		
2	Point	8068720	Cypress Ck at Katy-Hockley Rd nr Hockley, TX	29.560224	-95.000284	48.0	9.30	0.84	02/02	0	0.86	2.8	9.3	33	48	862	1976	2005	35	http://waterdata.usgs.gov/bun		
3	Point	8069740	Cypress Ck at House-Hall Rd nr Cypress, TX	29.859112	-95.717225	59.0	14.0	0.78	02/02	0.16	0.88	2.6	14	51	59	1010	1976	2005	35	http://waterdata.usgs.gov/bun		
4	Point	8068780	Little Cypress Ck nr Cypress, TX	30.016054	-95.697448	25.0	45.0	1.1	02/02	0.08	1.2	0.71	4.5	15	25	384	1986	2005	23	http://waterdata.usgs.gov/bun		
5	Point	8068800	Cypress Ck at Grant Rd nr Cypress, TX	29.973556	-95.586555	147	27.0	12	02/02	3.6	11	14	27	132	147	1540	1986	2005	19	http://waterdata.usgs.gov/bun		
6	Point	8068900	Cypress Ck at Stuebner-Arlene Rd nr Westfield, TX	30.00691	-95.511885	36.0	36.0	164	01/25	0.2	63	20	53	138	136	2080	1951	2005	66	http://waterdata.usgs.gov/bun		
7	Point	8069000	Cypress Ck nr Westfield, TX	30.025775	-95.428227	136	53.0	83	02/02	-9999	-9999	-9999	-9999	-9999	-9999	-9999	-9999	-9999	-9999	35	http://waterdata.usgs.gov/bun	
8	Point	8072730	Bear Ck nr Barker, TX	29.830713	-95.686891	18.0	3.90	3.1	02/02	0.05	3.3	1.1	3.9	12	18	245	1986	2005	33	http://waterdata.usgs.gov/bun		
9	Point	8072760	Langham Ck at W Little York Rd nr Addicks, TX	29.86717	-95.646812	17.0	8.70	13	02/02	2	13	3.2	8.7	21	17	96	1980	2004	11	http://waterdata.usgs.gov/bun		
10	Point	8073500	Buffalo Bayou nr Addicks, TX	29.761896	-95.605778	271	86.0	134	02/02	2.6	135	29	86	274	271	1730	1957	2007	65	http://waterdata.usgs.gov/bun		
11	Point	8073600	Buffalo Bayou at W Beef Dr, Houston, TX	29.762173	-95.557721	393	181	251	02/02	39	239	67	181	420	393	1730	1976	2007	39	http://waterdata.usgs.gov/bun		
12	Point	8073700	Buffalo Bayou at Piney Point, TX	29.746896	-95.523554	355	129	236	02/02	11	230	76	129	439	355	1720	1967	2007	39	http://waterdata.usgs.gov/bun		
13	Point	8074000	Buffalo Bayou at Houston, TX	29.760228	-95.405551	1,550	1,590	148	02/01	1460	-9999	1460	1590	1600	1550	1600	2005	2007	3	http://waterdata.usgs.gov/bun		
14	Point	8074020	Whiteoak Bayou at Alabonson Rd, Houston, TX	29.870781	-95.480496	67.0	30.0	16	02/02	13	17	20	30	67	104	245	2009	2005	9	http://waterdata.usgs.gov/bun		
15	Point	8074150	Cole Ck at Delhi Rd, Houston, TX	29.851337	-95.487996	3.30	3.50	28	02/01	0.12	-9999	1.3	3.5	4.7	3.3	10	1967	1975	22	http://waterdata.usgs.gov/bun		
16	Point	8074250	Brickhouse Gulch at Costa Rica St, Houston, TX	29.620804	-95.469355	6.50	5.50	5.0	02/02	1.11	5	2.8	5.5	6.2	6.5	23	1971	1979	17	http://waterdata.usgs.gov/bun		
17	Point	8074500	Whiteoak Bayou at Houston, TX	29.752208	-95.397161	90.0	47.0	56	02/02	0.9	51	20	47	72	80	1380	1940	1959	74	http://waterdata.usgs.gov/bun		
18	Point	8074540	Little Whiteoak Bayou at Trimble St, Houston, TX	29.792778	-95.380558	-9999	-9999	12	02/02	-999	-9999	-9999	-9999	-9999	-9999	-9999	-9999	-9999	-9999	-9999	39	http://waterdata.usgs.gov/bun
19	Point	8074760	Brays Bayou at Aleaf, TX	29.70912	-95.583	29.0	30.0	30	02/02	19	31	20	30	37	29	37	2009	2008	4	http://waterdata.usgs.gov/bun		
20	Point	8074800	Keegans Bayou at Roark Rd nr Houston, TX	29.656621	-95.562166	7.80	5.80	16	02/02	0.1	16	1.8	5.8	11	7.8	30	1965	1975	17	http://waterdata.usgs.gov/bun		
21	Point	8074810	Brays Bayou at Gessner Dr, Houston, TX	29.672322	-95.526277	112	87.0	97	02/02	49	95	65	87	146	112	273	2009	2005	9	http://waterdata.usgs.gov/bun		
22	Point	8075000	Brays Bayou at Houston, TX	29.697175	-95.412162	150	144	144	02/02	1.9	157	30	110	139	152	3470	1940	1959	74	http://waterdata.usgs.gov/bun		
23	Point	8075110	Brays Bayou at M.L.K. Jr Blvd, Houston, TX	29.714167	-95.338889	-9999	-9999	3,140	01/24	-999	-9999	-9999	-9999	-9999	-9999	-9999	-9999	-9999	-9999	-9999	39	http://waterdata.usgs.gov/bun
24	Point	8075400	Simms Bayou at Hiram Clarke St, Houston, TX	29.618844	-95.446052	18.0	16.0	4.8	02/02	3.1	4.7	10	16	21	18	72	1965	2005	40	http://waterdata.usgs.gov/bun		
25	Point	8075500	Simms Bayou at Houston, TX	29.674397	-95.289381	116	52.0	1,830	01/24	-999	-9999	-9999	-9999	-9999	-9999	-9999	-9999	-9999	-9999	-9999	39	http://waterdata.usgs.gov/bun
26	Point	8075600	Berry Bayou at Nevada St, Houston, TX	29.656919	-95.229101	5.50	4.50	5.6	02/02	3.6	5.8	3.3	4.5	6.3	5.5	9.6	2009	2007	4	http://waterdata.usgs.gov/bun		
27	Point	8075730	Vince Bayou at Pasadena, TX	29.684474	-95.216323	3.50	2.50	3.6	02/02	0.61	3.6	1.6	2.5	3.6	3.5	18	1996	2004	39	http://waterdata.usgs.gov/bun		
28	Point	8075763	Hunting Bayou at Hoffman St, Houston, TX	29.888837	-95.31327	3.60	3.60	2.3	02/02	1.4	2.2	1.8	3.6	5.5	3.6	6	2009	2007	4	http://waterdata.usgs.gov/bun		
29	Point	8075770	Hunting Bayou at H 610, Houston, TX	29.793282	-95.267991	12.0	11.0	7.0	02/02	2.4	7.4	7.9	11	14	12	36	1965	2004	45	http://waterdata.usgs.gov/bun		
30	Point	8075780	Greens Bayou at Cotton Rd nr Houston, TX	29.949112	-95.519693	-9999	-9999	19	02/02	-999	-9999	-9999	-9999	-9999	-9999	-9999	-9999	-9999	-9999	-9999	39	http://waterdata.usgs.gov/bun
31	Point	8075900	Greens Bayou nr US Hwy 75 nr Houston, TX	29.956809	-95.417994	24.0	18.0	30	02/02	4.3	28	11	18	24	14	107	1967	1950	31	http://waterdata.usgs.gov/bun		
32	Point	8076000	Greens Bayou nr Houston, TX	29.918278	-95.30688	63.0	39.0	51	02/02	0	51	17	39	58	63	822	1965	1959	58	http://waterdata.usgs.gov/bun		
33	Point	8076180	Garners Bayou nr Humble, TX	29.933861	-95.233961	35.0	21.0	28	02/02	7.9	29	12	21	32	35	147	1989	2005	17	http://waterdata.usgs.gov/bun		
34	Point	8076500	Halls Bayou at Houston, TX	29.861891	-95.334936	33.0	15.0	18	02/02	0.3	17	8.2	15	22	33	645	1957	1959	51	http://waterdata.usgs.gov/bun		
35	Point	8076700	Greens Bayou at Lay Rd, Houston, TX	29.89117	-95.232267	1,419	1,419	828	01/25	-999	-9999	-9999	-9999	-9999	-9999	-9999	-9999	-9999	-9999	-9999	39	http://waterdata.usgs.gov/bun
36	Point	8076997	Clear Ck at Mykawa St nr Pearland, TX	29.596899	-95.297437	38.0	41.0	26	02/02	6.8	25	15	41	58	38	62	2009	2007	4	http://waterdata.usgs.gov/bun		

- Part of the attribute table that summarizes soil types within watersheds using the Harris County soil dataset is depicted below.

RowID	STATION_NO	OZAHIL_LOAM	MAHATCHE_LOAM	KENNEY_LOAMY_FIN	HATLIFF_LOAM	WATERS	SEGNO_FINE_SANDY	HOCKLEY_FINE_SAN	WOCKLEY_FINE_SAI	GESSNER_LOAM	ATASCO_FINE_SAI	SEGNO_FINE_SAI_1	HOCKLEY_FINE_S_1
1	8067525	0	0	0	0	2025241.1684	0	0	0	424893.8396	0	0	0
2	8068325	21231.8446	0	0	2406427.5744	566218.2528	353886.408	8634820.3552	4458968.7408	46854560.4192	15358670.1072	0	3892750.488
3	8068720	0	0	0	0	353886.408	1910986.6032	3044223.1088	1203213.7872	58037370.912	16066442.9232	0	8142855.1488
4	8068740	0	0	0	0	0	0	0	566218.2528	21162407.1984	21020852.6352	0	0
5	8068780	0	0	0	0	495440.9712	0	1627877.4768	3326532.2352	75519359.467199	4317414.1776	0	1415545.632
6	8068800	1344768.3504	0	0	495440.9712	70777.2816	0	849327.3792	21374739.0432	15428447.3888	0	0	2194985.7296
7	8068900	0	70777.2816	0	0	283109.1264	638995.5344	0	1557100.1952	35671748.9264	21516293.6064	0	707772.816
8	8069000	70777.2816	353886.408	0	0	1910986.6032	495440.9712	778550.0976	283109.1264	68724740.4336	20383857.1008	353886.408	3397309.5168
9	8072730	0	0	0	0	0	0	0	0	638995.5344	0	0	0
10	8072760	0	0	0	0	0	778550.0976	0	0	1132436.5056	7360837.2864	0	0
11	8073500	4883632.4304	0	0	0	566218.2528	0	0	0	353886.408	15287392.8256	0	0
12	8073600	169854.7584	0	0	0	0	0	0	0	0	283109.1264	424863.6896	0
13	8073700	0	849327.3792	0	0	0	0	0	0	0	707772.816	0	0
14	8074000	0	1415545.632	0	0	0	0	0	0	10970478.648	2547982.1376	0	0
15	8074020	0	778550.0976	0	0	0	353886.408	0	0	2477204.856	26470703.3184	0	0
16	8074150	0	0	0	0	0	0	0	0	4388191.4592	0	0	0
17	8074250	0	0	0	0	0	0	0	0	0	778550.0976	0	0
18	8074500	0	0	0	0	0	0	0	0	0	424863.6896	0	0
19	8074540	0	0	0	0	0	0	0	0	0	0	0	0
20	8074760	0	212318.448	0	0	495440.9712	0	0	0	0	5732959.8096	0	0
21	8074800	0	0	0	0	0	0	0	0	0	70777.2816	0	0
22	8074810												

- Part of the attribute table produced in ArcGIS that summarizes soil types within watersheds using the National soil dataset is shown below.

Rowid	STATION_NO	WA	BO	W	AN	BB	LU	WC	VO	VS	KN	WO	OA	HOB	HF	BP	GU	KA	GE	HOA	SEA	SEB	IIA	WY	Z	
1	8067525	0	0	2309130	0	0	7144200	0	0	0	0	0	0	0	0	0	0	0	4215200	0	0	0	0	0	0	
2	8068325	0	7126200	4168800	0	0	0	0	0	0	2373390	512490600	2763000	46429200	6140700	539100	0	0	160631200	110502900	9519750	3912930	0	1685700	0	
3	8068720	132845400	0	3588930	0	0	0	0	0	0	0	625955400	0	249624900	0	0	0	0	161637300	44547300	2844990	7348680	4604670	5532300	0	
4	8068740	0	0	1632420	0	0	0	0	0	0	0	221849100	0	65500200	0	0	0	0	234256500	0	0	0	0	0	0	
5	8068760	0	4039200	5381100	0	0	0	0	0	0	0	514167000	0	33555200	0	0	0	0	46701900	21307500	1668710	1608930	0	0	0	
6	8068800	0	0	1598400	0	0	0	0	0	1033200	0	216539900	0	6784400	3907800	0	1747800	0	172893900	26028600	2781100	600300	1350720	5629500	0	
7	8068900	0	0	6679000	0	0	0	0	144630	1682640	0	399629800	0	19036000	3653800	0	1207800	0	231181200	8270100	20700	0	595500	0	0	
8	8069000	0	765000	8172900	0	0	0	0	0	0	3614400	743328900	1098900	4180500	1902780	0	998100	0	218565900	37832400	6974100	207000	4209300	2719350	341	
9	8072730	0	0	5455500	0	0	0	0	0	0	0	0	0	0	0	0	0	0	64206900	0	0	0	0	0	0	
10	8072760	0	0	7797600	0	0	0	0	0	0	0	10944000	0	0	0	0	0	0	82035900	0	0	0	0	0	0	
11	8073500	0	0	9631900	9469500	0	1600200	0	0	0	0	3372900	0	0	0	0	0	0	9067500	0	163353600	0	0	5057940	0	
12	8073600	0	0	63000	49180500	0	36274500	0	0	0	0	0	0	0	0	0	0	0	48392100	0	4608900	0	0	1620000	0	391
13	8073700	0	0	116100	33088500	0	810900	0	0	0	0	0	0	0	0	0	0	0	46364400	0	6012000	0	0	8611200	0	
14	8074000	0	0	231300	122813100	0	86356800	0	0	0	0	0	0	0	0	0	0	0	267536700	0	122111100	0	0	1475640	0	251
15	8074020	0	0	2930400	0	0	0	0	0	0	0	26044200	0	0	0	0	0	0	35288100	0	288397800	0	0	9736200	5130900	
16	8074150	0	0	0	0	0	0	0	0	0	0	0	0	0	0	0	0	0	1154700	0	45152100	0	0	0	0	
17	8074250	0	0	0	0	0	0	0	0	0	0	0	0	0	0	0	0	0	531000	18344700	0	0	0	0	0	
18	8074500	0	0	144000	17305200	0	0	0	0	0	0	0	0	0	0	0	0	0	575100	91249200	0	0	0	0	0	
19	8074540	0	0	0	878400	0	0	0	0	0	0	0	0	0	0	0	0	0	152397900	0	0	0	0	0	0	
20	8074760	18028600	0	1781190	0	8546780	2629800	0	0	0	0	0	0	0	0	0	819000	0	330166800	63243900	0	0	0	2309670	0	
21	8074800	0	0	0	0	1686600	1444500	0	0	0	0	0	0	0	0	0	0	0	0	479700	0	0	0	0	0	
22	8074810	0	0	189000	0	39440700	0	0	0	0	0	0	0	0	0	0	0	0	0	10656900	0	0	0	0	0	
23	8075000	447300	0	2837700	0	2771460	363384900	0	0	0	0	0	0	0	0	450000	0	0	0	16427700	0	0	0	0	0	
24	8075110	0	0	579600	3971700	0	165919500	0	0	0	0	0	0	0	0	0	0	0	0	0	0	0	0	0	0	
25	8075400	3353400	0	1923300	0	3254220	66001500	0	0	0	0	0	0	0	0	0	0	0	0	1906200	0	0	0	0	0	
26	8075500	0	0	1082700	0	1275300	301155300	0	0	0	0	0	0	0	0	631800	0	0	0	10774800	0	0	0	0	0	
27	8075605	0	0	0	0	0	86240700	0	0	0	0	0	0	0	0	578000	0	0	0	0	0	0	0	0	0	
28	8075730	0	0	711000	0	0	120598200	0	0	0	0	0	0	0	0	0	0	0	0	698400	0	0	0	0	0	
29	8075763	0	0	0	0	0	0	0	0	0	0	0	0	0	0	0	0	0	0	49660200	0	0	0	0	0	
30	8075770	0	0	331200	0	0	87901200	0	0	0	0	0	0	0	0	0	854100	0	29295000	0	0	0	0	0	0	
31	8075780	0	0	0	0	0	0	0	0	0	0	0	0	0	0	0	805500	0	35397900	3667500	0	0	0	0	78300	
32	8075900	0	0	1375200	0	0	0	0	0	0	0	84297600	0	0	0	0	796500	0	127119600	0	0	0	0	0	2341800	
33	8076000	0	1754100	342000	19070100	0	0	0	0	0	0	0	0	0	0	0	2486500	0	95197500	0	0	0	0	0	0	
34	8076180	0	1951200	217600	0	0	0	0	0	0	0	0	82118000	98195400	0	0	0	0	985500	209829600	0	0	0	0	5072400	0
35	8076500	0	0	207000	0	0	0	0	0	0	0	0	0	0	0	0	0	0	59696100	88060500	0	0	0	0	0	
36	8076700	0	1458200	2291400	92804400	0	0	0	0	0	0	1264500	150885200	0	0	103770	135680200	0	124503300	0	0	0	0	0	281	
37	8076997	737100	0	636300	0	1562400	1621800	268830	0	0	0	0	0	0	0	0	0	0	10054800	0	0	0	0	0	0	

Part of the attribute table that summarizes land cover classes using the 2008 Harris County land cover is shown below. There were 10 classes.

ID	STATION_NO	Developed_HI	Developed_LI	Developed_OS	Cultivated	Grassland_Shrub	Forest	Woody_Wetland	Herbaceous_Wetland	Barren	Water
1	8067525	4620600	6454800	1655100	9601200	1638900	1031400	4204800	1915200	169900	212940
2	8068325	10588500	15000300	2502000	31366800	19349100	1596510	2588400	3466800	2036700	538200
3	8068720	10169100	4501800	1990800	220773600	18099000	3859200	9082800	4486500	725400	160110
4	8068740	3027600	4651200	307800	52422300	7373700	358200	3337200	2240100	3528000	103500
5	8068780	4199400	2844900	213300	66356100	11950200	4622400	5168700	1775700	2062800	108990
6	8068800	12609000	31541400	3703500	9785900	13246200	6134400	8379000	1770300	2676600	872100
7	8068900	17274600	33218100	2600100	4972500	7114500	4998600	3744900	1559700	1556100	506700
8	8069000	25238700	48088800	4673700	5221800	14885100	8783100	4963500	2529000	2347200	792000
9	8072730	6080400	6231600	233100	31221000	4720500	1135800	1689300	319500	1199700	249300
10	8072760	10166400	13089600	871200	30876300	6358500	441900	183600	157500	3396600	216000
11	8073500	43434000	55096200	9936900	49317300	18979200	1345410	29934900	4824900	2979000	177480
12	8073600	16950600	15152400	1067400	0	27000	1423800	128700	20700	6300	93600
13	8073700	6753600	8360100	261900	0	0	927900	0	0	0	0
14	8074000	47232000	45483300	2812500	0	1044900	6678900	637200	453600	34200	47700
15	8074020	35544600	48051900	6468300	0	5843700	3303900	1040400	870300	124200	799200
16	8074150	9306900	5350500	892800	0	393300	199800	82800	71100	0	178200
17	8074250	14981400	11547900	1343700	0	178200	46800	127800	22500	0	66600
18	8074500	34827300	35913600	3412800	0	2818800	1961100	1055700	547200	107100	264600
19	8074540	25415100	25970400	1344600	0	127800	441900	235800	80100	11700	37800
20	8074760	68115600	88570800	21518100	133037100	24434100	2540700	36549000	7216200	7973100	431190
21	8										

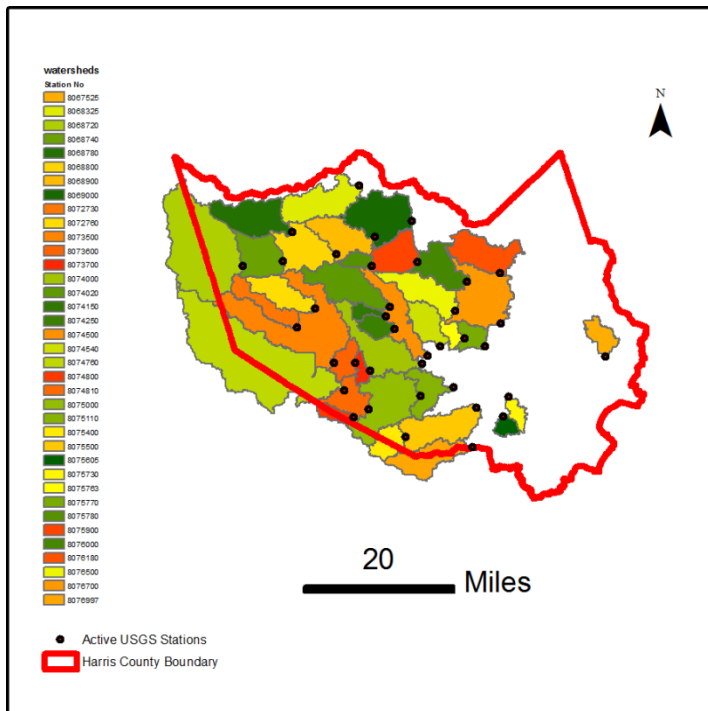


Figure A6.1 Active USGS stations and associated watersheds

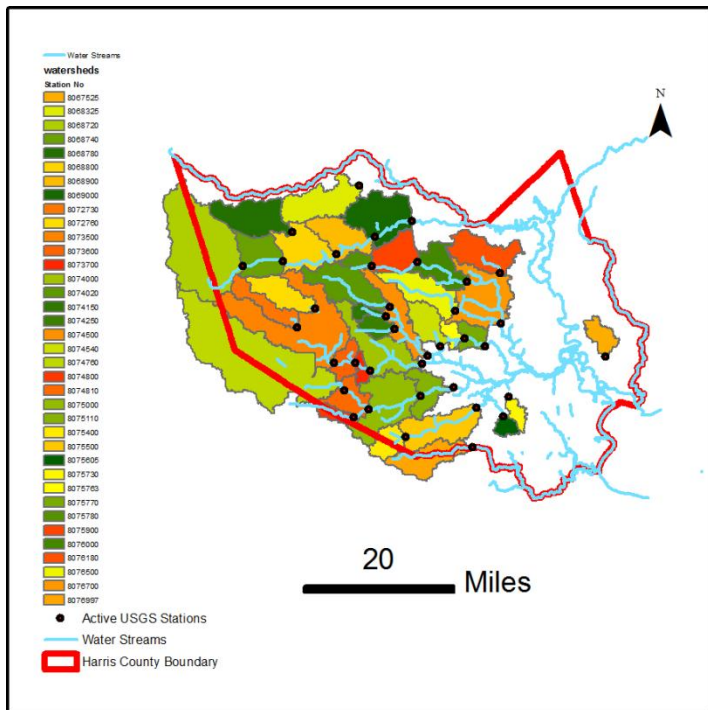


Figure A6.2 Active USGS stations and associated watersheds and surface-water streams

4. Runoff Calculation

The runoff at each monitoring station was calculated with the consideration of the upstream area that may influence each monitoring station. This is achieved by identifying the rain gages that are surrounding and within the watersheds. A total number of 99 rain gages is determined after excluding a number of gages that are associated with suspicious readings (i.e. the gages with the following IDs: 3380, 2480, 4160 and 4170). Then, the area of influence from each rain gage was constructed in ArcGIS using the Thiessen polygon algorithm, which can proportionally divide and distribute the gage coverage into gage regions – these regions are generally known as Thiessen or Voronoi polygons. The gage regions are intersected with the watershed layer, previously constructed, to exclude the parts that are located outside the watersheds. In this manner, the weight for each gage station is calculated as a percentage of the individual gage region's area to the upstream area of each monitoring station.

The direct runoff from each rainfall event is calculated using the NRCS Runoff Curve Number method. The method was developed by the U.S. Department of Agriculture and Natural Resources Conservation Service (NRCS), which is formally known as the Soil Conservation Service (SCS). The primary inputs into the method include the runoff curve number, rainfall and the drainage area size. The method is based on the principle that for a single storm; the ratio of actual soil retention after runoff begins to potential retention is equal to the ratio of direct runoff to the storm rainfall (USDA-SCS, 1985). This principle and after algebraic manipulation and simplifying assumptions results in equation (1) that is found in the National Engineering Handbook (USDA-SCS, 1985):

$$Q = \frac{(P-0.2S)^2}{P+0.8S} \quad (1)$$

Where:

Q is runoff (inch)

P is rainfall (inch)

S is the potential maximum soil moisture retention after runoff begins (inch). This parameter is calculated from next equation using the runoff Curve Number (CN):

$$S = \frac{1000}{CN} - 10 \quad (2)$$

The amount of water before runoff Ia (also named as initial abstraction), such as infiltration or rainfall interception by vegetation is directly related to S as in the equation (3).

$$Ia = 0.2S \quad (3)$$

The CN values are usually range from 30 to 100; lower numbers indicate low runoff while larger numbers are related to increasing runoff potential. The CN is an empirical parameter that is primarily related to soil characteristics and land use (surface cover). In general, the infiltration rate of the soil surface is affected by surface conditions and soil profiles. As soil profiles may be considerably altered due to urbanization, the hydrological soil groups (HSG) are established according to the texture of the surface soil as described in the next table

HSG Class	Soil Texture
A	Sand, loamy sand, or sandy loam
B	Silt loam or loam
C	Sandy clay loam
D	Clay loam, silty clay loam, sandy clay, silty clay, or clay

In general, the “Group A” soils are associated with the lowest runoff potentials and high infiltration rates even when thoroughly wetted, while the “Group D” soils are associated with the highest runoff potentials as they have very low infiltration rates when thoroughly wetted.

In this analysis, the hydrological soil groups are extracted from the NRCS soil data and it was found that only two soil groups (i.e. C and D) are located within the investigated watersheds. These are illustrated in following Appendix 7 figures.

Our investigation also recognized that determining the CN values for a range of land use/cover can be narrowed down to two main categories: impervious and pervious surfaces. For this purpose, the national impervious data set was used to calculate the percentage of imperviousness for upstream areas of the monitoring stations and the CN for the C and D hydrological groups are given a value of 98. The pervious category for C and D hydrological groups were given average weighted numbers based on the land use/cover types and their percentages classes within the upstream areas. As a result, three groups of CN values were created: 1) CN value for impervious surfaces; 2) CN values for previous surfaces with hydrological soil group C (range between 73 and 83); and 3) CN values for previous surfaces with hydrological soil condition D (range between 79 and 86). The three groups of CN values are then combined based on the percentage of impervious and pervious surfaces and their individual CN values of each upstream area.

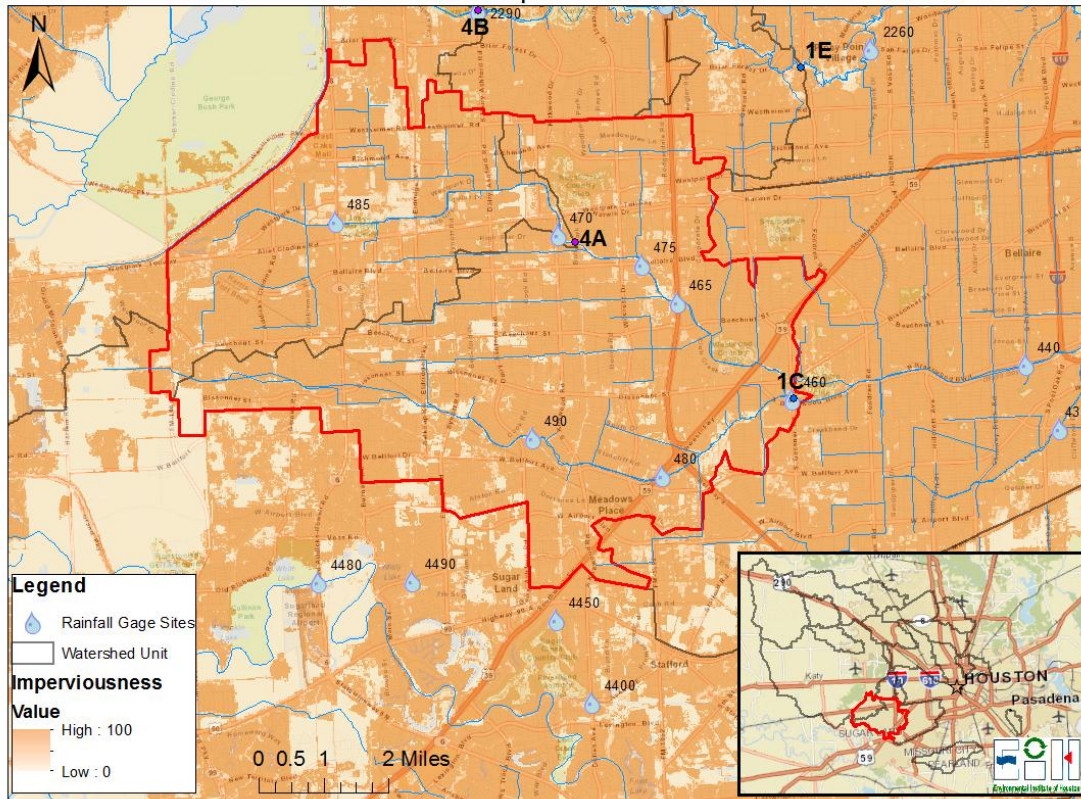
Finally, the runoff at each monitoring station was calculated for all hourly and daily rainfalls using equations 1 and 2 and once the rainfall exceeds the initial abstraction as expressed in equation 3. The upstream area of each watershed and the weights of each rain gage were used to calculate the total runoff at each monitoring station.

References:

USDA-SCS. 1985. National Engineering Handbook, Section 4 – Hydrology. Washington, D.C.: USDA-SCS.

Appendix 7: Hydrological Soil Types and Imperviousness by Site Specific Watersheds.

Site 1C Imperviousness



Site 1C Hydrological Soil Types

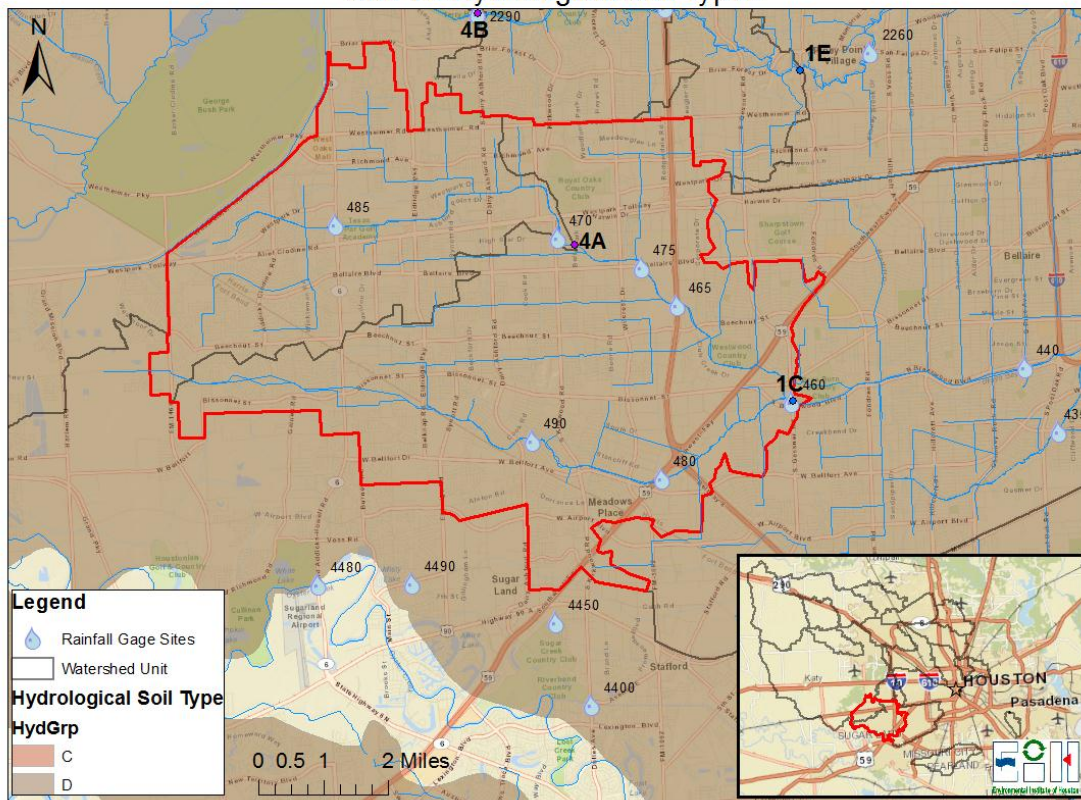


Figure A7.1. Site 1C imperviousness and hydrological soil types.

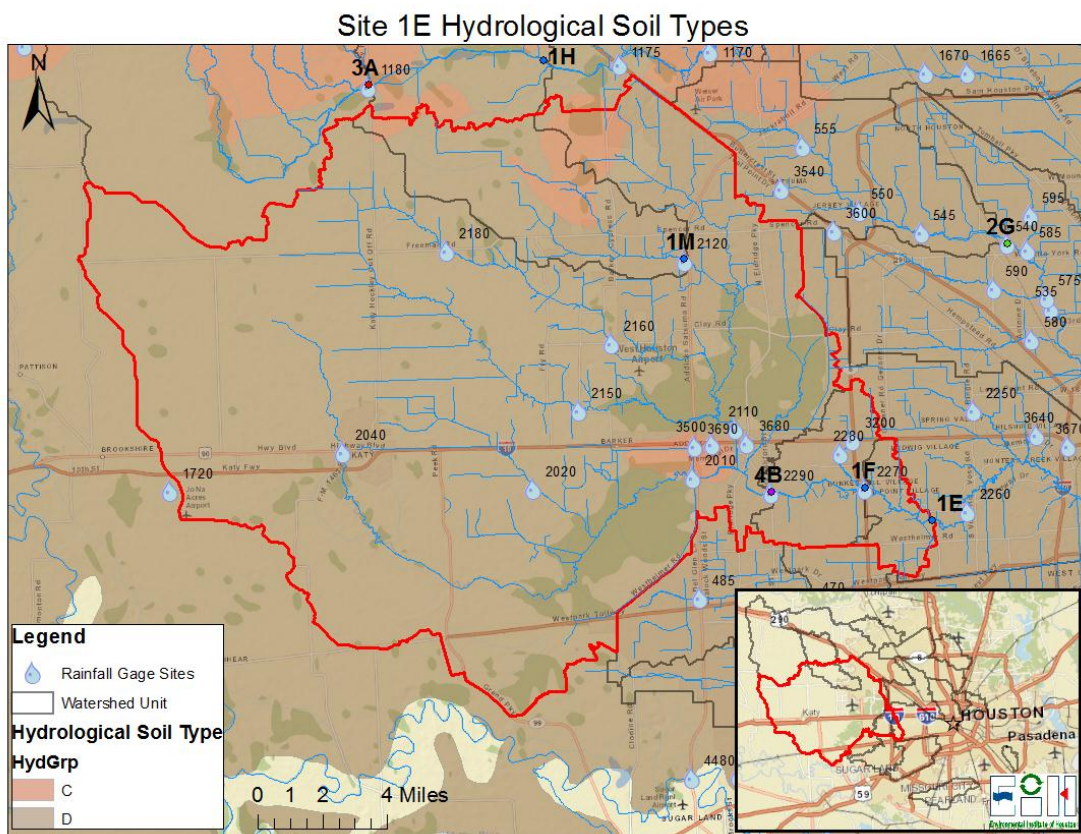
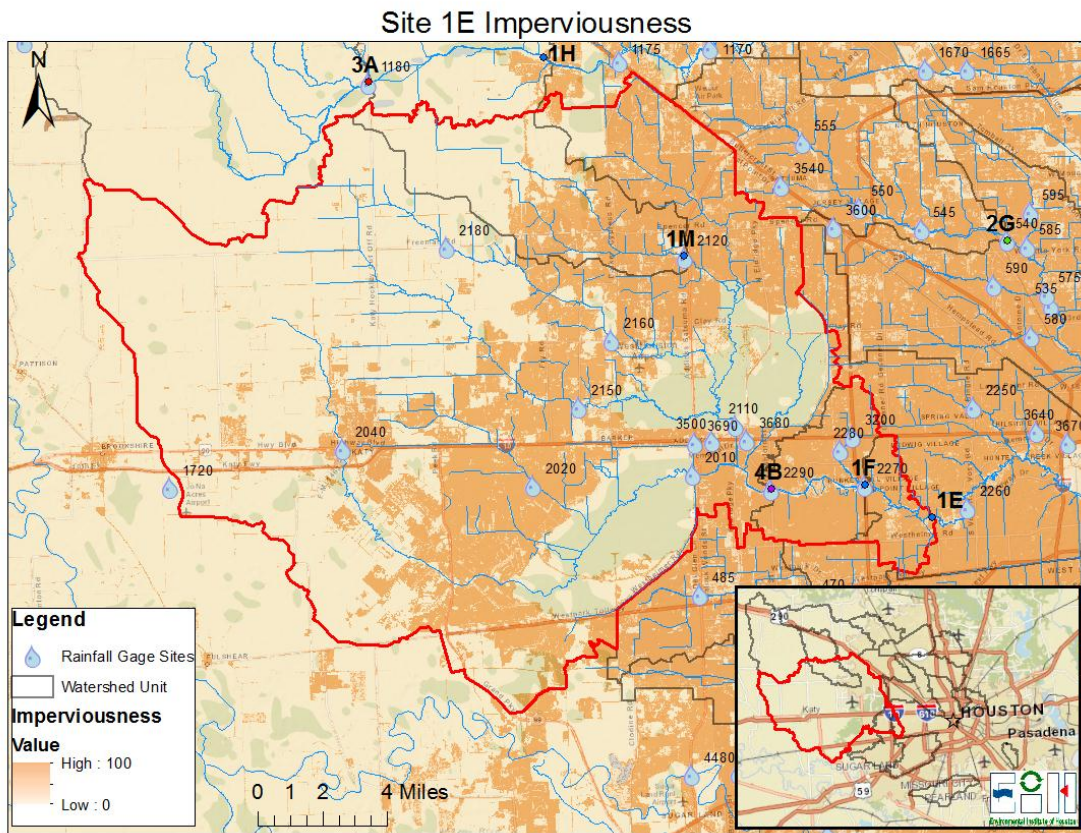


Figure A7.2. Site 1E imperviousness and hydrological soil types.

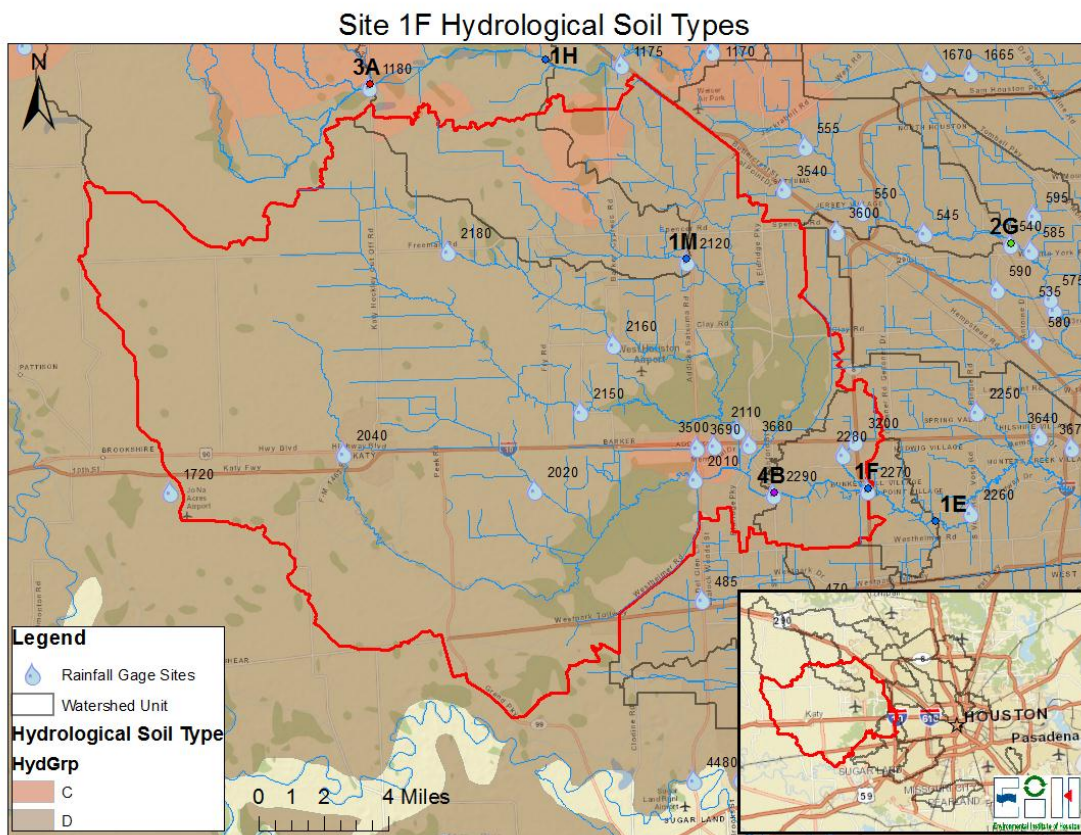
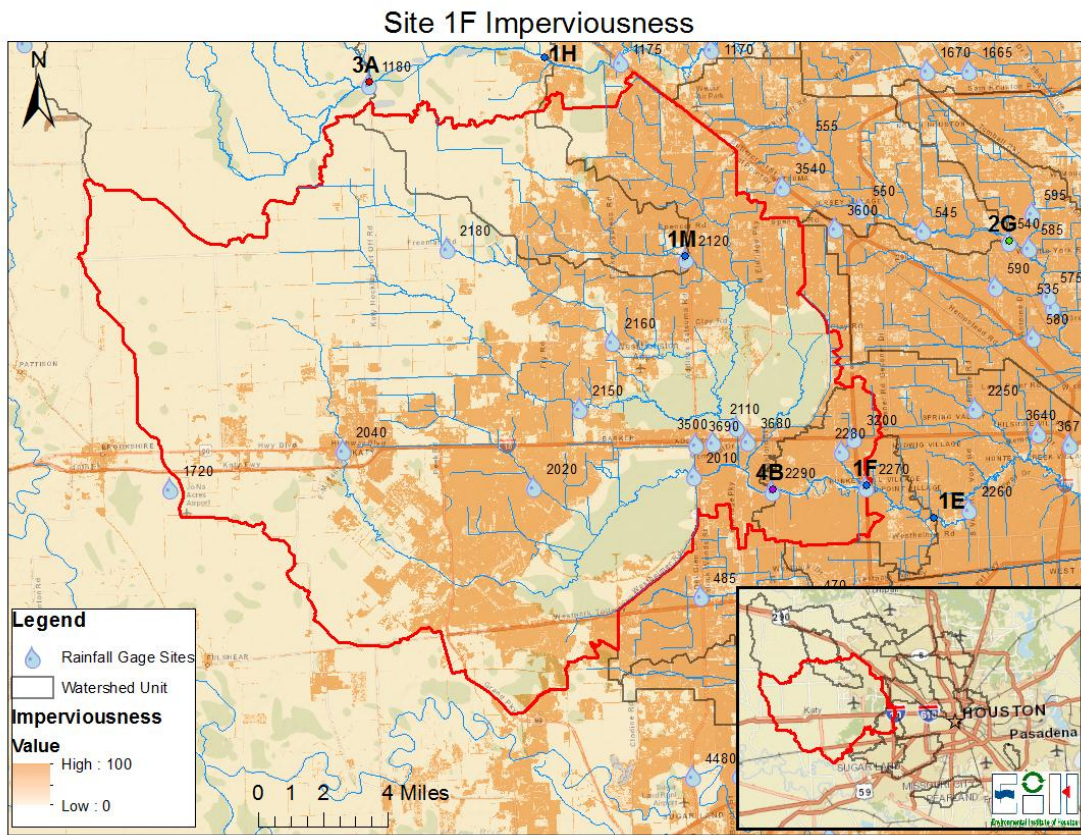
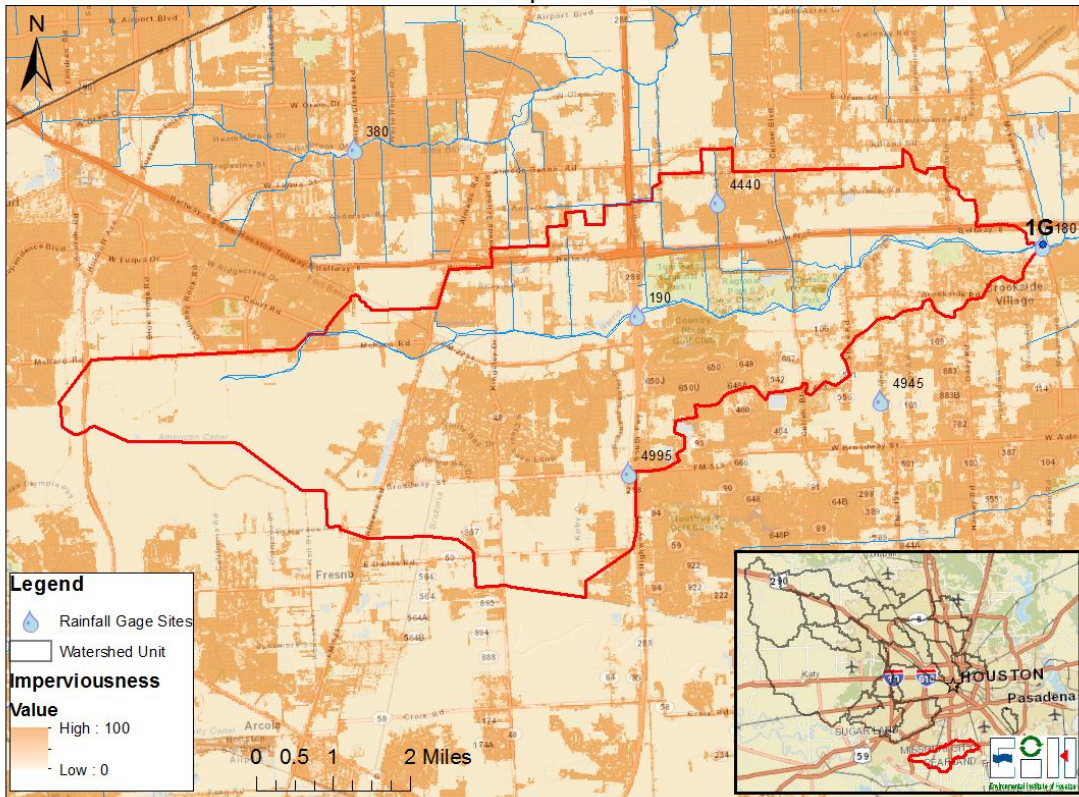


Figure A7.3. Site 1F imperviousness and hydrological soil types.

Site 1G Imperviousness



Site 1G Hydrological Soil Types

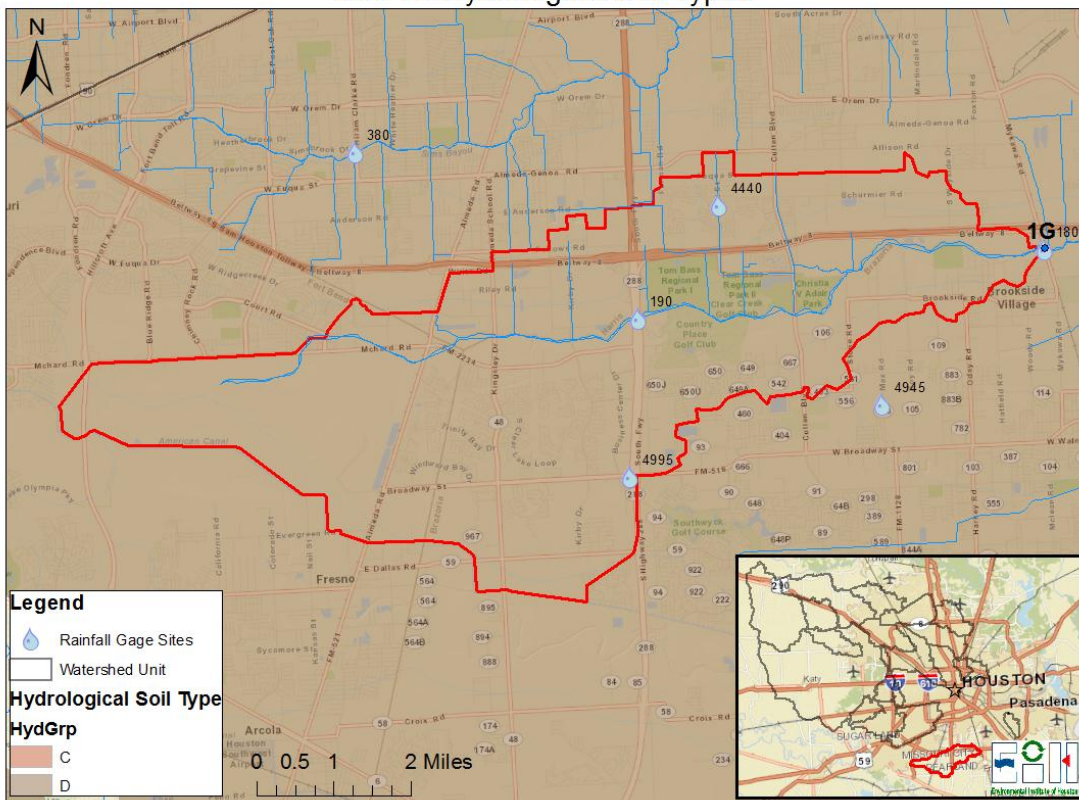
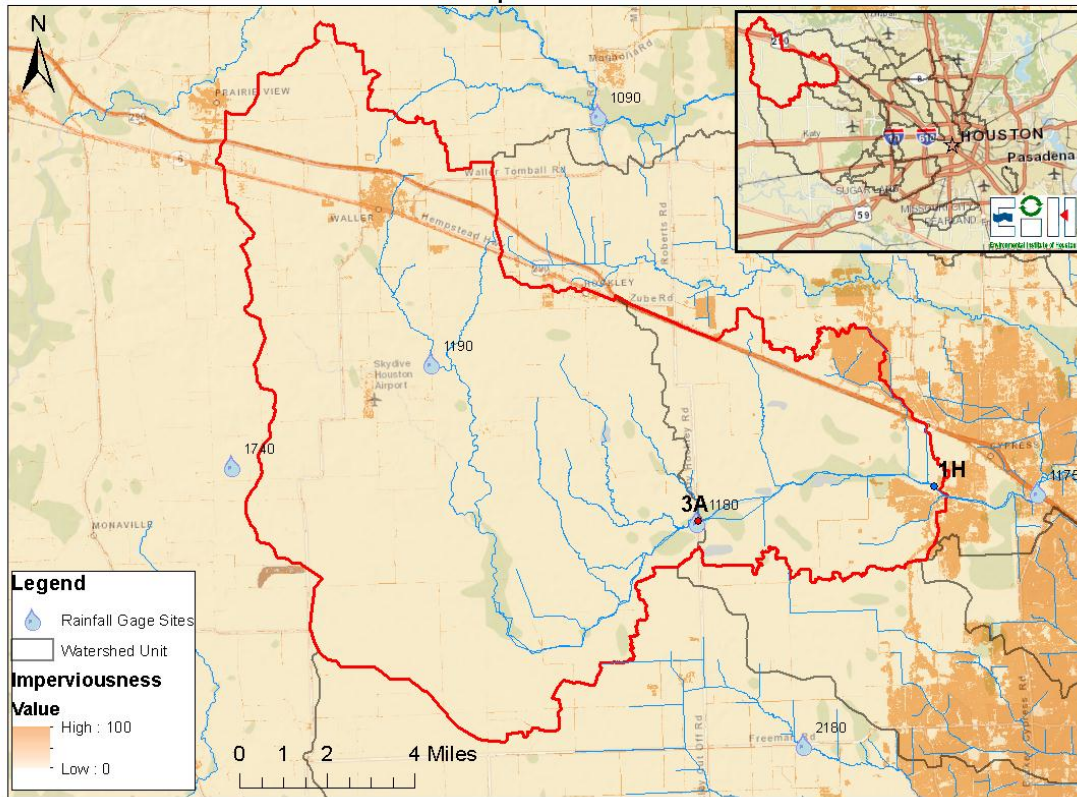


Figure A7.4. Site 1G imperviousness and hydrological soil types.

Site 1H Imperviousness



Site 1H Hydrological Soil Types

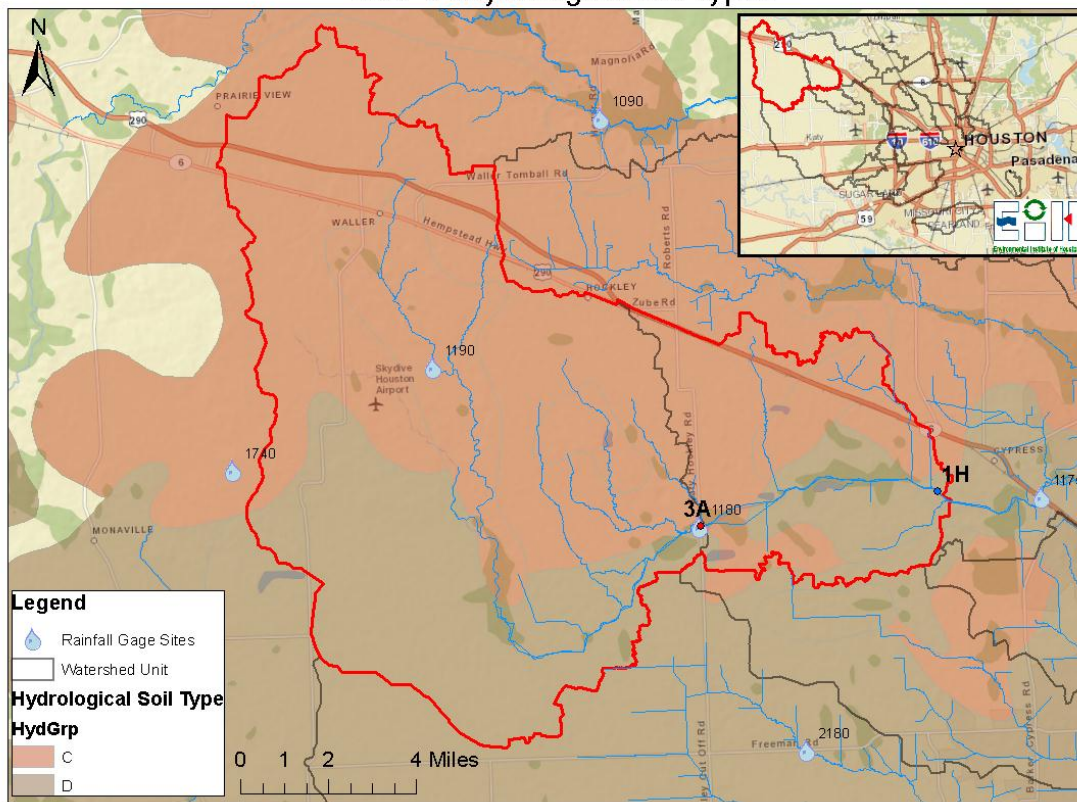
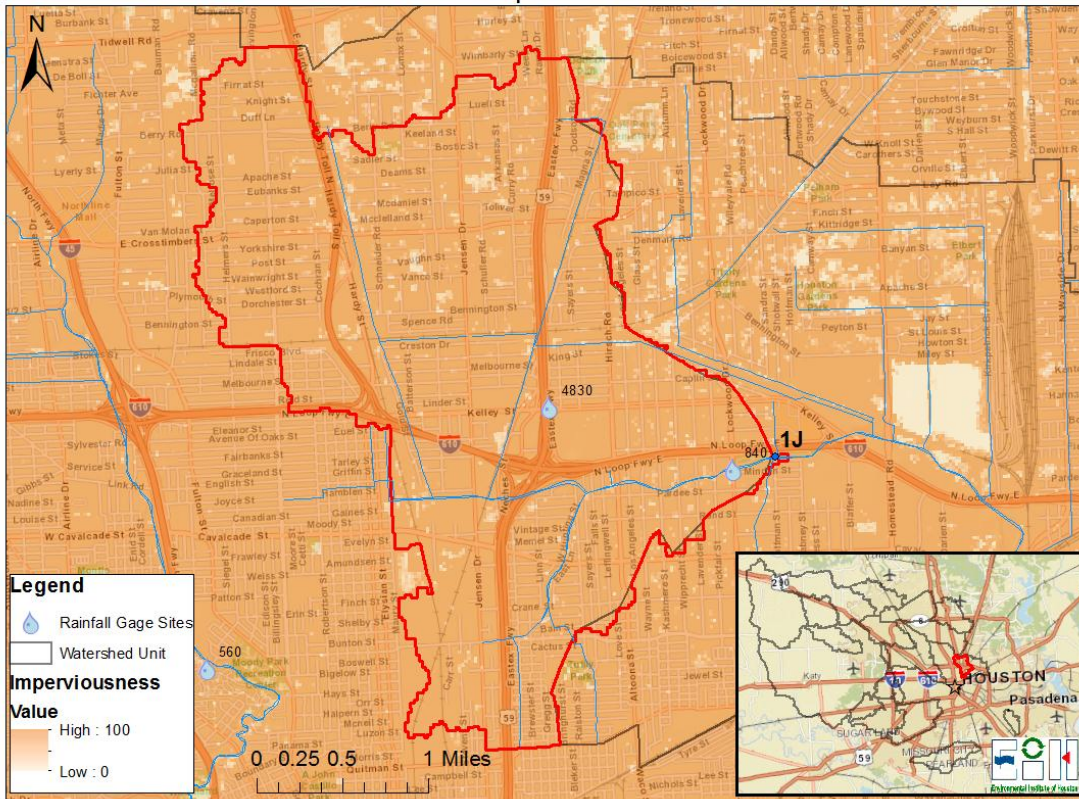


Figure A7.5. Site 1H imperviousness and hydrological soil types.

Site 1J Imperviousness



Site 1J Hydrological Soil Types

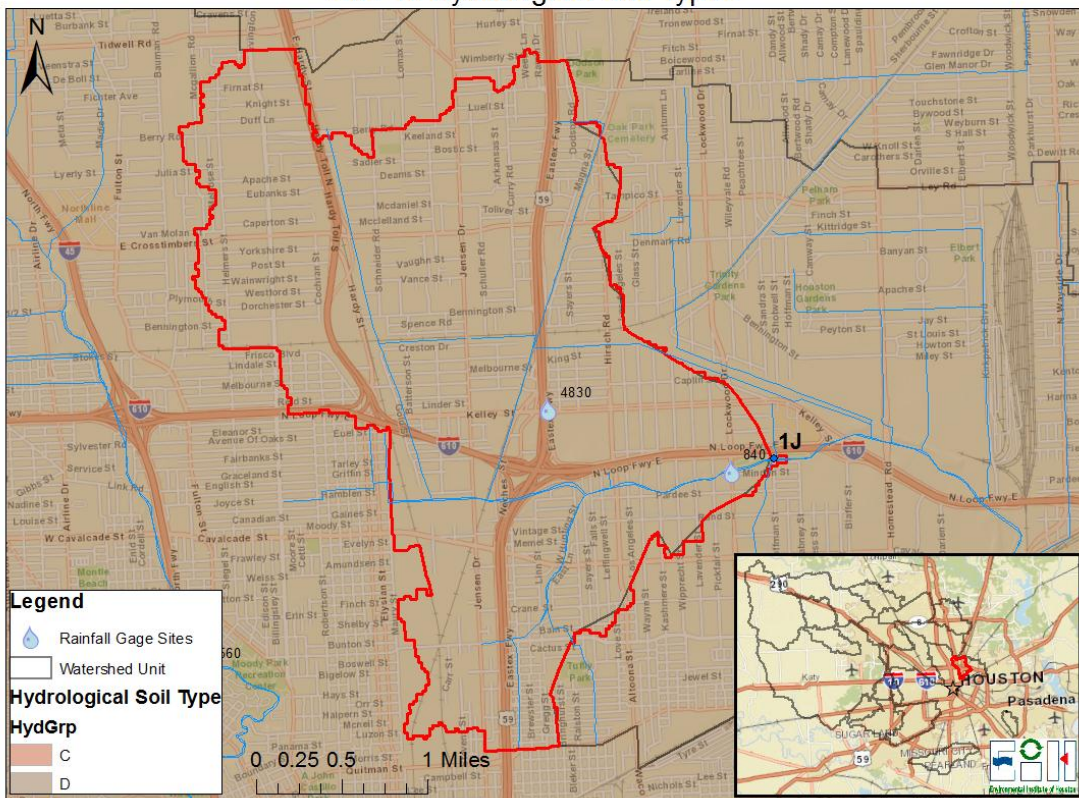
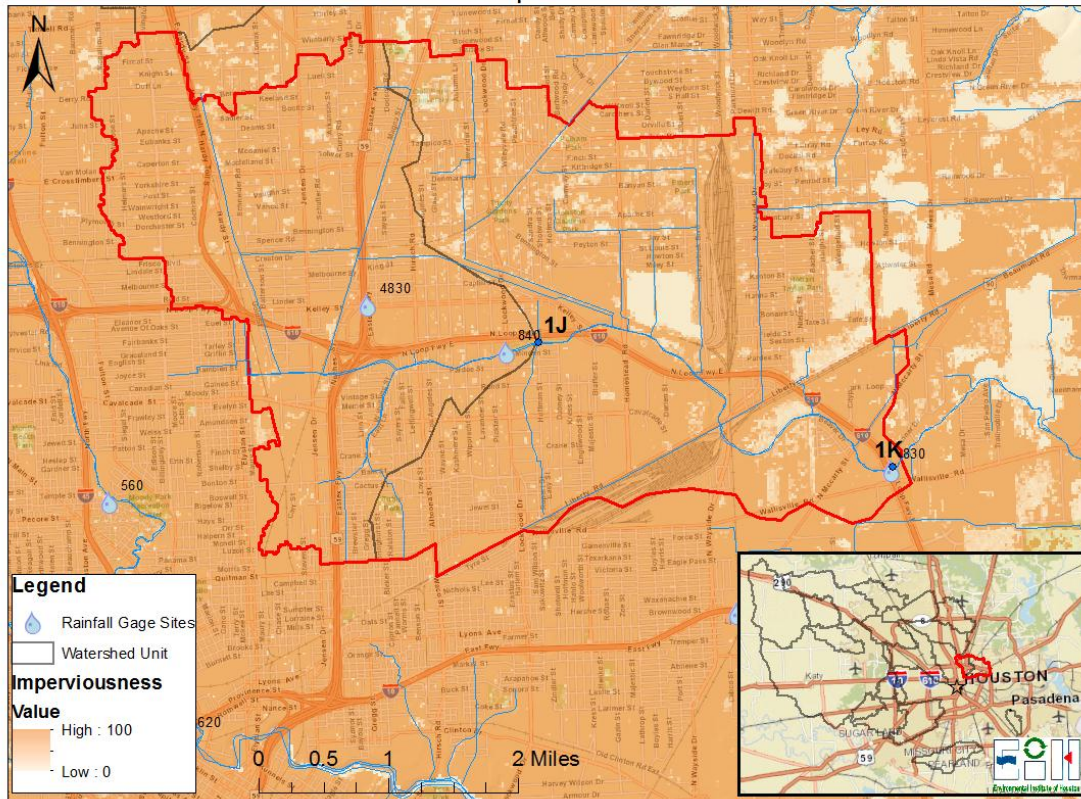


Figure A7.6. Site 1J imperviousness and hydrological soil types.

Site 1K Imperviousness



Site 1K Hydrological Soil Types

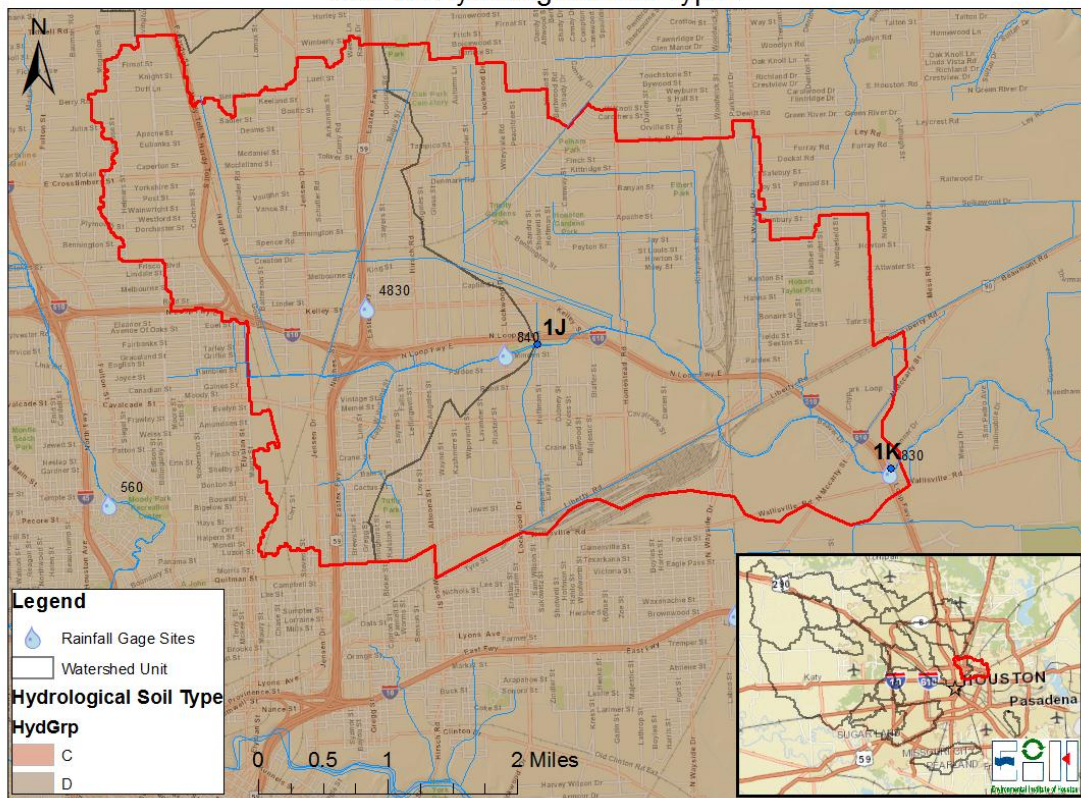
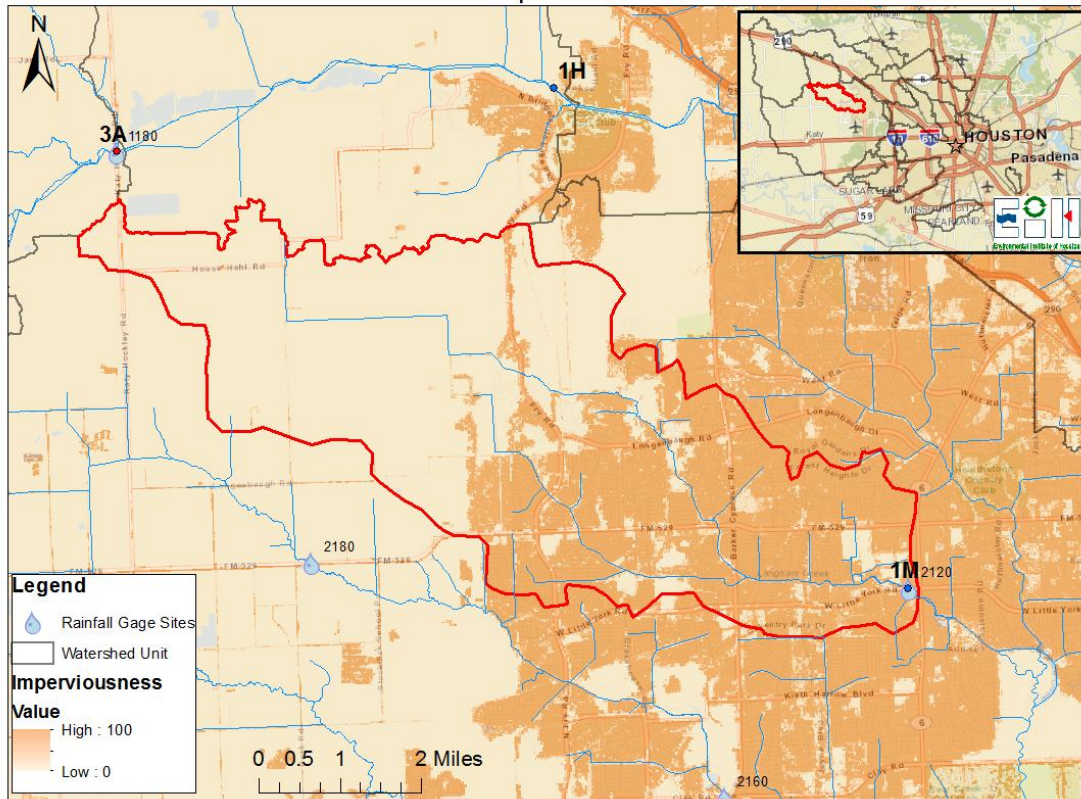


Figure A7.7. Site 1K imperviousness and hydrological soil types.

Site 1M Imperviousness



Site 1M Hydrological Soil Types

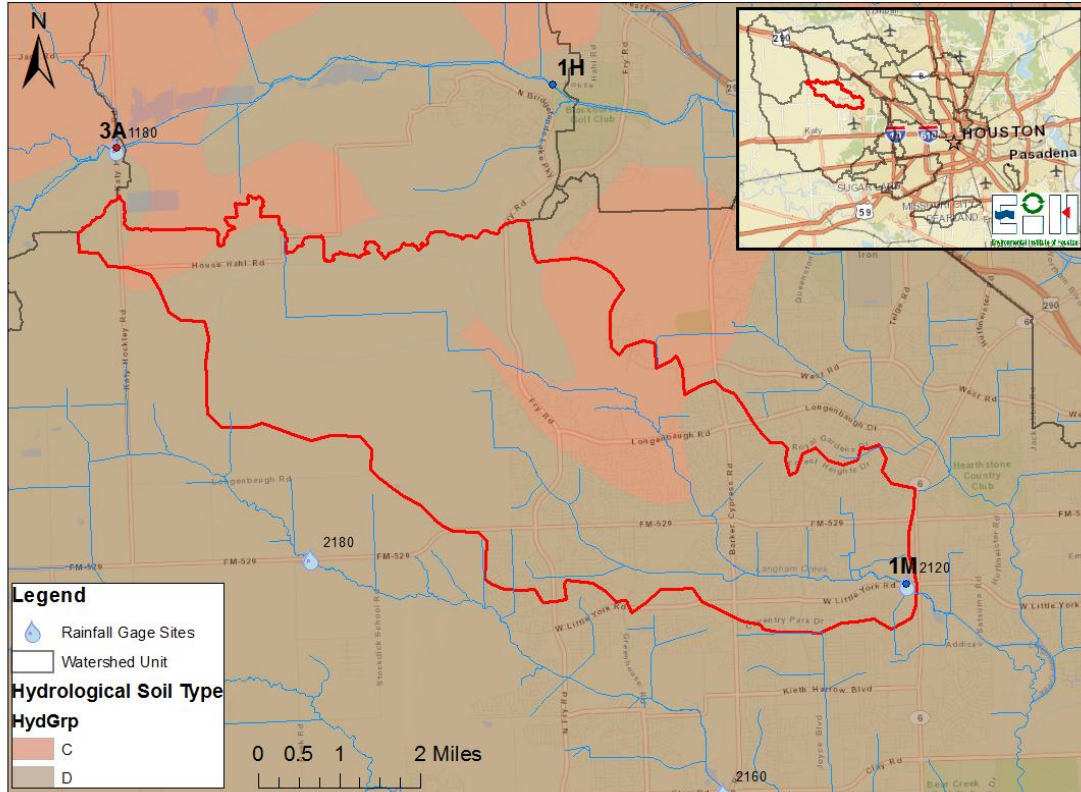
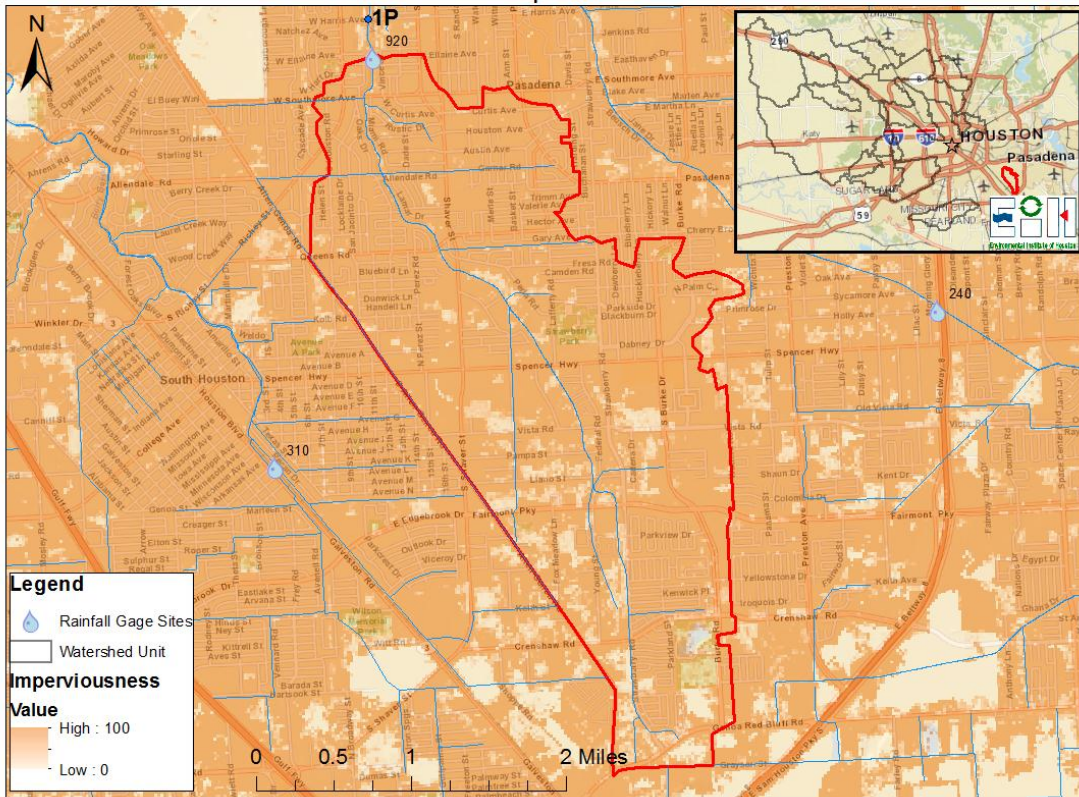


Figure A7.8. Site 1M imperviousness and hydrological soil types.

Site 1P Imperviousness



Site 1P Hydrological Soil Types

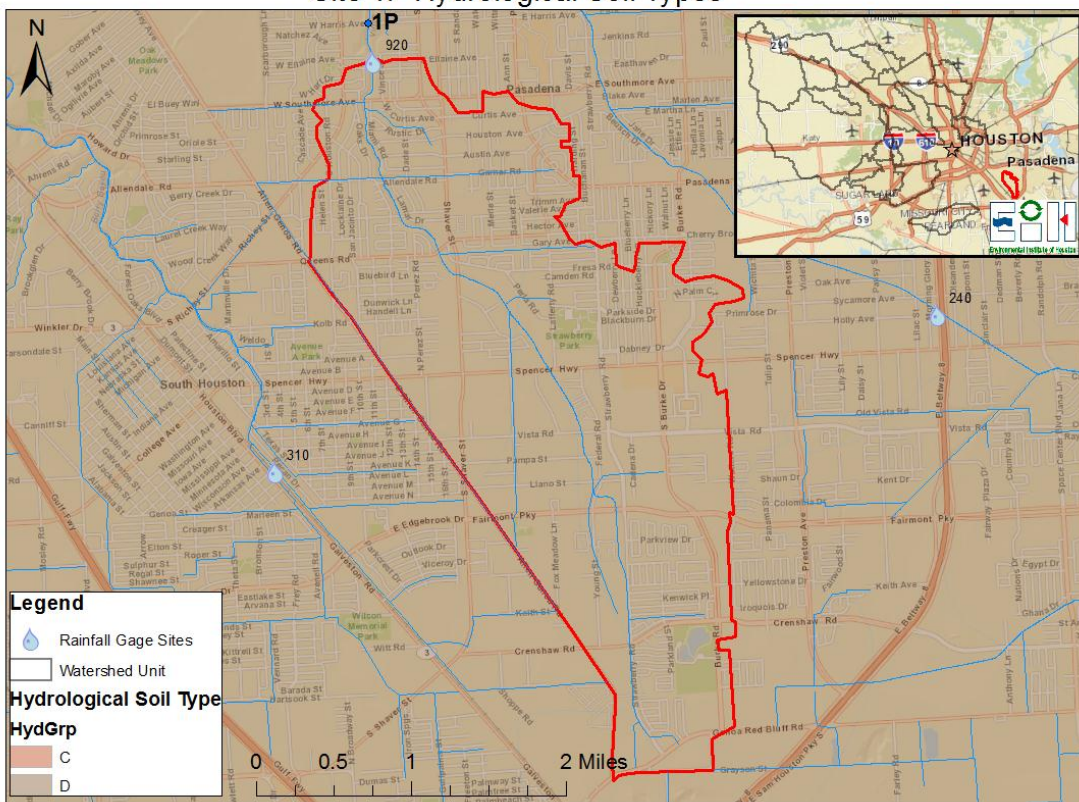
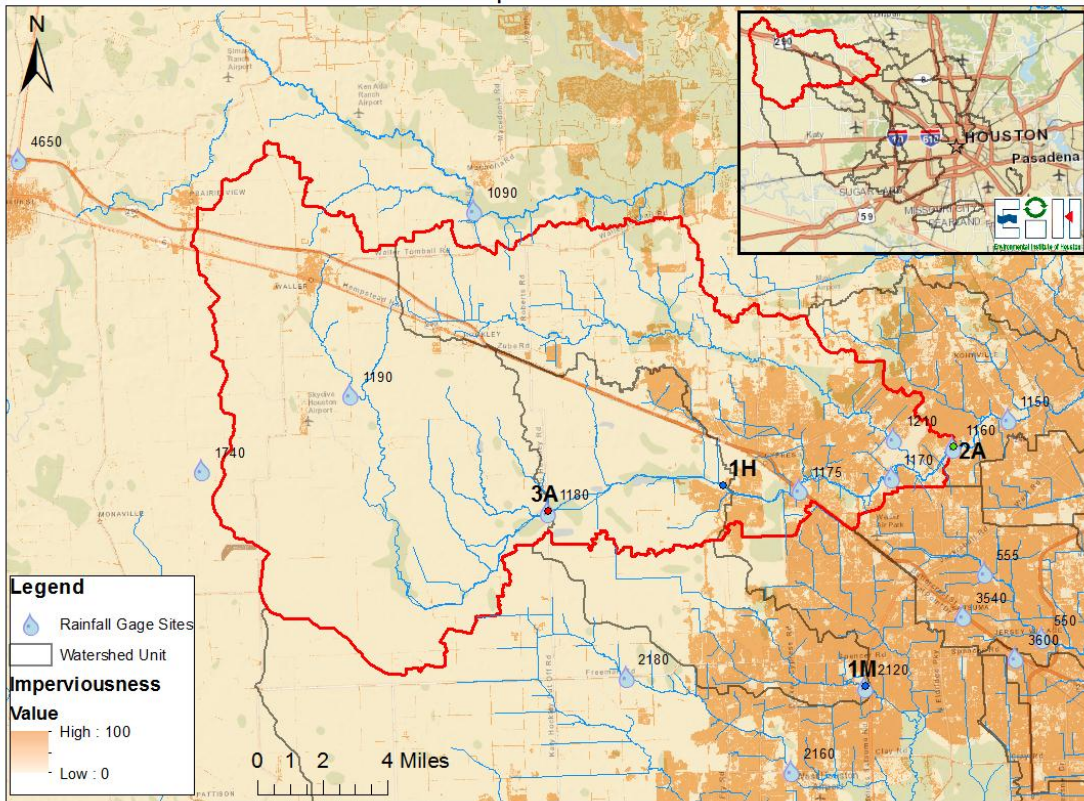


Figure A7.9. Site 1P imperviousness and hydrological soil types.

Site 2A Imperviousness



Site 2A Hydrological Soil Types

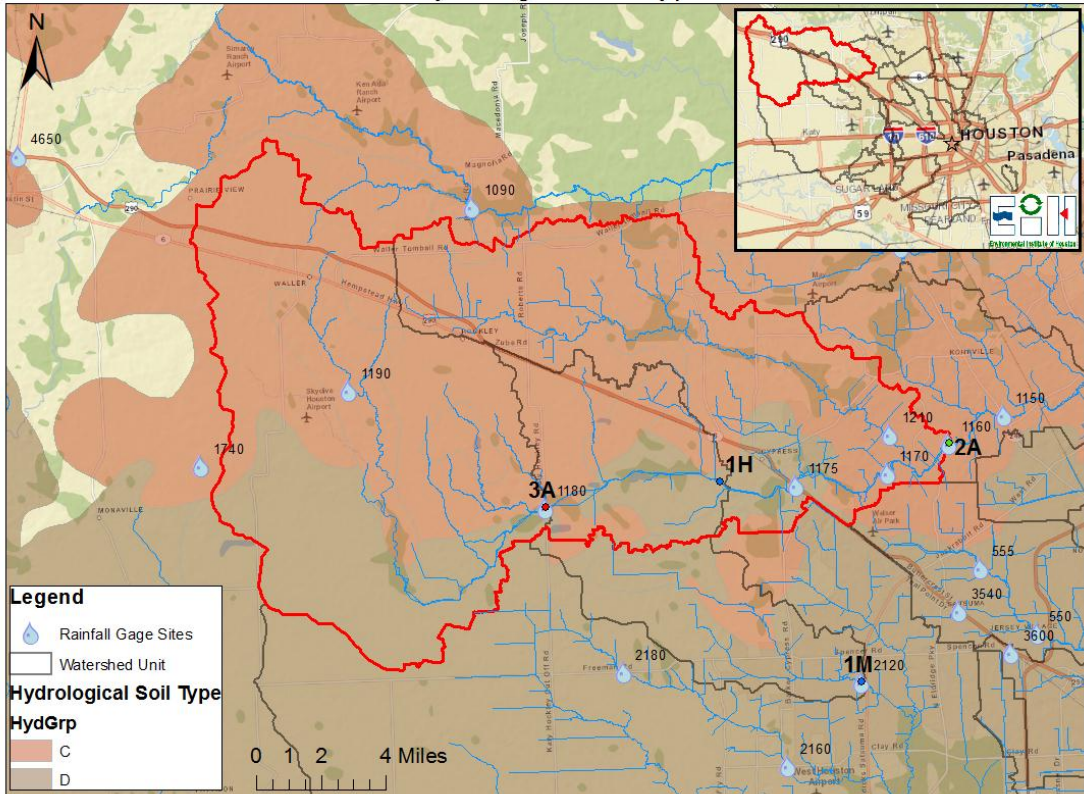
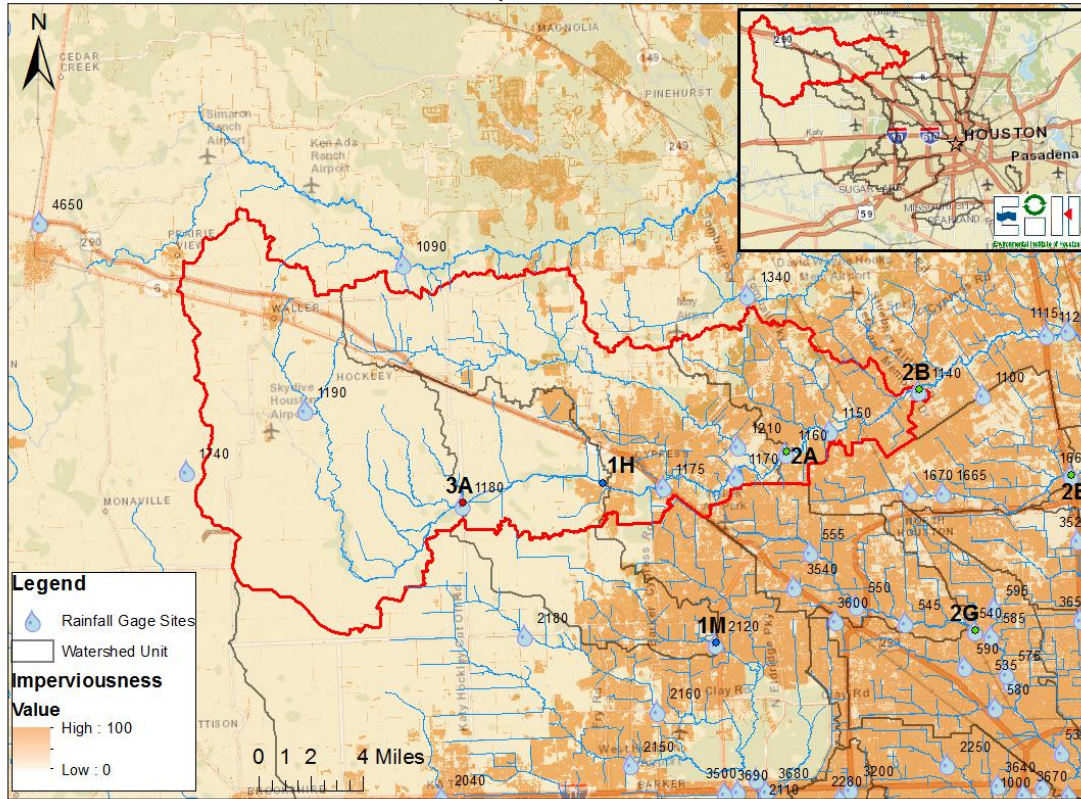


Figure A7.10. Site 2A imperviousness and hydrological soil types.

Site 2B Imperviousness



Site 2B Hydrological Soil Types

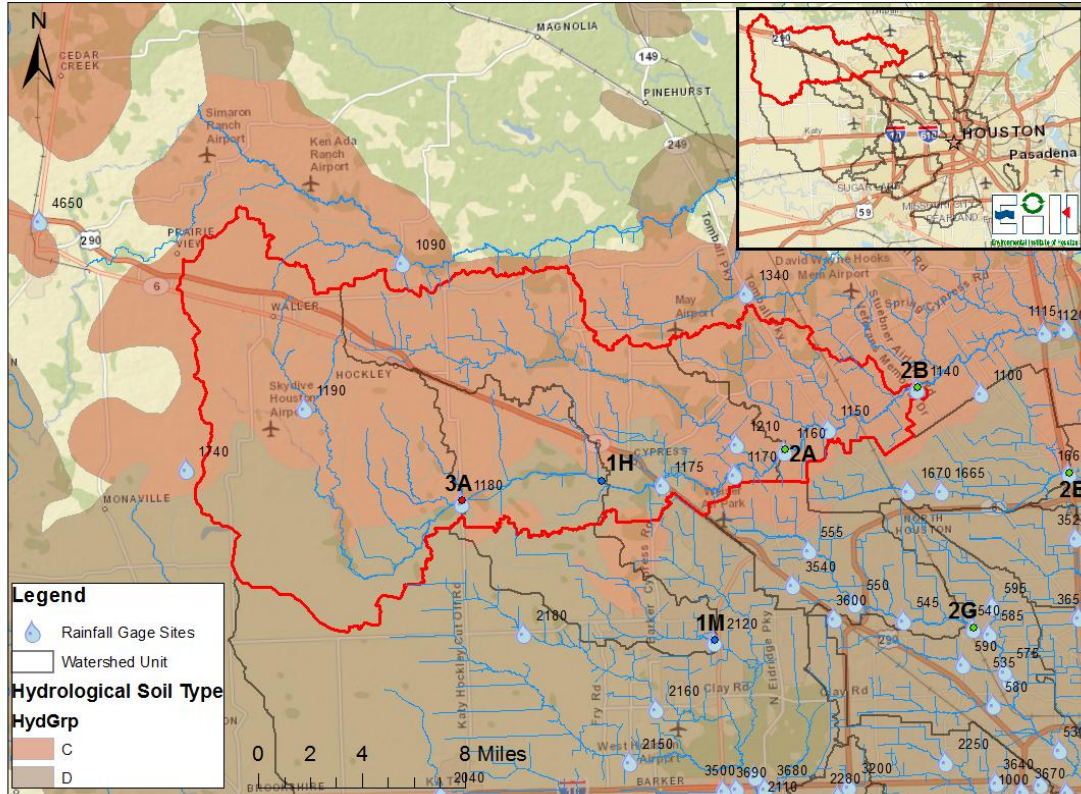
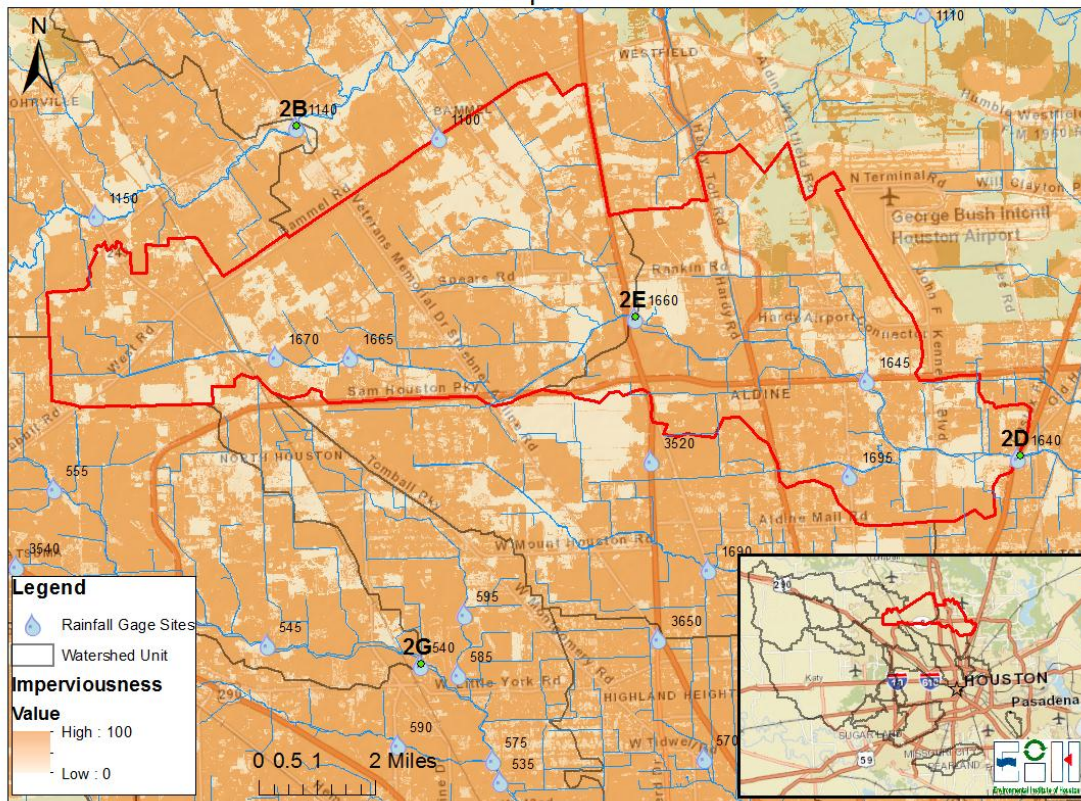


Figure A7.11. Site 2B imperviousness and hydrological soil types.

Site 2D Imperviousness



Site 2D Hydrological Soil Types

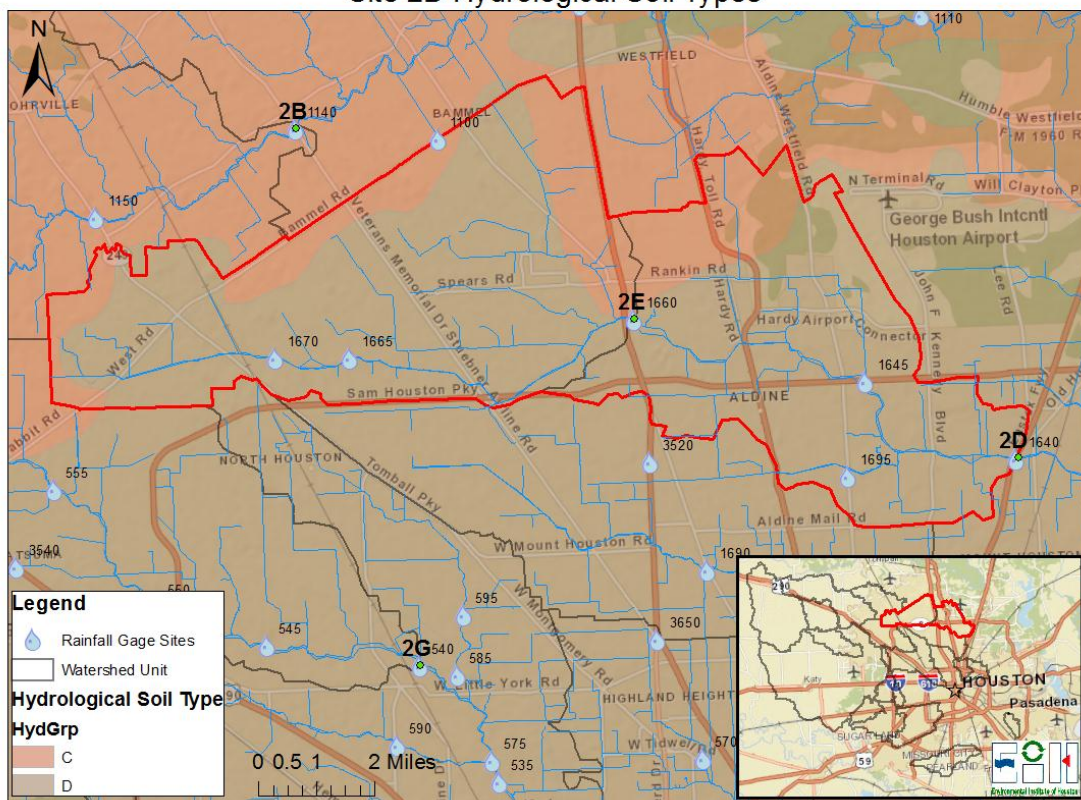
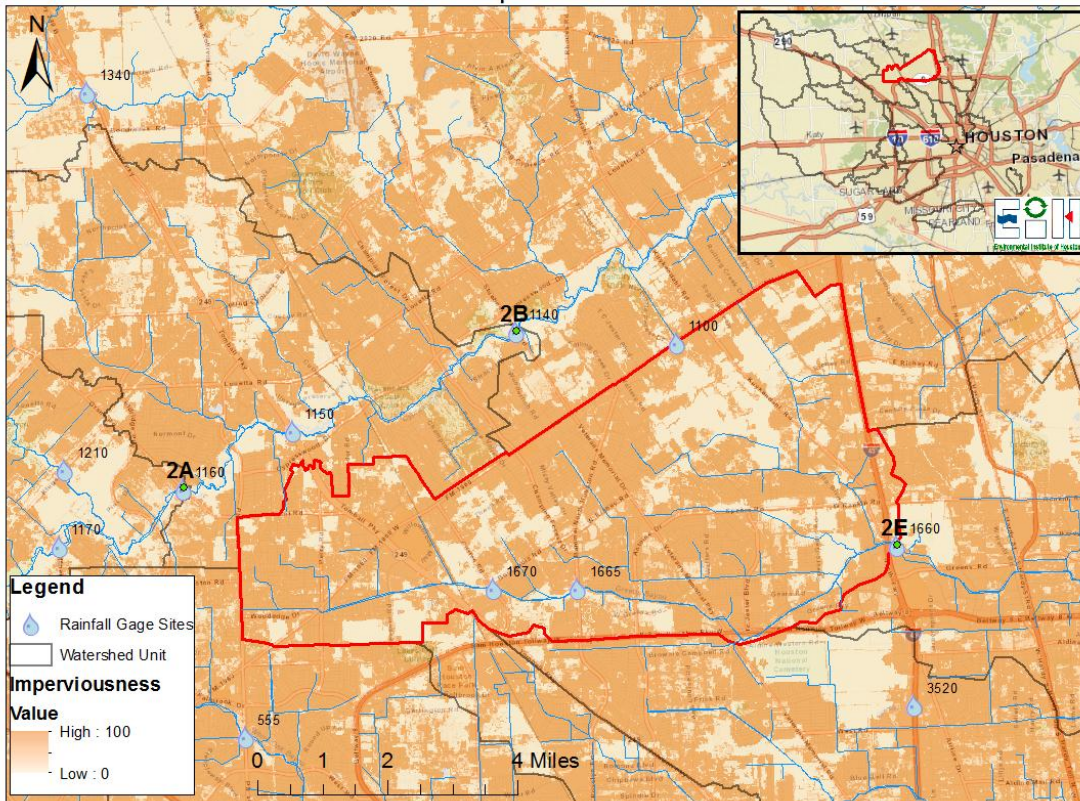


Figure A7.12. Site 2D imperviousness and hydrological soil types.

Site 2E Imperviousness



Site 2E Hydrological Soil Types

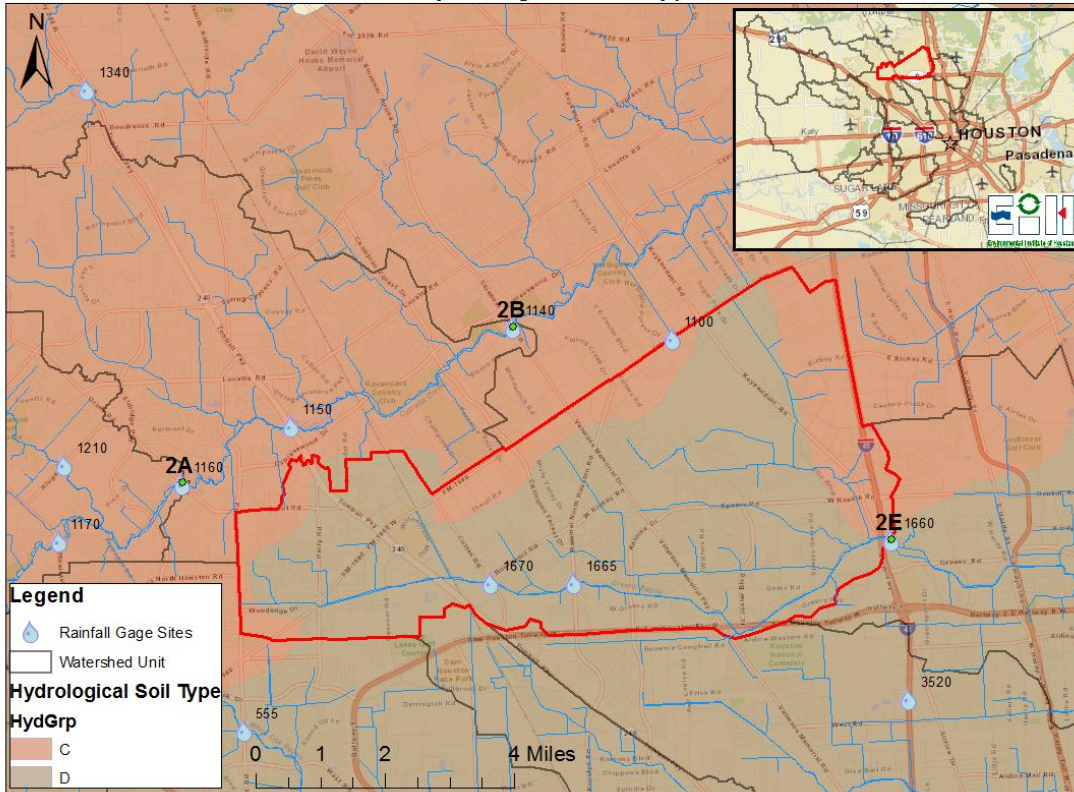
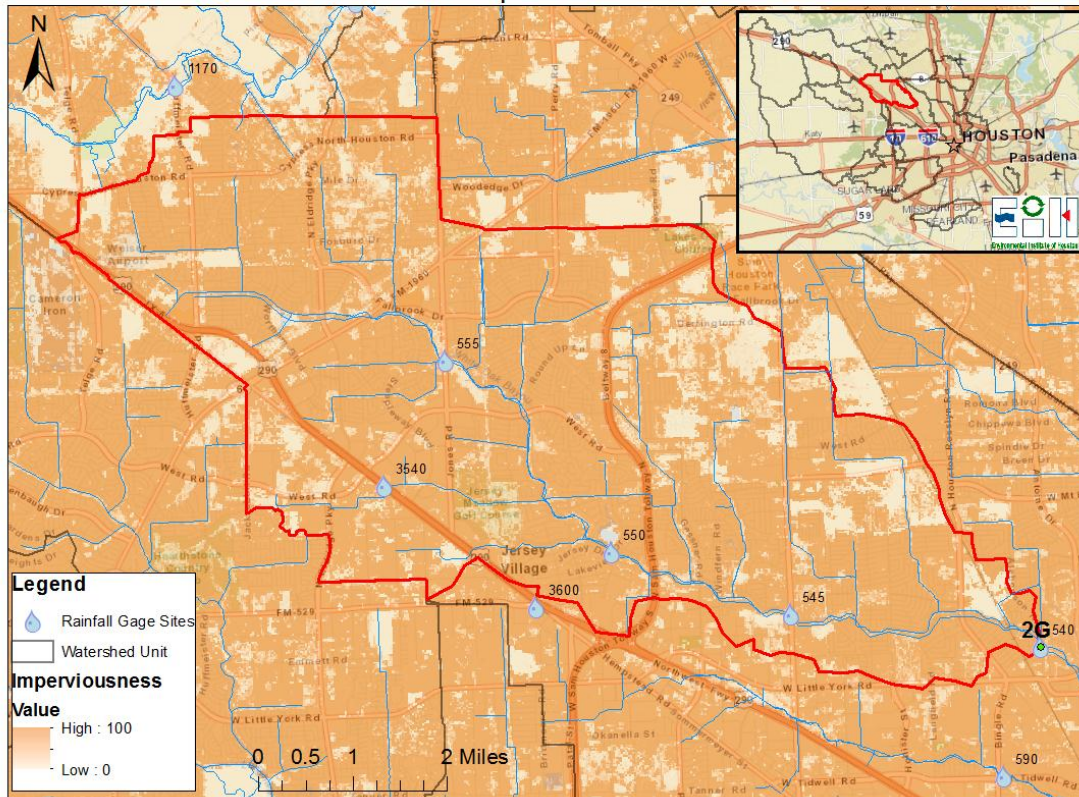


Figure A7.13. Site 2E imperviousness and hydrological soil types.

Site 2G Imperviousness



Site 2G Hydrological Soil Types

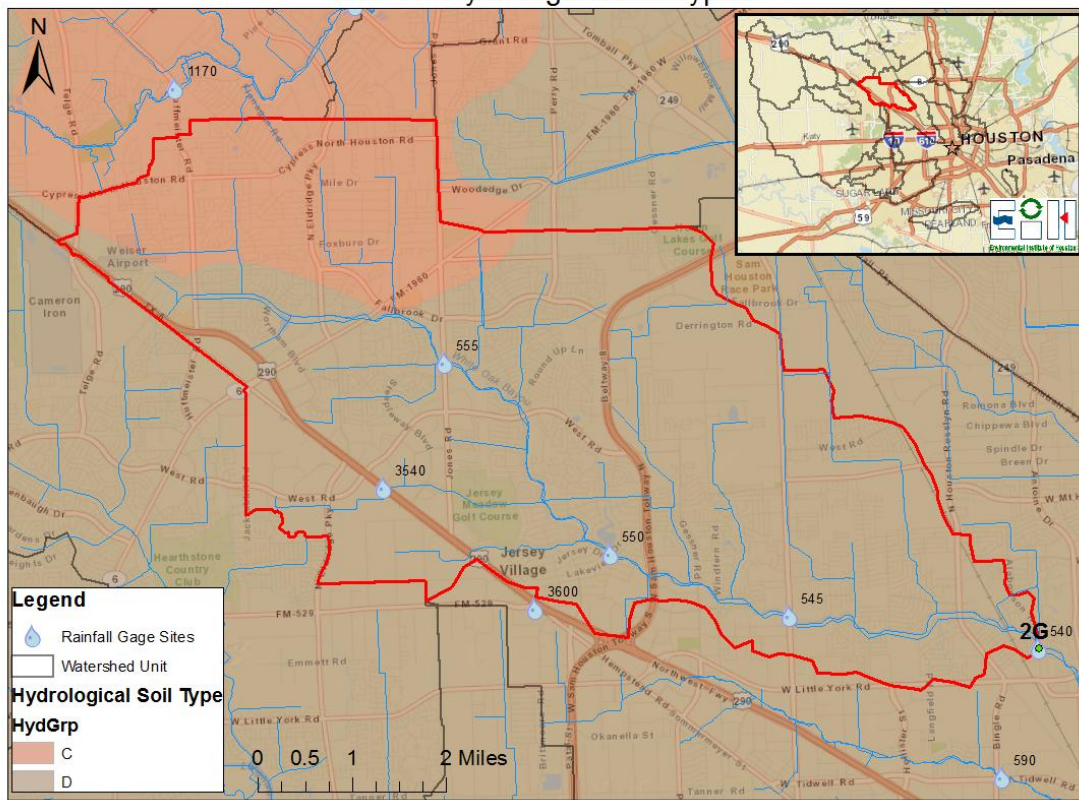
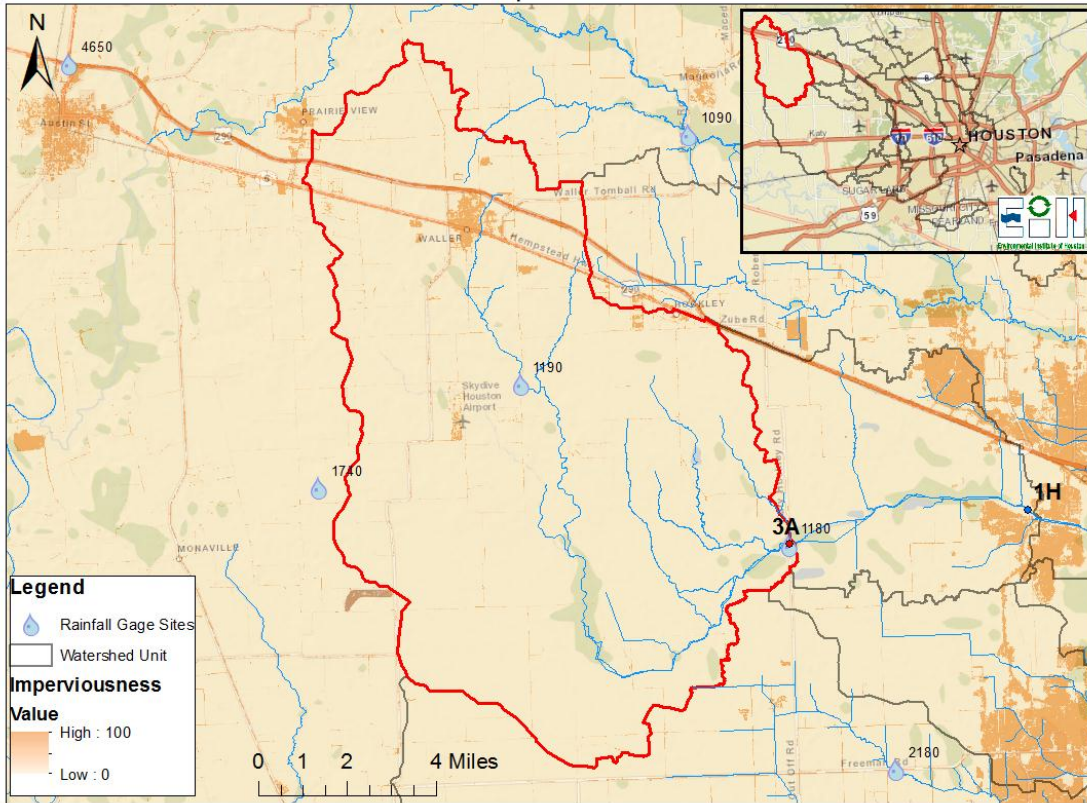


Figure A7.14. Site 2G imperviousness and hydrological soil types.

Site 3A Imperviousness



Site 3A Hydrological Soil Types

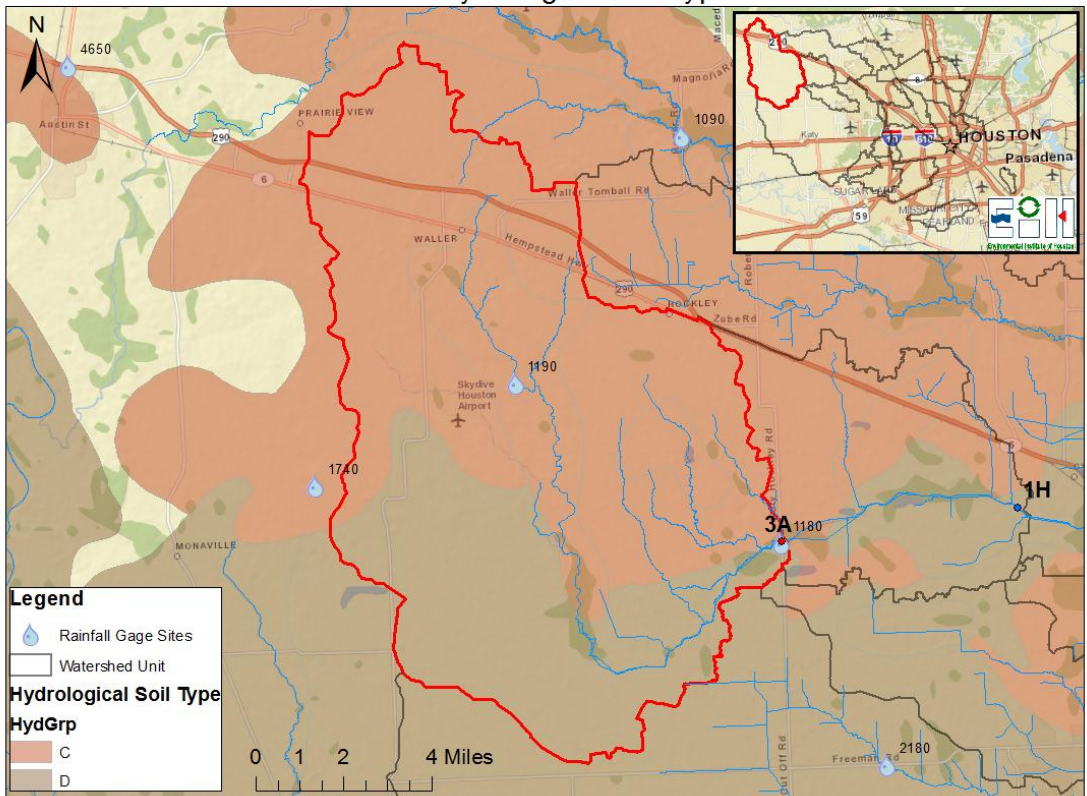
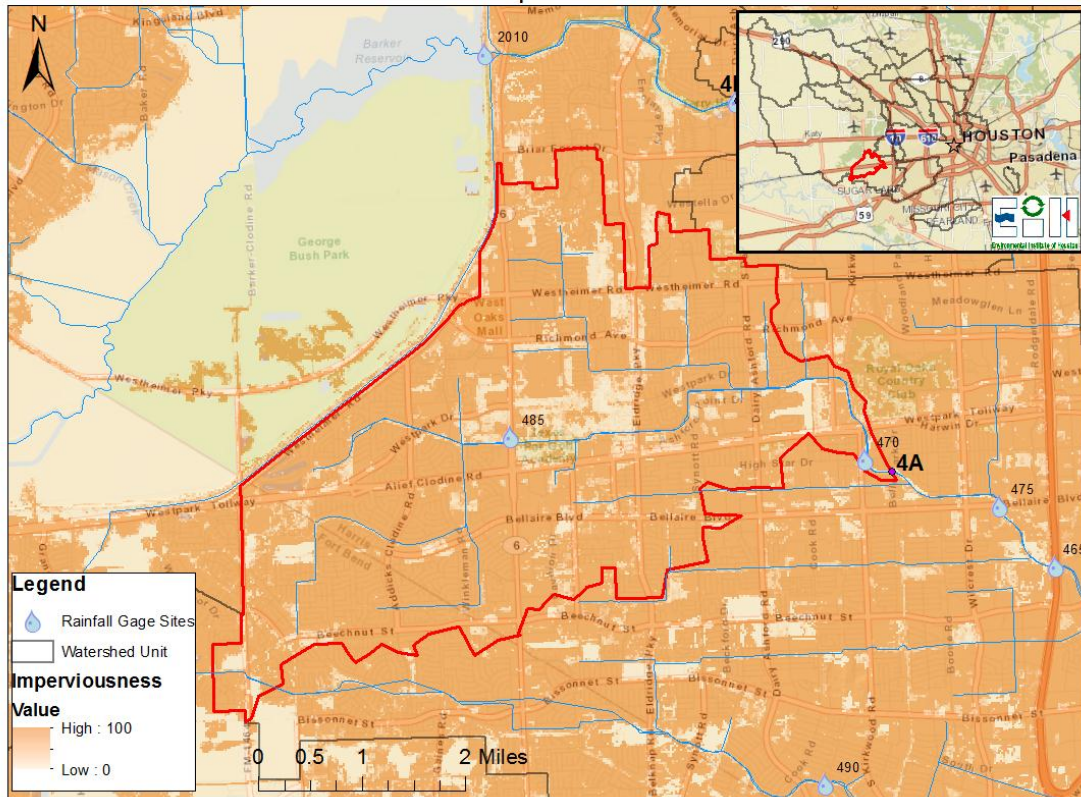


Figure A7.15. Site 3A imperviousness and hydrological soil types.

Site 4A Imperviousness



Site 4A Hydrological Soil Types

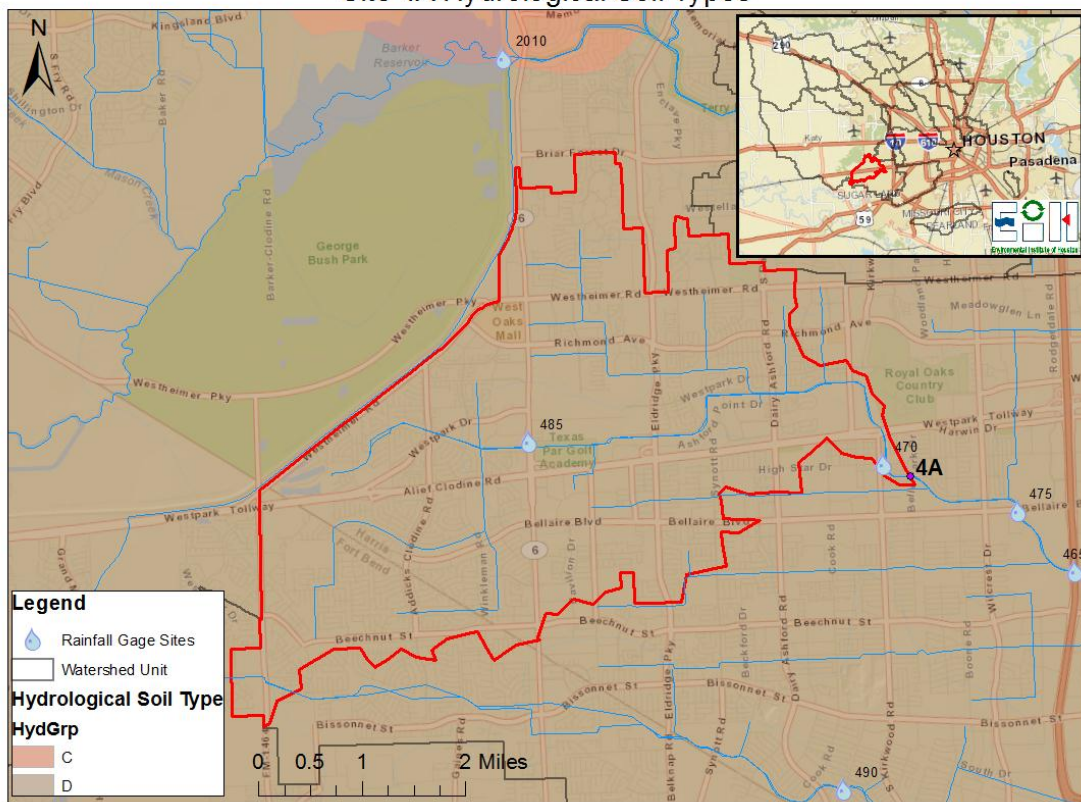


Figure A7.16. Site 4A imperviousness and hydrological soil types.

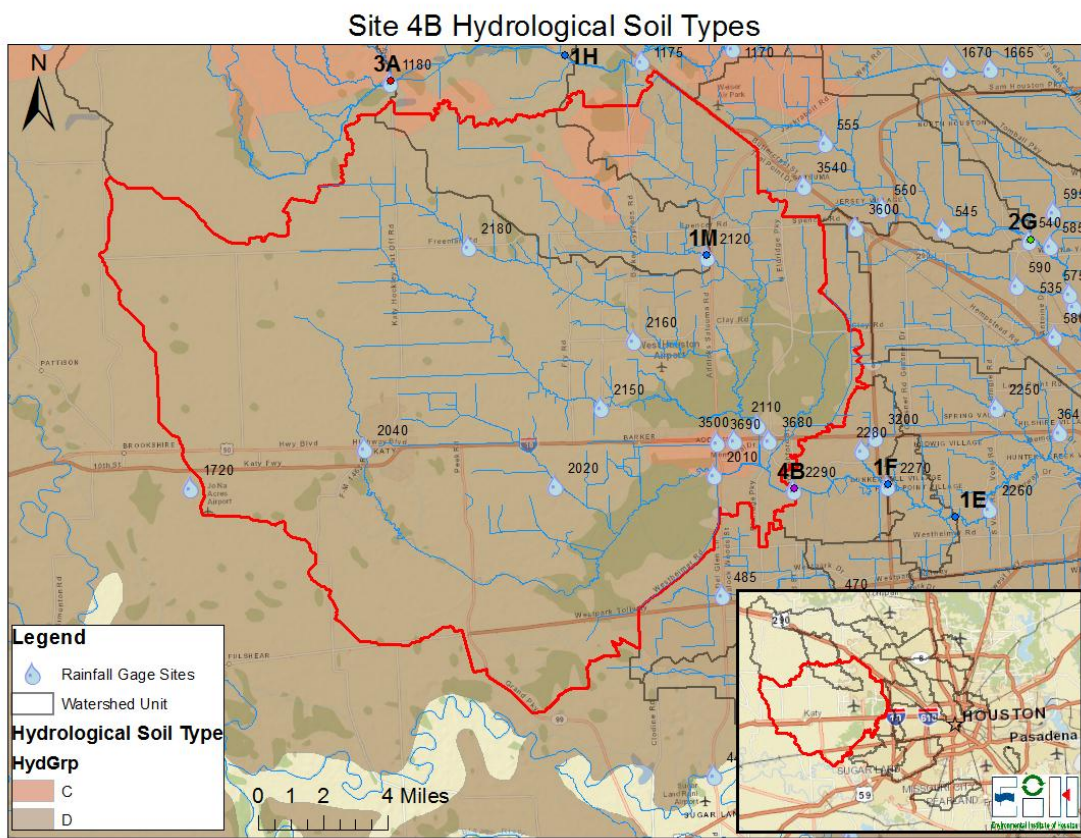
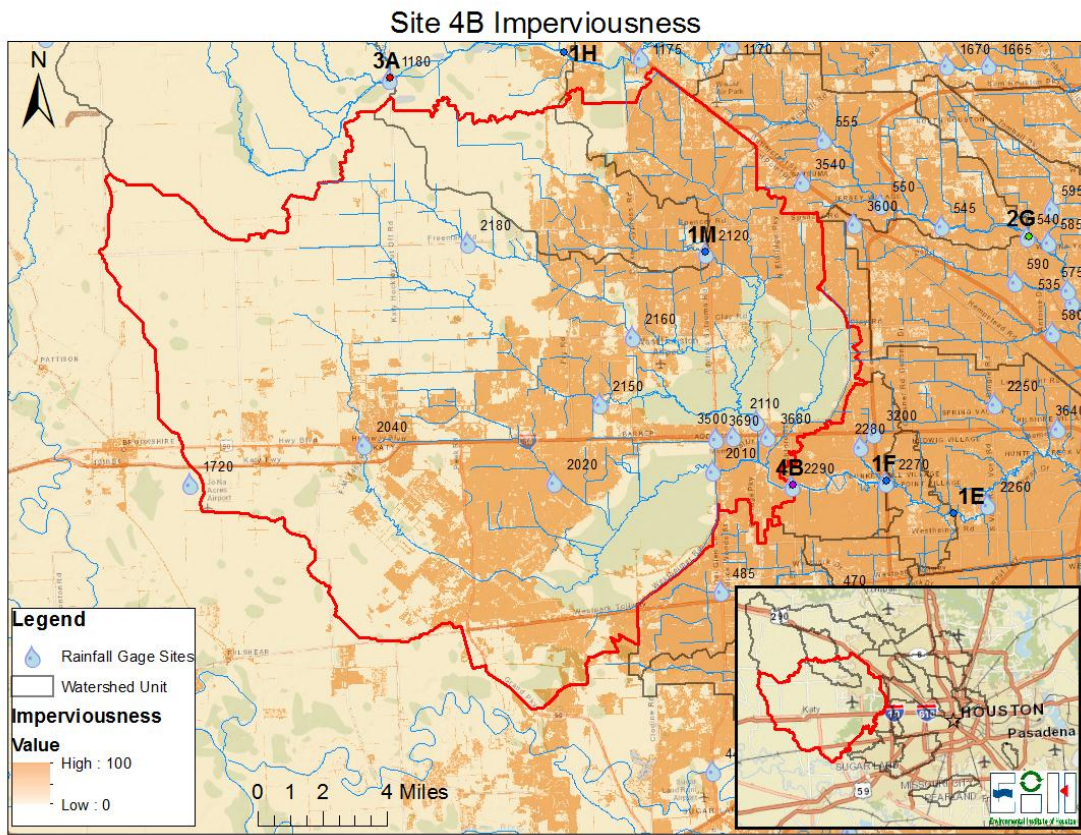


Figure A7.17. Site 4B imperviousness and hydrological soil types.

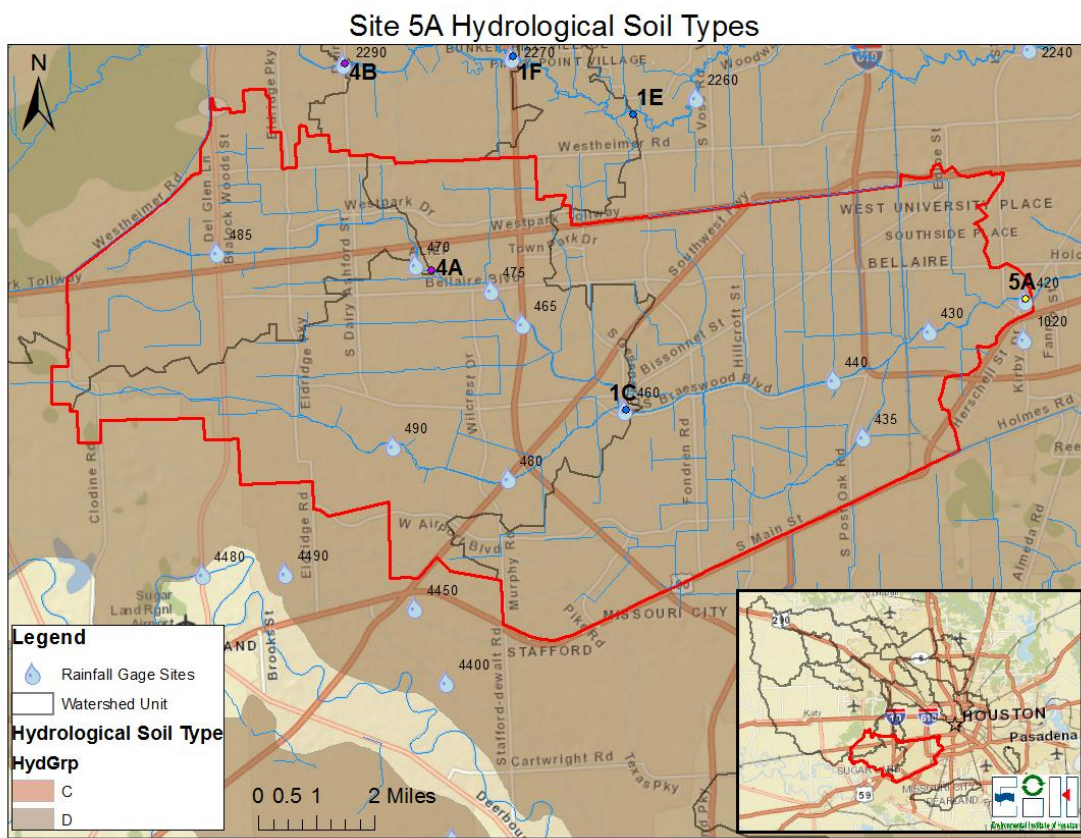
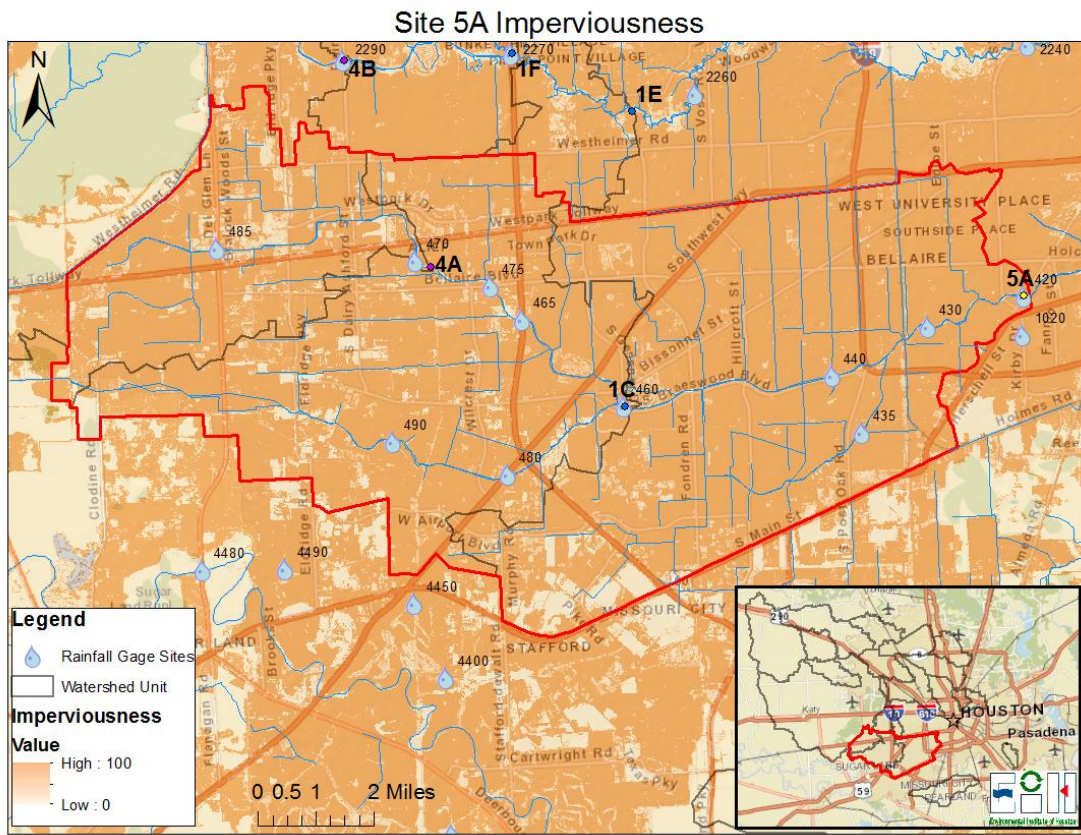
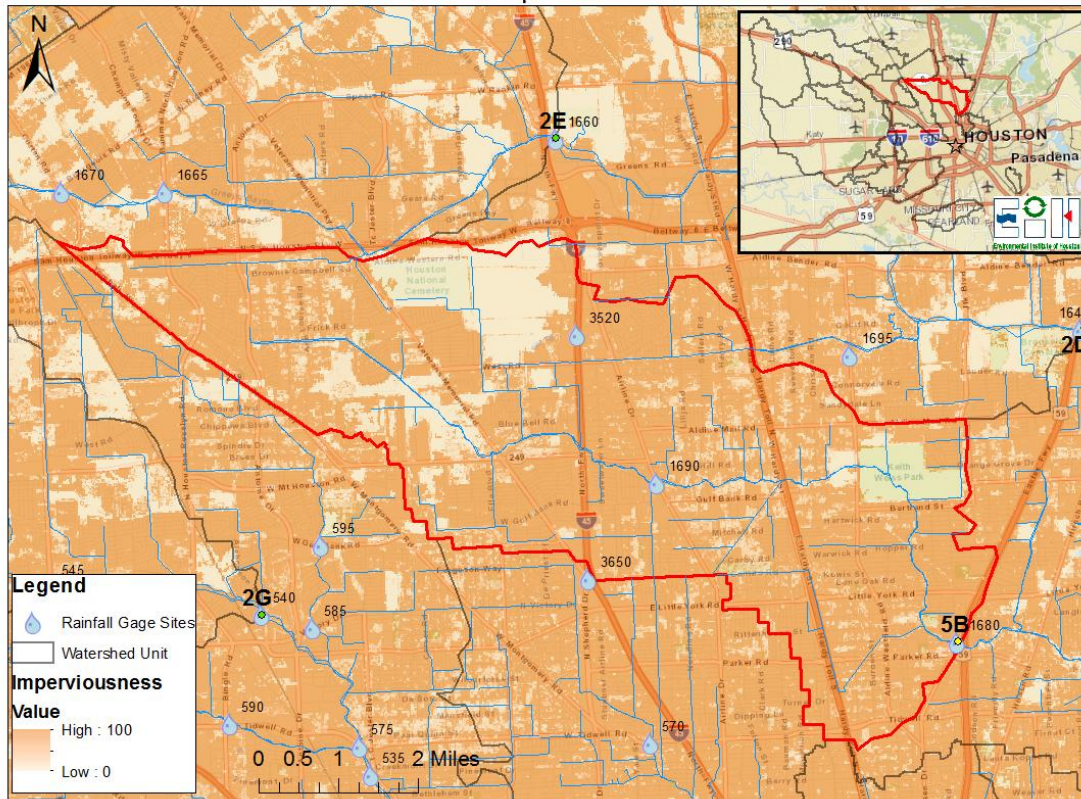


Figure A7.18. Site 5A imperviousness and hydrological soil types.

Site 5B Imperviousness



Site 5B Hydrological Soil Types

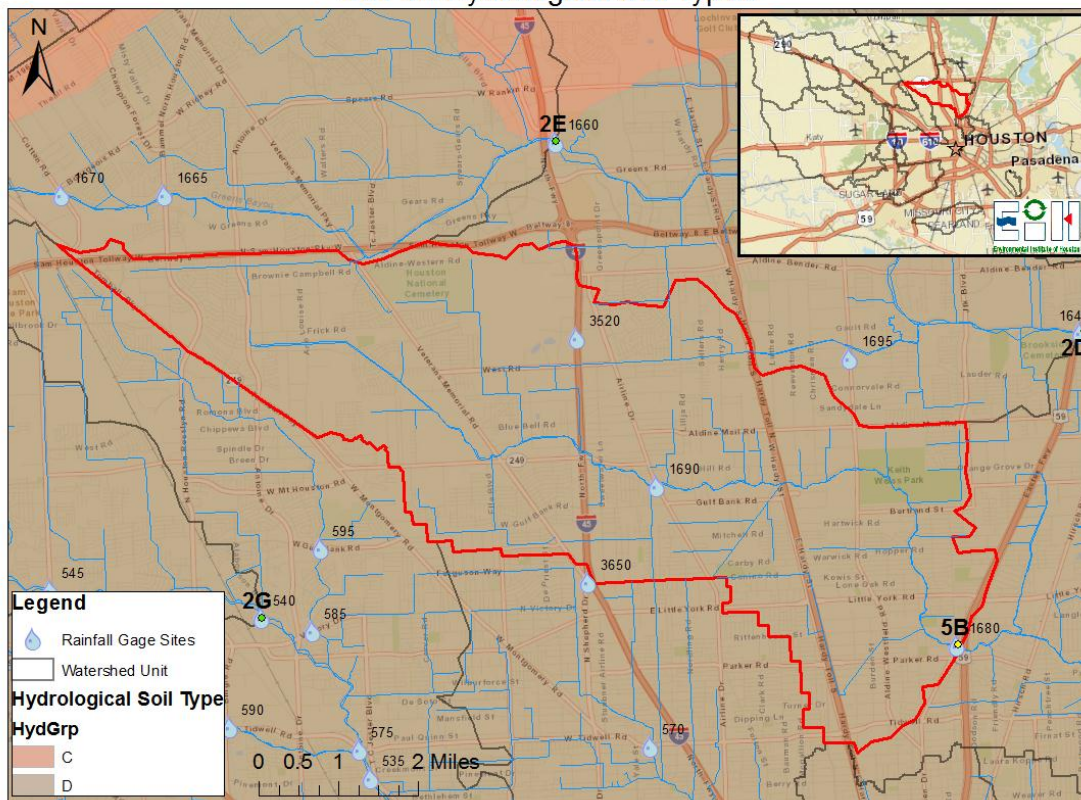
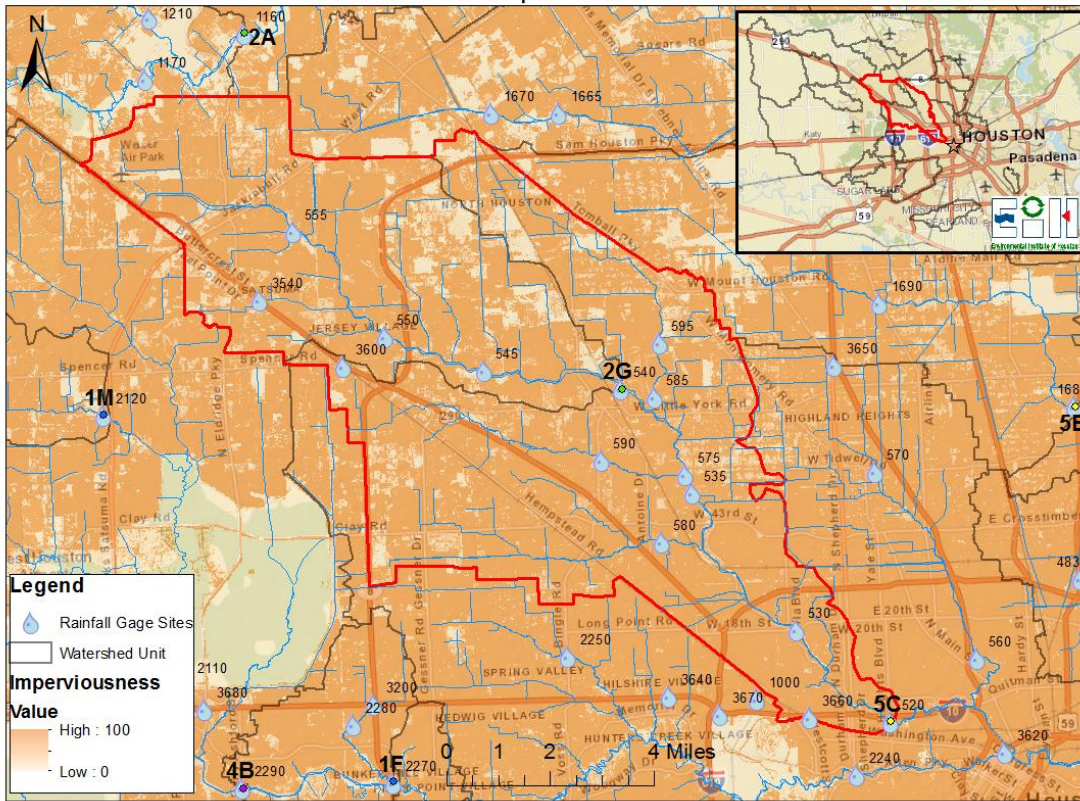


Figure A7.19. Site 5B imperviousness and hydrological soil types.

Site 5C Imperviousness



Site 5C Hydrological Soil Types

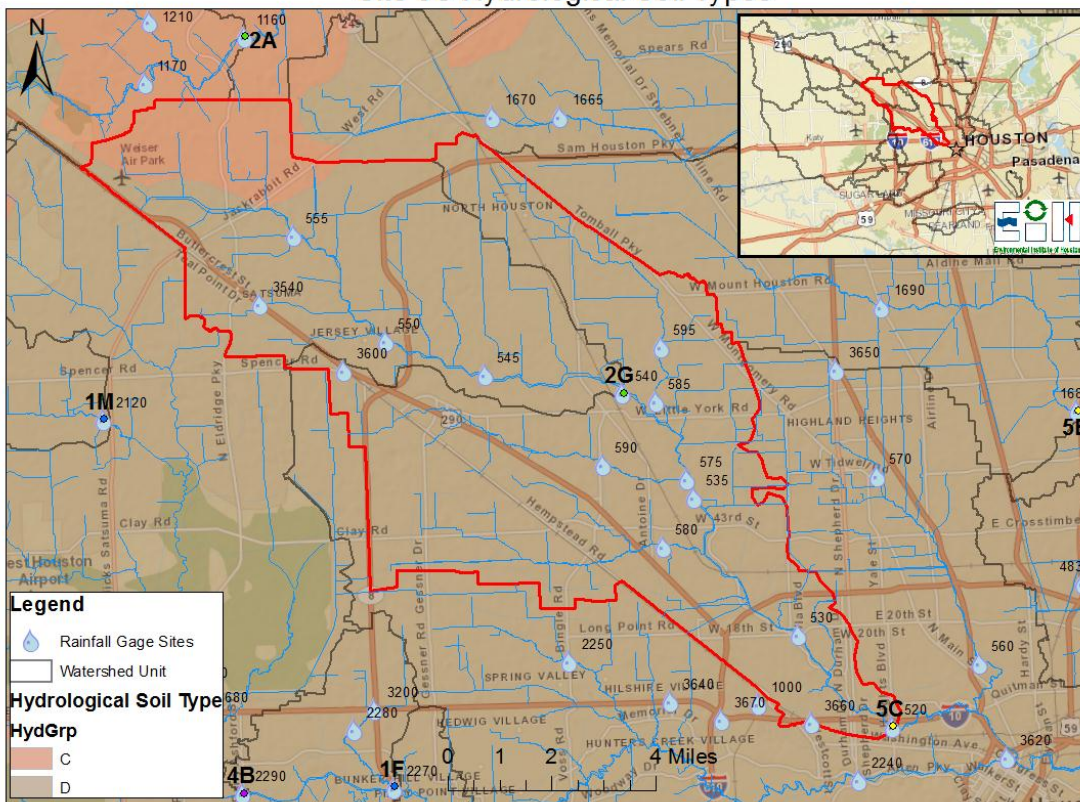


Figure A7.20. Site 5C impervious land area and hydrological soil types.

Appendix 8: Parent 2010 Historical Data Review Database (Electronic Supplement)

*See Compact Disk at Rear of Report for Electronic Supplements

Appendix 9: Historical Database (Electronic Supplement)

9.A: Harris County Historical Data

9.B: EIH CRP NTU Historical Database

*See Compact Disk at Rear of Report for Electronic Supplements

Appendix 10: Deployed Sonde Data (Electronic Supplement)

*See Compact Disk at Rear of Report for Electronic Supplements

Appendix 11: Flow Data (Electronic Supplement)

*See Compact Disk at Rear of Report for Electronic Supplements

Appendix 12: Rainfall Data (Electronic Supplement)

12.A. Daily Rainfall Data

12.B. Hourly Rainfall Data

*See Compact Disk at Rear of Report for Electronic Supplements

Appendix 13: Master Data (Electronic Supplement)

13.A. Master Database

13.B. Lab Bench Sheets

13.C. Field Datasheets

*See Compact Disk at Rear of Report for Electronic Supplements

Appendix 14: ArcGIS Runoff Data (Electronic Supplement)

*See Compact Disk at Rear of Report for Electronic Supplements